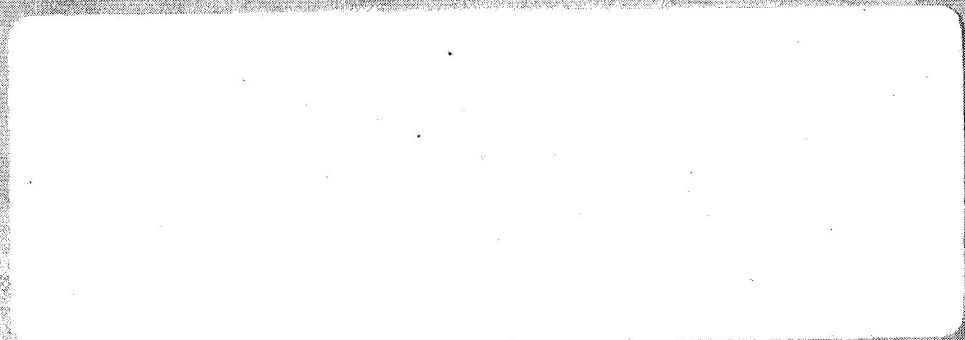


mi



FACILITY FORM 602

ACCESSION NUMBER N68-19391

PAGES 206

(NASA CR OR TMX OR AD NUMBER) CP-93679

(THRU) _____

(CODE) 1

(CATEGORY) 30


GPO PRICE \$ _____

CSFTI PRICE(S) \$ _____

Hard copy (HC) 3.10

Microfiche (MF) .65

ff 653 July 66



PHILCO-FORD CORPORATION
Space & Re-Entry Systems Division
Newport Beach, California

Publication No. UG-4289

SPACE AND RE-ENTRY SYSTEMS

FINAL REPORT DEVELOPMENT OF ADVANCED SOIL SAMPLER TECHNOLOGY VOLUME II OF II

Prepared for: Space Sciences Division
Jet Propulsion Laboratory
California Institute of Technology
4800 Oak Grove Drive
Pasadena, California 91103

Contract No.: 951935

Reporting Period: 28 June 1967 to 31 January 1968

Prepared by: George P. Zebal
George P. Zebal, Program Engineer
Wilfred H. Bachle
Wilfred H. Bachle, Design Engineer

Approved: Robert P. Thompson
Robert P. Thompson, Manager, Space
Applications and Explorations Activity
R. A. Mills
R. A. Mills, Program Manager



PHILCO-FORD CORPORATION
Space and Re-entry Systems Division
Newport Beach, California • 92663

APPENDIX A

SOIL MODELS FOR LABORATORY TESTING

APPENDIX A

CONTENTS

SOIL MODELS FOR LABORATORY TESTING

Nevada No. 60 Sand

Olivine Basalt Silt

Soil Model I-2 Pumice

Soil Models II-1a, II-1b, II-1c, and II-1d

Nevada No. 60 Sand of Varying Thickness over a
Pumice Base

Soil Model III-3 Sandstone

Soil Model PR Pebble Rubble

Soil Model IV-1 Infected Sand

Soil Model IV-3 Cemented Sand with Filaments

Soil Model IV-4 Lichen Covered Basalt

Soil Model IV-5 Organic Incrustations

LIST OF TABLES

TABLE		PAGE
A-1	Composition of Pisgah Crater Olivine Basalt	A-7
A-2	Soil Model III-3, Sandstone, Control Sample	A-13
A-3	Preparation of Homogeneously Infected Nevada No. 60 Sand	A-19

LIST OF FIGURES

FIGURE		PAGE
A-1	Particle Size Distribution Curve for Nevada No. 60 Sand Control Sample.	A-5
A-2	Particle Size Summation Curve for Nevada No. 60 Sand . .	A-6
A-3	Particle Size Distribution Curve for Basalt Silt Control Sample	A-8
A-4	Particle Size Summation Curve for Basalt Silt	A-9
A-5	Pumice Model in DWB Testing Bin	A-10
A-6	Sandstone Model in DWB Testing Bin	A-10
A-7	Particle Size Distribution Curve for Sandstone Control Sample	A-14
A-8	Particle Size Summation Curve for Sandstone	A-15
A-9	Particle Size Distribution Curve for Pebble Rubble . . .	A-16
A-10	Particle Size Summation Curve for Pebble Rubble	A-17
A-11	Pebble Rubble Model in DWB Testing Bin	A-18
A-12	Cemented Sand with Filaments Model	A-18
A-13	Yellow Crustose Lichen Colony on a Basalt Cinder Boulder	A-21
A-14	Barnacle-studded Unfinished Concrete Test Surface . . .	A-21

APPENDIX A
SOIL MODELS FOR LABORATORY TESTING

This appendix presents detailed descriptions of the soil models utilized in the laboratory testing phase of the program. The ensuing chapters will describe the models in terms of composition, particle size and size distribution, texture and structure. Where organic materials are present, their character will be described and pictured.

Nevada No. 60 Sand

This sand was utilized in a pure state as the unnumbered noncohesive sand model (see the test matrix, Table 3-3) and as the noncohesive surface layer of the sand over pumice models (Nos. II-1a, II-1b, II-1c and II-1d). The Nevada No. 60 sand was originally selected to represent a typical terrestrial desert dune sand having a grain size distribution similar to that described by Bagnold. It was commercially obtained from a natural dune source in Clarke County, Nevada. Mineralogically, it is wholly composed of water white to buff to reddish brown, slightly iron-stained, well rounded to subrounded, quartz grains. For testing purposes, the model is maintained in a loose state. Since the individual grains are well rounded, an easily sheared uncompacted material is obtained.

The particle size distribution and summation curves for Nevada No. 60 sand are designated on Figures A-1 and A-2, respectively.

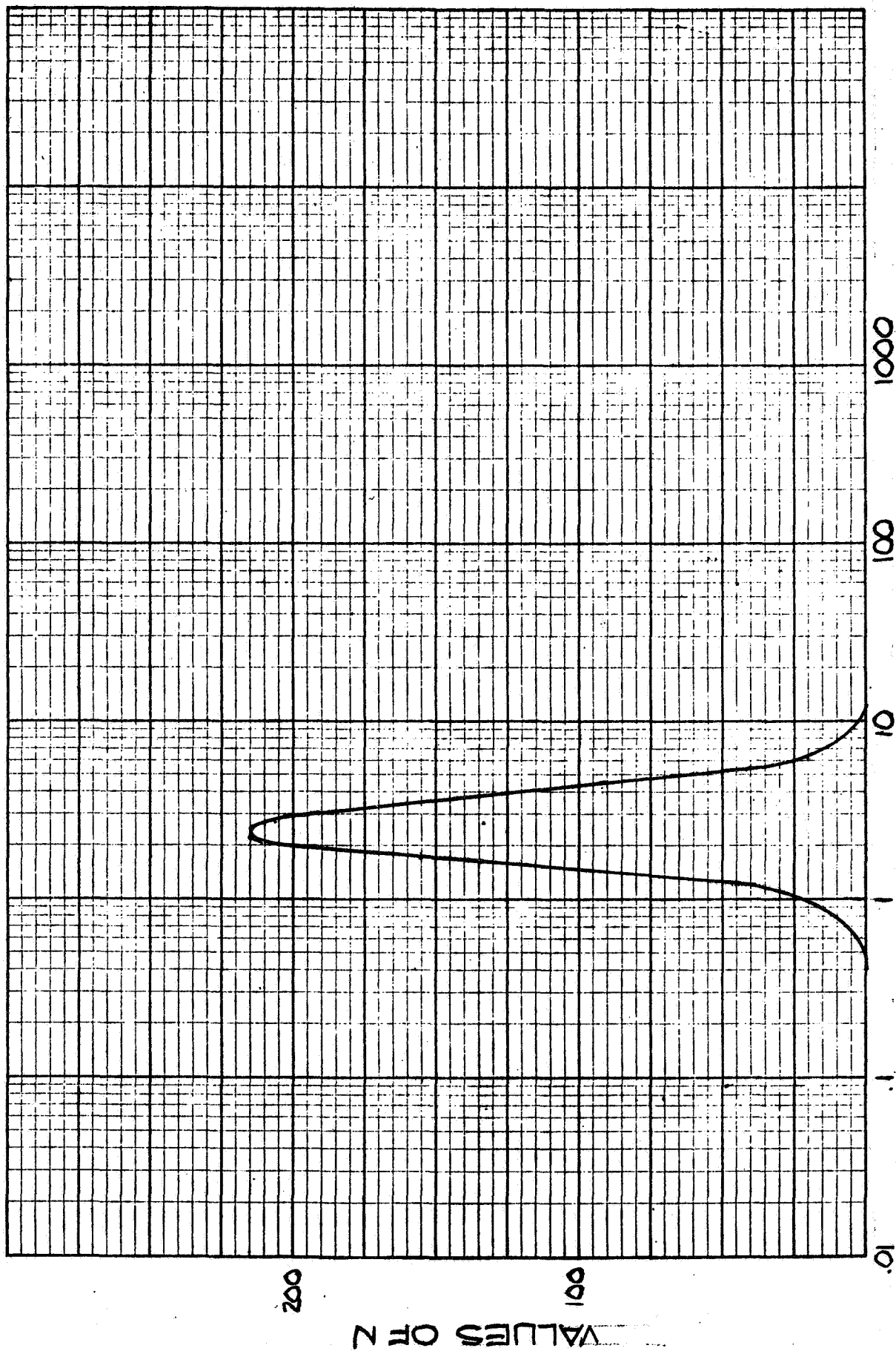


FIGURE A-1 PARTICLE SIZE DISTRIBUTION CURVE FOR NEVADA 60 SAND CONTROL SAMPLE

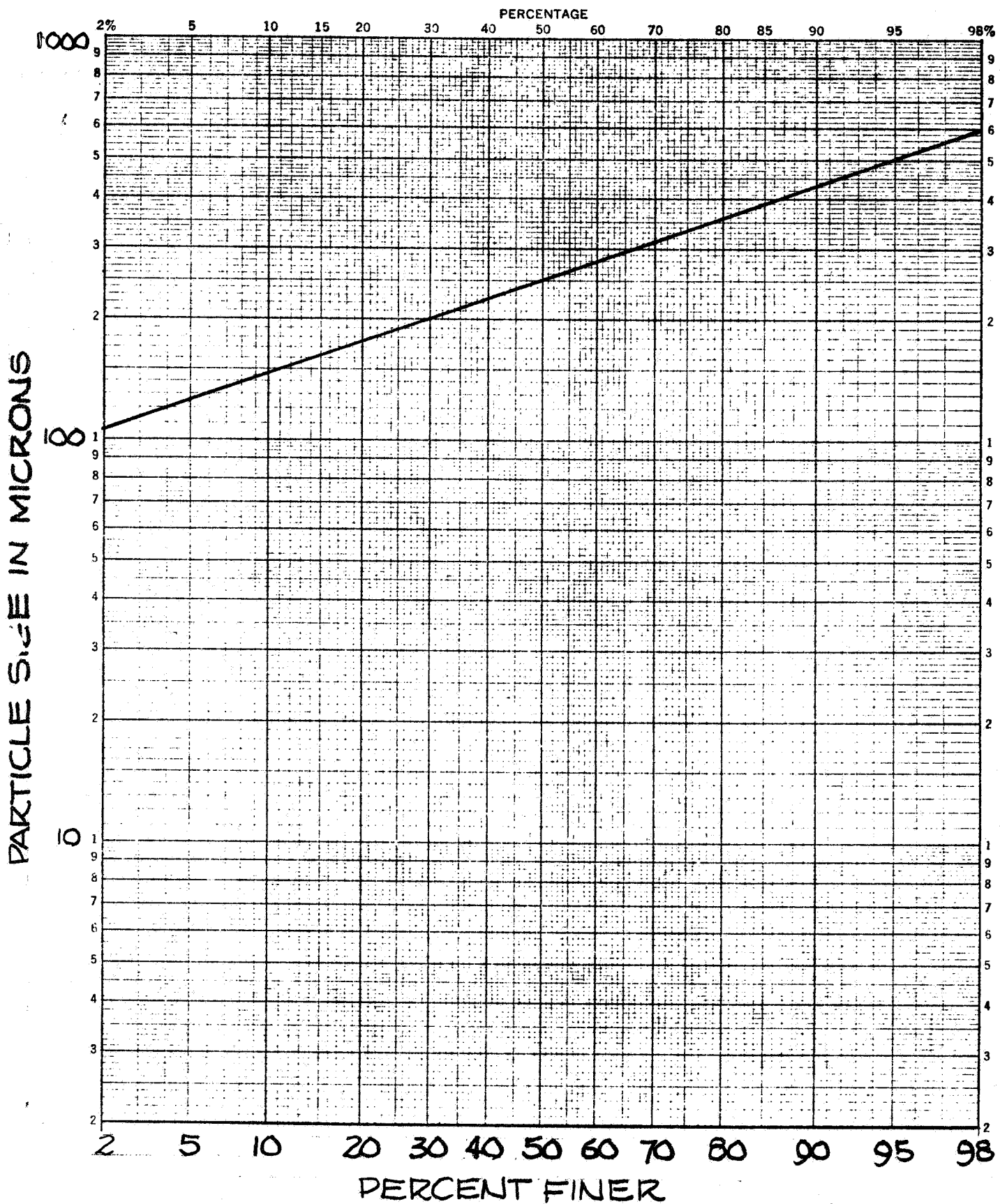


FIGURE A-2 PARTICLE SIZE SUMMATION CURVE
NEVADA 60 SAND

Olivine Basalt Silt

The basalt silt was tested in a pure state as the unnumbered cohesive silt model (see the test matrix, Table 3-3) and as the silt-size component of the pebble rubble model (No. PR). The basalt silt was selected as a laboratory test model because of its geologically undifferentiated character which may express an affinity to undifferentiated lunar and planetary crusts, and its grain size and cohesive nature. Cohesion is obtained for testing purposes through a combination of extremely angular grain shape and natural packing due to handling. It was prepared by mechanically crushing Pisgah Crater olivine basalt cobbles until the desired product passed through a 230 mesh screen (particle size $< 62 \mu$).

The composition of Pisgah Crater olivine basalt was obtained from petrographic analyses of thin-sections cut from pahoehoe flow fragments. The composition of the feldspar minerals was checked by an X-ray diffraction analysis. The average composition was ascertained to be that shown in Table A-1.

TABLE A-1

COMPOSITION OF PISGAH CRATER OLIVINE BASALT

Mineral Group	Mineral	Percent	
Plagioclase feldspar		35	
	Andesine		20
	Anorthite		15
Pyroxene		40	
	Augite		25
	Hypersthene		15
Accessory minerals		25	
	Olivine		20
	Magnetite		5
		100%	100%

Particle size distribution and summation curves for basalt silt are shown on Figures A-3 and A-4.

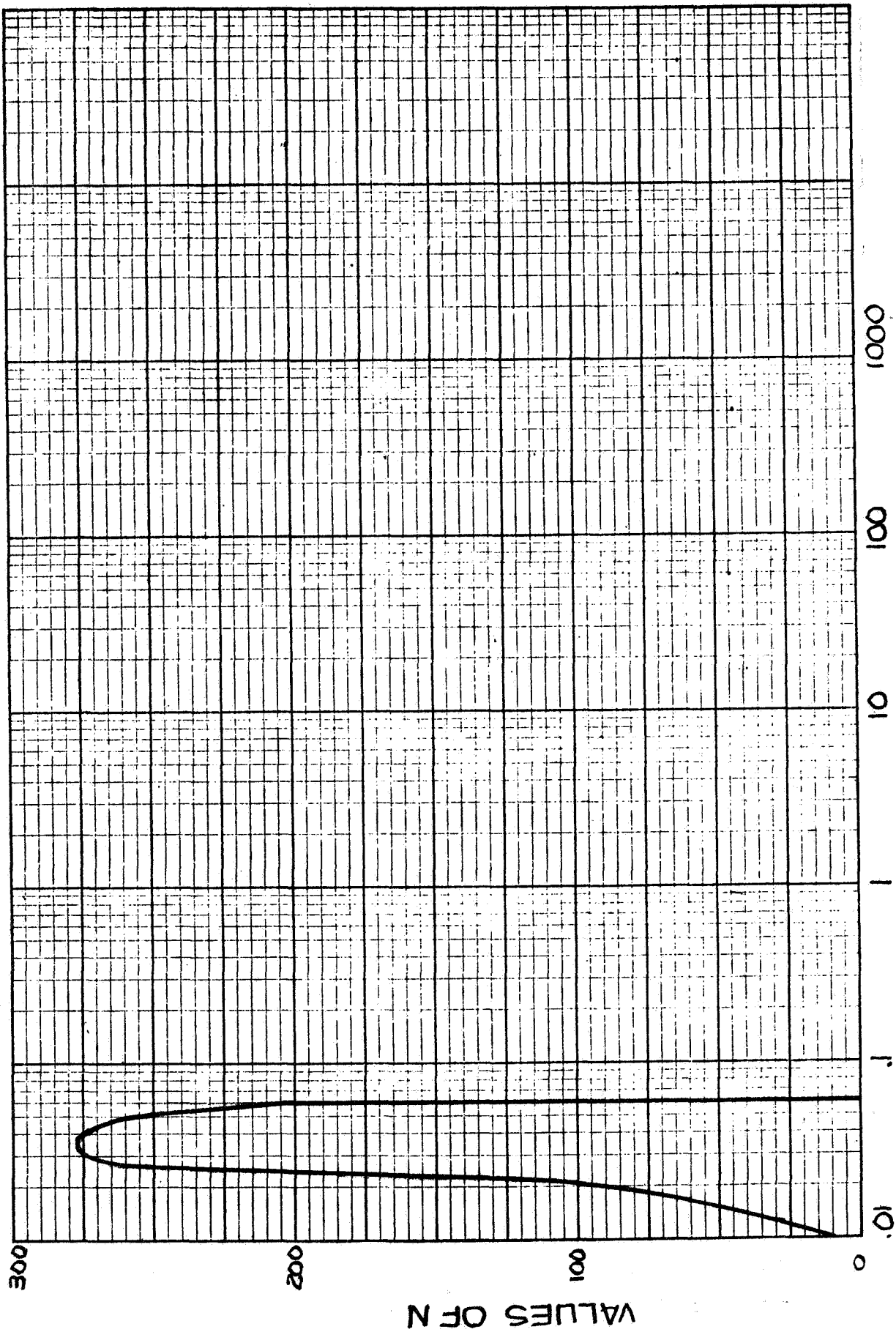


FIGURE A-3 PARTICLE SIZE DISTRIBUTION CURVE FOR
BASALT SILT CONTROL SAMPLE

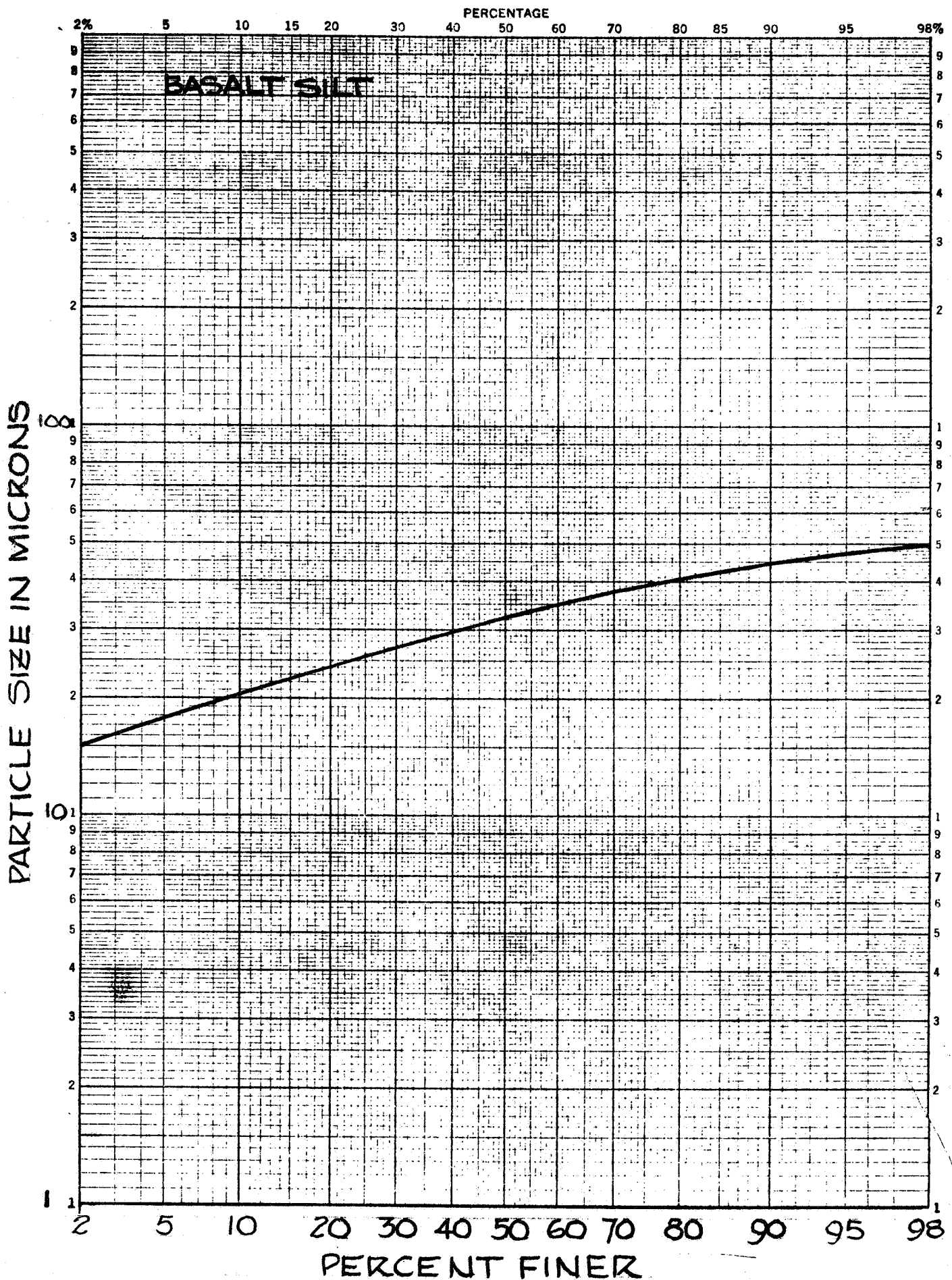


FIGURE A-4 PARTICLE SIZE SUMMATION CURVE

Soil Model I-2 Pumice

Pumice was used in the preparation of two laboratory models. In a pure state, blocks of pumice were laid end to end, as illustrated in Figure A-5, to demonstrate the ability of the VCS and DWB samplers to collect samples from a completely outgassed, very cellular, hard and brittle type of surface flow material that may represent lava surfaces in reduced atmospheric pressure environments such as the Moon and Mars. Vesicular surfaces of this nature may provide ideal organic microenvironments. The pumice was commercially obtained from a source near Mono Lake, Lee Vining, Mono County, California. It was supplied in cut blocks measuring 12x11x6 inches suitable for direct emplacement into the VCS and DWB sampling bins as shown in Figure A-5. The pumice is mineralogically a water white silica glass. Flow banding is prominent (as denoted in the darker blocks in Figure A-5) due to the presence of minor amounts of impurities, dominantly oxides of magnesium and iron. The individual vesicles making up the cellular structure of this type of pumice vary in diameter from 0.1 to 15 mm; the average diameter is 1.5 mm. Because of the flow structure most of the vesicles are oval to sinuously contorted. The walls separating vesicles often tend to be bundles of tubes with glass walls varying from 10 to 50 μ in thickness. Beneath the microscope, a hand specimen appears to be composed of interwound silky fibers trending parallel to the flow banding with each fiber a tube. The collections of interwound fibers, in turn, enclose the vesicles in a sponge-like manner.

Soil Models II-1a, II-1b, II-1c and II-1d, Nevada No. 60 Sand of Varying Thickness over a Pumice Base

Pumice was utilized as the base material because it tends to simulate outgassed flow material and Nevada No. 60 sand was used as the surface layer because of its dune-like, noncohesive and easily sheared character. In addition, the two materials are so unlike that the sand grains and equally sized glass shards could be easily separated under the microscope and the sample collecting effectiveness of the samplers analyzed.

Descriptions of Nevada No. 60 sand and Mono Lake pumice are provided above and by Figures A-1 and A-2. The preparation of the models is described in Table 2-2 of the test plan.

Soil Model II-3 Sandstone

The sandstone model was designed to afford a cohesive particulate material having a dense but very irregular surface. Blocks of sandstone up to 12 inches in length were irregularly distributed along the length of the DWB sampling bin for testing as shown by Figure A-6. The sandstone blocks were obtained by Philco-Ford personnel from an excavation on the Irvine Ranch, Corona del Mar, California. The sandstone can be generally described as a buff, limonite-stained, weakly cemented (Fe_2O_3 and CaCO_3), fine to very

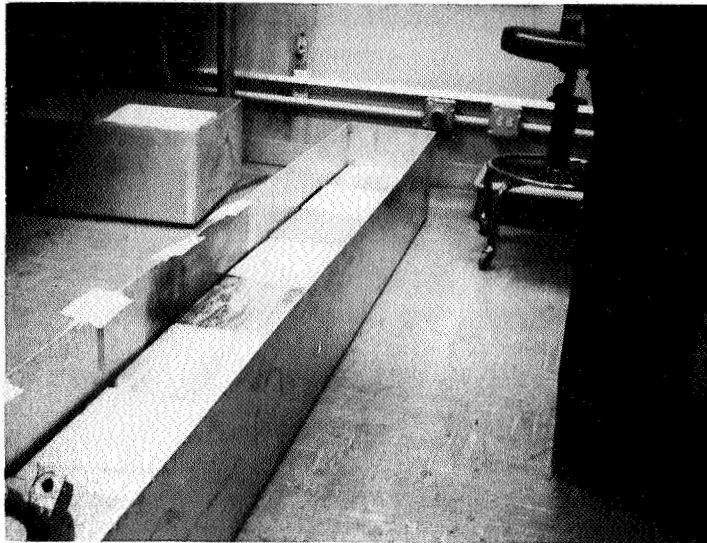


FIGURE A-5
PUMICE MODEL IN DWB TESTING BIN

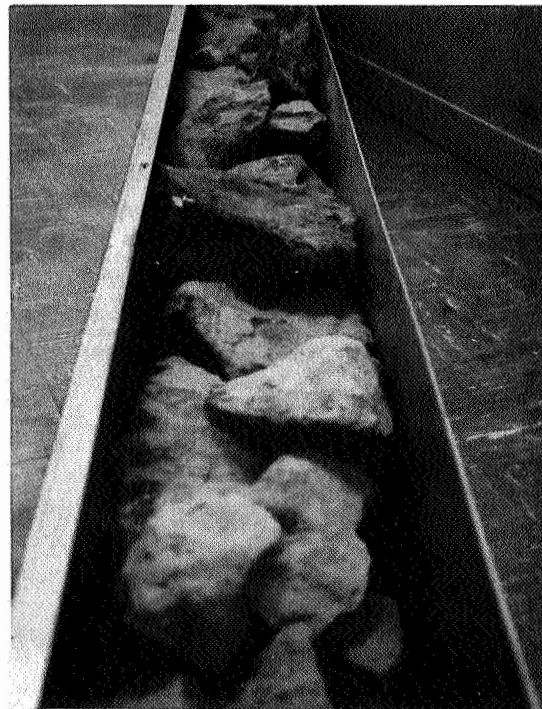


FIGURE A-6
SANDSTONE MODEL IN DWB TESTING BIN

fine grained, slightly silty, upper Miocene sandstone. An abundance of plant remains and complete lack of marine fossils suggests that it was formed in an estuarine or deltaic environment. A detailed breakdown of its mineralogical composition is provided on Table A-2.

The particle size distribution and summation curves for the sandstone model are presented on Figures A-7 and A-8. The sandstone was broken down by soaking several representative fragments in water, autoclaving to dryness and, finally, manually crushing lumps that had recemented in the autoclave.

Soil Model PR Pebble Rubble

The pebble rubble material was manufactured from mechanically crushed Pisgah Crater olivine basalt. The absolute grain size range lies between 0.5 μ and 76 mm. The particle size distribution curve, Figure A-9, and the summation curve, Figure A-10, illustrate the particle distribution between these extremes. This model was designed to represent an impact rubble composed of crushed material. Three types of particulate material were intermixed to fabricate the test model. The parent rock from which all three types were obtained were boulders and cobbles of pahoehoe type lava from the Pisgah Crater flow complex. The pebble component was removed as the initial product of a Gates jaw crusher; material from 10 to 76 mm was obtained. Jaw crushed material was further reduced by passing through a gyratory crusher set for approximately 10 mm; this produced the sand-sized material, 62 μ to 2 mm. Due to the processing described above, a paucity of material in the 7 to 12 mm range was obtained as demonstrated by the particle size distribution curve of Figure A-9. Three additional pulverizing cycles beyond the jaw crusher were utilized to obtain the silt fraction. This fraction included material that passed wholly through a 230 mesh screen; a product with a grain size range of 0.5 to 62 μ . Equal amounts of these products were mixed to yield the pebble rubble model tested. The resultant rubble is pictured in Figure A-11.

Soil Model IV-1 Infected Sand

Nevada No. 60 sand was contaminated with Bacillus subtilis var. niger spores to provide about 1×10^5 spores per gram of sand. The dry spores, obtained from R. K. Hoffman, Ft. Detrick, Maryland, assayed 1×10^5 spores per gram. Assay procedures for spores and spores mixed with sand are described in Appendix C. The manner in which spores and sand were mixed is noted in Table A-3. The composition and particle size range of Nevada No. 60 sand is shown on Figure A-1 and A-2.

TABLE A-2

SOIL MODEL III-2, SANDSTONE, CONTROL SAMPLE

Caught on Sieve No.	Quantity Grams	Description
10	0.14	Very fine grained gravel composed of: Greasy gray, angular quartzite pebbles, 2 to 5 mm - 40% Fossil root, stem and leaf fragments: 60%
18	0.13	Very coarse sand as follows: Quartzite as above - 50% Snow white to rusty, subangular to subrounded α quartz - 30% Fossil plant fragments as above - 20%
35	0.60	Coarse grained sand as follows: Quartzite as above - 10% α quartz species (70%) (a) Water white, translucent, well rounded grains - 45% (b) Water white to orange to buff to dark red angular to subangular grains - 15% (c) Snow white, angular to subrounded grains - 10% Fossil plant fragments as above - 15% Golden yellow to light brown muscovite mica flakes - 5%
60	2.43	Medium grained sand: Quartzite - Trace α quartz species as above (75%) (a) 45% (b) 25% (c) 5% Fossil plant fragments - 5% Muscovite mica flakes - 20%
120	18.69	Fine grained sand: α quartz species as above (80%): (a) Trace (b) 60% (c) 20% Fossil plant fragments - Trace Muscovite flakes - 20% Dark resinous brown magnetite - Trace
230	39.70	Very fine grained sand: α quartz species (90%): (a) Trace (b) 70% (c) 20% Fossil plant fragments - Trace Muscovite flakes - 5% Magnetite - 5%
325	2.66	Quartz silt composed of: α quartz species as above (85%): (a) Trace (b) 65% (c) 20% Muscovite flakes - Trace Magnetite - 15%
Cup	2.35	Very fine grained quartz silt (very little clay): α quartz species (> 95%): (a) Trace (b) > 85% (c) 10% Muscovite flakes - Trace Magnetite - < 5% Clay - Trace
Total	66.70	

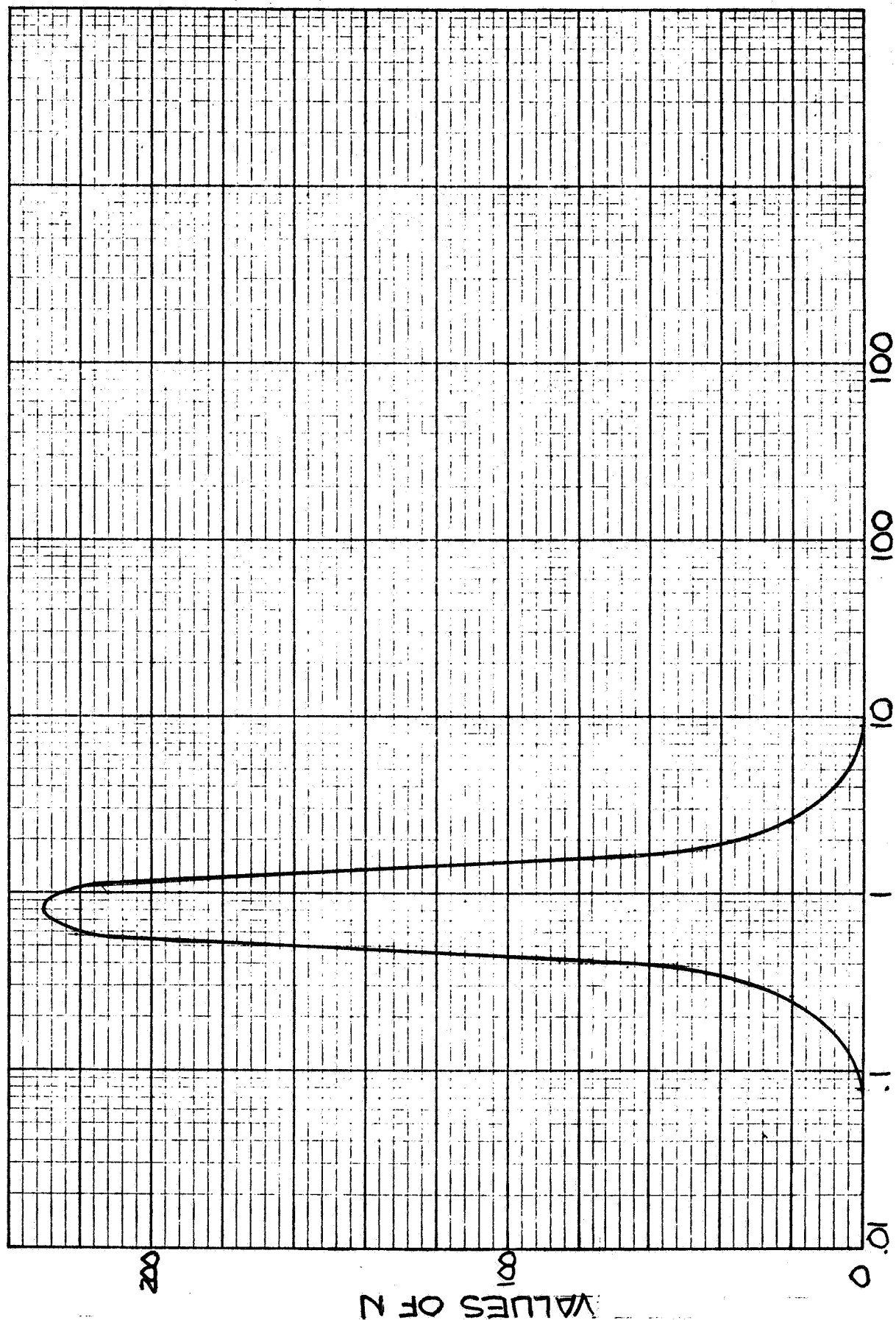


FIGURE A-7 PARTICLE SIZE DISTRIBUTION SANDSTONE CONTROL

PARTICLE SIZE IN MILLIMETERS

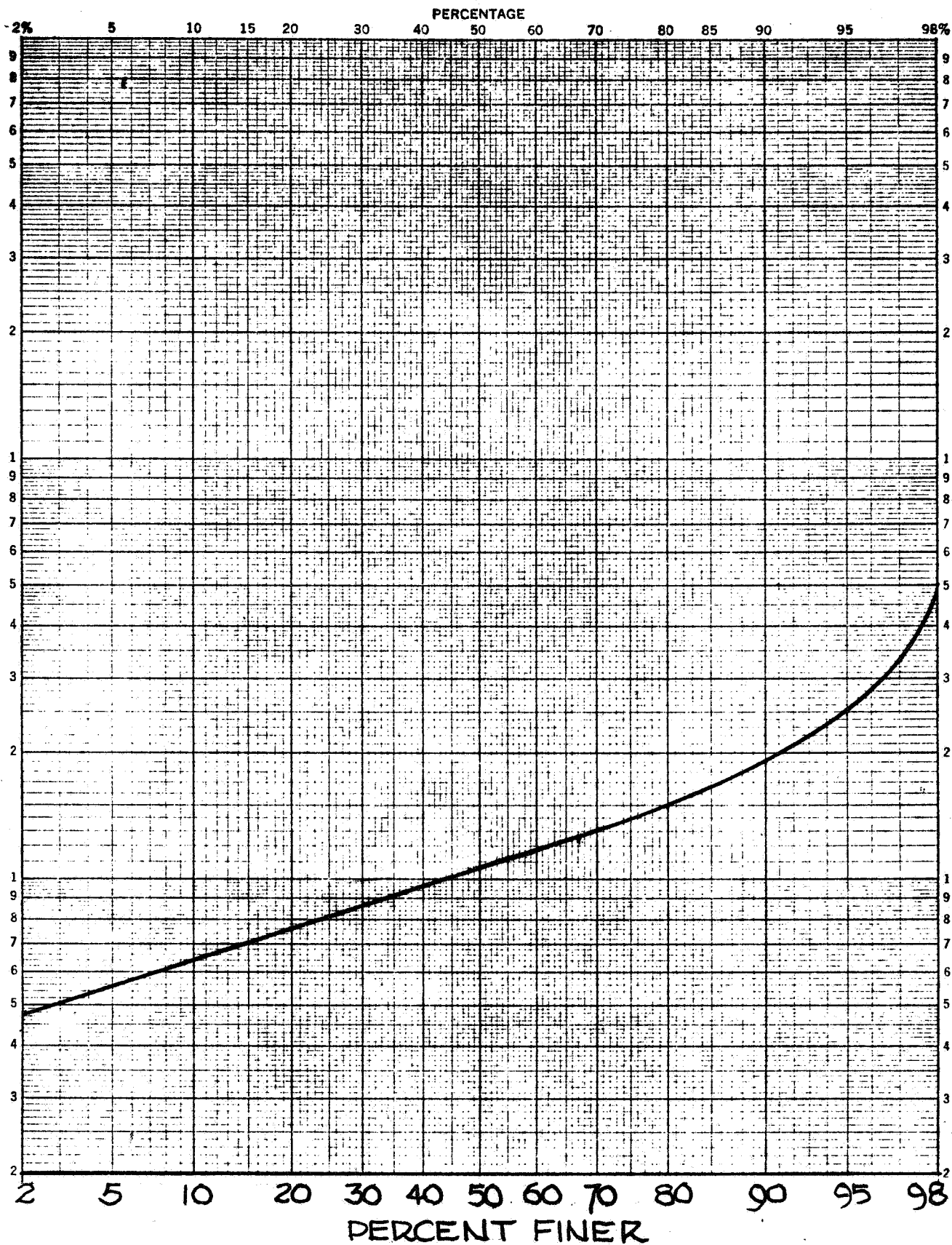


FIGURE A8 PARTICLE SIZE SUMMATION CURVE
SANDSTONE CONTROL SAMPLE

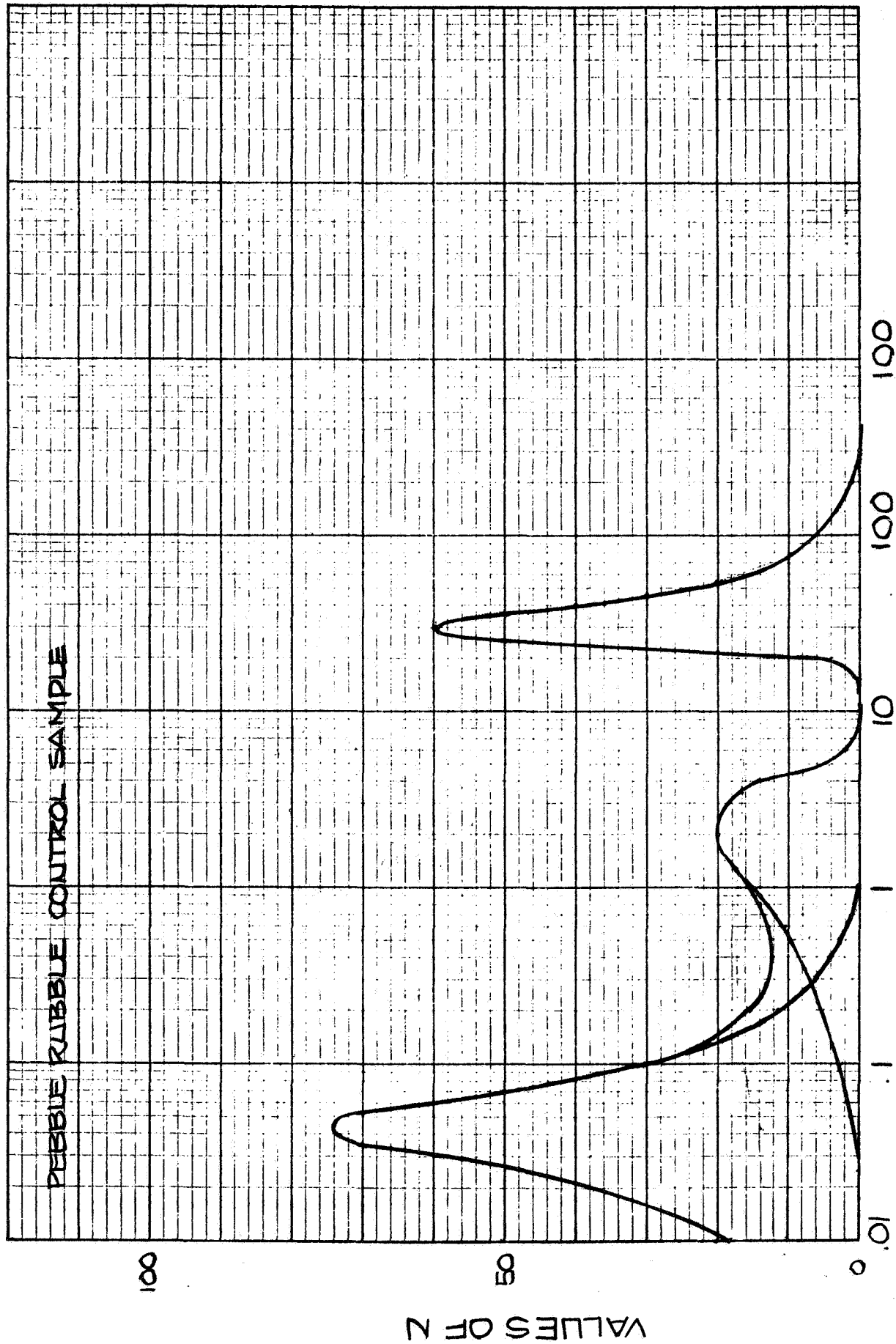


FIGURE A9 PARTICLE SIZE DISTRIBUTION CURVE

PARTICLE SIZE IN MILLIMETERS

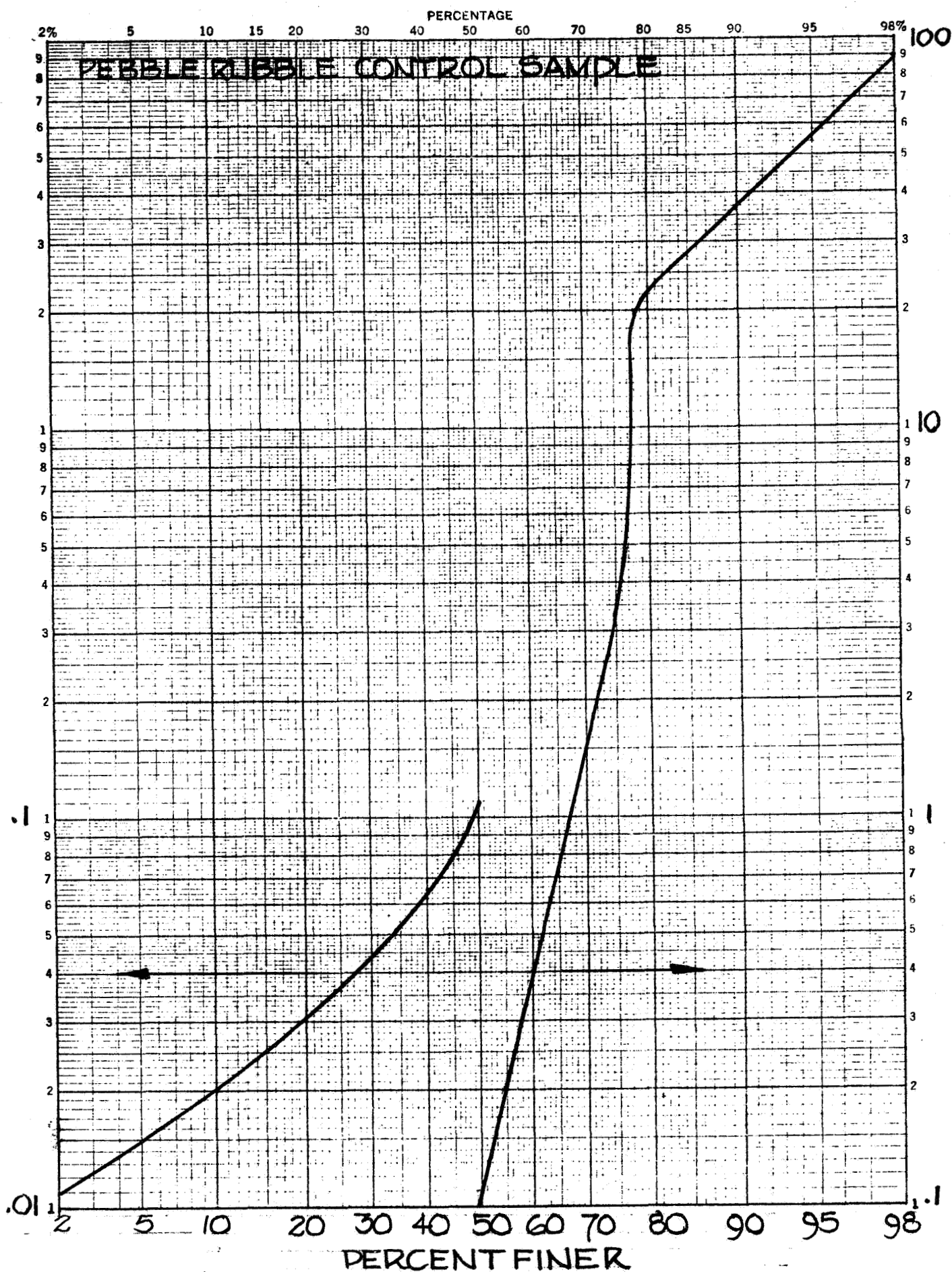


FIGURE A-10 PARTICLE SIZE SUMMATION CURVE

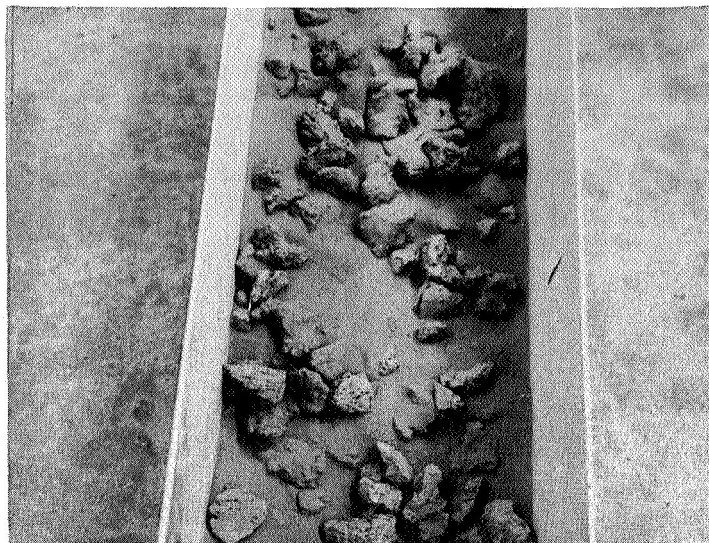


FIGURE A-11
PEBBLE RUBBLE MODEL IN DWB TESTING BIN



FIGURE A-12
CEMENTED SAND WITH FILAMENTS MODEL

TABLE A-3

PREPARATION OF HOMOGENEOUSLY INFECTED NEVADA 60 SAND

(a)	Fifty mg of <u>B. subtilis</u> spores added to 11 lbs of Nevada 60 sand.
(b)	Mix the 11 lbs of infected sand for 5 minutes on a rotating ball mill (balls were not used).
(c)	Remove 1 lb of sand prepared in "b" above and add to 10 lbs of fresh sand.
(d)	Mix for 5 minutes on a rotating ball mill as in "b" above.
(e)	Repeat "c" and "d" 10 times, combining all mixes into an aluminum testing bin measuring 6 x 12 x 12 inches.
(f)	Dilution plate count assays of controls and sampled sand specimens (see Appendix C).

Cultures prepared from the sand before the spores were added had a very low bacterial count and did not include organisms which resembled the B. subtilis var. niger colony. This indicated that it was not necessary to sterilize the sand before spores and sand were combined.

Soil Model IV-3 Cemented Sand with Filaments

This model was designed to represent a cohesive soil containing organic filamentary or root-like structures. It was fabricated from Nevada No. 60 sand and common cement with a 10:1 ratio of aggregate to cement. While the mixture was in a viscous state filaments of sphagnum moss were liberally introduced to produce a product wherein the filament density is at least 10 filaments per square inch. The rough, filament-studded surface of this model is shown within its wooden test bin in Figure A-12.

Soil Model IV-4 Lichen Covered Basalt

Among the terrestrial xerophytic plants, the symbiotic association of a fungus and an alga that constitutes a lichen displays the greatest environmental tolerance. The lichens are early colonizers of devastated areas, e.g., lava flows, and are predominant forms in low elevation, low latitude deserts as well as high latitude tundra and high elevation alpine floras. For these reasons a lichen-like form may be the organic adaptation naturally selected by Martian organisms. It was also desirable to utilize an encrusting organism that was indigenous to an extremely rough surface like basalt cinder masses. Basalt boulders liberally strewn with

lichens were collected from the extremely dry southern slope of the interior crater wall of the Pisgah Crater cinder cone. Figure A-13 shows a group of crustose yellow lichens on a highly irregular and microvesicular basalt cinder mass. The lichen colony measures 2 inches by 3/4 inch and the face of the rock is 3 inches wide. Dozens of pieces of basalt bearing similar colonies of lichens were hand emplaced in the DWB sampling bin for testing in a manner that would provide an irregular surface estimated to be approximately 15 percent lichen covered.

Soil Model IV-5 Organic Incrustations

The organic incrustation model was selected to simulate the presence of fossils or viable encrusting organisms whose skeletal remains or tests were contained within or welded to a rock surface with an adhesion similar to that of the rock itself. For these reasons, microporous cement surfaces containing large numbers of small tidewater barnacles affixed thereto were chosen to represent this test example. These barnacles are uniquely qualified for this purpose. When the free-swimming larval stage finally commences to attach itself to a host, it secretes CaCO_3 into the pores of the host and, if the host is a fine grained cohesive rock such as a piece of unfinished cement, the shell becomes anchored to the rock with a tenacity equal to the cohesiveness of the calcareous shell of the animal and, in this case, the cohesion of the host rock. Figure A-14 illustrates a flat piece of unfinished concrete, approximately 10 inches wide supporting several hundred individual barnacles. The barnacles are round to oval, measure 0.3 to 0.4 cm in diameter, contain a small central port providing access to the hollow interior, and possess deeply sculptured ridges radiating from the aperture. The relief of the barnacle-studded surface varied from 0.1 to 0.15 cm. Although collected alive from the tidal zone along the Newport Beach jetty, the tests were conducted after the material had been sun-dried for approximately two months. The flat blocks of concrete were hand emplaced in the DWB test bin to provide a relatively flat test surface that was approximately 10 percent barnacle-covered.



FIGURE A-13
YELLOW CRUSTOSE LICHEN COLONY ON A BASALT
CINDER BOULDER

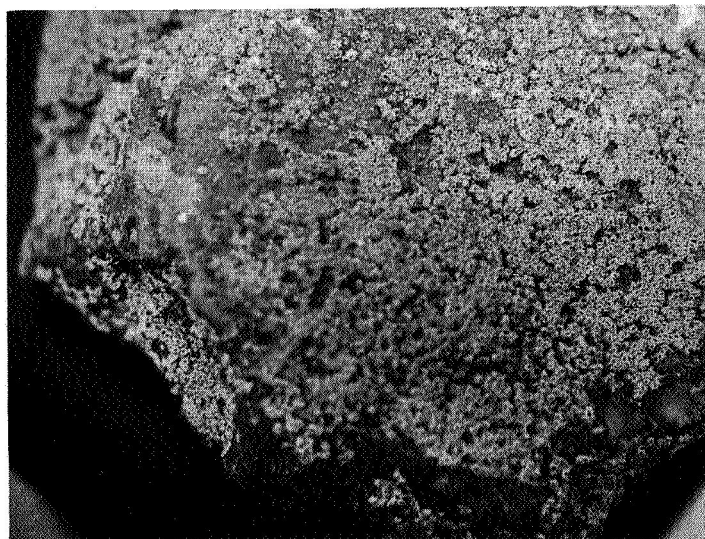


FIGURE A-14
BARNACLE-STUDED UNFINISHED CONCRETE
TEST SURFACE

APPENDIX B

DESCRIPTION OF FIELD TEST SITES

APPENDIX B

CONTENTS

DESCRIPTIONS OF FIELD TEST SITES

Kelso Dunes Area

Terrain Model A Dune Sand

Pisgah Crater Area

Terrain Model B Dry Lake Duricrust

Terrain Model C Pahoehoe Basalt

Terrain Model D Aa Basalt

Terrain Model E Compacted Cinders

Terrain Model F Desert Pavement

LIST OF TABLES

TABLE		PAGE
B-1	Location of Field Test Sites.	B-6
B-2	Temperatures at Sample Site A	B-8
B-3	Explanation for Geologic Map of Pisgah Crater Area.	B-10
B-4	Explanation for Geologic Map of Pisgah Playa Lake Area. . .	B-14

LIST OF FIGURES

FIGURE		PAGE
B-1	Soil Model A - Kelso Dune Sand	B-7
B-2	Geologic Map of Pisgah Crater Area	B-9
B-3	Soil Model B - Dry Lake Duricrust	B-12
B-4	Geologic Map of Pisgah Playa Lake Area	B-13
B-5	Soil Model C - Pahoehoe Basalt	B-17
B-6	Soil Model D - Aa Basalt	B-18
B-7	Soil Model E - Compacted Cinders	B-20
B-8	Soil Model F - Desert Pavement	B-21

APPENDIX B
DESCRIPTIONS OF FIELD TEST SITES

The field sites were originally recommended to test the range of materials capable of being sampled, the operating modes and the mechanical and biological effectiveness of JPL and Philco-Ford model soil samplers. The sites were selected to represent natural environments having the following qualifications:

- (1) Similarity to suspected Martian environments.
- (2) Minimal biological populations and activity.
- (3) Availability of a multiple array of subenvironments.
- (4) Presence of adverse conditions, such as soil dryness and low atmospheric humidity, duricrusts and blowing sand and dust.
- (5) Proximity to JPL and Philco-Ford laboratories to reduce transport requirements for accessory equipments.

Pisgah Crater and Kelso Dunes, San Bernardino County, California, offered these qualifications within the following subenvironments:

- (1) Dunes.
- (2) Duricrusts.
- (3) Compacted cinders (cf welded tuffs).

(4) Natural desert pavements.

(5) Pahoehoe and aa-type basalt flows.

The locations of Pisgah Crater and the Kelso Dunes are denoted on the plot of a portion of Southern California, Figure 2-1 in Section 2. The specific locations of the subenvironments tested are described on Table B-1. The ensuing paragraphs will describe the general field test areas and the specific test sites in order to relate these natural desert environments and the sampled subenvironments to planetary environments that will some day be biologically and geologically sampled.

The Pisgah Crater and Kelso Dunes areas lie in the Mojave Desert of Southern California. The Mojave Desert is the westernmost part of the Basin and Range Province of the Southwestern United States and Northeastern Mexico. This province has been block-faulted into an intricate series of long narrow ranges separated by aggraded desert plains. Most of these intermontane desert plains are centripetally drained with playa lakes occupying the closed basin lows. The test areas lie near the northern border of the Sonoran Desert Section of the Basin and Range Province. In this section most of the ranges are shorter and less elevated than in the Great Basin Section to the north and east. Most of the ranges are composed of complexly faulted blocks of Tertiary to recent lava flows of andesitic and basaltic composition. Some ranges consist of Tertiary continental clastic sediments, Mesozoic granite, Paleozoic silicified limestones and some pre-Cambrian metamorphic rocks. The Pleistocene to recent covering of these aggraded desert basins are derived, therefore, from a complex series of sources. However, since most of the more recent sediments veneering the localized basins are derived from adjacent ranges, their content reflects local source materials.

Kelso Dunes Area

The Kelso Dunes are a permanent whaleback dune complex covering more than 60 square miles. Prevailing winds are directed from either due west or northeast with more constant winds from the west but stronger winds from the northeast. A constant source of sediments is provided by flood stages on the Mojave River which disappears underground near the Kelso Dunes (see Figure 2-1).

Terrain Model A Dune Sand

The specific location chosen to represent Soil Model A, typical dune sand, consisted of an isolated plot, containing 800 square feet, which lay on the broad crest of a recently formed traveling dune spilling into a dry wash. The isolated plot is shown in the general view of Figure B-1. The surface of the plot was clear of vegetation but patches of dune grass and

TABLE B-1
LOCATION OF FIELD TEST SITES

<u>Area</u>	<u>Type</u>	<u>Name</u>	<u>Section</u>	<u>Two-RGE</u>	<u>County</u>
Kelso Dunes	A	Dune sand	NE $\frac{1}{4}$ Sec. 3	T.9N., R.12E.	San Bernardino, Calif.
Pisgah Dry Lake	B	Playa duricrust	NW $\frac{1}{4}$ Sec. 27	T.8N., R.5E.	San Bernardino, Calif.
Pisgah Crater	C	Pahoehoe basalt	NW $\frac{1}{4}$ Sec. 32	T.8N., R.6E.	San Bernardino, Calif.
Pisgah Crater	D	Aa basalt	NW $\frac{1}{4}$ Sec. 32	T.8N., R.6E.	San Bernardino, Calif.
Pisgah Crater	E	Compacted cinders	NW $\frac{1}{4}$ Sec. 32	T.8N., R.6E.	San Bernardino, Calif.
Pisgah Crater	F	Desert pavement	NW $\frac{1}{4}$ Sec. 32	T.8N., R.6E.	San Bernardino, Calif.



GENERAL VIEW



CLOSE UP VIEW

FIGURE B-1. SOIL MODEL A - KELSO DUNE SAND

isolated bushes of catclaw and greasewood grew adjacent to the plot. The surface sloped evenly east at 10° and was wholly covered by eolian ripple marks upon which were superimposed a few recent tracks of small mammals (fox and pack rat) and reptiles (lizards) and many distinctive tracks of insects (stink bugs). Structurally the dune exhibited well developed eolian topset cross bedding with laminae varying in thickness from 1.5 to 6.5 mm; the laminae were accentuated by abundant grains of black magnetite and ilmenite. The surface of the dune was dry but, despite the fact that it had not rained since early August, dampness was encountered at depths varying from 12.5 to 20 cm across the dune. The line of demarcation between dry and damp sand was very sharp at these depths.

During the sampling operation at Kelso Dunes, the weather was clear, the humidity low, and the wind was variable, dominantly westerly and southerly, at less than 8 mph. Air and subsurface temperatures were monitored during testing as follows in Table B-2.

TABLE B-2

TEMPERATURES AT SAMPLE SITE A

Location	Temperature, $^{\circ}\text{C}$ and Time			
	Min.	Time	Max.	Time
Air, 12 inches above ground				
Direct sun	18.2	0800	26.9	1430
Shade	18.2	0830	26.0	1400
Subsurface, 1/8 inch deep	25.9	0845	33.0	1445
Subsurface, 2 inches deep	15.0	0915	22.0	1415

A control sample was taken as a representative sample of the entire isolated plot by combining samples from each of the four corners of the plot. A grain size and petrographic analysis of this standard sample for Soil Model A, Kelso dune sand, appears in Appendix D.

Pisgah Crater Area

The Pisgah Crater area contains the remaining five test sites: duricrust, compacted cinders, desert pavement and pahoehoe and aa basalt surfaces. Pisgah Crater itself is a cinder cone. The cone is completely surrounded by lava flows covering approximately 40 square miles. The flows and cinder cone are post-Pleistocene in age; the former having covered a pre-flow playa lake and tend to conform to the Pleistocene drainage patterns. The lava flows emanated from fissures flanking the cinder cone. The order of events during the formation of the flow complex was (see Figure B-2 and Table B-3):

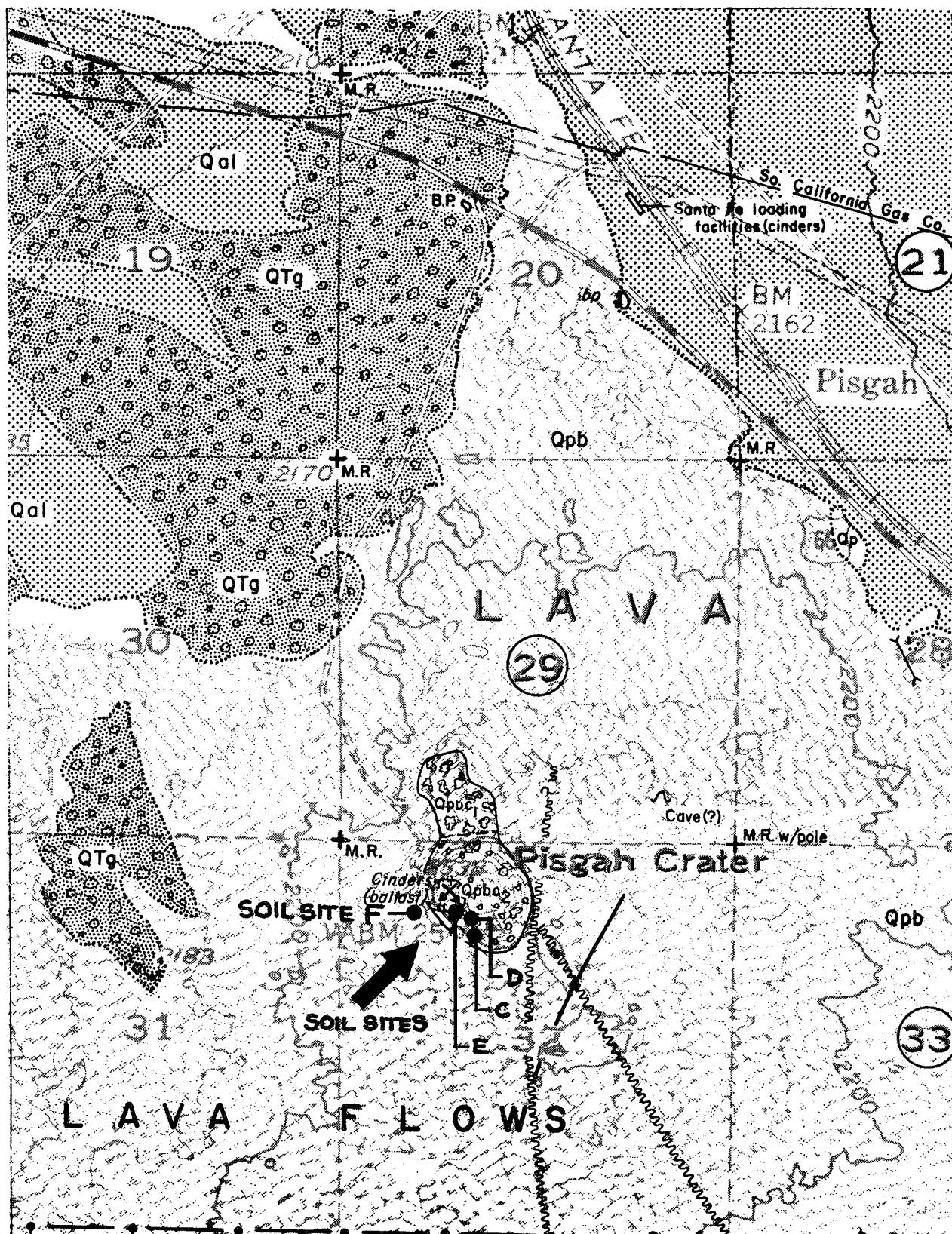


FIGURE B-2. GEOLOGIC MAP OF PISGAH CRATER AREA

<div>Quaternary</div> <div>Recent</div> <div>Pleistocene</div>		<u>EXPLANATION</u>	
		<div>Qa1 / Qp</div>	Surficial deposits composed of gravelly and sandy alluvium (Qa1); locally clay and sandy playa deposits (Qp).
		<div>Qpb / Qpbc</div>	Basalt flows (Qpb) and basaltic cinders (Qpbc).
		<div>Qpbc₂</div>	Basaltic cinders, coarse to fine.
		<div>Qpbc₁</div>	Basaltic cinders and rubble, very coarse to blocky.
		<div>Qpb</div>	Olivine basalt flows, aa and pahoehoe types.
		<div>QTg</div>	Older gravel and sand with abundant pre-Pisgah basalt volcanic cobbles; locally includes weakly cemented silt and silty clay.
		<u>SYMBOLS</u>	

M. R.	Section corner, mound of rocks	Contact between deposits
		~~~~~	Major fault
B. P. or bp	Borrow pit (gravel)	—	Minor fault
		∩	Lava cave
		>—<	Lava tube

TABLE B-3. EXPLANATION FOR GEOLOGIC MAP OF PISGAH CRATER AREA

- (1) Formation of viscous pahoehoe basalt flows covering the maximum area.
- (2) Formation of veneer of very viscous aa basalt from most active fissures.
- (3) Development of the cinder cone.

The pahoehoe (smooth, ropy lava) and aa (blocky, very rough lava) test sites were formed directly from the cooling of surface flows. The desert pavement site was laid down as a mass of water-laid basalt and cinder pebble, sand, silt and clay in a small basin surrounded by lava flows. Wind later exhumed the pebbles and created the pavement mosaic by blowing away the sand-silt-clay matrix material. The compacted cinders were deposited at the toe of the crater by gravity and impact. Later wind-blown fine materials, sand to clay, were sifted onto the upper surface and, through the action of rain water, caused to permeate the porous cinder mass. The duricrust test site is a part of the surface of a playa lake formed by a recent fault. The fine playa sediments, dominantly fine sand, silt and clay were both wind and water deposited.

#### Terrain Model B Dry Lake Duricrust

The duricrust or evaporated playa lake isolated plot, containing 1,925 square feet of surface area, covered an unblemished segment of a recent playa formed by water and sediment entrapment against lava beds on the downthrown side of a recent fault. The dry lake is 4,500 feet long and 700 feet wide. The thickness of playa sediments varies from 4 feet at the northeast corner to 2.7 feet at the southwest corner; at each corner basalt cobbles were encountered at these depths. No visible dampness existed to these depths. The isolated plot and a detailed photograph of the playa surface is shown on Figure B-3. A geologic map of the sediments and igneous rocks surrounding the Pisgah Playa Lake is denoted on Figure B-4 and Table B-4. The surface of the plot was clear of vegetation and absolutely level. The surface is wholly covered with desiccation cracks, 1/16 to 1/8 inch wide and up to 3/4 inch deep. The cracks produce irregular polygons averaging 4 to 9 inches in diameter and 1/8 inch thick. While the polygons are produced by major cracks, they often contain minor cracks within their boundaries. Earlier generations of polygons are occasionally present denoted by slightly raised ridges where the former desiccation cracks existed. Many of the cracks were sand-silt filled and many polygons overlay thin lenses of sandy silt. The polygons themselves were formed from an evaporated clay-silt crust, averaging 1/16 inch in thickness, which was weakly cemented by calcite. Cementation, however, was strong enough to permit small polygons to maintain their structural integrity when removed by a trowel. This cementation also causes small duricrust flakes to exist in almost all mechanically obtained samples. Structurally, the



GENERAL VIEW



CLOSE UP VIEW

FIGURE B-3 . SOIL MODEL B-DRY LAKE DURICRUST



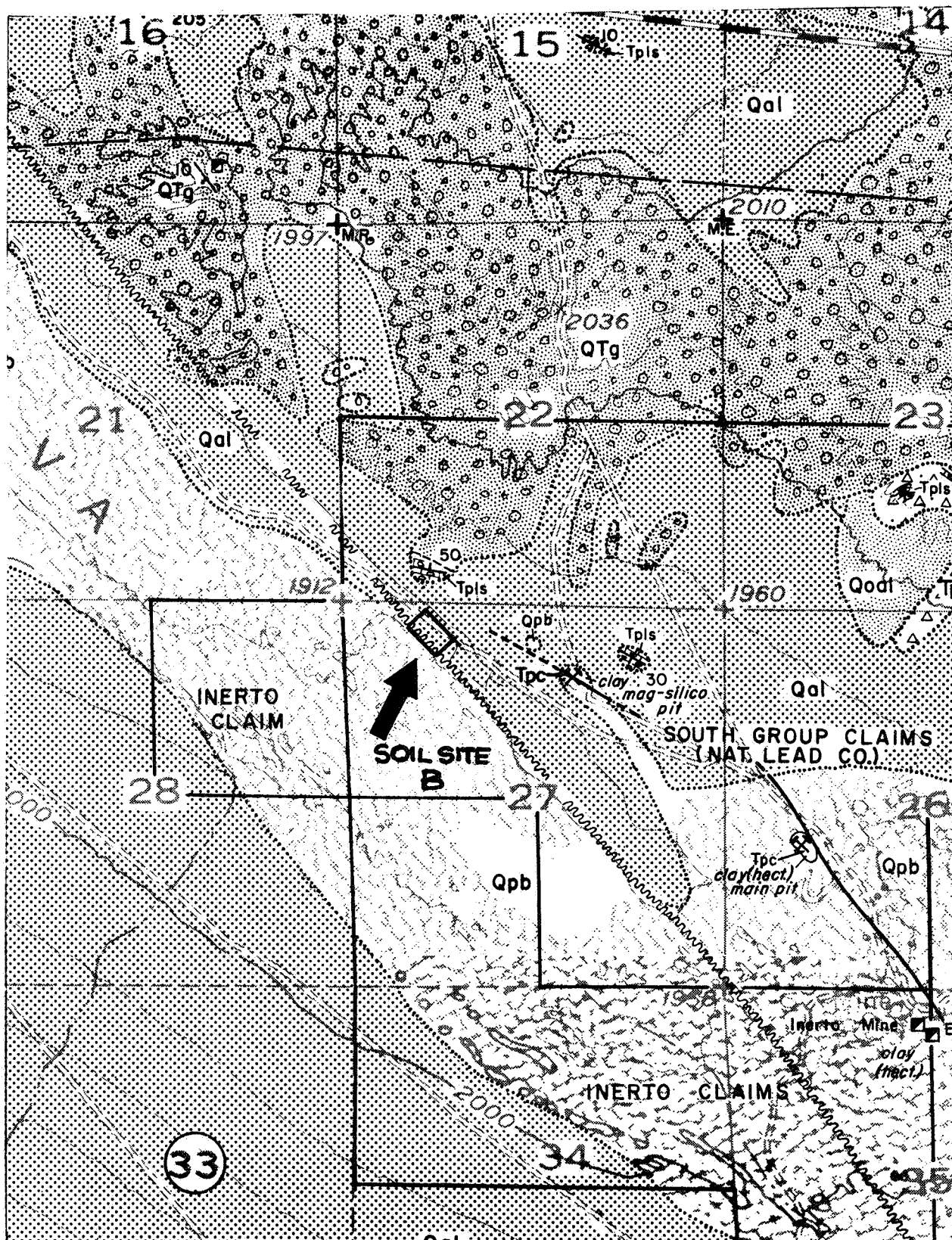




FIGURE B-4. GEOLOGIC MAP OF PISGAH PLAYA LAKE AREA



# EXPLANATION

Quaternary	Recent	Qa1 / Qp	Surficial deposits of gravelly and sandy alluvium (Qa1); locally clay and sandy playa deposits (Qp).
		Qpb	Olivine basalt flows, pahoehoe type.
	Pleistocene	Qoa1	Older surficial deposits derived from older deposits of mixed composition; sands and gravels, locally dissected.
			UNCONFORMITY
		QTg	Gravel and sand with abundant volcanic cobbles; locally includes weakly cemented silt and silty clay.
			UNCONFORMITY
Tertiary	Miocene	Tpu / Tpls / Tpc	Sedimentary tuff, limestone and clay.
		Tpu	Volcanic tuff and bedded tuffaceous sediments.
		Tpls	Silicified limestone.
		Tpc	Bentonitic clay (hectorite) locally associated with limestone.

# SYMBOLS


- M. E. Section corner, mound of earth ..... Contact between deposits
- M. R. Section corner, mound of rocks  Major fault
- Minor fault

TABLE B-4. EXPLANATION FOR GEOLOGIC MAP OF PISGAH PLAYA LAKE AREA

deposit below the thin surface crust is remarkable uniform. The sand and silt content and the mineral content is remarkably constant with depth. Only the calcite cementing material decreases with depth; in fact, it appears to be concentrated in the crust, for a sample at a depth of 2 inches showed no appreciable calcite content by X-ray diffraction scan.

A control sample was obtained by combining samples from two diametrically opposed corners of the plot. Two grain size analyses of the standard control sample for Soil Model B, Pisgah Playa Lake duricrust, appear in Appendix D. One is a gross standard sample, characterized by a high percentage of "duricrust flakes," wherein the clay and silt are bound by calcite and moisture into flakes which, when sieved, appear as coarse to medium grained sand. Many of the samplers collected material of this nature. The other analysis in Appendix D, treats the grain size and composition of the control sample after sonication to disperse the cemented clay-silt duricrust flake aggregate. This latter analysis presents an absolute picture of the components of the duricrust soil model.

#### Terrain Model C Pahoehoe Basalt

A pahoehoe basalt flow terrain was chosen as a soil model for three reasons:

- (1) A relatively smooth-surfaced vesicular type of basalt may be a common planetary and lunar surface material.
- (2) A vesicular basalt may be biologically important because of a myriad number of shielded microenvironments offered to viable organisms and because the individual vesicles may serve as wind-gathered organic particle sinks.
- (3) The challenge offered by this type of material may tax the sample gathering effectiveness of the samplers being field tested.

Soil Model C represents pahoehoe basalt - a vesicular type of lava whose lower viscosity permitted hardening into low, broad, smooth-surfaced (on a large scale) arches (many covering lava tubes having diameters of 10's of feet) and corrugated ropy forms. This model consisted of a gently sloping (maximum 4°) dome of pahoehoe basalt covering 1,500 square feet and cracked into polygons (incipient columnar structure) averaging 1½ - 2½ feet in diameter. The surface also contains several major joints or closed cracks bounding blocks and exhibiting relief up to 2 inches. The basalt surface is wholly vesicular with bubble-pits varying in size from < 1/2 to < 1/16 inch in diameter. Some small slabs of loose exfoliated

basalt lie on the surface. There was visible evidence of sand and silt size debris in cracks, joints and many of the larger vesicles. The isolated plot and a view of the surface texture is shown on Figure B-5.

During the sampling operation conducted on the pahoehoe basalt model, the day was cloudy but bright with a slight breeze from the northwest. Surface temperatures varied from 28.7°C to 31.2°C. Air temperatures, measured 12 inches above the basalt surface, were between 25.8°C and 26.5°C.

#### Terrain Model D Aa Basalt

The aa-type basalt flow terrain was utilized as a soil model for the reasons listed under pahoehoe basalt and in addition because the surface area per square foot of soil surface is greatly magnified affording a large number of shielded microenvironments for viable organisms and organic particles.

Soil Model D consists of aa basalt - a supremely rough, angular, blocky type of lava extruded onto the surface in such a remarkably viscous state that the flow maintains a steep front wall as it advances across a surface like a bulldozer, spalling off large blocks of hardened lava. This front wall and the general surface of the flow freezes into jagged blocks that are negotiated with great difficulty on foot. The rough aa basalt model, contained 700 square feet with approximately 600 square feet covered by aa basalt. The isolated plot lay on the front of a frozen advancing flow covering pre-existing pahoehoe basalt flows. The general surface slope was 18°, locally steeper, with several small basins wherein finer materials (sand and silt) have collected. The isolated plot and a detailed view of the block-studded flow surface are pictured in Figure B-6. The individual aa blocks are fantastically contorted, angular and vesicular and range from coarse gravel (> 1 inch) to 2 feet in diameter, hence surface relief is of this magnitude. The entire mass is interlocked to form a very rough and rigid surface. Since the deposit is remarkably porous, a great deal of fine wind blown material is present in the interblock areas.

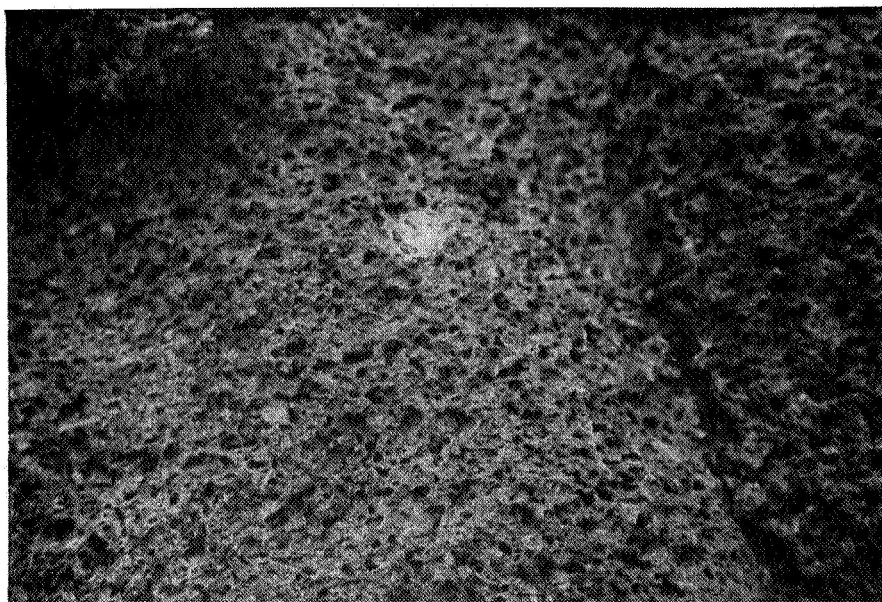
During the sampling operation, which was conducted in the morning, the day was clear and bright with slight westerly breezes. A minimum surface temperature of 13.0°C was obtained in the shade; surface sunlit temperatures ranged from 21.0 to 22.0°C. Air temperatures, 5 feet above ground level varied between 21.4°C and 24.8°C.

#### Terrain Model E Compacted Cinders

A welded tuff model was originally proposed but the welded tuffs in the Pisgah Crater area are restricted to the older Tertiary volcanics and are, therefore, much too indurated and altered to afford a representative model. A compacted cinder model with a very broad grain size range was chosen as a sampler-challenging substitute.



GENERAL VIEW

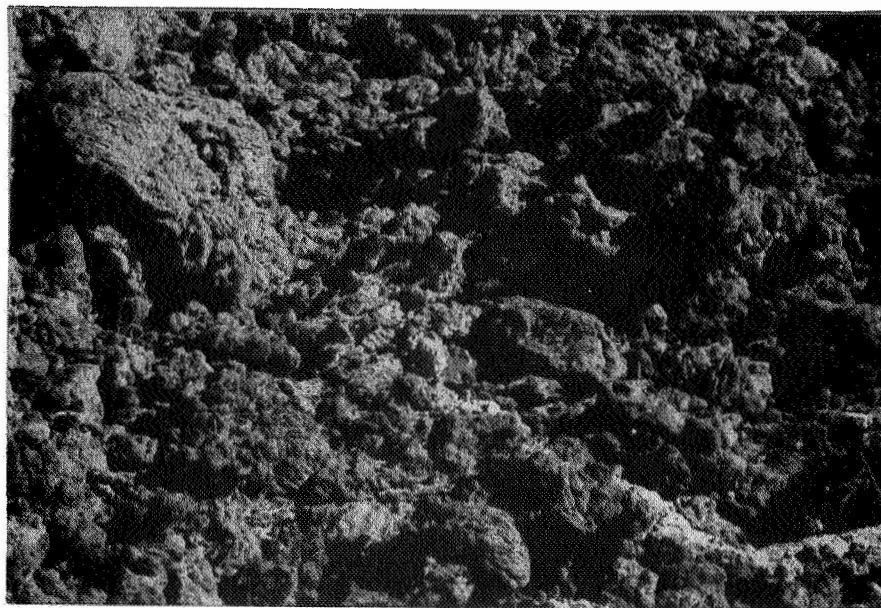


CLOSE UP VIEW .

FIGURE B-5. SOIL MODEL C - PAHOEHOE BASALT



GENERAL VIEW



CLOSE UP VIEW

FIGURE B-6 . SOIL MODEL D - aa BASALT

The location chosen to represent Soil Model E, compacted volcanic cinders, was contained in an isolated plot of 805 square feet lying at the base of the Pisgah cinder cone. The isolated plot is pictured in Figure B-7. The compacted cinder deposit is composed of a key-seated matrix of very angular oxidized (red) and relatively unoxidized (black to iridescent) basalt cinders and volcanic bombs. The cinders and bombs vary in size from cobbles up to 8 inches in diameter to coarse sand ( $< 2$  mm). Both the cinders and bombs are composed of low density, highly out-gassed, microcellular basalt pumice. The deposit is fairly homogeneous with depth and was laid down as the toe of a crudely bedded cinder talus slope at the base of the cinder cone. During its formation it was liberally sprinkled with impacting volcanic bombs. The entire deposit has been injected with windblown and water-percolated sand, silt and clay. A small ravine cuts the west edge of the isolated plot. Here the deposit is exposed to a depth of 4 feet. This bank shows that a crude stratification exists. In beds 2 to 8 inches thick, very coarse grained bombs and cinders ( $1\frac{1}{2}$  - 3 inches) graded downwards into less coarse cinders ( $< 1/2$  inch). Two holes were dug to depths of  $3\frac{1}{2}$  feet at the northwest and southwest corners of the plot; to these depths no dampness was recorded.

During sampling operations, the weather was calm and cloud cover ranged from complete absence to almost complete cover. Both surface and air temperatures ranged from  $24.0^{\circ}\text{C}$  to  $27.0^{\circ}\text{C}$  under these conditions.

#### Terrain Model F Desert Pavement

The desert pavement isolated plot chosen to represent Soil Model F consisted of 1500 square feet located in a small basin-like re-entry surrounded by pahoehoe basalt flows. The isolated plot is pictured in Figure B-8. The undisturbed pavement surface was composed of a mosaic of very angular olivine basalt pebbles and isolated cobbles. This mosaic covers and protects a substrate composed of sand, silt and clay size particles also containing abundant basalt pebbles and a few cobbles. The absolute grain size of the mosaic ranges from 5 inches to coarse sand particle sizes ( $< 2$  mm). The range in particle sizes of the specific model where testing was accomplished was 1.5 inches to coarse sand. The thickness of the deposit was 18 inches where a concentration of basalt cobbles was encountered. Structurally, the deposit tended to be zoned into the following layers from top to bottom:

- (1) Surface pavement mosaic averaging  $< 1$  inch in thickness.
- (2) Very weakly cemented crust composed of sand-silt-clay mixture with rare basalt pebbles and averaging  $3/4$  inch in thickness.



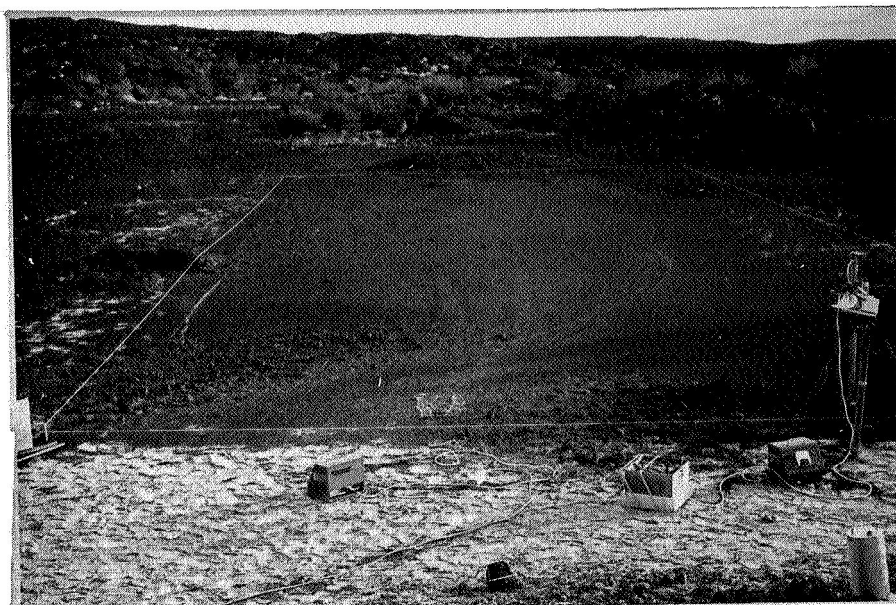
GENERAL VIEW



CLOSE UP VIEW

FIGURE B-7. SOIL MODEL E - COMPACTED CINDERS





GENERAL VIEW



CLOSE UP VIEW

FIGURE B-8. SOIL MODEL F - DESERT PAVEMENT



(3) Approximately 16 inches of intermixed basalt pebbles, sand, silt and clay with the number of pebbles increasing with depth.

(4) Basal layer of basalt cobbles below 18 inches.

The mosaic or pavement surface affords a very adequate protective surface from wind erosion but it has no surface integrity when disturbed.

During the sampling operation, surface and air temperatures were monitored. The minimum surface temperature was measured at 0815 at 23.8°C; a maximum temperature of 37.5°C was measured at 11:45. The air temperature, one foot above the ground with a breeze blowing (< 8 mph) varied from 26.0°C to 29.4°C during the operation.

APPENDIX C

VIABILITY AND BIOCHEMICAL ASSAY PROCEDURES

## APPENDIX C

The procedures, materials, and equipment employed in the biological effectiveness evaluation of the field test samples are described on the following pages.

The general system for viability analysis utilized up to 10.0 grams of mixed soil sample weighed directly from the storage bottle into a sterile aluminum foil dish. Samples were weighed out to the nearest 0.1 gram. The sample was placed into a sterile 90 ml distilled water blank to provide (approximately) a 10 to 1 dilution of the soil. Water was added to dilution bottles for samples weighing less than 2.0 grams to provide the initial 10 to 1 dilution. Tenfold serial dilutions were made using 10 ml volumes pipetted to successive 90 ml distilled water blanks to obtain 3 suitable consecutive dilutions for plating. Three plates each of egg albumen agar (EAA), soil extract agar (SEA), and yeast extract agar (YEA) were inoculated at each dilution. One-tenth milliliter of suspension was spread on each plate with a sterile bent-glass spreader (hockey-stick). Inverted plates were incubated at room temperature for from 13 to 24 days before the colonies on them were counted. Storage in closed corrugated paper cartons maintained the agar in a suitably moist condition during this incubation.

Plates were counted using a Quebec colony counter. To aid counting, many plates were flooded with 0.2% triphenyl tetrazolium chloride thereby giving the red formazan color to punctiform colorless colonies. Scratching colonies with an inoculating needle helped differentiation of bacteria and actinomycetes. Actinomycete colonies often resembled mold colonies on YEA and often required microscopic verification.

### C.1 ASSAY PROCEDURE FOR VIABLE PARTICLE CONTENT OF SOIL

1. Place 10 grams of the soil specimen into 90 ml of sterile water contained in an 8-ounce bottle.

2. Shake the bottle 25 times to disperse contents.

3. Using a sterile 10-ml pipette, transfer, immediately, a 10-ml aliquot of the suspension into 90 ml of sterile water in an 8-ounce bottle. This second suspension corresponds to a  $10^{-2}$  concentration, or a 100-fold dilution, of the specimen.

4. Continue to dilute 10-ml aliquots serially into 90-ml portions of sterile water in 8-ounce bottles until 3 appropriate consecutive tenfold dilutions are obtained.

5. Place a 0.1-ml aliquot of each dilution on 3 plates each of SEA, EAA, and YEA.

6. Distribute the inoculum over the surface of the agar with a sterile glass hockey stick.

7. Incubate the cultures inverted at room temperature for at least 10 days.

Materials used:

1. SEA (soil extract agar). Prepare a soil extract by adding 1 kg of soil to 1.5 liters of water. Autoclave for 30 minutes at 121°C. Cool and filter the material through a Buchner funnel. Add 20 g of Difco Bacto-agar (Difco certified), 0.5 g of dibasic potassium phosphate, 0.1 g of dextrose, to 1 liter of the soil extract. Mix and autoclave at 121°C for 20 minutes. A soil specimen from the Philco-Ford Newport Beach site was used to prepare soil extract agar (SEA) for the preliminary laboratory analysis. The SEA for evaluation of field test specimens used an extract of JPL No. 76-2, a Mojave desert sand-gravel mix containing some caliche.
2. EAA (egg albumen agar). Prepare egg-albumen solution by dissolving 0.25 mg of egg albumen (Difco certified) in 10 ml of 0.1 Normal sodium hydroxide. To the egg-albumen solution, placed in a 1500-ml flask, add 15 g Difco Bacto-agar (Difco certified), 1.0 g dextrose, 0.5 g dibasic potassium phosphate, and 0.2 g of magnesium sulfate heptahydrate. Adjust pH to 6.8 using hydrochloric acid and autoclave at 121°C for 20 minutes.
3. YEA (yeast extract agar). To 15 g of Difco Bacto-agar (Difco certified) in a 1500-ml flask, add 1.0 g Yeast Extract (Difco certified), 1.0 g dextrose, 0.5 g potassium nitrate, 1.0 g dibasic potassium phosphate, 0.1 g calcium chloride, 0.1 g sodium chloride, and 0.01 g ferric chloride. Mix and autoclave at 121°C for 20 minutes.
4. Sterile disposable plastic petri dishes.

## C.2 ASSAY PROCEDURE FOR CARBON CONTENT OF SOIL

1. Weigh out a 10-g sample of the soil to be assayed for carbon content.

2. Using not more than 15 ml of carbon-dioxide-free water wash the sample into the bottom of the Allison reaction vessel.

3. Attach the reaction vessel to the analysis system. To verify that the system is leak free, evacuate the system through the CO₂-collection bulb. Weigh the bulb at 10-minute intervals. The weight will not change if the system is leak free. Record tare weight.

4. Draw 15 ml of carbonates digestion acid into the reaction vessel.

5. Close valve to vacuum and then pass CO₂-free air into the system through the drying column. When the bubblers start to bubble, carefully open the valve to the vacuum.

6. Close valve to vacuum and then pass air into the system through the Mikhobite column (removes carbon dioxide). When the bubbler starts to bubble, slowly open the valve to the vacuum so that bubbles form at the rate of 6 to 8 per second.

6. While continuously passing CO₂-free air through the system apply a flame 5 to 6 cm high to the reaction vessel. Boil 3 to 5 minutes. If white fumes (SO₃) rise above the second bulb of the condenser, reduce heating. Heat slowly at first to prevent silver sulfate bubbler from clogging when the soil has a high chloride content.

7. Remove flame and continue to pass CO₂-free air through the system for at least 10 minutes. Maintain the bubbling rate at 6 to 8 per second.

8. Remove and weigh the CO₂ collection (absorption) bulb. The increase in weight is caused by carbonates in the sample.

9. Replace the CO₂-collection bulb.

10. Add 1 g of K₂Cr₂O₇ to the material in the reaction vessel and then promptly reattach the reaction vessel to the analysis system.

11. Draw 15 ml of organic-carbon digestion acid into the reaction vessel.

12. Repeat steps 5, 6, and 7.

13. Remove and weigh the CO₂-collection bulb. The increase in weight is caused by organic carbon in the sample.

Materials used:

1. Mikhobite, a carbon dioxide absorbent (The Frederick G. Smith Co., Columbus, Ohio).
2. Potassium Iodide solution, dissolve 100 g of KI in 100 ml of water.
3. Saturated silver sulfate solution.
4. Anhydrone (anhydrous magnesium perchlorate).
5. Granular zinc, 30-mesh.
6. Sulfuric acid, concentrated.
7. Potassium dichromate ( $K_2Cr_2O_7$ ).
8. Carbonates digestion acid. Dissolve 57 ml of concentrated sulfuric acid and 92 g of ferrous sulfate heptahydrate in 600 ml of water. Cool and then dilute to 1000 ml. This solution is approximately 2 Normal sulfuric acid and contains 5% of ferrous sulfate as an antioxidant. Keep well stoppered.
9. Organic carbon digestion acid. Dissolve 400 ml of 85% phosphoric acid ( $H_3PO_4$ ) in 600 ml of concentrated sulfuric acid. Keep well stoppered.

Equipment used:

1. A modification of the Allison wet-combustion analysis system in which the opportunities for leaks and loss of sample are reduced. This system is described by Allison (1960, 1965).

### C.3 ASSAY PROCEDURE FOR ALPHA-AMINO NITROGEN CONTENT OF SOILS

Weigh out 5 g of the soil to be assayed for alpha-amino nitrogen. Place this soil in a 125-ml flask compatible with the Liebig condenser.

Add 20 ml of 6 Normal hydrochloric acid and then 2 drops of octyl alcohol and mix by swirling.

Add boiling stones and then connect flask to a Liebig condenser. Heat flask with a mantle until contents boil gently.

Reflux overnight to obtain hydrolysate.

Cool contents of flask (hydrolysate) and pass hydrolysate through Whatman GF/A filter paper, using a small Buchner funnel and filter flask.

Wash hydrolysis residue with small portions of distilled water. Keep filtrate volume less than 60 ml.

Transfer hydrolysate to a 200-ml beaker.

Neutralize hydrolysate to pH 6.0 by addition of 5 Normal sodium hydroxide, then adjust pH to 6.5 to 6.9 by addition of 0.5 Normal sodium hydroxide. Avoid producing an alkaline hydrolysate.

Transfer hydrolysate to a 100-ml volumetric flask and dilute to volume with washings from beaker and pH meter electrodes.

Transfer 5 ml of the hydrolysate of the hydrolysate to a steam distillation flask.

Add 1 ml of 0.5 normal sodium hydroxide to the flask.

Pass steam through the steam distillation apparatus.

Adjust distillation rate to 7 to 8 ml per minute.

Adjust water flow through condenser so that the distillate temperature is at or below 22°C.

Heat flask in a boiling water bath for 20 minutes to reduce volume to 2 ml.

Cool flask and add, first, 500 mg of citric acid and then 100 mg of ninhydrin.

Immerse flask in a boiling water bath and swirl continuously for 1 minute, then without swirling allow the flask to remain in the boiling water bath for an additional 9 minutes.

Cool flask to room temperature then add 10 ml of phosphate-borate buffer and 1 ml of 5 normal sodium hydroxide.

Connect flask to steam distillation apparatus and distill ammonia liberated from the hydrolysate (by the ninhydrin) into a collection flask containing 20 ml of boric acid indicator solution. Continue distillation until 35 ml of distillate have been collected.

Titrate the distillate with 0.10 normal sulfuric acid to a grey-pink endpoint. One ml of this acid is equivalent to 1.4 milligrams of alpha-amino nitrogen in the hydrolysate aliquot or 5.6 milligrams per gram of soil assayed.



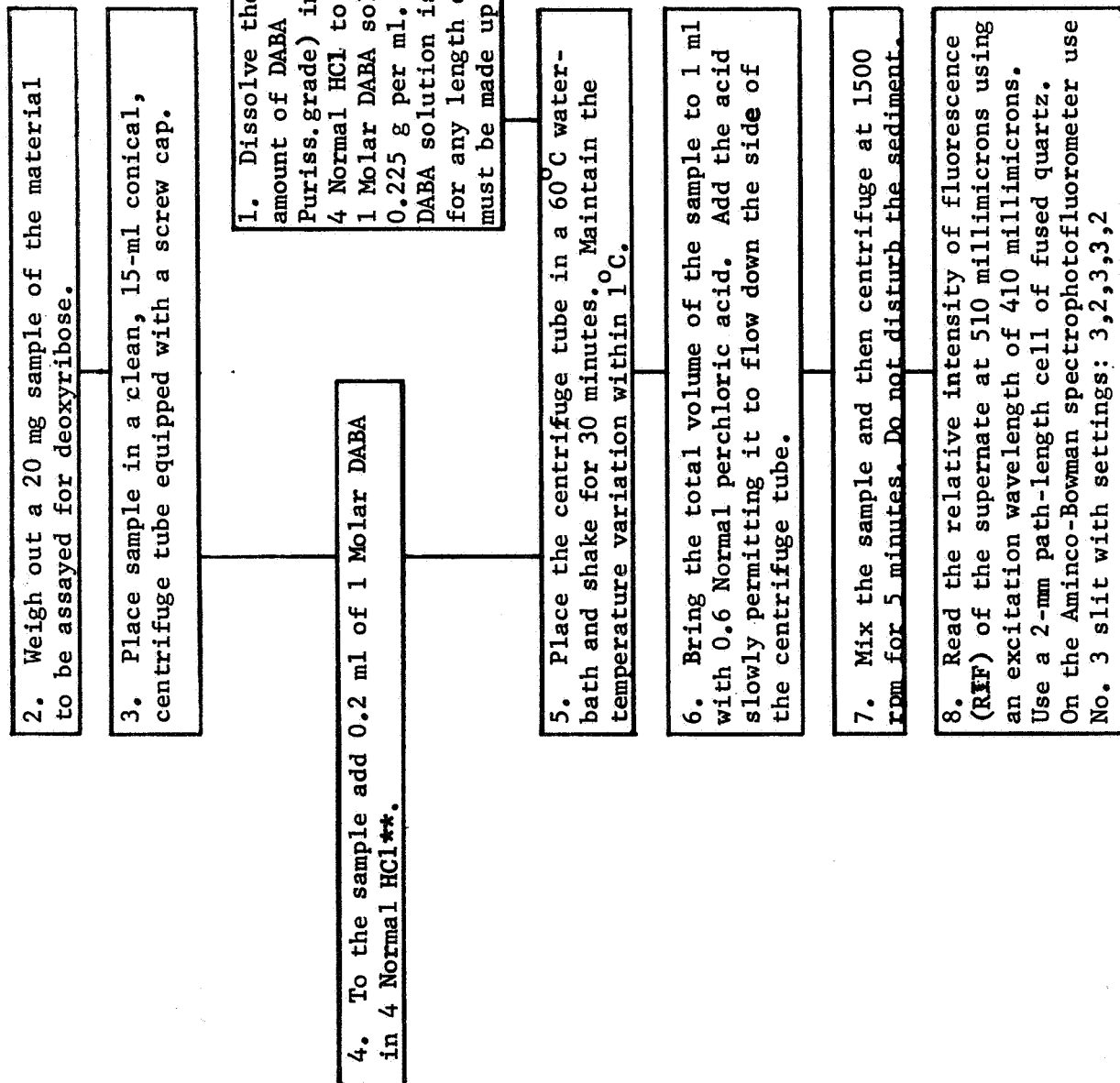
Materials used:

1. Phosphate-borate buffer, pH 11.2. Dissolve 100 g of  $\text{Na}_3\text{PO}_4 \cdot 12\text{H}_2\text{O}$  and 25 g of  $\text{Na}_2\text{B}_4\text{O}_7 \cdot 10\text{H}_2\text{O}$  in 900 ml of water. Dilute to 1 liter.
2. Boric acid indicator solution. Dissolve 20 g of pure  $\text{H}_3\text{BO}_3$  in about 700 ml of hot water, and transfer the cooled solution to a 1-liter volumetric flask containing 200 ml of ethanol and 20 ml of mixed indicator solution prepared by dissolving 0.330 g of brom cresol green and 0.165 g of methyl red in 500 ml of ethanol. After mixing the contents of the flask, add approximately 0.05 Normal sodium hydroxide cautiously until a color change from pink to pale green is just detectable when 1 ml of the solution is treated with 1 ml of water. Then dilute the solution to volume with water.
3. n-Octyl alcohol
4. Sulfuric acid
5. Hydrochloric acid
6. Sulfuric acid

Equipment used:

1. Steam distillation apparatus
2. Refluxing apparatus
3. Microburette.

#### C.4 ASSAY PROCEDURE FOR DEOXYRIBOSE



*If stored at 4°C, Puriss. DABA solution may be used up to the seventh day. Freshly prepared DABA solution was used in all tests, however.

**The alternate procedure uses 4 Normal perchloric acid rather than 4 Normal hydrochloric acid in Steps 1 and 4. In Step 5 the temperature is 55°C rather than 60°C and the time 90 minutes rather than 30 minutes.

Materials used:

1. DABA (3, 5-Diaminobenzoic acid dihydrochloride, M. W. 225.08), Aldrich Chemical Company, Inc., Milwaukee, Wisconsin.  
Puriss. grade (Aldrich No. 11,383-2)  
Practical grade* (Aldrich No. D 1282-1)
2. Hydrochloric acid, 10 Normal, fluorometric grade, Hartman-Leddon Co., Philadelphia, Pennsylvania.
3. Hydrochloric acid, 4 Normal, fluorometric grade. Dissolve 40 ml of 10 Normal fluorometric grade hydrochloric acid in ultrapure water and dilute to 100 ml.
4. Ultrapure water. Hartman-Leddon Co., Philadelphia, Pennsylvania.
5. Perchloric acid, 10 Normal, fluorometric grade, Hartman-Leddon Co., Philadelphia, Pennsylvania.
6. Perchloric acid, 4 normal. Prepare in a manner analogous to that for 4 Normal HCl.
7. DNA, ex-Herring sperm, grade A, Calbiochem, Los Angeles.
8. DOR (deoxyribose), Aldrich Chemical Company, Inc., Milwaukee, Wisconsin.

Equipment used:

1. Spectrophotofluorometer, Aminco-Bowman with standard fused-quartz cuvettes and Aminco-Bowman X-Y recorder.
2. Centrifuge, International Equipment Company, Model 5.

---

*This material must be purified by preparing first a 1 Molar solution, adding activated charcoal (U.S.P./Merck), shaking, storing overnight at 4°C, and filtering to remove the charcoal. The purified material is straw-yellow.

APPENDIX D  
SOIL SAMPLE ANALYSIS

APPENDIX D  
SOIL SAMPLE ANALYSIS  
CONTENTS

SECTION

- D.1 SOIL ANALYSIS METHODOLOGY
  - D.1.1 Sieving Procedure
  - D.1.2 Clay Analysis Procedure
  - D.1.3 Mineralogical Composition Analysis Procedure
  - D.1.4 Particle Size Distribution Analysis Procedure
- D.2 FIELD TEST SITE CONTROL SAMPLE ANALYSIS
  - D.2.1 Particle Size Distribution Analysis
    - D.2.1.1 Test Site A, Kelso Dune Sand
    - D.2.1.2 Test Site B, Pisgah Drylake Duricrust
    - D.2.1.3 Test Site E, Compacted Cinders
    - D.2.1.4 Test Site F, Desert Pavement
  - D.2.2 Clay Analysis
  - D.2.3 Mineralogical Composition
- D.3 FIELD SAMPLE DISTRIBUTION CURVES
  - D.3.1 Test Site A, Kelso Dune Sand
  - D.3.2 Test Site B, Duricrust
  - D.3.3 Test Site E, Compacted Cinders
  - D.3.4 Test Site F, Desert Pavement

APPENDIX D  
LIST OF TABLES

TABLE		PAGE
D-1	Assay Procedure for Clay Content of Soil. . . . .	D-9
D-2	Effect of Sonication on Soil Suspensions. . . . .	D-11
D-3	Clay Content of Selected Soil Specimens . . . . .	D-40
D-4	Soil Model A, Kelso Dune Sand, Control Sample Composition	D-43
D-5	Soil Model B, Pisgah Playa Lake, Control Sample - Composition of Gross Sample after Dry Sieving . . . . .	D-45
D-6	Soil Model B, Pisgah Playa Lake, Control Sample - Composition after Dispersion and Sedimentation Treatment.	D-46
D-7	Composition of Pisgah Crater Olivine Basalt . . . . .	D-44
D-8	Soil Model E, Compacted Basalt Cinders, Control Sample Composition. . . . .	D-48
D-9	Soil Model F, Pisgah Crater Desert Pavement, Control Sample Composition. . . . .	D-49

# LIST OF FIGURES

FIGURE		PAGE
D-1	Typical Soil Particle Size Distribution Curve. . . . .	D-13
D-2	Derivation of Percent Finer Curve from Distribution Curve. . . . .	D-14
D-3	Subdistribution Synthesization . . . . .	D-17
D-4	Comparison of Typical Sands. . . . .	D-19
D-5	Particle Size Distribution for Kelso Dune Sand (Log-log Plot) . . . . .	D-20
D-6	Particle Size Distribution for Kelso Dune Sand (Semilog Plot) . . . . .	D-21
D-7	Summation Curve Duricrust Control Sample . . . . .	D-23
D-8	Particle Size Distribution for Duricrust (Log-log Plot). .	D-24
D-9	Particle Size Distribution for Duricrust (Semilog Plot). .	D-25
D-10	Summation Curve for Compacted Cinders. . . . .	D-27
D-11	Particle Size Distribution for Compacted Cinders (Log-log Plot) . . . . .	D-28
D-12	Particle Size Distribution for Compacted Cinders (Semilog Plot) . . . . .	D-29
D-13	Integrated Summation Curve for Compacted Cinders . . . . .	D-30
D-14	Summation Curve for Desert Pavement < 2 mm Diameter. . . .	D-32

FIGURE		PAGE
D-15	Particle Size Distribution for Desert Pavement < 2 mm Diameter (Log-log Plot) . . . . .	D-33
D-16	Particle Size Distribution for Desert Pavement < 2 mm Diameter (Semilog Plot) . . . . .	D-34
D-17	Integrated Summation Curve for Desert Pavement < 2 mm Diameter . . . . .	D-35
D-18	Summation Curve for Desert Pavement . . . . .	D-36
D-19	Particle Size Distribution for Desert Pavement (Log-log Plot) . . . . .	D-37
D-20	Particle Size Distribution for Desert Pavement (Semilog Plot) . . . . .	D-38
D-21	Integrated Summation Curve for Desert Pavement . . . . .	D-39
D-22	Summation Curve, Sample 1, Site A . . . . .	D-52
D-23	Distribution Curve, Sample 1, Site A . . . . .	D-53
D-24	Summation Curve, Sampler 2, Site A . . . . .	D-54
D-25	Distribution Curve, Sampler 2, Site A . . . . .	D-55
D-26	Summation Curve, Sampler 3, Site A . . . . .	D-56
D-27	Summation Curve, Sampler 4, Site A . . . . .	D-57
D-28	Summation Curve, Sampler 5, Site A . . . . .	D-58
D-29	Summation Curve, Sampler 6, Site A . . . . .	D-59
D-30	Summation Curve, Sampler 8, Site A . . . . .	D-60
D-31	Summation Curve, Sampler 9, Site A . . . . .	D-61
D-32	Summation Curve, Sampler 10, Site A . . . . .	D-62
D-33	Distribution Curve, Sampler 10, Site A . . . . .	D-63
D-34	Summation Curve, Sampler 11, Site A . . . . .	D-64
D-35	Distribution Curve, Sampler 11, Site A . . . . .	D-65



FIGURE		PAGE
D-36	Summation Curve, Sampler 2, Site B . . . . .	D-68
D-37	Distribution Curve, Sampler 2, Site B. . . . .	D-69
D-38	Summation Curve, Sampler 4, Site B . . . . .	D-70
D-39	Summation Curve, Sampler 5, Site B . . . . .	D-71
D-40	Summation Curve, Sampler 6, Site B . . . . .	D-72
D-41	Summation Curve, Sampler 7, Site B . . . . .	D-74
D-42	Distribution Curve, Sampler 7, Site B . . . . .	D-75
D-43	Summation Curve, Sampler 8, Site B . . . . .	D-76
D-44	Summation Curve, Sampler 9, Site B . . . . .	D-77
D-45	Summation Curve, Sampler 10, Site B . . . . .	D-78
D-46	Distribution Curve, Sampler 10, Site B . . . . .	D-79
D-47	Summation Curve, Sampler 2, Site E . . . . .	D-82
D-48	Distribution Curve, Sampler 2, Site E . . . . .	D-83
D-49	Summation Curve, Sampler 4, Site E . . . . .	D-84
D-50	Distribution Curve, Sampler 4, Site E . . . . .	D-85
D-51	Summation Curve, Sampler 6, Site E . . . . .	D-86
D-52	Distribution Curve, Sampler 6, Site E . . . . .	D-87
D-53	Summation Curve, Sampler 7, Site E . . . . .	D-88
D-54	Distribution Curve, Sampler 7, Site E . . . . .	D-89
D-55	Summation Curve, Sampler 9, Site E . . . . .	D-90
D-56	Distribution Curve, Sampler 9, Site E . . . . .	D-91
D-57	Summation Curve, Sampler 11, Site E . . . . .	D-92
D-58	Distribution Curve, Sampler 11, Site E . . . . .	D-93

FIGURE		PAGE
D-59	Summation Curve, Sampler 2, Site F . . . . .	D-96
D-60	Distribution Curve, Sampler 2, Site F. . . . .	D-97
D-61	Summation Curve, Sampler 4, Site F . . . . .	D-98
D-62	Distribution Curve, Sampler 4, Site F. . . . .	D-99
D-63	Summation Curve, Sampler 5, Site F . . . . .	D-100
D-64	Distribution Curve, Sampler 5, Site F. . . . .	D-101
D-65	Summation Curve, Sampler 6, Site F . . . . .	D-102
D-66	Distribution Curve, Sampler 6, Site F. . . . .	D-103
D-67	Summation Curve, Sampler 7, Site F . . . . .	D-104
D-68	Distribution Curve, Sampler 7, Site F. . . . .	D-105
D-69	Summation Curve, Sampler 9, Site F . . . . .	D-106
D-70	Distribution Curve, Sampler 9, Site F. . . . .	D-107
D-71	Summation Curve, Sampler 10, Site F. . . . .	D-108
D-72	Distribution Curve, Sampler 10, Site F . . . . .	D-109

## APPENDIX D

### SOIL PARTICLE SIZE DISTRIBUTION ANALYSIS AND MINERALOGICAL COMPOSITION

The subject of soil analysis for particle size distribution and mineralogical composition is comprehensive enough to warrant some special treatment. For this reason and to maintain clarity in the text of the body of this report, this subject is discussed independently in this appendix.

#### D.1 SOIL ANALYSIS METHODOLOGY

This section reviews the procedures and methods used to process the soil sample and to analyze the data. In general, the intent was to compare the samples collected by the soil samplers at the field test sites to a control sample obtained from each test site. Obviously, no control samples were taken at either of the basalt test sites. Since most of the soil samplers were surface or near subsurface samplers, the control was collected over an area to a shallow depth of one to two inches. Care must be exercised in obtaining these samples to ensure that a representative sample is obtained and that it is large enough so that it contains a statistically representative population of particle sizes. For example, the larger the maximum size particles that are contained in the sample, the larger the control sample must be to ensure that the gravel size distribution is representative.

##### D.1.1 SIEVING PROCEDURE

The first step in processing these samples to determine the particle size distribution is to separate the soil into cuts of finite size ranges. The very large gravel size material above one centimeter in diameter were removed by hand and separated into various cuts by measurement. All material below one centimeter was separated by sieving. Coarse sieves

were used to separate the particles between two millimeters and one centimeter in diameter. The openings of these screens decreased from 10 millimeters in 2 millimeter intervals. From 2 millimeters on down, the screen mesh size decreased by a factor of two down to a mesh opening of 63 microns. A 44 micron screen was the finest mesh screen used.

After separating the sample into cuts for the size ranges mentioned above, these cuts were weighed from which the percentages finer could be calculated. This data was then plotted on log-probability graph paper. Any extrapolation or smoothing of the data was performed in these plots. Using these plots, distribution curves as a function of particle size were derived using a method given by R. A. Bagnold in "The Physics of Blown Sand and Desert Dunes." This method as applied here is described in greater detail later in this section. The distribution curves obtained in this manner for the control samples are given in Section 2 of this appendix and those obtained for the soil samplers are given in Section 3 of this appendix. Only those samples of 10 grams or more in size were subjected to this type of analysis. These distributions were then compared to detect the character of the changes, if any, that the sampler may have made in the collected sample for a particular test site.

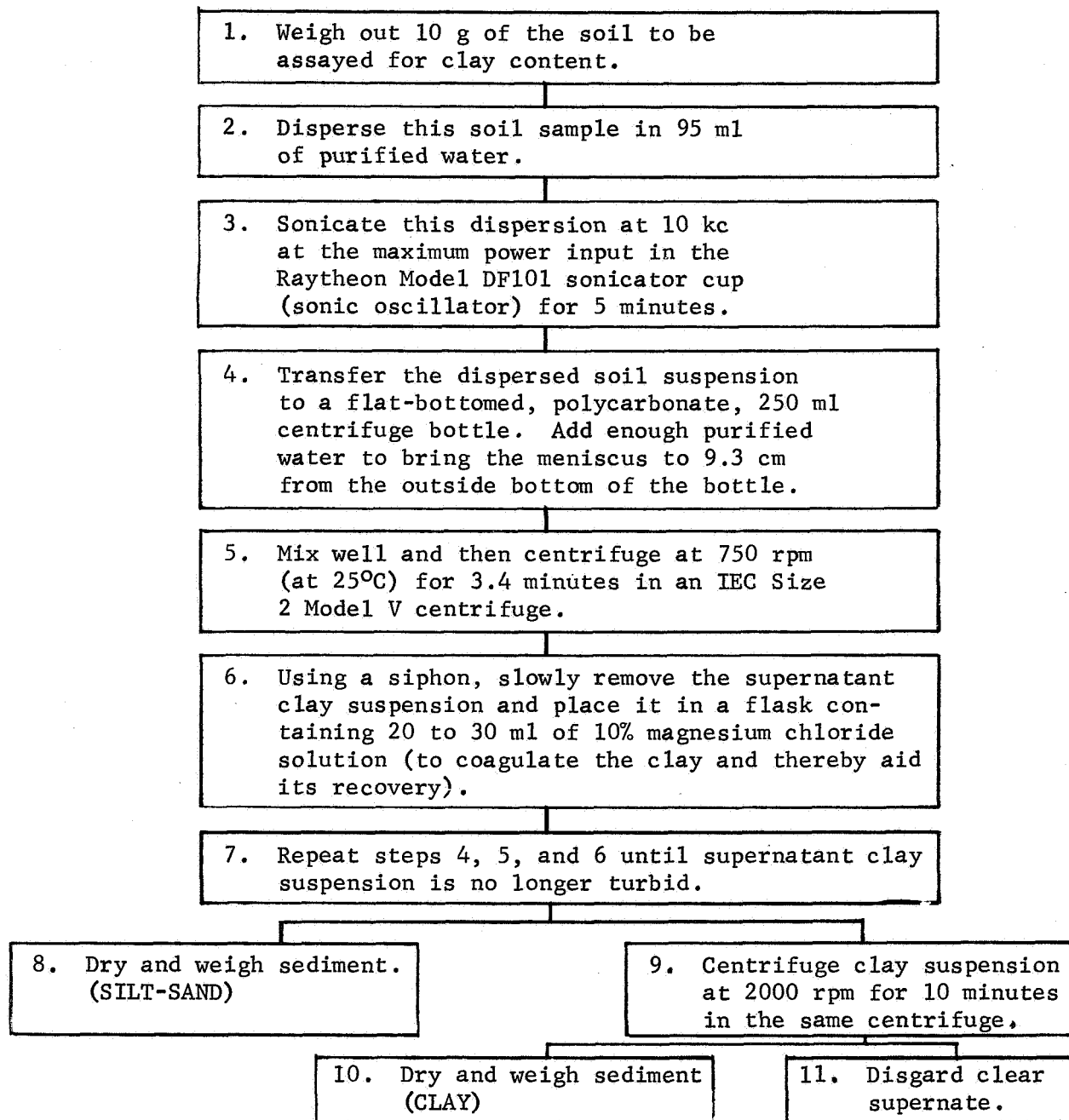
The results of this analysis is, in many instances, qualitative rather than quantitative. Many repeated runs would be required to establish the quantitative reliability of this type of data; however, in several cases it is felt that the characteristics of the sampler in acquiring a soil sample can be identified with reasonable reliability.

#### D.1.2 CLAY ANALYSIS PROCEDURE

In soil, particular minerals tend to occur within defined size ranges (Whittig, 1965). This tendency for specific colloidal minerals to concentrate within specific size fractions is the net result of their resistance to weathering and the intensity of the weathering they experience. The more resistant minerals, such as montmorillonite, persist in the finer clay fractions whereas the crystal structure and composition of the less resistant minerals, such as feldspars and mica, are destroyed before weathering reduces them to particles of size typical of clay. For this reason, a mineralogical analysis of a clay-silt mixture often gives a good, though rough, estimate of the distribution of particle sizes between those characteristic of clay and those characteristic of silt. Both mineralogical and sedimentation analyses were employed in this investigation. Not all specimens, however, were subjected to both methods of analysis. The procedure used in the clay sedimentation analysis is given in Table D-1. This procedure was used in the preliminary laboratory work preceding the analysis of the field test samples on Pisgah soil samples P1, P2, and P3 to check out the procedure. The results of this preliminary work are discussed in the following paragraphs.

TABLE D-1

ASSAY PROCEDURE FOR CLAY* CONTENT OF SOIL



*Consists of particles smaller than 2 microns.

The sedimentation analysis used employed a procedure suitable for preparing clay specimens for X-ray diffraction studies. This standard method (Whittig, 1965) separates a soil into clay and a silt-sand fraction by centrifugal sedimentation. The standard methods also usually involve pretreatments (Kunze, 1965) of the soil specimen with acid, hydrogen peroxide, and sodium dithionite to remove carbonates, organic matter, and iron oxides which cement clay particles to silt and sand particles and to each other. Moreover, the clay is usually suspended in saturated sodium chloride solution to prevent aggregation of the clay by divalent ions normally present in the soil.

Because of this cementation, specific procedures are required to ensure dispersion of the clay particles before sedimentation analysis. Among the Pisgah soils P1, P2, and P3, discussed in Section 5.1.1 of this report, less than 3% of the individual specimens passed through the 44-micron sieve, yet some of these soils contained upwards of 8% clay.

Recently, Edwards and Bremner (1967) reported the use of sonic vibration in soil analysis to disperse clay particles, thereby obviating the need for the pretreatments or the sodium chloride suspension medium. These investigators claim that many of the artifacts characteristic of the standard methods are eliminated by sonic dispersion. However, the problems associated with the centrifugation, such as sharpness of separation at a particular particle size are retained.

The method used in the present investigation for dispersing clay was based on Edwards' and Bremner's results. However, it used a more powerful, 250-watt rather than 60-watt, Raytheon Model DF101 sonic oscillator (sonicator) and the frequency was 10 kc rather than 9 kc. Because of these differences, the effect of sonic treatment time on the specimen was measured.

Equivalent portions of the duricrust control specimen were sonicated in approximately 45 ml of water for several different periods of time. The suspensions were stored in 100 ml graduated cylinders. The appearance of the suspensions after 8 days of storage are described in the table. After 15 days of this storage, the water above the sediment was clear. At the fifteenth day discrete algal colonies populated on the surface of the sediment in both specimens which received no sonication. On the twenty-first day the surfaces of these sediments were covered with algae. No algal colonies were seen in the sonicated specimens. Although Edwards and Bremner found no tendency of the sonic dispersed clay to flocculate during a 9 day quiescent storage period, Table D-2 clearly shows that the more intense treatment does induce clay flocculation. On the basis of the results shown in Table D-1, 5 minutes of sonication appears to be optimum for this procedure.

TABLE D-2

## EFFECT OF SONICATION ON SOIL SUSPENSIONS

Sonication Minutes	Location and Appearance of Zone, ml markings					
	Sediment	Flocc	Turbidity	Haze	Faint Haze	Clear
0 0} replicates	0-3				3-45	
3	0-4		4-38	38-45		45-48
5	0-5		5-35	35-40		40-45
10	0-11	11-40				40-45
25	0-10	10-35				35-45

## D.1.3 MINERALOGICAL COMPOSITION PROCEDURES

This section presents the mineralogical composition analyses of the control samples and describes the methods of deriving these compositional analyses. The composition of the pahoehoe- and aa-type basalts were derived from petrographic analyses of thin-sections cut from pahoehoe flow fragments and observed under a petrographic microscope. The composition of the sand-size grains was determined by means of a petrographic microscope but the percentage of constituents was counted by using a 15 power binocular microscope and a standard sedimentary particle counting grid. Silt size particles were identified by means of correlation with the composition of sand particles and by X-ray diffraction analyses and the percentage of constituents estimated beneath a 45 power binocular microscope using a counting grid. The mineral composition and constituent percentage population for clay-size particles was determined by X-ray diffraction scans of the separated clays.

## D.1.4 PARTICLE SIZE DISTRIBUTION ANALYSIS PROCEDURE

The following discussion is devoted to explaining the method used to derive the distribution curves used in the evaluation of the sampler's performance.

This method utilizes a graphical display of the data from which trends and typical characteristics may be described in a systematic manner.

It is well known that many things can be described with some sort of distribution curve. This has been found to be typically true of soils and other natural occurring phenomena such as meteorite distribution by size, the frequency of occurrence of chance events, etc. This curve is shown qualitatively in Figure D-1 for three different ways of presentation where the percentage of the population at any given grain size is given in terms of weight. Most soils resemble a normal distribution if the logarithm of the grain size is used as the abscissa as shown in part B of Figure D-1. When this curve is plotted against grain size as shown in part A of this figure, it is seen that a skewed distribution actually exists such that there is usually a broader distribution by weight in the coarse grain material than in the fine grain material. This is probably a result of the cube law which says that the volume of the particle and hence the weight increases or decreases as the cube of the diameter. Bagnold found in his work with dune sands that further simplification of the shape of this curve could be achieved by plotting the logarithm of the percentage of the sample by weight against the logarithm of the particle size as shown in part c of Figure D-1.

In general this will allow the curve on each side of the peak to be fitted with a straight line. The slopes of these lines are the same only if the curve is symmetrical. The feature of this plot which can be utilized to advantage is that it provides a systematic means of detecting trends and extrapolating the experimental data where needed. It is also easier to describe a complex mixture as a combination of simple distributions from which the percentage of a particular distribution existing in the the total sample can be determined; i.e., the relative percentage of sand size material composed of silt or gravel size material. This will be explained more fully subsequently.

From the distribution curve the percent finer curve may be derived by integration as shown in Figure D-2. The area under the curve in part A of the figure must be equal to 100 percent since this represents the total sample. If the distribution curve is symmetrical the peak of the distribution curve is the mean grain size and 50 percent of the material by weight is finer than this size. The distribution curve could be obtained directly from the experimental data and is frequently plotted as a histogram as shown by the dotted lines in part A of Figure D-2. Alternatively, the percentage finer or summation curve can also be computed directly from the experimental data. It was our experience that better results are obtained by plotting the percent finer curve on logarithmic probability graph paper and deriving the distribution curve from this plot. Any smoothing of the curve through the data that may be necessary can be more easily accomplished on this plot and will introduce less errors. Also, where there are only a



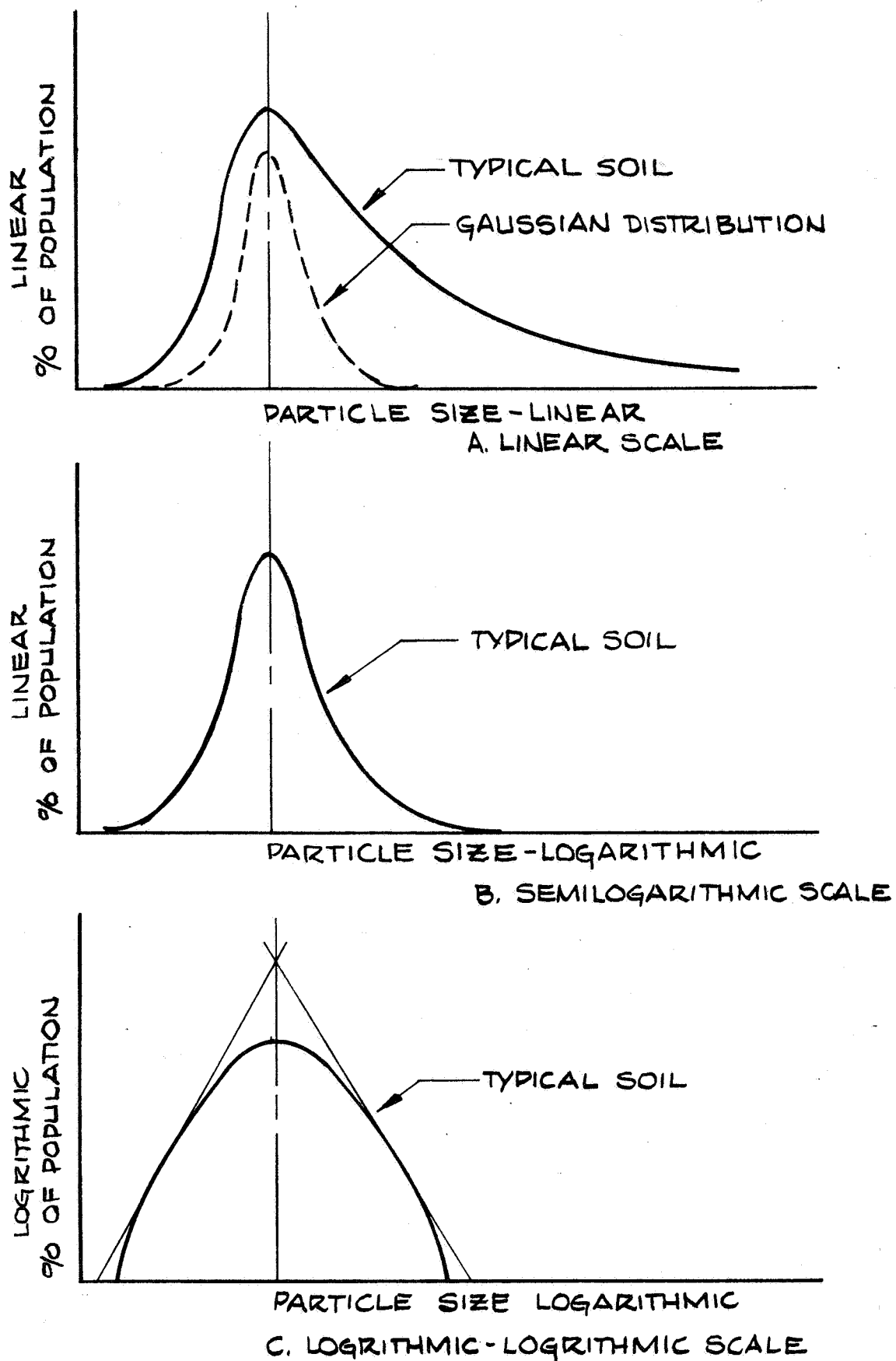
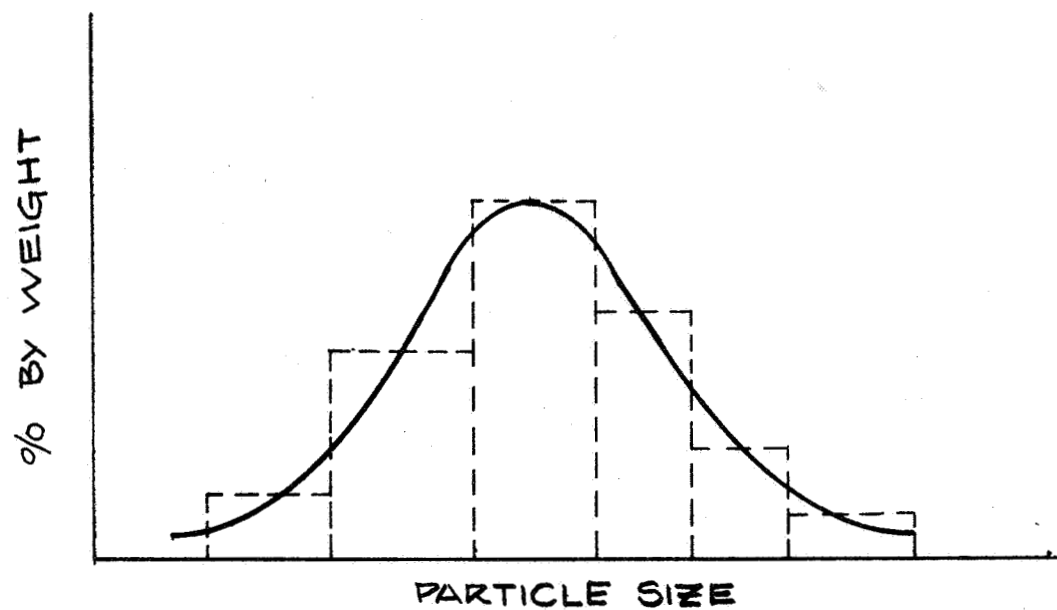
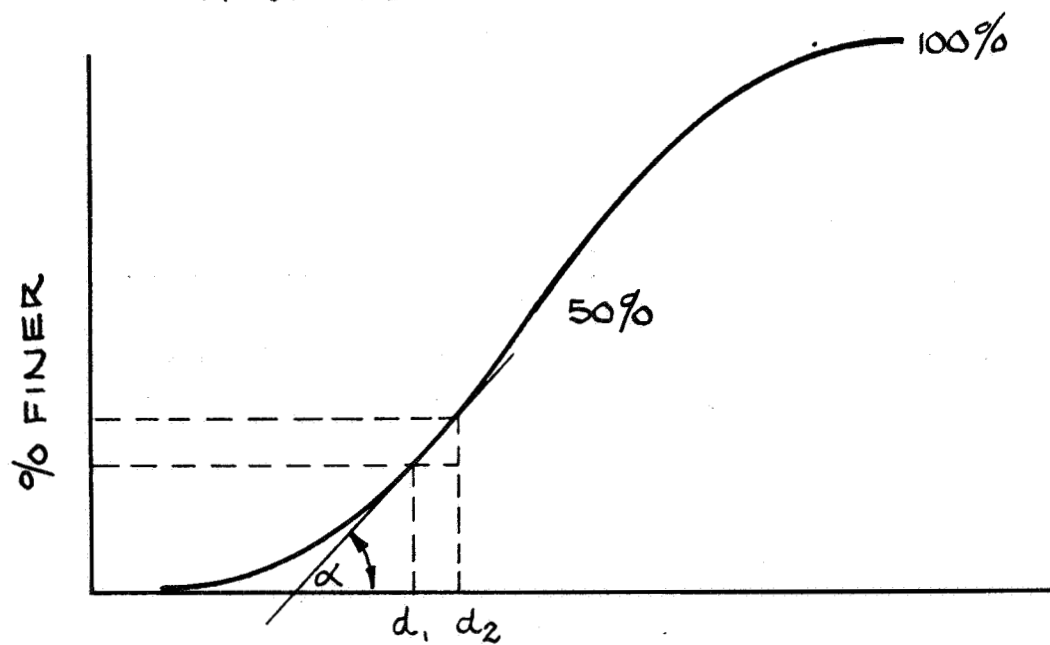


FIGURE D-1. TYPICAL SOIL PARTICLE SIZE DISTRIBUTION CURVES



A. DISTRIBUTION CURVE



B. PERCENT FINER OR SUMMATION CURVE

FIGURE D-2. DERIVATION OF PERCENT FINER CURVE FROM DISTRIBUTION CURVE

few data points, intermediate values can be more systematically selected. Mathematically the ordinate of the distribution curve is the derivative or the slope of the percent finer curve. This can be expressed as

$$\tan \alpha = \frac{P_2 - P_1}{\log d_2 - \log d_1} = \frac{\Delta p}{\log \frac{d_2}{d_1}} = N.$$

From this equation it is seen that some convenient particle size ratio can be selected to provide the requisite points to construct a distribution curve. It is noted here that the value of N calculated in this manner is not the actual percentage by weight; however, it is directly proportional to it. Because of the large amount of data that were processed in a rather limited time, these plots were used directly rather than being rectified to actual percentages. As long as these curves are used consistently in this manner the same results are obtained and direct comparisons can legitimately be made. It was found that care and some exercise of judgment is required in selecting the appropriate particle size ratio  $d_2/d_1$ . If too small a ratio is used the accuracy with which the percent finer curve can be read approaches that of the calculation and erratic results are obtained. If the ratio is too large insufficient points are obtained to identify the shape of the distribution curve.

In order to check the results, after the distribution curve and the sub-distributions were derived these curves were integrated graphically to produce a percentage finer or summation curve. This derived percentage finer curve was then compared against the original experimental data. Surprisingly good agreement was achieved in these checks. The application of this analysis method is illustrated in Section D.2.1 in which the particle size distributions for the field test control samples are discussed.

At this point it is pertinent to review the characteristics of a soil sample which can be identified from these curves. If a summation curve is a straight line on conventional probability paper the distribution is a normal or Gaussian distribution with a peak at the same particle size as the 50 percent point. The slope of the line is the standard deviation of the sample. Thus, the flatter the slope the lower the deviation and the narrower is the spread of particle sizes contained in the sample. Conversely, the steeper the slope the broader is the distribution of particle sizes. A straight line on the logarithmic-probability paper represents a skewed distribution.

The presence of more than one simple distribution is indicated by a sharp knee or change in slope occurring between two relatively straight segments of the summation curve. These are more easily identified on the distribution curve as indicated by the presence of more than one peak. In some cases two distinct peaks may not exist. The presence of two or more distribution populations is usually indicated if a hump or bulge occurs on a limb of the distribution curve. Another feature observed is that if a portion of the sample at either end of the distribution is discarded and the distribution is determined for the remaining sample, the general shape of the curve for the remaining portion is preserved although the absolute magnitude of percentages change causing the curve to be displaced or shifted vertically.

Knowing the characteristics of these curves, it is possible to analyze a complex distribution and to synthesize the simple subdistributions and percentages of these which are required to produce the overall distribution. Figure D-3 illustrates the steps which are followed in this analysis. The distribution curve for the complex sample is shown as a solid line in part A of this figure in a log-log plot. Two simple population subdistributions making up this complex distribution are labeled A and B. The shaded area is where the population of these two overlap. The dashed line sloping down to the right is the coarse limb of population B and the dashed line sloping down to the left is the fine limb of population A. In order to locate the position of these limbs it is known that at point 0 the values of the ordinates at 0' is equal for each subpopulation because they cross each other. The magnitude of the value at 0' must then be half the value of the envelope curve at 0 since the two subpopulations add to determine the envelope population. The slope of the coarse limb of population B is determined by the fact that from the peak of the envelope curve towards point 0 the population in this limb dominates in the envelope curve. The slope of this limb must then be essentially the same as that in the envelope curve. The coarse limb of population B is displaced toward the left slightly so that the sum of the ordinates for populations A and B are equal to that in the envelope curve. Since no real clues exist for establishing the slope of the fine limb for population A, a symmetrical shape is assumed. This is generally true for many soils, particularly sand.

Having established the shape of the distribution curve for populations A and B on the log-log plot, these curves are then replotted on the similog paper as shown in part B of Figure D-3. A graphical integration of these curves produces the summation curves as shown in part c of this figure. The dashed curves are the summation curves for the subpopulations A and B and the sum of these add to give the total summation curve as shown by the solid line. A check on the consistency of the analysis can be made by comparing the derived summation curve to that obtained by plotting the original experimental data. A slight shift in the location of the curve

may occur but the shape is usually preserved remarkably well. Admittedly, there is a considerable amount of judgment which must be exercised in an analysis of this type; however, surprisingly consistent results were obtained in evaluating the control samples from the test sites in this way.

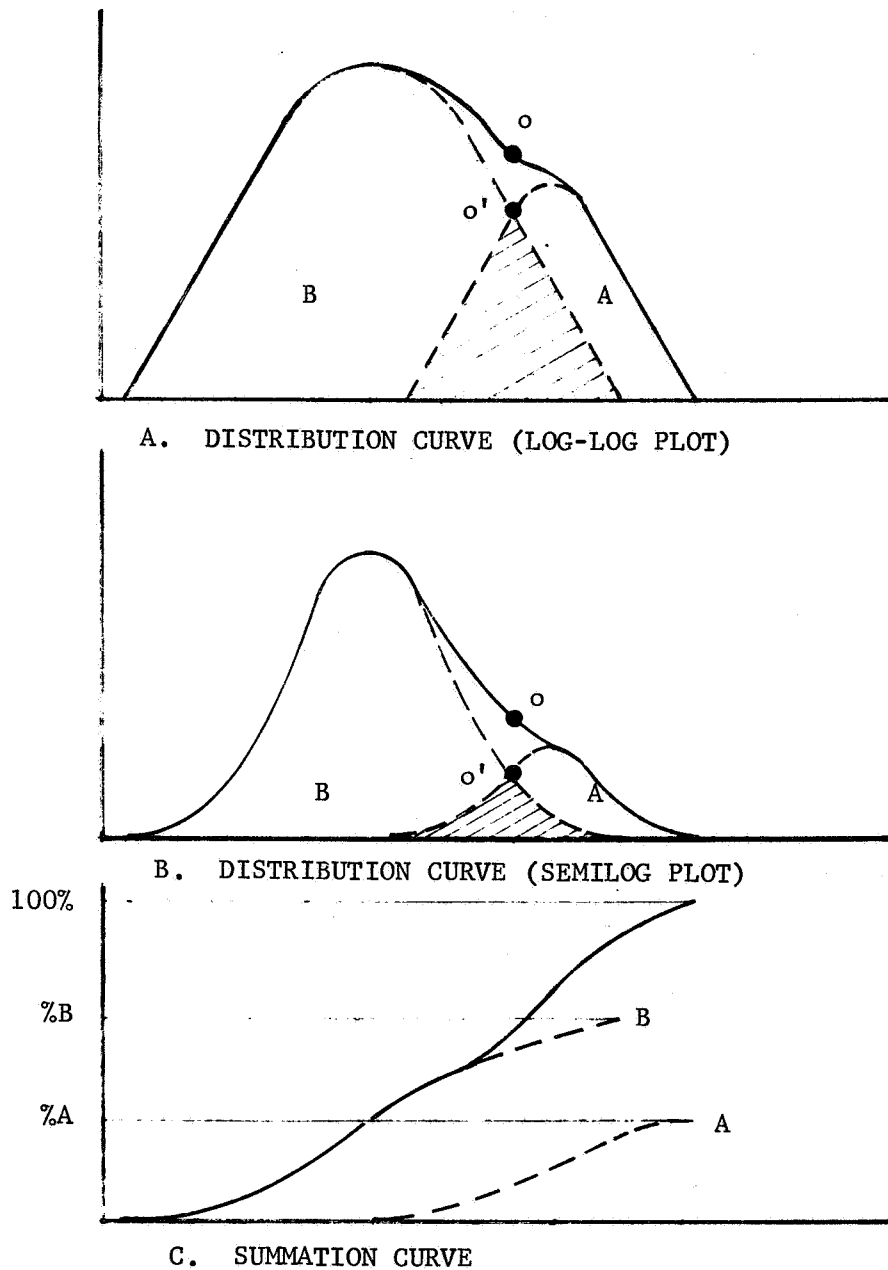


FIGURE D-3. SUBDISTRIBUTION SYNTHESIZATION

D.2 FIELD TEST SITE CONTROL SAMPLE ANALYSIS

## D.2 FIELD TEST CONTROL SAMPLE ANALYSIS

The control samples taken at four of the field test sites were analyzed to determine their physical characteristics and mineralogical composition. These analyses are presented in this section. Section D.2.1 treats the particle size and distribution analysis and Section D.2.2 treats the mineralogical compositional analysis.

### D.2.1 PARTICLE SIZE DISTRIBUTION ANALYSIS

This section presents the results of the dry sieving and graphical analysis procedures described earlier in this appendix for each of the control samples.

#### D.2.1.1 TEST SITE A, KELSO DUNE SAND

The characteristic percent finer curve obtained for this soil sample is given in Figure D-4. For the sake of comparison two other sands are plotted. The Nevada 60 sand is a sieved cut that was used in the laboratory testing. The Yuma dune sand is from data presented by M. G. Bekker at the "Proceedings of the 1st International Conference on the Mechanics of Soil-Vehicle Systems," 1961. It is interesting to note that the standard deviation for each of these sands is the same. Only the mean grain size varies, although not very drastically.

The log-log plot of the distribution curve for the Kelso dune sand is shown in Figure D-5. The value of this plot in extrapolating the shape of the curve can be seen by the way the light straight lines fit the heavy solid line. The heavy solid line is the range covered by the experimentally determined data. This curve is replotted on semilog paper in Figure D-6 which shows the characteristically narrow and symmetrical distribution that most sands exhibit.

- - - - YUMA DUNE SAND  
 - - - - NEVADA GO SAND  
 - - - - KELSO DUNE SAND

PARTICLE SIZE - MILLIMETERS

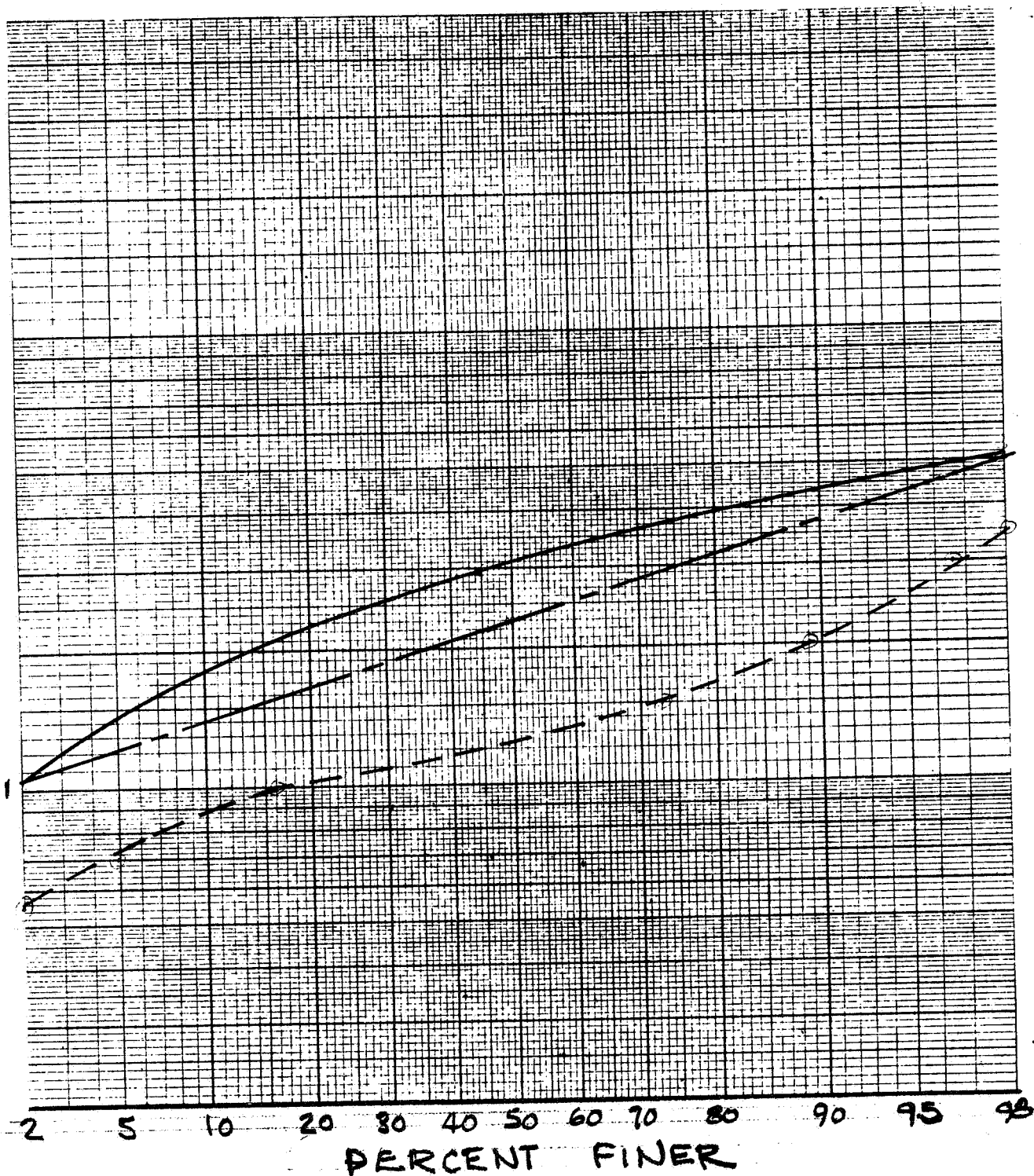


FIGURE D-4 COMPARISON OF TYPICAL SANDS



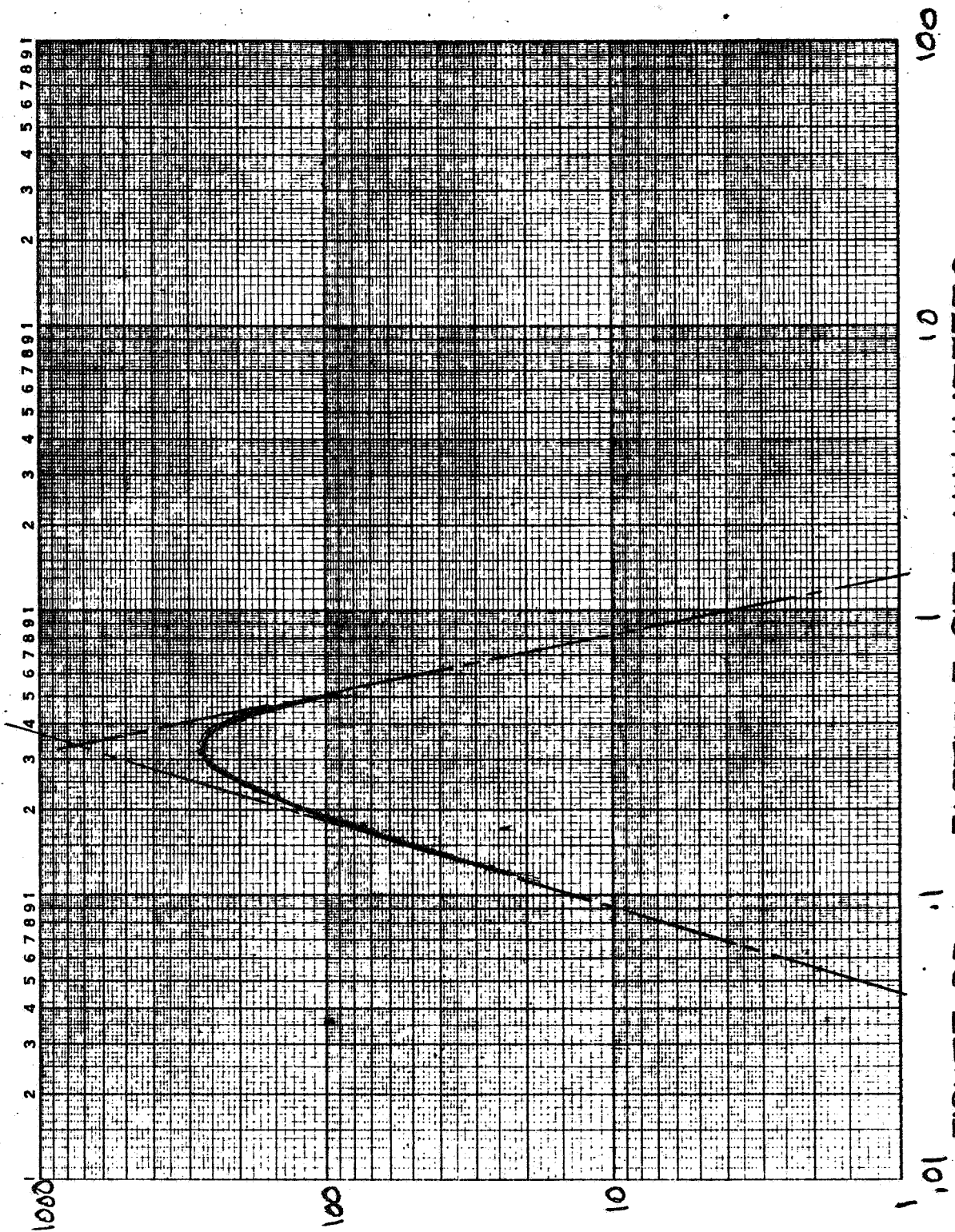


FIGURE D5 PARTICLE SIZE - MILLIMETERS  
PARTICLE SIZE DISTRIBUTION KELSO DUNE SAND

VALUE OF N

359-06  
FEL & CO. INC.  
7 CYCLES X 60 DIVISIONS

MODEL

DATE

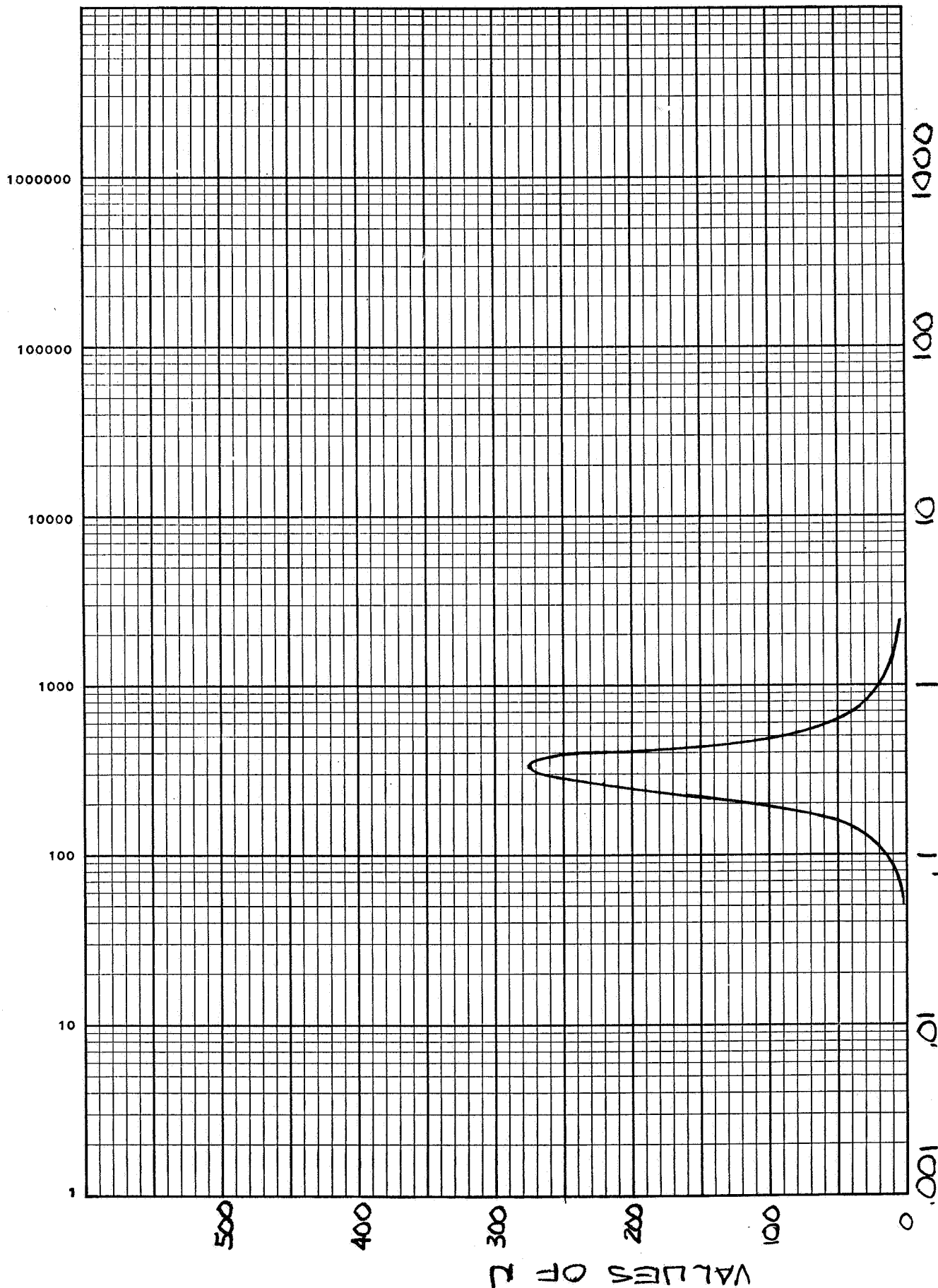


FIGURE D6  
PARTICLE SIZE DISTRIBUTION KELSODUNE SAND

#### D.2.1.2 TEST SITE B, PISGAH DRY LAKE DURICRUST

The particle size distribution for this model is particularly difficult to assess. In the field this soil was lightly cemented together. In the dry sieving analysis, the particles were broken down manually by crushing and abrasion and then were dry sieved. The percentage finer curve is shown in Figure D-7 as the curve labeled A. Curve B in this figure was obtained using dispersion and sedimentation techniques. The log-log plot of the distribution curve for duricrust is given in Figure D-8 and the semilog plot is given in Figure D-9. It is seen that the peak of the distribution curve occurred at the same particle size for both methods of analysis. The net effect of using the dispersal technique was to break down some of the agglomerated coarse grains into fine material. This is indicated by the change in slopes of the coarse and fine limbs of the distribution curve in Figure D-8. Also, a hump in the fine limb of the curve appeared indicating that this soil is a mix of two simpler distributions which would appear to consist of a narrow distribution of sand and a broader distribution of silt size material.

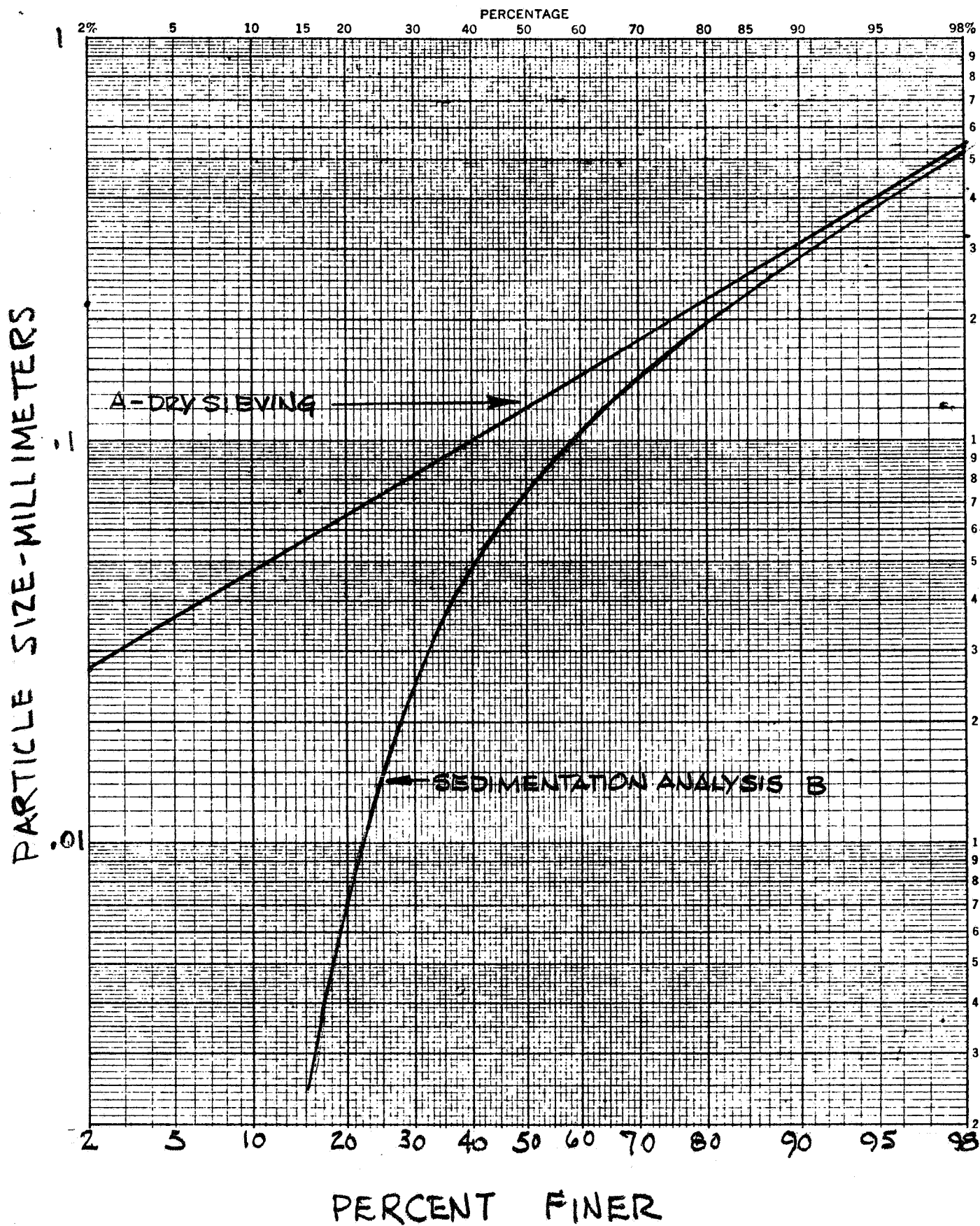


FIGURE D7 SUMMATION CURVE  
DURICRUST CONTROL SAMPLE

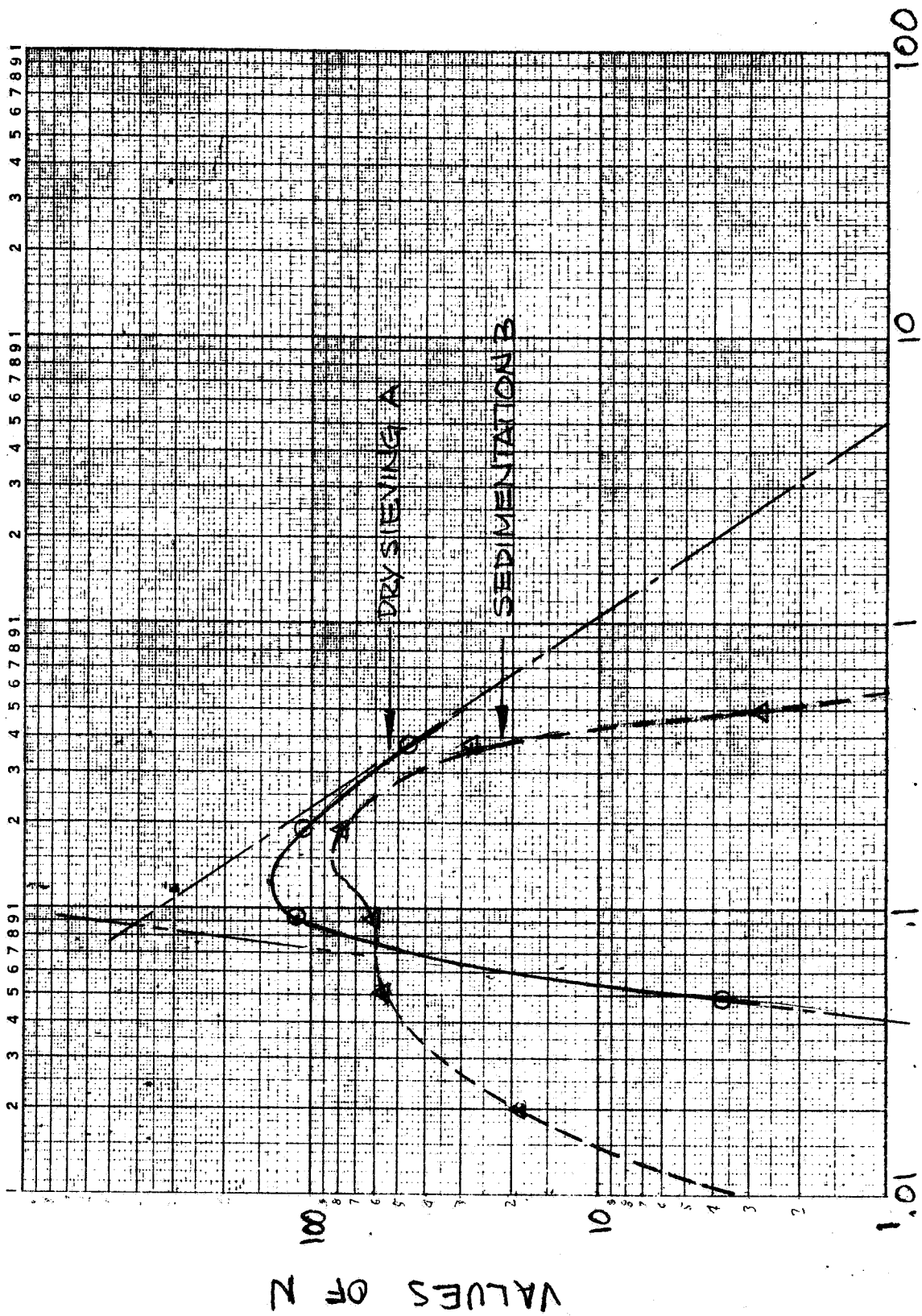


FIGURE D8 PARTICLE SIZE - MILLIMETERS  
PARTICLE SIZE DISTRIBUTION PLURICRUST

MODEL

DATE

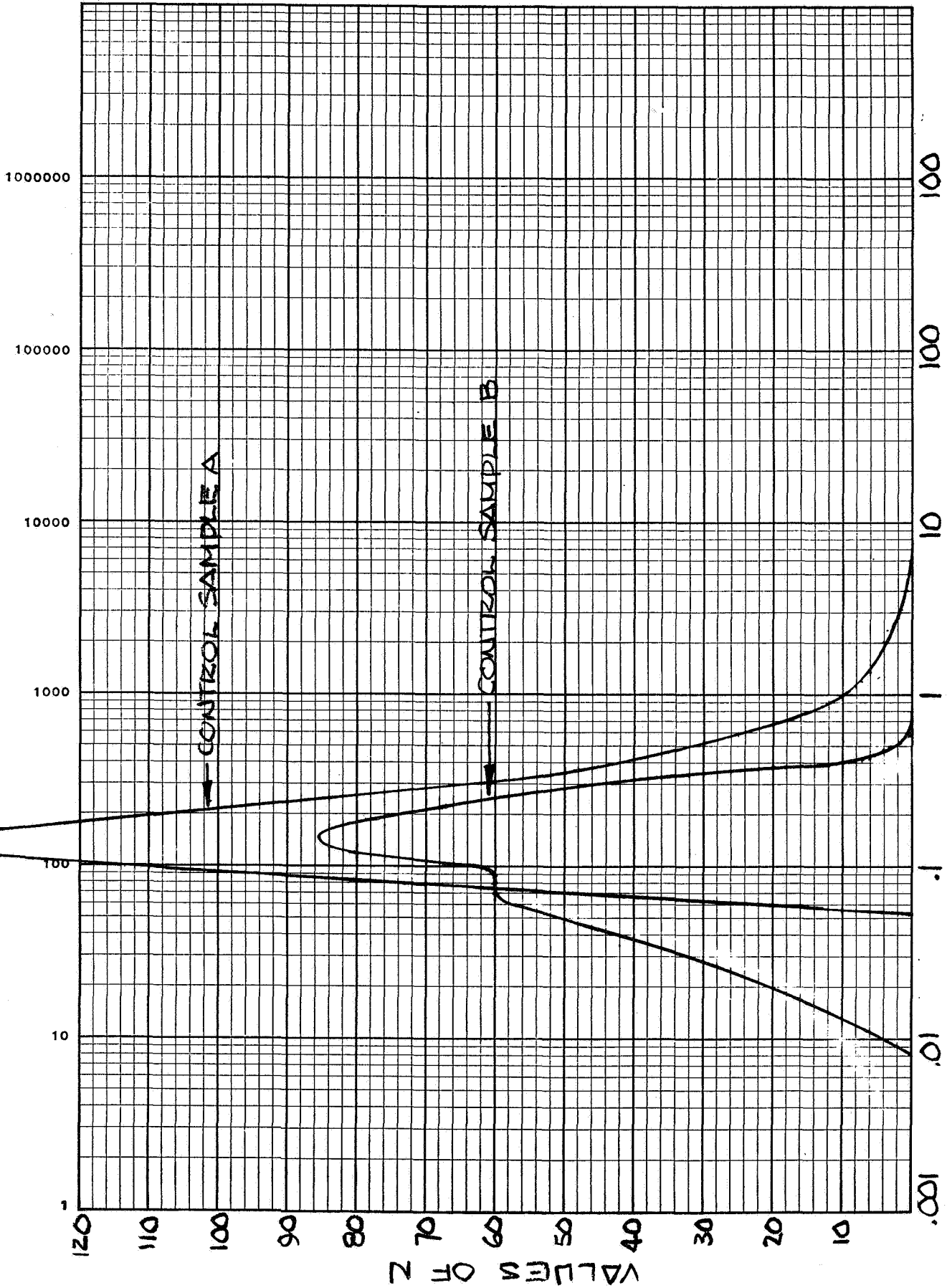


FIGURE D9  
PARTICLE SIZE DISTRIBUTION DURICRUST

#### D.2.1.3 TEST SITE E, COMPACTED CINDERS

The control sample for this test site soil has a very broad distribution of sizes consisting of everything from fine material up to moderately coarse gravel. The summation or percentage finer curve is given in Figure D-10. The distribution curve derived from this data is given in Figure D-11 as a log-log plot and in Figure D-12 as a semilog plot. It can be seen that this soil is a mixture of moderately coarse gravel and what appears to be a fine sand like material in which the gravel dominates. Integration of the distribution curve as shown in Figure D-13, shows that 82 percent of this model is gravel and the remaining 18 percent is finer material. It is noted that this soil is a mix of two distinct populations with very little overlap. There are two peaks in the distribution curve. One occurs at 80 microns which is like fine sand. The other occurs at 25 millimeters which is like coarse pebbles.



PARTICLE SIZE - MILLIMETERS

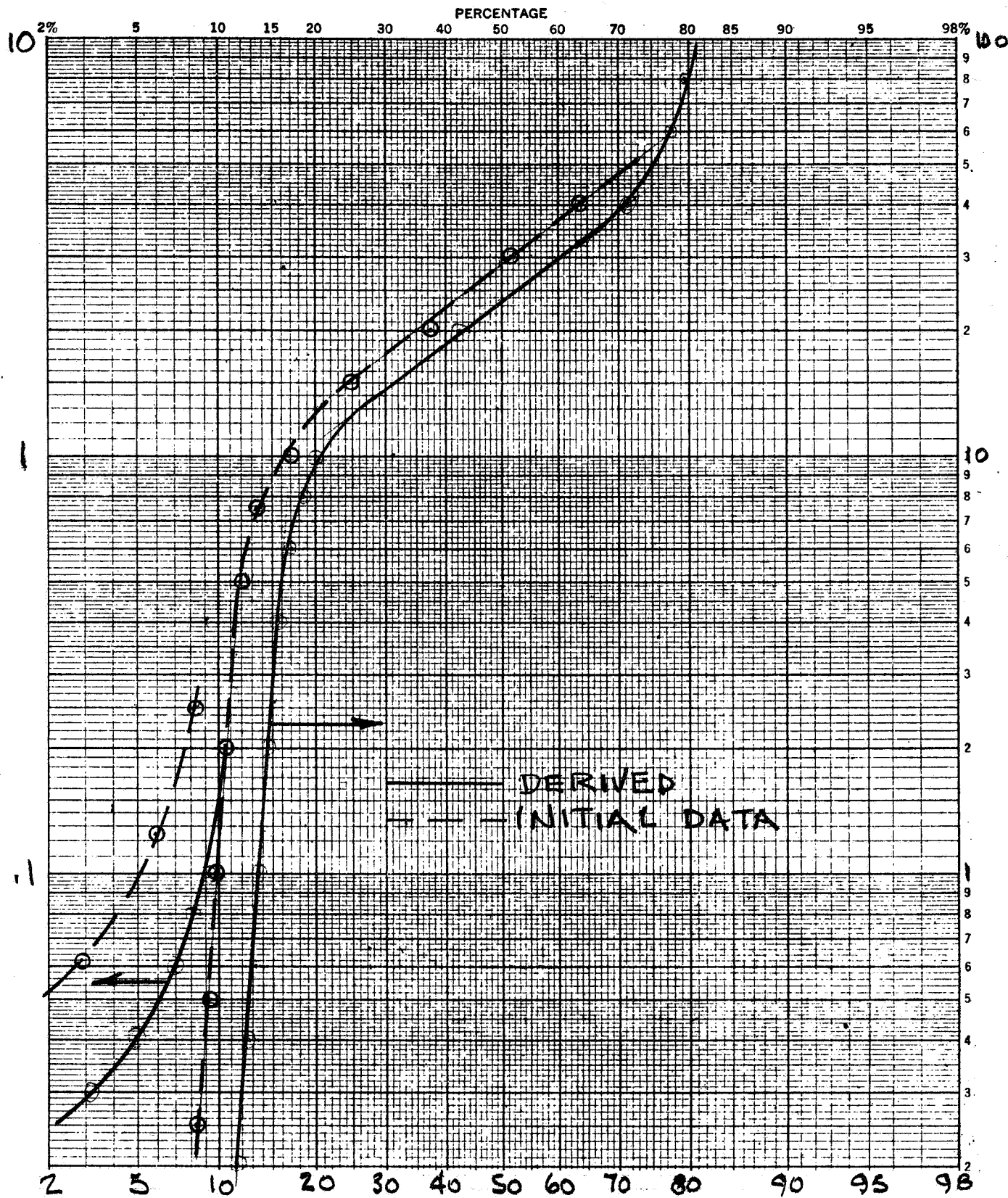


FIGURE D10 PERCENT FINER  
PARTICLE SIZE DISTRIBUTION COMPACTED CINDERS



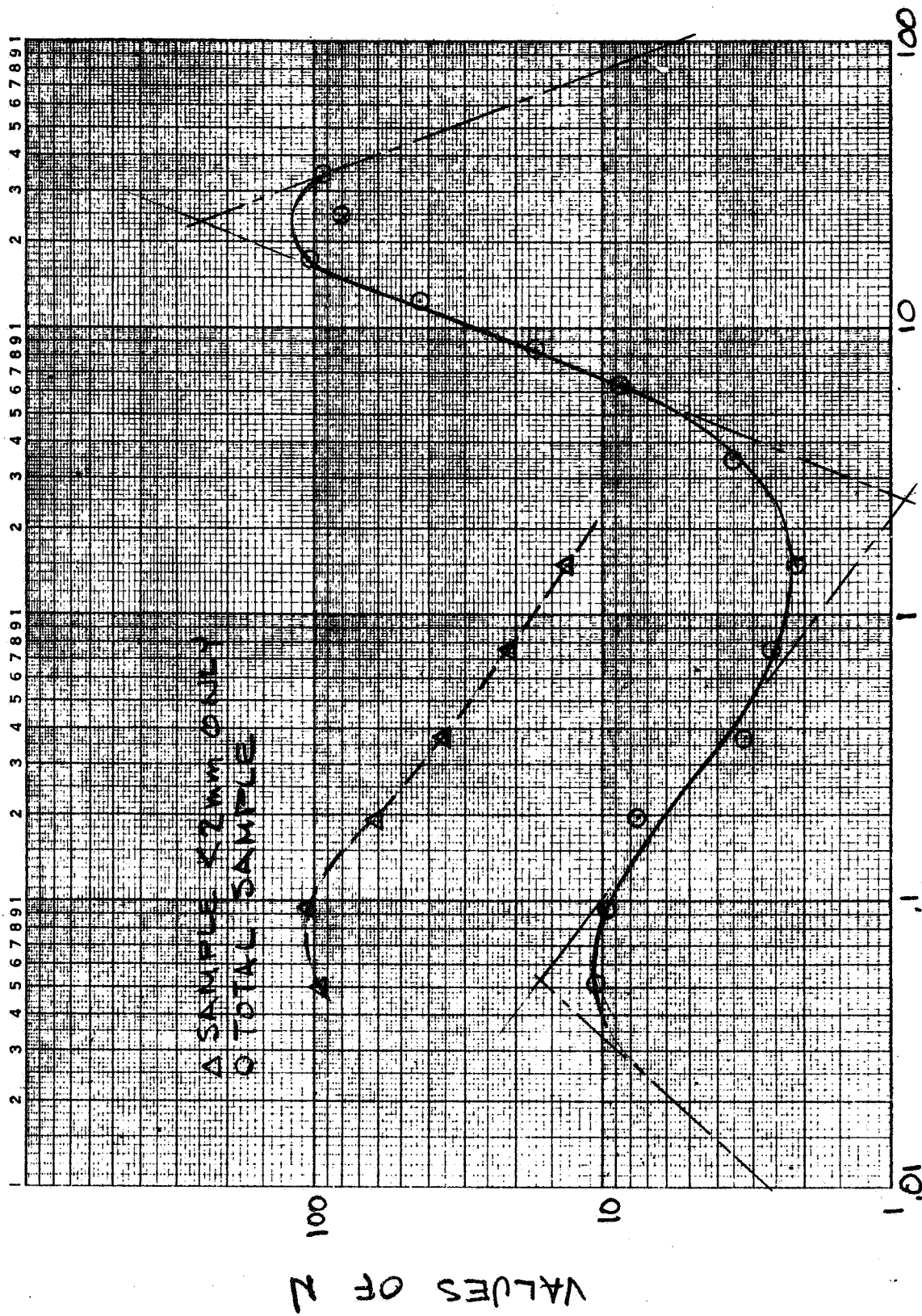


FIGURE D11 PARTICLE SIZE - MILLIMETERS  
PARTICLE SIZE DISTRIBUTION - COMPACTED CINDERS

MODEL

DATE

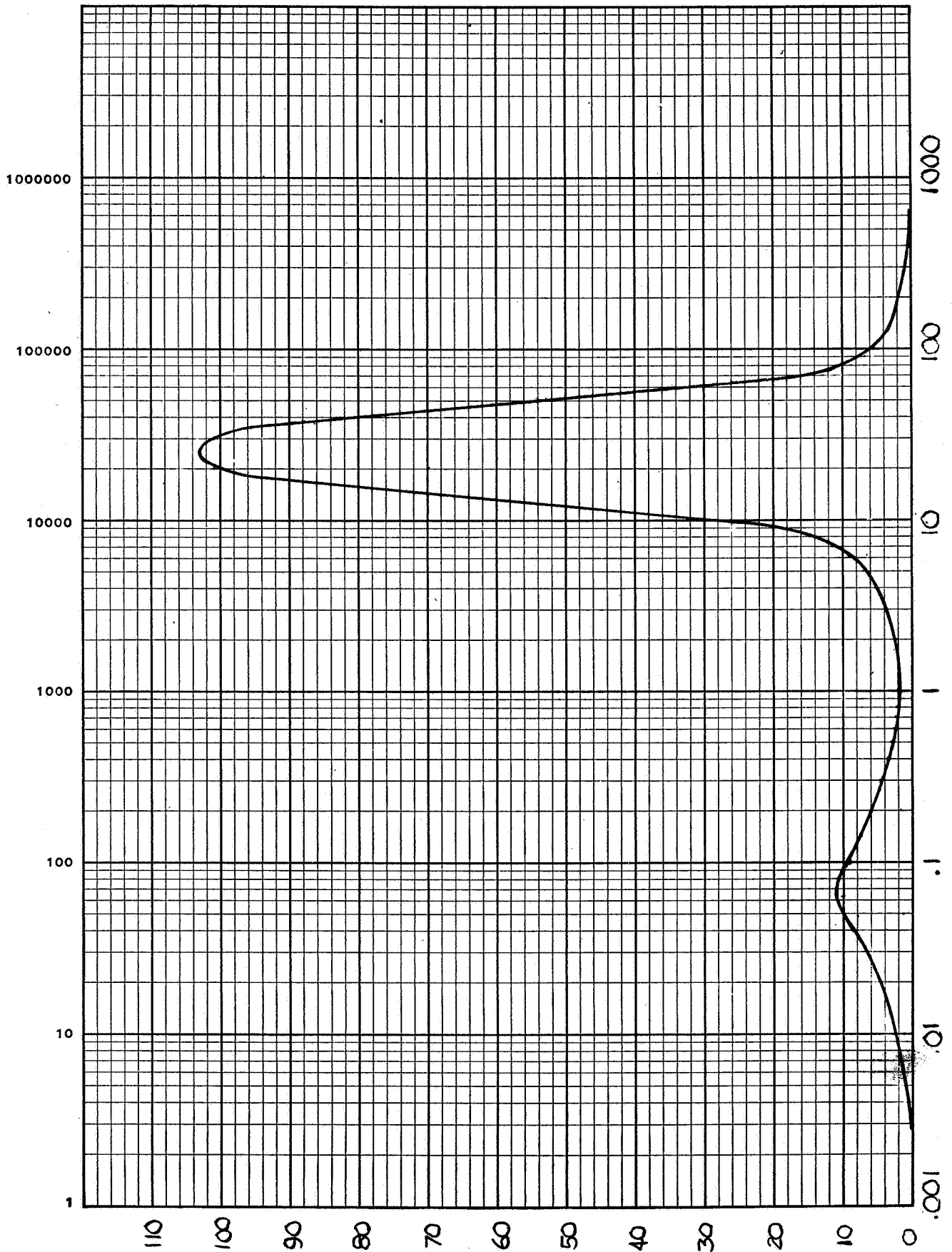


FIGURE D12 PARTICLE SIZE DISTRIBUTION COMPACTED CINDERS

VALUES OF N

1-LOG MIC 159-8  
FEL & CO. MADE IN U.S.A.  
7 CYCLES X 60 DIVISIONS

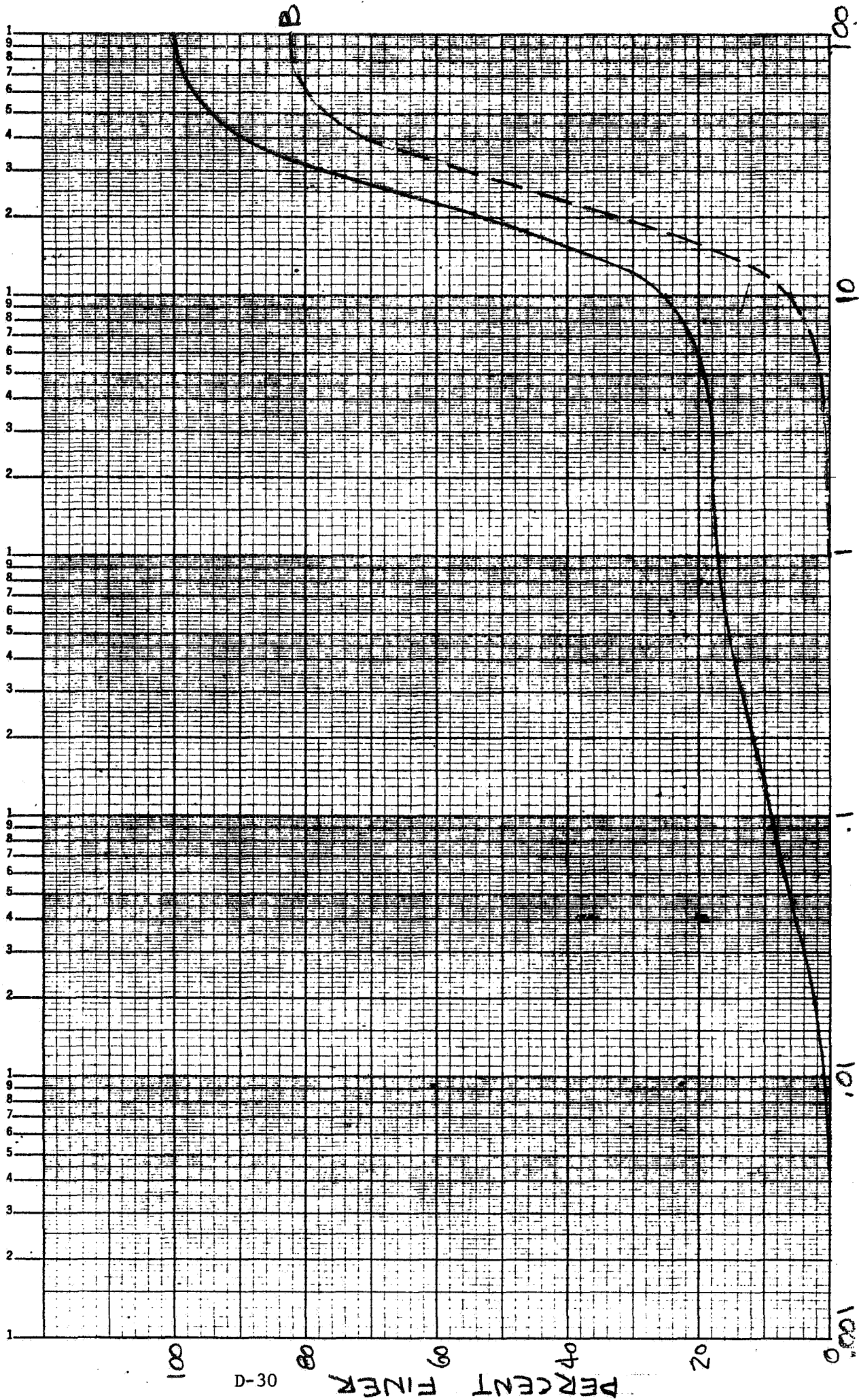


FIGURE D13 COMPACTED CINDERS SUMMATION CURVE  
 DATE

#### D.2.1.4 TEST SITE F, DESERT PAVEMENT

This soil model was analyzed in two ways. Originally a distribution was determined only for that material passing through a 10 mesh screen. This was the type data presented in the 5th monthly progress report and is shown in Figure D-14. Four separate samples of this control sample were sieved and are shown as the experimental points. The tight grouping of these points indicated that the sieving technique produced consistent results and a reasonably high confidence level in this data can be concluded. Figure D-15 shows the log-log plot of the distribution curve derived and the two subpopulations which were synthesized. This data is replotted in Figure D-16 on semilog paper. The integrated summation curve is given in Figure D-17. Based on this data, it would be concluded that this sample is a mixture of about 90 percent sand and 10 percent coarser grade of sand. In actual fact population A is the tail of a much coarser pebble population as will be seen.

Figure D-18 shows the summation curve for the total sample. Both the initial data curve and that derived through analysis are shown. Again it is noted that the shape of the curve is well preserved. Figure D-19 shows the distribution curve in the log-log plot and the synthesized subpopulations. The dashed curve is that derived for that portion of the sample below 2 mm in diameter. Again the shape of the distribution curve for the fine material is preserved but a distortion due to the overlap between populations A and B can be seen in the bulge on the coarse limb side of the curve. The semilog plot of this curve is given in Figure D-20 and the integrated summation curve is shown in Figure D-21. From this curve it is seen that population A comprises 53 percent of the total sample and population B comprises 47 percent of the total. In sieving this material to obtain the necessary data points, all the material above the 10 mesh screen was weighed and the percentage of the material in the sample larger than 2 millimeters was determined to be about 40 percent. If the point on the total summation curve in Figure D-21 at a particle size of 2 millimeters is read, it is seen that 59 percent of the total sample is less than 2 millimeters in size. This leaves 41 percent coarser than 2 millimeters which correlates exceptionally well with the initially measured experimental data. Referring back to Figure D-20, it is seen that this soil also has two peaks with one at 100 microns and the other at 4 to 5 millimeters. These are characteristic of sand and fine pebbles respectively.

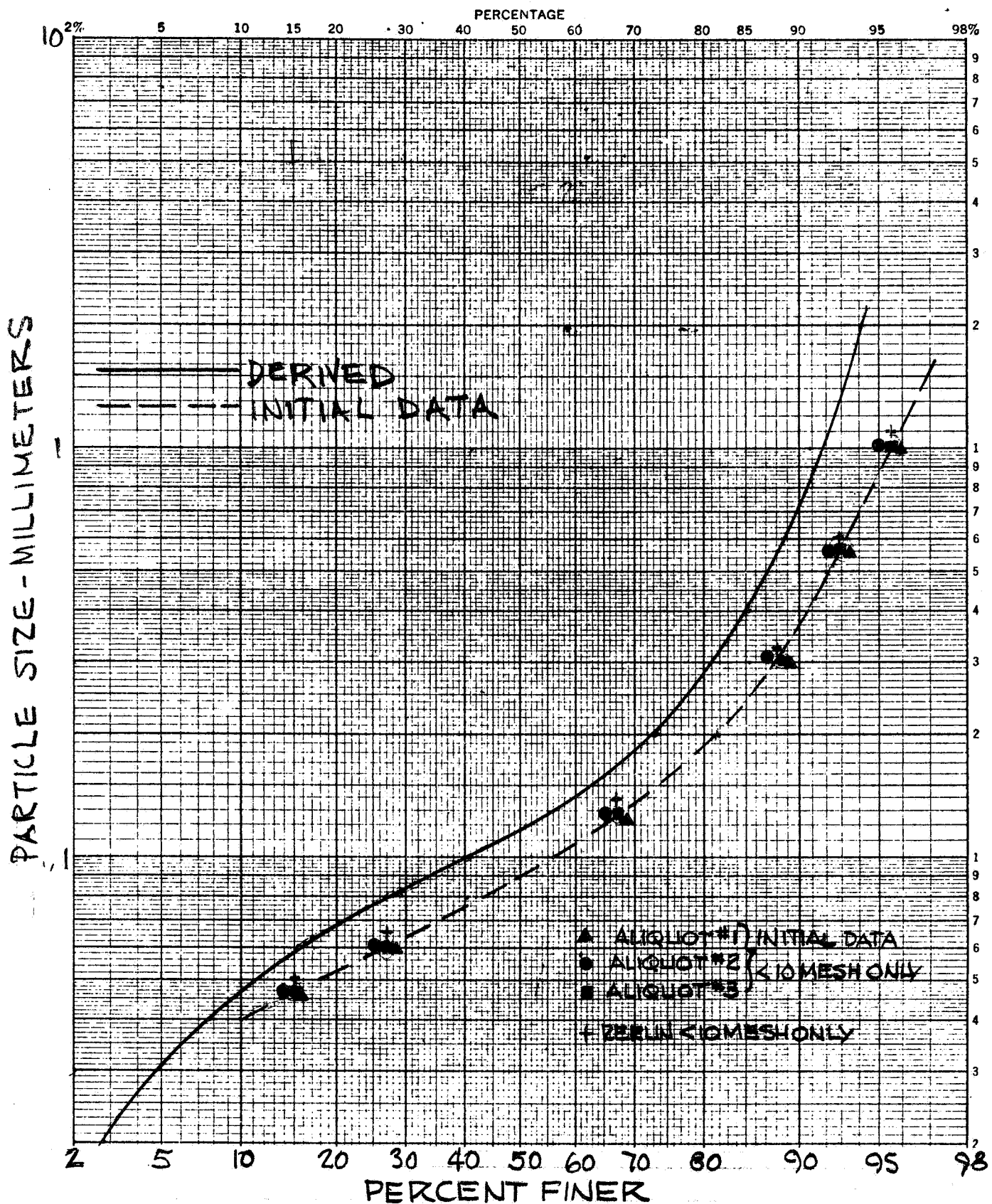
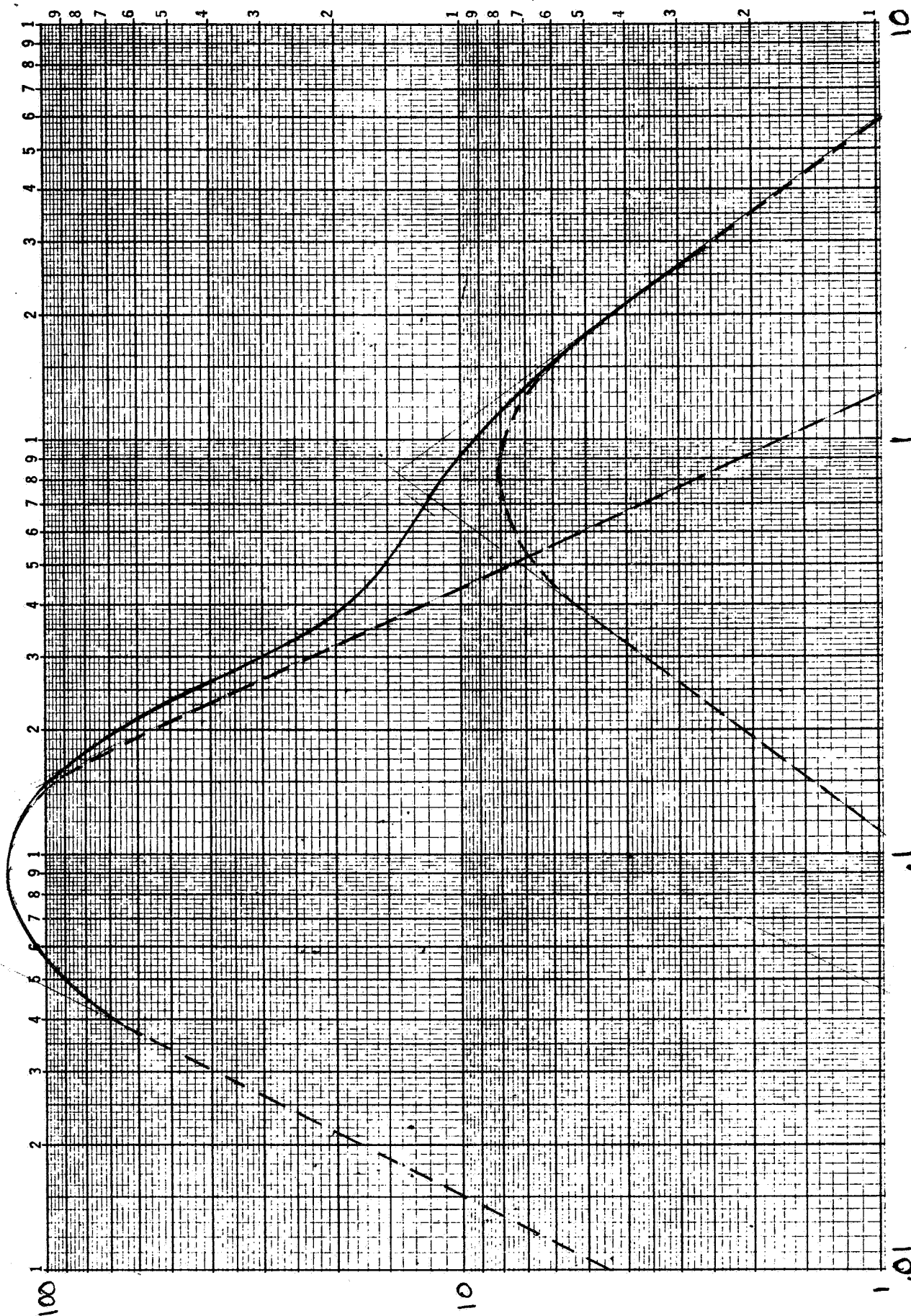


FIGURE D14 PARTICLE SIZE DISTRIBUTION  
DESERT PAVEMENT < 2MM DIAMETER





VALUES OF N

FIGURE D-15 PARTICLE SIZE IN MILLIMETERS  
PARTICLE SIZE DISTRIBUTION-DESERT PAVEMENT <2MM DIAMETER

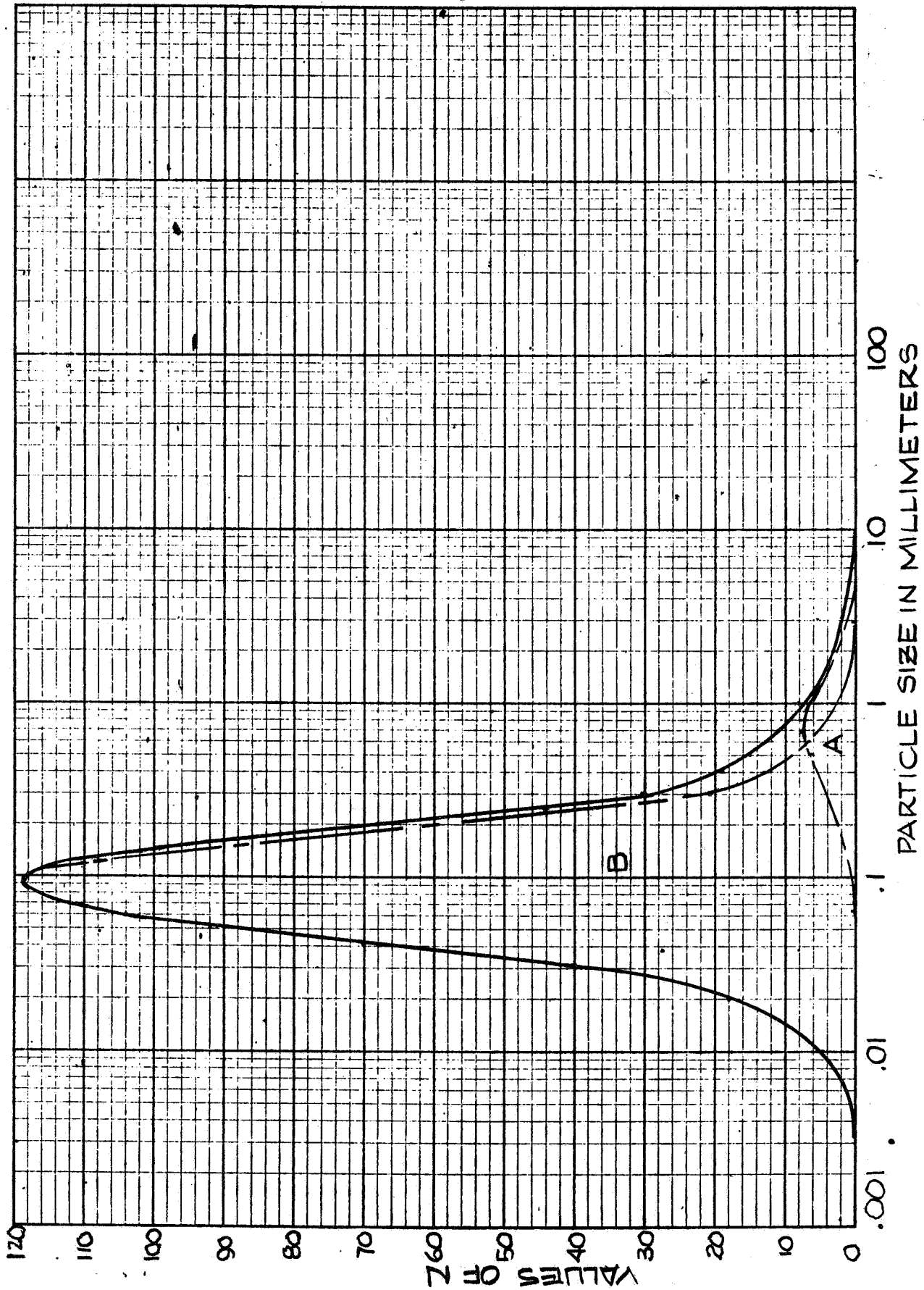


FIGURE D16 PARTICLE SIZE DISTRIBUTION DESERT PAVEMENT

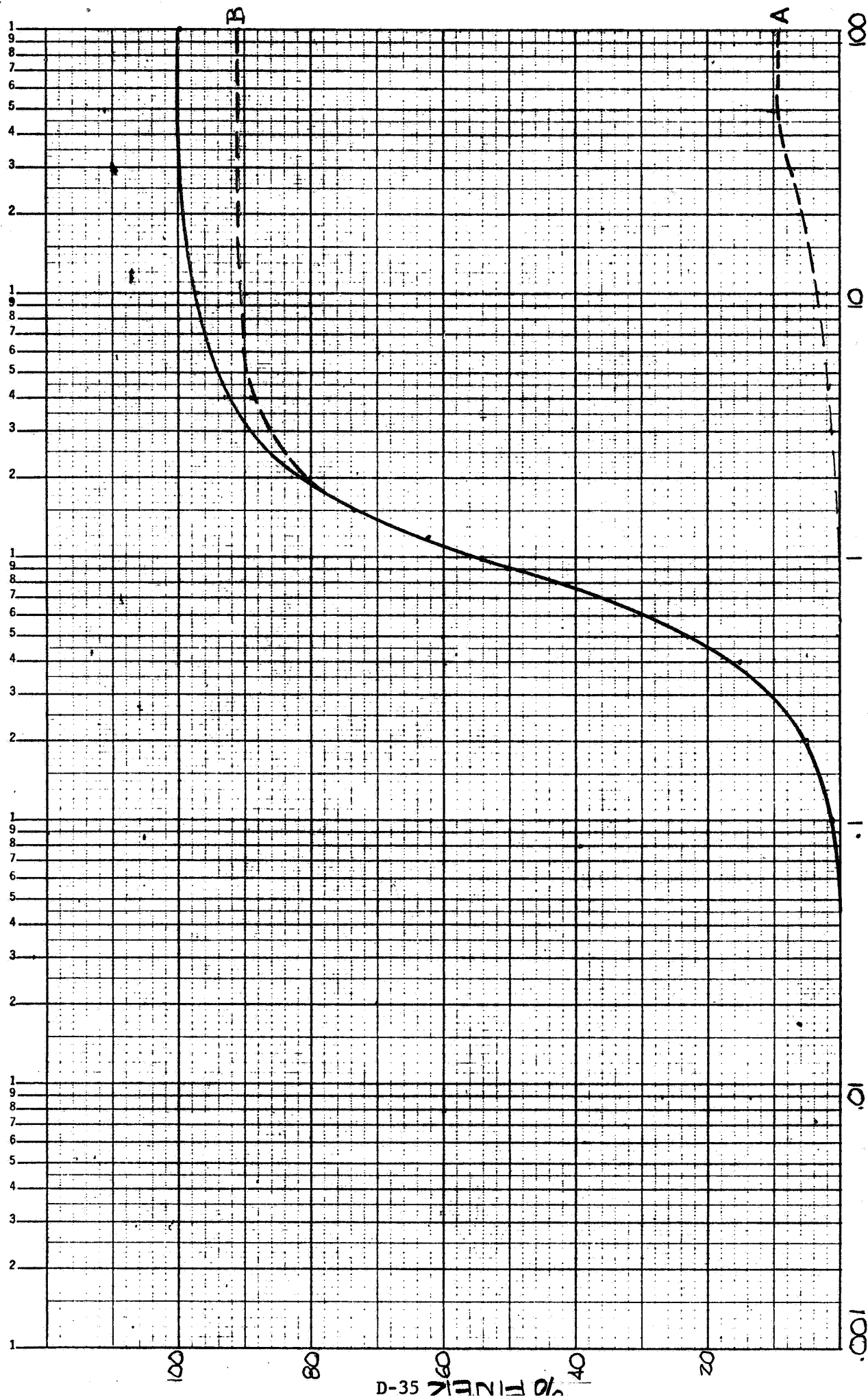


FIGURE D17 DESERT PAVEMENT < 2MM DIAMETER  
SUMMATION CURVE



PARTICLE SIZE - MILLIMETERS

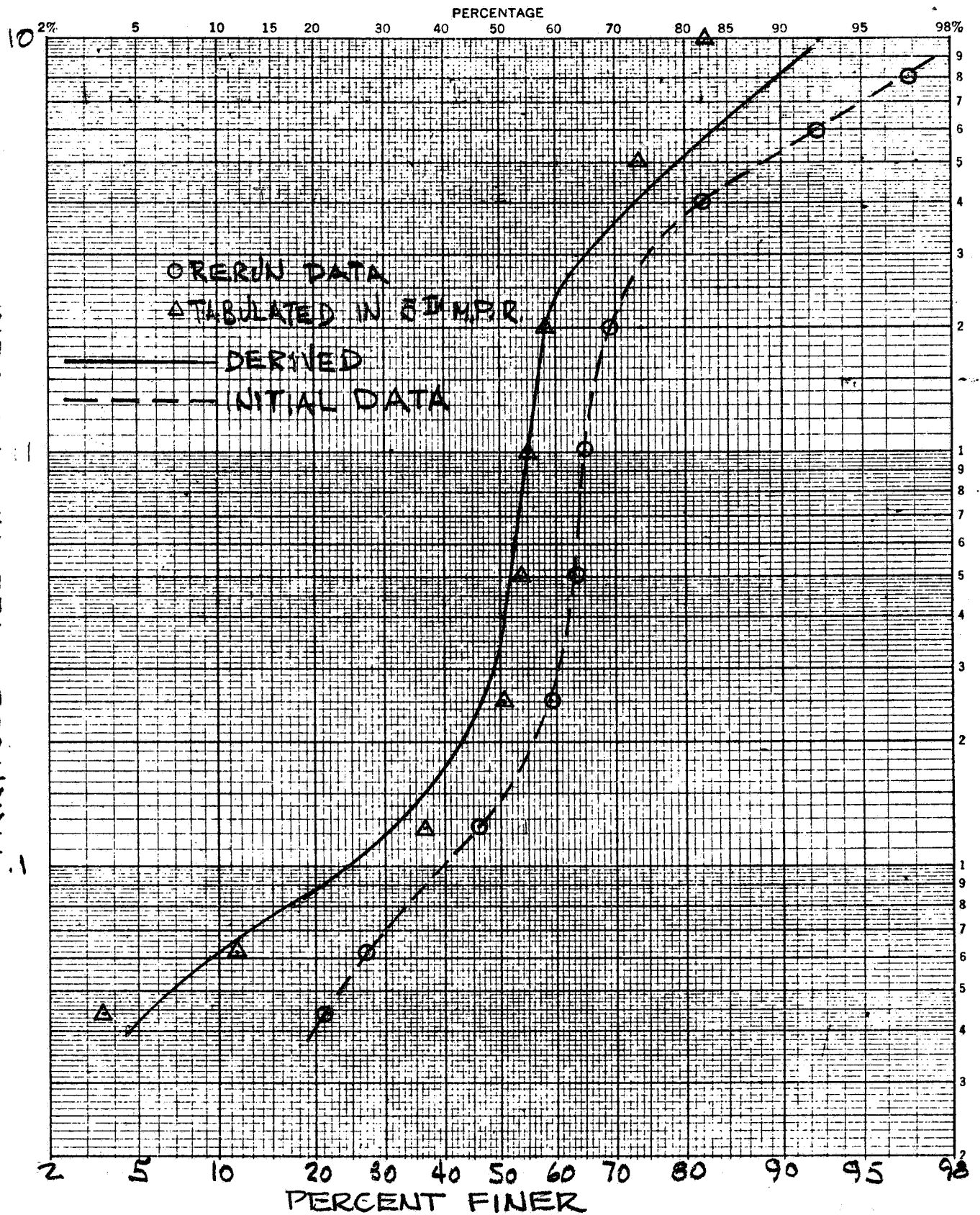


FIGURE D18 PARTICLE SIZE DISTRIBUTION  
 DESERT PAVEMENT-TOTAL SAMPLE

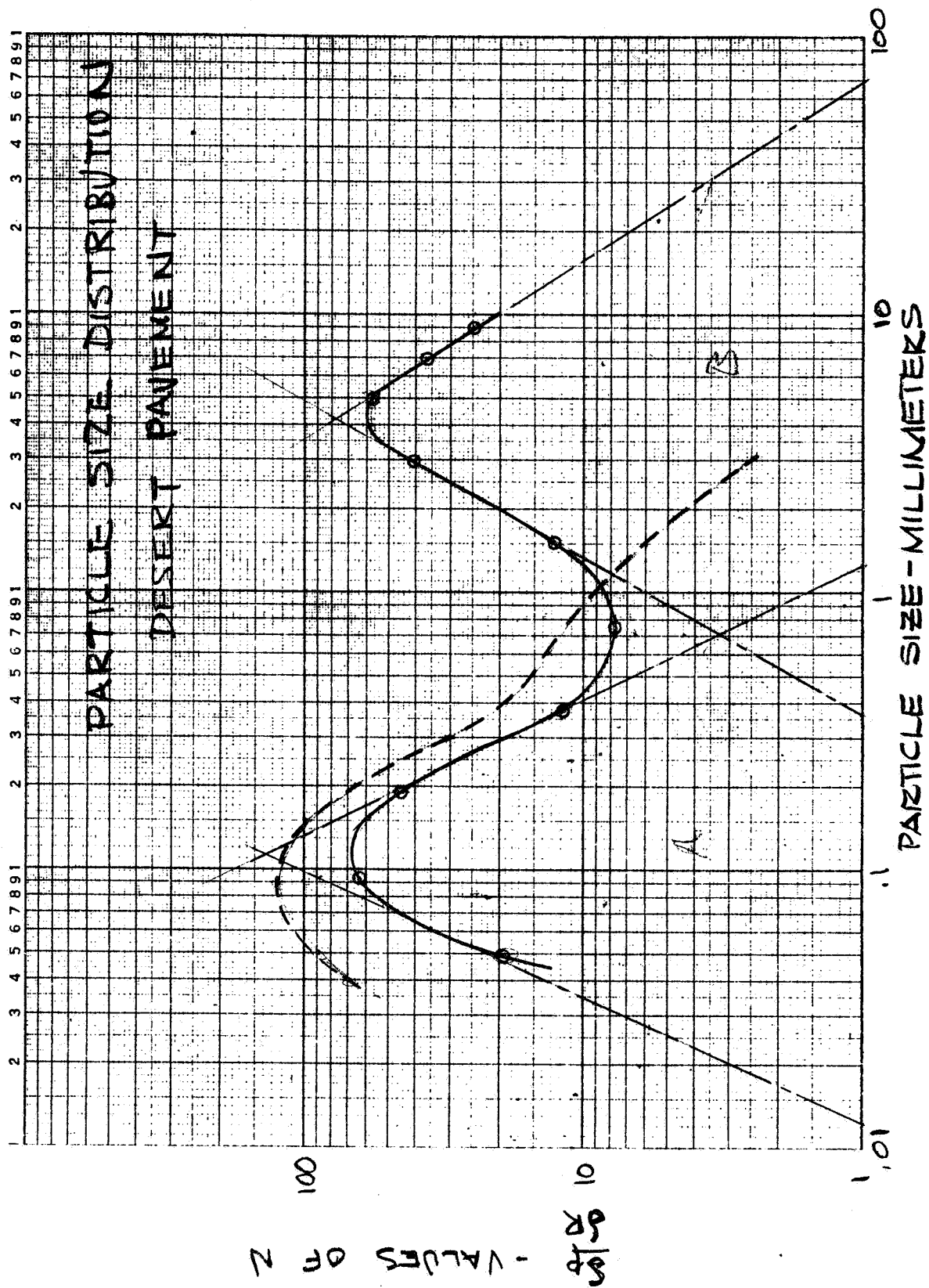


FIGURE D19 PARTICLE SIZE DISTRIBUTION - DESERT PAVEMENT

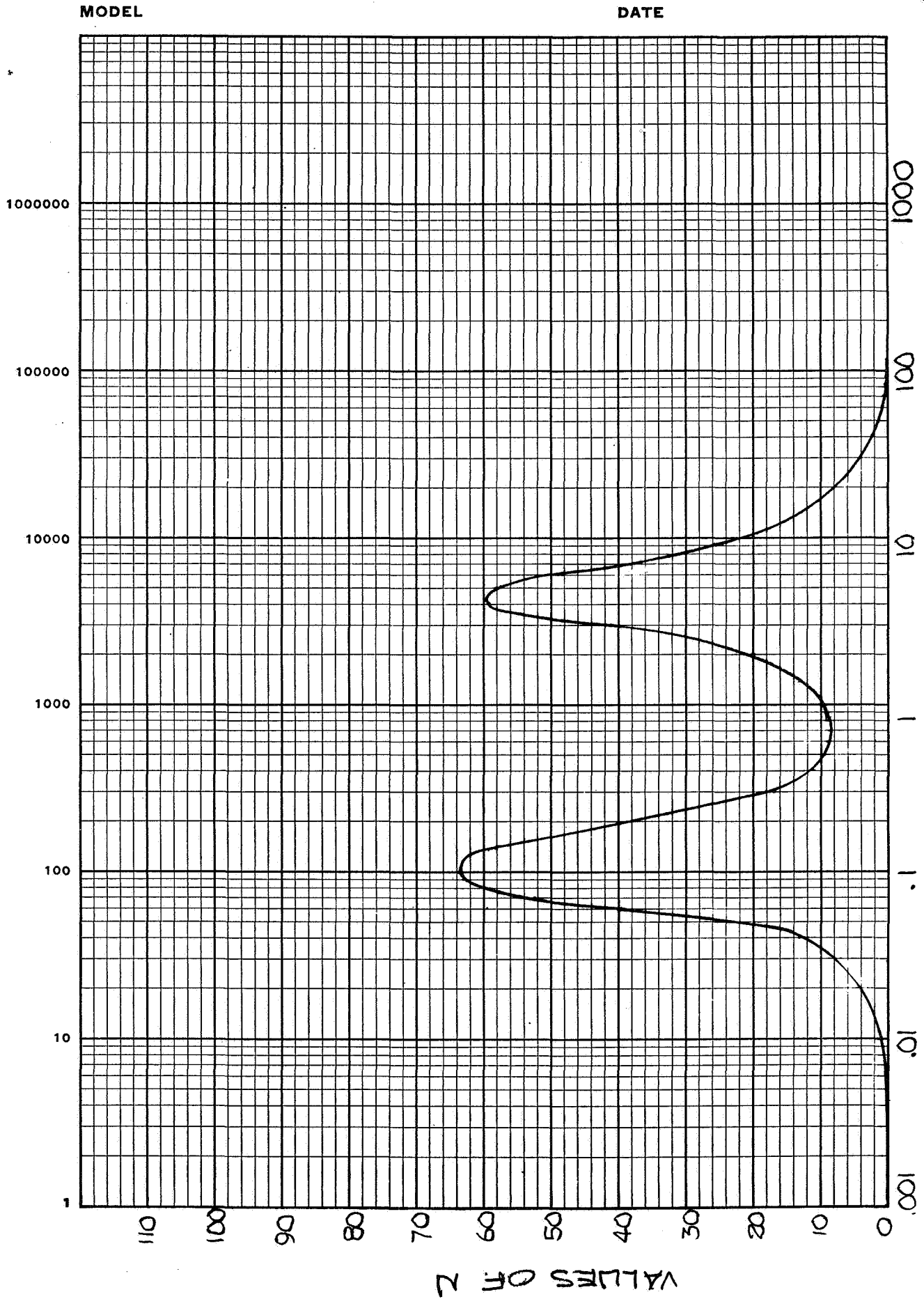
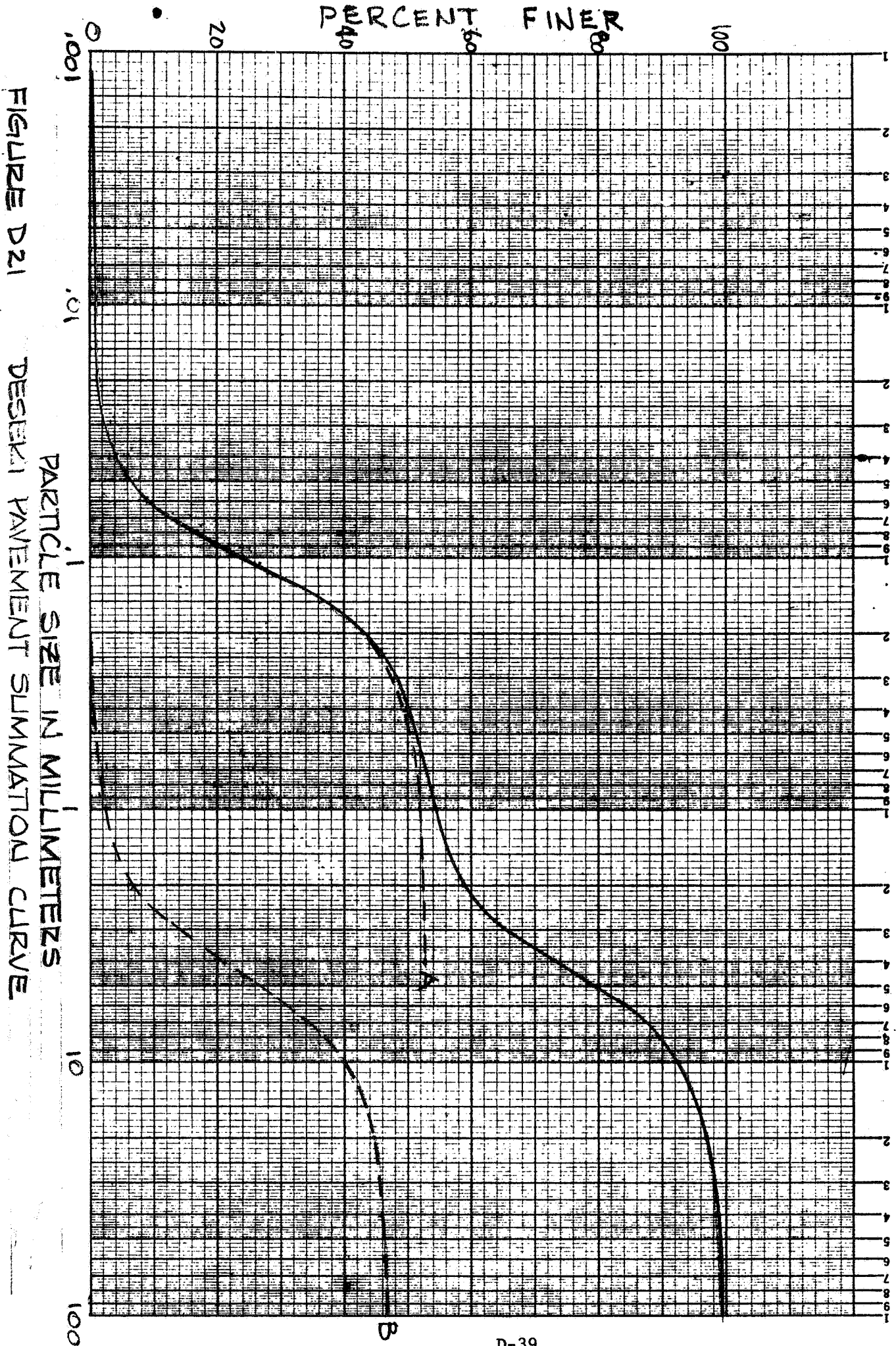


FIGURE D 20 PARTICLE SIZE IN MILLIMETERS  
 PARTICLE SIZE DISTRIBUTION DESERT PAVEMENT



### D.2.2 CLAY ANALYSIS

Control samples from the dunes, the duricrust, compacted cinders, and the desert pavement test sites were separated into clay (particles smaller than 2 microns) and silt-sand fractions using the Edwards-Bremner dispersion techniques and centrifugal sedimentation (Whittig, 1965). The assay procedure outlined in Table D-2 was used. The clay was recovered from the water used to wash the sand-silt particles by the addition of 10% magnesium chloride solution followed by high speed centrifugation. The duricrust, desert pavement, and compacted cinder silts required 3 washings to remove the clay from them using only one period of sonication. The clay was removed from the dune silt in 2 washings. Moreover, the clay removed from dune silt did not flocculate on addition of magnesium ion, indicating either high organic or unusual mineralogical composition. To confirm the correctness of the 5-minute sonication the clay fractionation was performed on replicate specimens one of which received a 5 minute sonic treatment and the other a 10 minute sonic treatment. The results are shown in Table D-3.

TABLE D-3  
CLAY CONTENT OF SELECTED SOIL SPECIMENS

Specimen	Period of Sonication, min	Weight of Clay, g	Weight of Silt-Sand, g	Clay Content, per cent
A-Dune Sand Control	5	0.0757	4.1426	1.8
	10	0.1335	5.0823	2.6
B-Duricrust Control	5	0.9124	4.4492	17.0
	10	0.6212	1.9909	23.8
F-Desert Pavement Control	5	0.3458	4.5295	7.1
	10	0.3822	3.8083	9.1
E-Compacted Cinder Control	5	0.3889	9.0524	4.1
2B2	5	1.4673	8.2613	15.1
9B2	5	1.1967	7.0706	14.5
10B2-1	5	0.2556	2.1727	10.5
10B2-2	5	0.9267	5.2186	15.1
10B3X	5	0.3636	2.0177	15.3
10B4	5	0.4717	9.0101	5.0

The effect of sonication beyond 5 minutes' duration appears to be that of breaking up the silt particles so that the sediment density is decreased and the number of large clay particles increased. The amount of clay found in the specimens receiving 5-minute treatments correlates roughly with the amount of clay minerals found in the same specimens by X-ray diffraction analysis. In the case of the dunes silt-sand, the sedimentation estimate of the clay content is possibly high because the material which has a clay-like sedimentation rate does not coagulate with divalent ions as clay minerals should. Part of this material may be organic or disintegrated feldspar or mica silt particles. It is important to note that a good correlation was obtained for the clay content derived by the above method and that obtained by estimates from the X-ray diffraction analysis.

The experimental results indicate that samplers 2 and 9 collect soil specimens containing approximately the same clay content as the control specimen. The gravity dump collected sample obtained by sampler 10 in run number 10B2-2 also did not affect the clay content of the soil. However, the pneumatically collected sample taken by this sampler during the sampling run designated as 10B2-1 indicates a 30 percent loss in clay content. This loss is probably due to clay size material being ejected at the outlet of the cyclone collector. The effluent from the cyclone collector for sampler 10 was collected during the gravity dump cycle for the third run at the duricrust site which is designated 10B3X in Table D-3. It is noted that the clay content of this sample is approximately the same as the control indicating that the heavy effluent observed to emanate from the cyclone collector and blower of this sampler was not selectively rejecting clay at this time. It should be reiterated that the funnel outlet tended to clog allowing the chamber to fill itself rather full. Continual rapping was required to cause the soil sample to fall out of the funnel into the collection bottle. Thus, at least intermittently the outlet to the cyclone was the only means of exit from the collector. This fact, coupled with the reduced efficiency of the cyclone because of the large quantity of soil in the funnel and cylindrical portion of the cyclone collector, undoubtedly explains the nonselective loss of sample through the outlet to the cyclone collector and the blower.

Because the finest clay particles were concentrated on the very surface of the duricrust test site, even the control sample could not be representative of the material which each sampler attempted to acquire. For example, sampler 2 abrades only the top surface to a depth less than one millimeter while sampler 9 collected to a depth of 32 millimeters. Sampler 10 samples to a depth of 1 to 2 millimeters which is also very shallow. The effect of wind on this sampler is indicated by wind run 10B4 [1] shows that two-thirds of the clay fraction was lost during acquisition. This is interesting since the wind did not cause any apparent degradation in the total weight of sample collected, yet apparently removed the clay size material during acquisition by the wire brush.

Clay analyses on samples collected by the sampler mechanisms were not performed for the other test sites.

### D.2.3 MINERALOGICAL COMPOSITION

The mineralogical composition of the sieved and sonically separated fractions of the soil models representing each test site are shown on Tables D-4 to D-9.

#### KELSO DUNES AREA

##### Soil Model A, Dune Sand

The typical dune sand control sample lacked particles in the plus 10 mesh ( $> 2$  mm) and the minus 325 mesh ( $< 44\mu$ ) range. The composition of particles in the sand and silt range are shown on Table D-4. A clay separation was performed and a small residue derived. However, this residue did not coagulate with divalent ions as clay minerals should. Most of this material may be organic and/or sonically disintegrated feldspar or mica particles and hydrated, grain-coating, mineral oxides. Beneath the microscope, no clay-size particles were observed.



TABLE D-4  
SOIL MODEL A, KELSO DUNE SAND, CONTROL SAMPLE  
COMPOSITION

Caught on Sieve No.	Quantity grams	Description
10	--	No pebbles or gravel present.
18	.01	Yellow to tawny, slightly iron-stained, subangular to subrounded, pitted, frosted, very coarse sand: $\alpha$ quartz - 100%
35	.58	Coarse sand with the following composition: $\alpha$ quartz species - 99% (a) Pale to deep yellow to orange to light brown, iron-stained, subrounded to well rounded, highly frosted grains - 35% (b) Glassy, transparent, unfrosted, subangular (probably local Granite Mountains source) grains - 30% (c) Milky white, well rounded, highly frosted grains - 25% (d) Greasy gray to glassy translucent, subrounded and pitted in intimate association with weakly magnetic ilmenite - 9% Magnetite; strongly magnetic, black, well rounded grains - 1% Apatite; pale green, well rounded grains - Trace Garnet; greasy purplish-red, subrounded to well rounded, highly frosted grains - Trace Tourmaline (?); nonmagnetic, black, well rounded rods - Trace Biotite; golden to dark brown flakes - Trace
60	13.91	Medium sand, as above, abundance percentages as above.
120	5.98	Fine sand, as above: $\alpha$ quartz species - 85% Ilmenite w/quartz - 8% Magnetite - 6% Biotite - 1% Apatite, garnet and tourmaline - Trace
230	1.40	Very fine sand, as above: $\alpha$ quartz species - 80% Magnetite - 15% Ilmenite - 4% Tourmaline - 1% Apatite, biotite, and garnet - Trace
325	.10	Silt similar in composition to above sand but tending to be more angular: $\alpha$ quartz species - 80% Magnetite - 10% Tourmaline - 5% Ilmenite - 5% Apatite, biotite and garnet - rare
Cup	.03	Silt, as above, almost wholly angular: $\alpha$ quartz species - 90% Magnetite - 5% Ilmenite - 3% Tourmaline - 2% Apatite and garnet - rare No very fine silt or clay size particles present
Total	22.01	



## PISGAH CRATER AREA

### Soil Model B, Dry Lake Duricrust

Two analyses are provided for this material as shown on Figures D-7 to D-9 presented earlier in this appendix. The gross control sample analysis, denotes the character of the gross sample derived from sieving. This material contains most of the clay and fine silt fractions, bound by moisture and calcite, in the form of "duricrust flakes" which form a large percentage of the sand-size fractions ( $62\mu < d < 2\text{mm}$ ). Table D-5 gives the composition of this gross sample. Another control sample analysis, labeled B on Figures D-7 to D-9, was performed after the "duricrust flakes" had been dispersed and the clay fraction isolated. Table D-6 gives the absolute composition of the Pisgah Playa Lake duricrust soil.

### Soil Models C and D, Pahoehoe and Aa Basalt

The average compositions of Pisgah Crater pahoehoe and aa basalts are essentially identical. The average composition of these flow phase olivine basalts is given in Table D-7.

TABLE D-7

COMPOSITION OF PISGAH CRATER OLIVINE BASALT

Mineral Group	Mineral	Percent	
Plagioclase feldspar		35	
	Andesine		20
	Anorthite		15
Pyroxene		40	
	Augite		25
	Hypersthene		15
Accessory minerals		25	
	Olivine		20
	Magnetite		5
		100%	100%

TABLE D-5

SOIL MODEL B, PISGAH PLAYA LAKE, CONTROL SAMPLE  
COMPOSITION OF GROSS SAMPLE AFTER DRY SIEVING

Caught on Sieve No.	Quantity grams	Description
10	0.01	Black to dark brown, vesicular to pitted, angular olivine basalt pebbles; many pits and vesicles filled with very fine grained, slightly altered feldspar and/or limonite; and white, microcrystalline, angular $\alpha$ quartz grains. Basalt - 65% $\alpha$ quartz - 35%
18	0.02	Very coarse sand and duricrust flakes as follows: Basalt - 5% $\alpha$ quartz species (60%) (a) White to yellow-brown, subangular to subrounded grains - 40% (b) Water white, transparent, angular to subangular grains - 15% (c) White to yellow to light brown to dark red, iron-stained, microcrystalline, rounded grains - 5% (d) Milky white, angular to subangular grains - Trace (e) Greasy gray to purplish gray, subangular to subrounded grains - Trace Duricrust flakes; small tabular plates composed of clay-size grains weakly cemented with calcite - 30% Biotite, golden to dark brown, eroded "books" and flakes - 5% Organic debris (small stem fragments, frayed vegetable fibers) - Trace
35	0.26	Coarse sand and duricrust flakes as above.
60	4.13	Medium sand and duricrust flakes as above with some earthy red basalt cinder grains: Basalt grains - Trace Basalt cinders - 5% $\alpha$ quartz grains - 50% Duricrust flakes - 40% Biotite flakes - 5% Organic debris - Trace
120	6.38	Fine sand and duricrust flakes as above with an increased amount of basalt cinders and angular, water white $\alpha$ quartz grains: Basalt cinders - 15% $\alpha$ quartz species (55%): (a) 10% (b) 40% (c) Nil (d) 5% (e) Tr Duricrust flakes - 20% Biotite flakes - 10%
230	7.86	Very fine sand and duricrust flakes as above: Basalt cinders - 5% $\alpha$ quartz grains - 35% Duricrust flakes - 50% Biotite flakes - 10%
325	2.13	Silt, identical in composition to the very fine sand above.
Cup	0.88  (0.66)  (0.22)	The -44 $\mu$ sample present in the cup can be tentatively divided into silt and clay fractions as follows: 4 $\mu$ - 44 $\mu$ : Very fine silt fraction Very fine angular $\alpha$ quartz grains - 50% Andesine and anorthite grains - 45% Biotite - 5% < 4 $\mu$ : Clay fraction Monmorillonite (60%) and chlorite (40%) - 100%
Total	21.67	Note: This description covers a gross sample in the form collected; when the duricrust flakes are broken down the grain-size percentages will change markedly. See Table D-6.

TABLE D-6

SOIL MODEL B, PISGAH PLAYA LAKE, CONTROL SAMPLE  
COMPOSITION AFTER DISPERSION AND SEDIMENTATION TREATMENT

Caught on Sieve No.	Quantity Grams	Description
10	0.010	Very fine basalt and quartz pebbles, as before. Basalt - 65% $\alpha$ quartz - 35%
18	0.014	Very coarse sand as follows: Basalt - 8% $\alpha$ quartz species (85%): (a) 57% (b) 21% (c) 7% (d) Tr (e) Tr Biotite - 7% Organic debris - Trace
35	0.182	Coarse sand identical to above.
60	2.478	Medium sand with some earthy red basalt cinder grains: Basalt - Trace Basalt cinders - 9% $\alpha$ quartz species (82%): (a) 55% (b) 20% (c) 7% (d) Tr (e) Tr Biotite - 9% Organic debris - Trace
120	5.104	Fine sand with increasing basalt cinder and water white, angular $\alpha$ quartz grains: Basalt cinders - 19% $\alpha$ quartz species (68%): (a) 12% (b) 50% (c) Nil (d) 6% (e) Tr Biotite - 13%
230	3.930	Very fine sand: Basalt cinders - 10% $\alpha$ quartz species (70%): (a) 12% (b) 51% (c) None (d) 7% (d) Tr Biotite - 20%
325	1.870	Coarse silt identical to very fine sand above.
4 $\mu$ - 44 $\mu$	4.376	Medium to fine silt as follows: $\alpha$ quartz species (50%): (a) 9% (b) 36% (c) None (d) 5% (e) Tr Andesine and anorthite grains - 45% Biotite - 5%
<4 $\mu$	3.706	Clay as follows: Montmorillonite - 60% Chlorite - 40%
Total	21.67	Note: This description illustrates the completely broken-down composition of the Pisgah Playa Lake duricrust soil.

#### Soil Model E, Compacted Basalt Cinders

The compacted basalt cinders control sample, when analyzed by dry sieving and clay dispersal and sedimentation processes, yielded a composition for each grain-size fraction isolated that is given in Table D-8. The composition of the basalt cinders is basically similar to the average composition of the olivine basalt flow phase material denoted in Table D-7.

#### Soil Model F, Desert Pavement

The composition of the desert pavement control sample is given in Table D-9. The basalt pebbles are wholly pahoehoe flow phase basalt, hence of identical composition to that shown for the parent material in Table D-7.

TABLE D-8  
SOIL MODEL E, COMPACTED BASALT CINDERS, CONTROL SAMPLE  
COMPOSITION

Caught on Sieve No.	Quantity grams	Description																														
10	82.30	Dark brown to deep reddish brown, very angular, very porous and pitted, slightly limonite stained, basalt cinder pebbles, and micro-bombs as follows: <table><tr><th>No. fragments</th><th>Type</th><th>Max. dimensions, cm</th></tr><tr><td>(34.0) { 1</td><td>Cinder</td><td>4.3</td></tr><tr><td>1</td><td>Bomb</td><td>4.1</td></tr><tr><td>(10.6) 2</td><td>Cinders</td><td>3.0 - 4.0</td></tr><tr><td>(13.1) 3</td><td>Cinders</td><td>2.0 - 3.0</td></tr><tr><td>(11.8) 11</td><td>Cinders</td><td>1.5 - 2.0</td></tr><tr><td>( 7.0) 18</td><td>Cinders</td><td>1.0 - 1.5</td></tr><tr><td>( 3.1) 20</td><td>Cinders</td><td>0.75 - 1.0</td></tr><tr><td>( 1.4) 23</td><td>Cinders</td><td>0.50 - 0.75</td></tr><tr><td>( 1.3) 68</td><td>Cinders</td><td>0.20 - 0.50</td></tr></table>	No. fragments	Type	Max. dimensions, cm	(34.0) { 1	Cinder	4.3	1	Bomb	4.1	(10.6) 2	Cinders	3.0 - 4.0	(13.1) 3	Cinders	2.0 - 3.0	(11.8) 11	Cinders	1.5 - 2.0	( 7.0) 18	Cinders	1.0 - 1.5	( 3.1) 20	Cinders	0.75 - 1.0	( 1.4) 23	Cinders	0.50 - 0.75	( 1.3) 68	Cinders	0.20 - 0.50
No. fragments	Type	Max. dimensions, cm																														
(34.0) { 1	Cinder	4.3																														
1	Bomb	4.1																														
(10.6) 2	Cinders	3.0 - 4.0																														
(13.1) 3	Cinders	2.0 - 3.0																														
(11.8) 11	Cinders	1.5 - 2.0																														
( 7.0) 18	Cinders	1.0 - 1.5																														
( 3.1) 20	Cinders	0.75 - 1.0																														
( 1.4) 23	Cinders	0.50 - 0.75																														
( 1.3) 68	Cinders	0.20 - 0.50																														
18	0.59	Irridescent black, dull tan to lustrous brown and lustrous dark red to earthy red basalt cinder sand, very angular, very porous, highly vesicular and pitted; many pits and vesicles filled with very fine grained, slightly altered feldspar and/or limonite. Basalt cinders - 100%																														
35	0.71	Coarse basalt cinder sand as above with trace of organic debris (stem fragments and frayed vegetable fibers).																														
60	0.88	Medium basalt cinder sand as above with some $\alpha$ quartz grains and mica flakes as follows: Basalt cinders - 75% $\alpha$ quartz species - (20%): (a) Snow white to yellow to tan, subrounded grains - 15% (b) Water white, transparent, angular to subangular grains - 5% (c) Snow white to yellow to pink, microcrystalline, rounded to well rounded grains - Trace Biotite, golden yellow to dark brown, cleavage flakes - 5%																														
120	2.10	Fine basalt cinder and $\alpha$ quartz sand with mica flakes as above: Basalt cinders - 60% $\alpha$ quartz species as above (25%): (a) 5% (b) 15% (c) 5% Biotite flakes as above - 15%																														
230	2.71	Very fine basalt cinder and $\alpha$ quartz sand as above: Basalt cinders - 35% $\alpha$ quartz species as above (60%): (a) 15% (b) 40% (c) 5% (d) Greasy gray to purplish gray, subangular to subrounded grains - Trace Biotite flakes as above - 5% Free magnetite grains - Trace Anorthite, greasy gray, subrounded, frosted laths - Trace																														
325	1.44	Silt composed of the following materials: $\alpha$ quartz species, tending to be angular to subangular (90%): (a) 25% (b) 45% (c) 20% (d) Trace Biotite flakes - 10% Free magnetite grains - Trace Anorthite laths - Trace																														
Cup	1.30	The -44 $\mu$ material present in the cup can be divided into silt and clay fractions as follows:																														
	(0.90)	4 $\mu$ - 44 $\mu$ : Very fine silt fraction Very fine angular $\alpha$ quartz grains - 55% Andesine and anorthite grains - 45%																														
	(0.40)	< 4 $\mu$ : Clay fraction Montmorillonite (60%) and chlorite (40%) - 100%																														
Total	92.03																															

TABLE D-9

SOIL MODEL F, PISGAH CRATER DESERT PAVEMENT, CONTROL SAMPLE  
COMPOSITION

Caught on Sieve No.	Quantity grams	Description
10	12.70	Very angular, highly pitted olivine basalt pebbles as follows; surface pavement material; <div><div>No. fragments</div><div>Max. dimensions, cm</div></div> <div><div>(3.7)</div><div>1</div><div>2.8</div></div> <div><div>(1.6)</div><div>4</div><div>1.0 - 1.25</div></div> <div><div>(2.8)</div><div>14</div><div>0.5 - 1.0</div></div> <div><div>(4.6)</div><div>159</div><div>0.2 - 0.5</div></div>
18	0.86	Very angular, highly pitted fragments of olivine basalt and black to dark red, dull earthy to vitreous to iridescent pumaceous basalt cinders; many pits filled with very fine grained, slightly altered feldspar and/or limonite; 60% surface pavement and 40% subsurface material: Basalt and basalt cinders - 100%
35	0.61	Coarse basalt and basalt cinder sand as above with white, translucent, sub-angular and light tan, iron-stained, subrounded, highly frosted $\alpha$ quartz grains; wholly subsurface material: Basalt and basalt cinders - 90% $\alpha$ quartz - 10%
60	0.88	Medium black and red basalt cinder and black basalt sand as above (50%) with $\alpha$ quartz sand (40%) having the following composition: $\alpha$ quartz species: <div><div>(a)</div><div>Snow white to yellow to pink, microcrystalline, rounded to well rounded grains - 25%</div></div> <div><div>(b)</div><div>Milky, subangular grains - 10%</div></div> <div><div>(c)</div><div>Water white, transparent, angular to subangular grains - 5%</div></div> <div><div>(d)</div><div>Greasy gray to purplish gray, subangular to subrounded grains - Trace</div></div> Golden yellow to dark brown cleavage plates of biotite - 10% Andesine-anorthite, greasy gray, subrounded laths, frosted - Trace Organic debris (seeds, small stems) - Trace Note: Basalt fragments are weakly magnetic due to magnetite content.
120	4.12	Fine basalt, basalt cinder, and $\alpha$ quartz sand as above: Basalt and basalt cinders - 25% $\alpha$ quartz grains as above - 60% Biotite - 15% Free magnetite grains - Trace Andesine-anorthite laths, greasy gray, subrounded, frosted - Trace
230	7.63	Very fine basalt cinder and $\alpha$ quartz sand as above: Basalt cinders - 20% $\alpha$ quartz grains tending to be angular to subangular - 75% Biotite - 5% Free magnetite grains - Trace
325	2.36	Silt composed of the following: Basalt cinders, earthy red - 10% $\alpha$ quartz species (85%): <div><div>(a)</div><div>Snow white to yellow, subrounded grains - 45%</div></div> <div><div>(b)</div><div>Water white, transparent, angular grains - 25%</div></div> <div><div>(c)</div><div>Milky white, subangular grains - 15%</div></div> Free magnetite grains - 5% Andesine-anorthite laths, subrounded, frosted - Trace Biotite flakes - Trace
Cup	1.10  (0.50)  (0.60)	The -44 $\mu$ sample can be divided into silt and clay fractions as follows:  4 $\mu$ - 44 $\mu$ : Very fine silt fraction Very fine angular $\alpha$ quartz grains - 70% Andesine and anorthite grains - 30%  < 4 $\mu$ : Clay fraction Montmorillonite (55%) and chlorite (45%) - 100%
Total	21.18	

This page intentionally blank.

D.3.1 TEST SITE A, KELSO DUNE SAND

Particle Size Distribution Curves



### D.3 FIELD SAMPLE DISTRIBUTION CURVES

This section presents the curves obtained for those sampler mechanisms which acquired a sufficiently large sample to justify a particle size analysis. In general a summation or percentage finer curve is given on one page and the facing page has the corresponding distribution curve, where it exists. Distribution curves were not derived where inspection of the summation curve was adequate to arrive at a conclusion. These curves are grouped according to the test site to which they apply. At the beginning of each group will be a short subparagraph which will serve to act as dividers and also to summarize the salient points for that group. Within a group, the curves are arranged in a sequence corresponding to the sampler number assigned to each mechanism in the body of the text.

#### D.3.1 TEST SITE A, KELSO DUNE SAND

This section contains Figures D-22 through D-25 for samples taken at test site A. In general most of the samplers appear to sample this soil without severe alteration of the distribution which is to be expected. Only samplers numbers 1, 2 and 10 appear to have collected samples with altered distributions. The alteration observed for sample run 1A3¹, Figures D-22 and D-23, and 10A7¹, Figures D-32 and D-38, could be attributed to the effect of the wind blowing the fines away, since the distribution appears to have narrowed with the peak moving to a coarser grain size. This same effect is noted to a lesser degree for run 10A3 with no wind. Here the effect may be due to the sorting action of the cyclone collector since a loss of fines is indicated.

Sampling run 2A3, Figures D-24 and D-25, is unique in that the peak has shifted to a finer grain size and the distribution has broadened considerably. This result is to be expected since the perforations in the cylinder at which the soil enters will exclude the larger grains in preference to the fines.

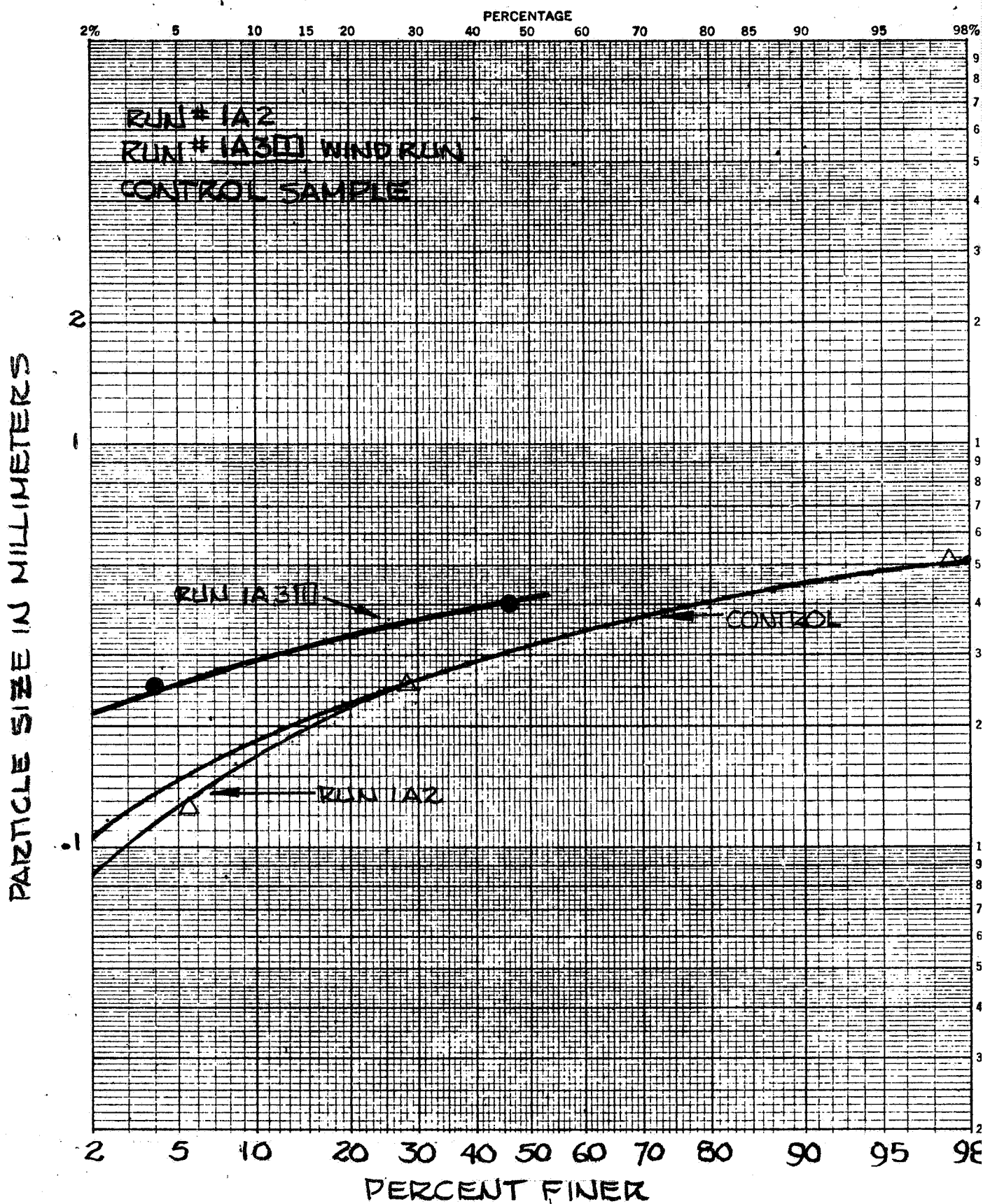


FIGURE D22. PARTICLE SIZE SUMMATION CURVE  
KELSO DUNE SAND

MODEL

DATE

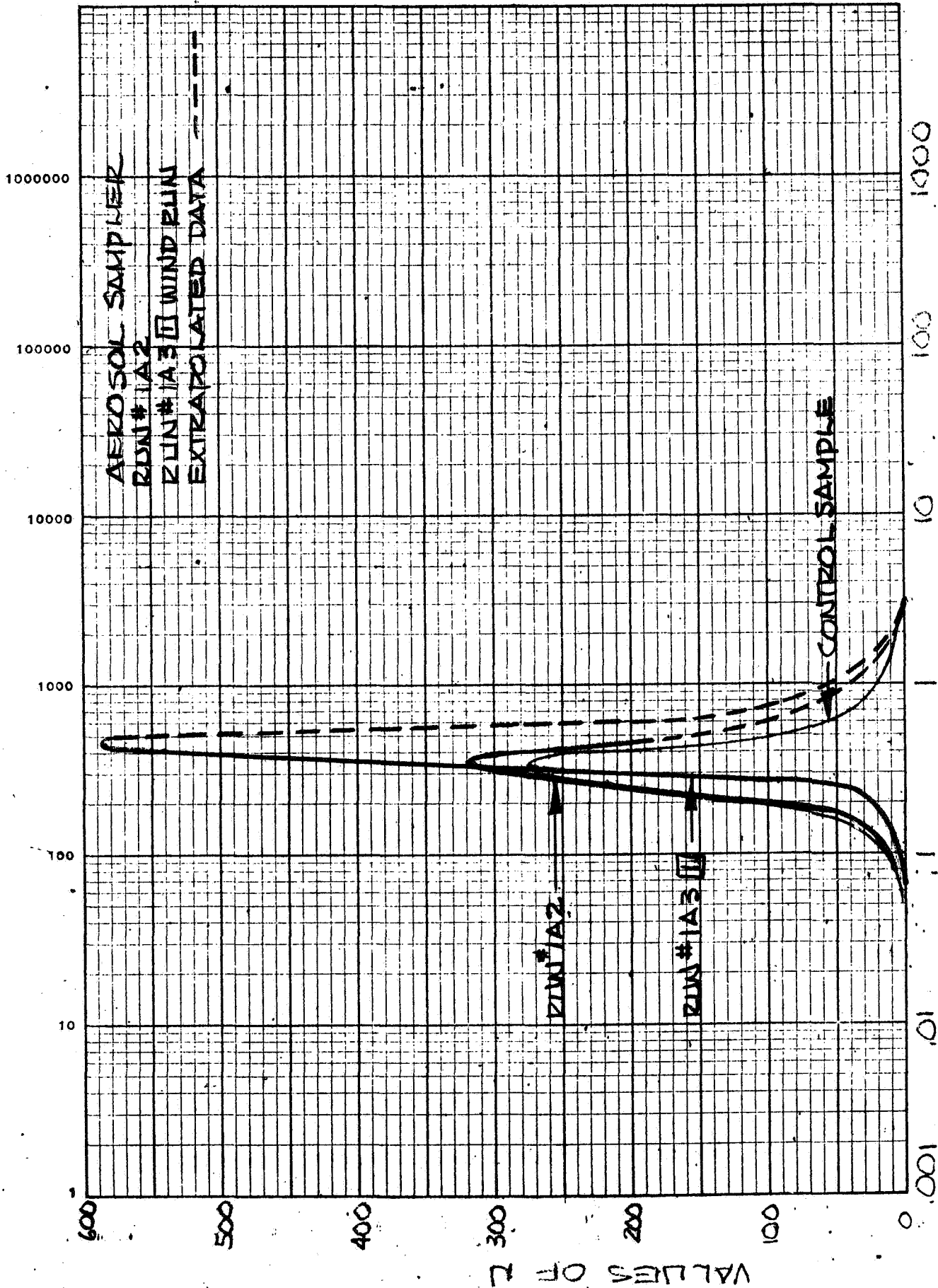


FIGURE D23  
PARTICLE SIZE DISTRIBUTION KELSO DUNE SAND

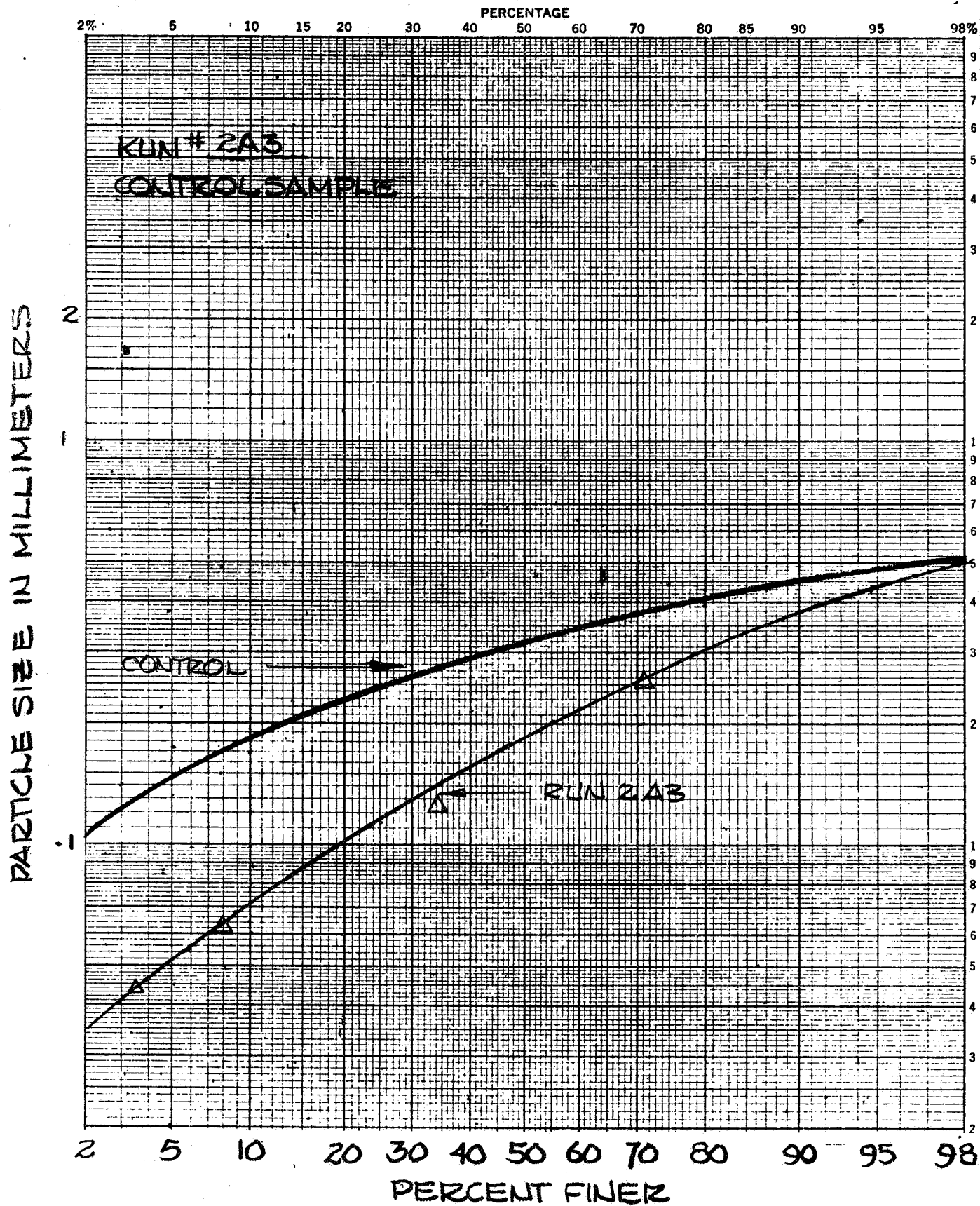


FIGURE D24 PARTICLE SIZE SUMMATION CURVE  
KELSO DUNE SAND

MODEL

DATE

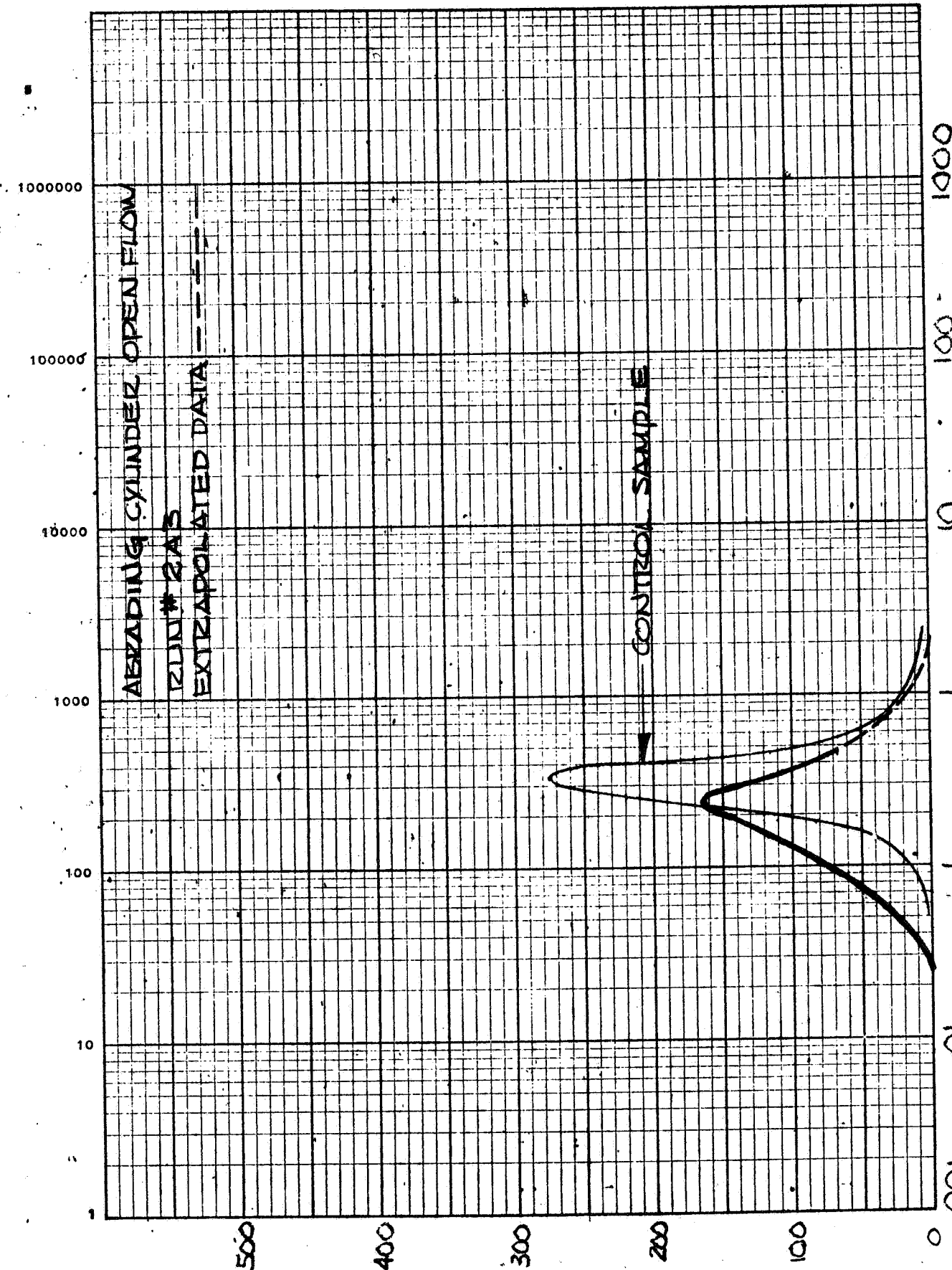


FIGURE D25  
PARTICLE SIZE DISTRIBUTION KELSO DUNE SAND



PARTICLE SIZE IN MILLIMETERS

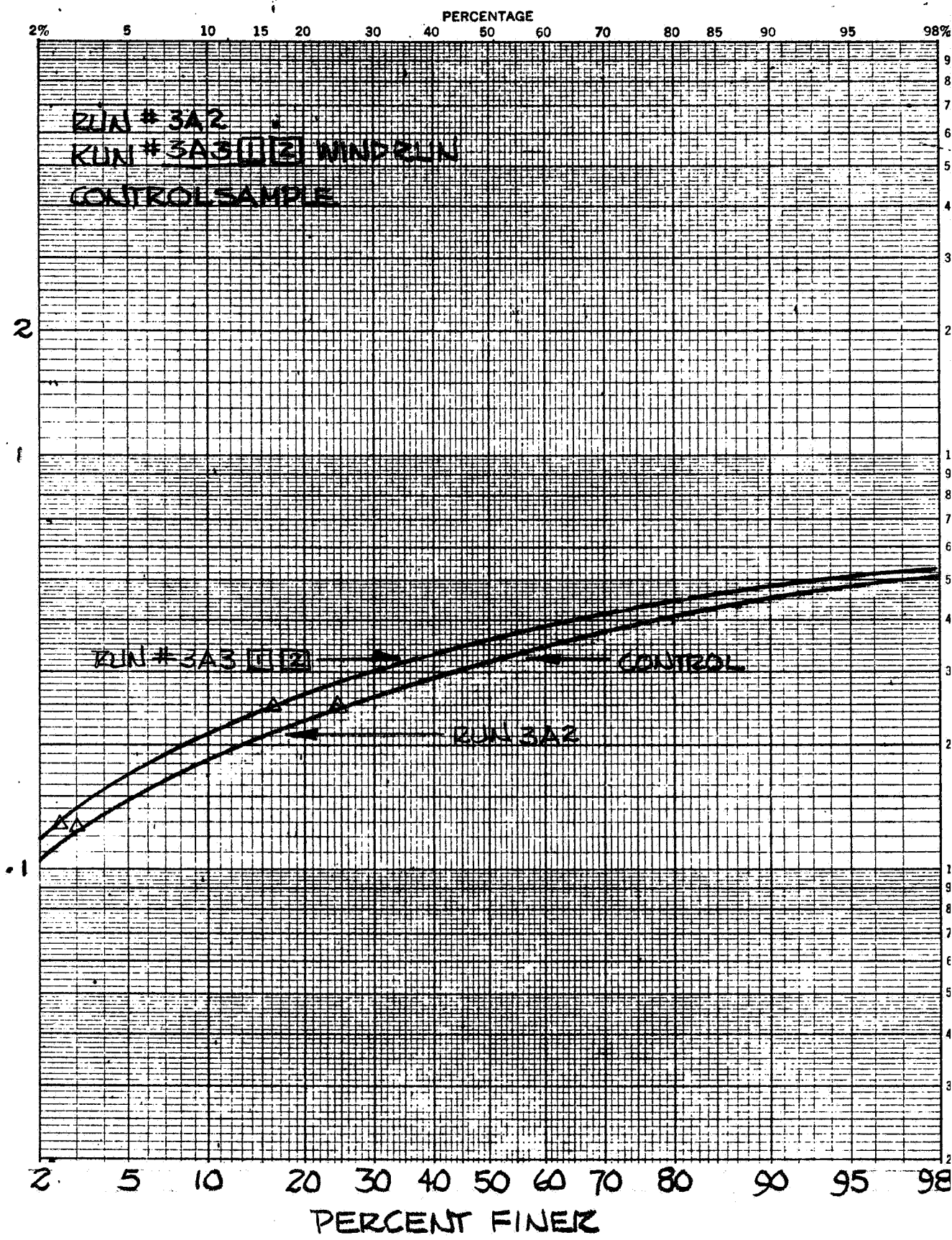


FIGURE D26 PARTICLE SIZE SUMMATION CURVE  
KELSO DUNE SAND

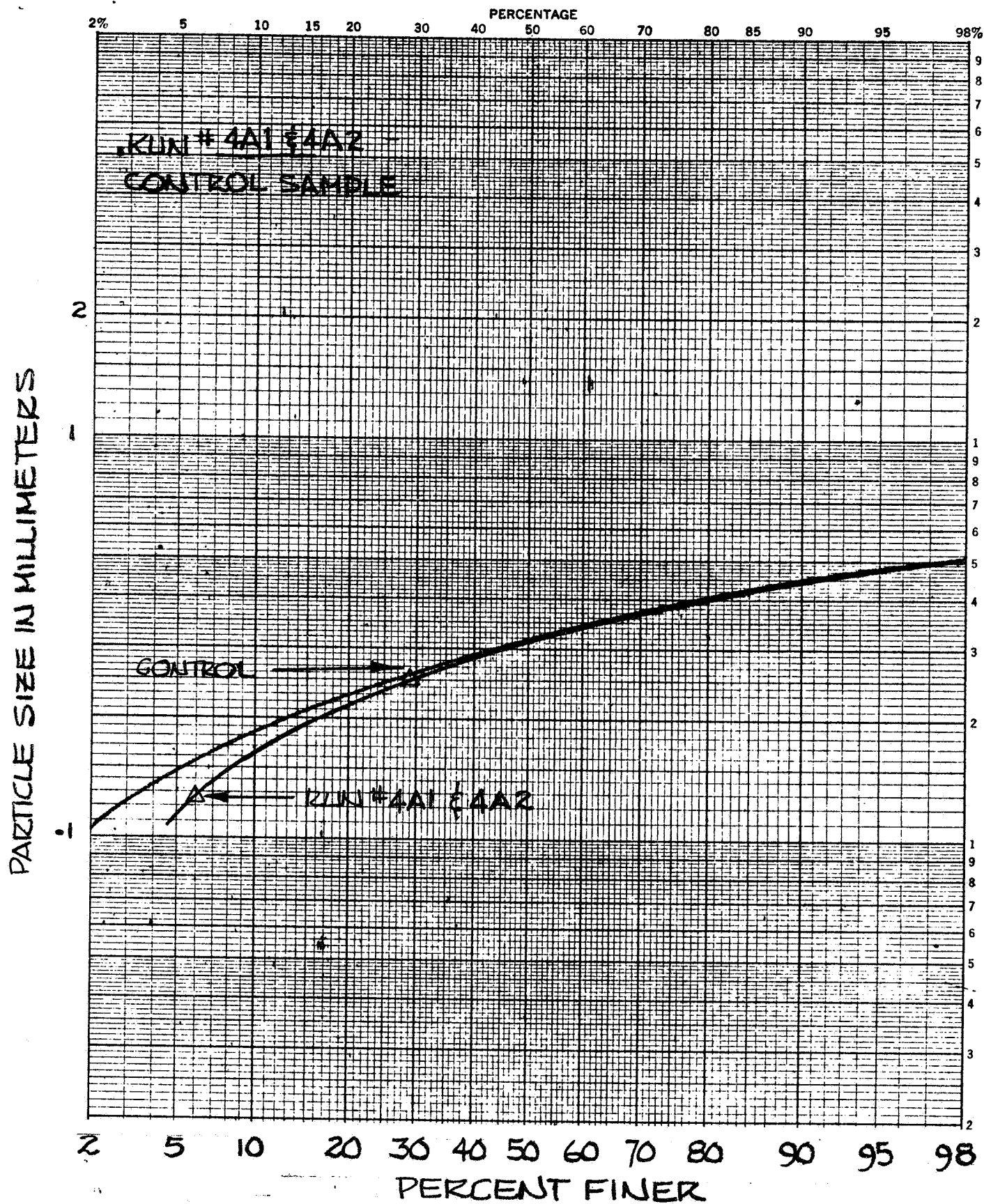


FIGURE D27 PARTICLE SIZE SUMMATION CURVE  
KELSO DUNE SAND

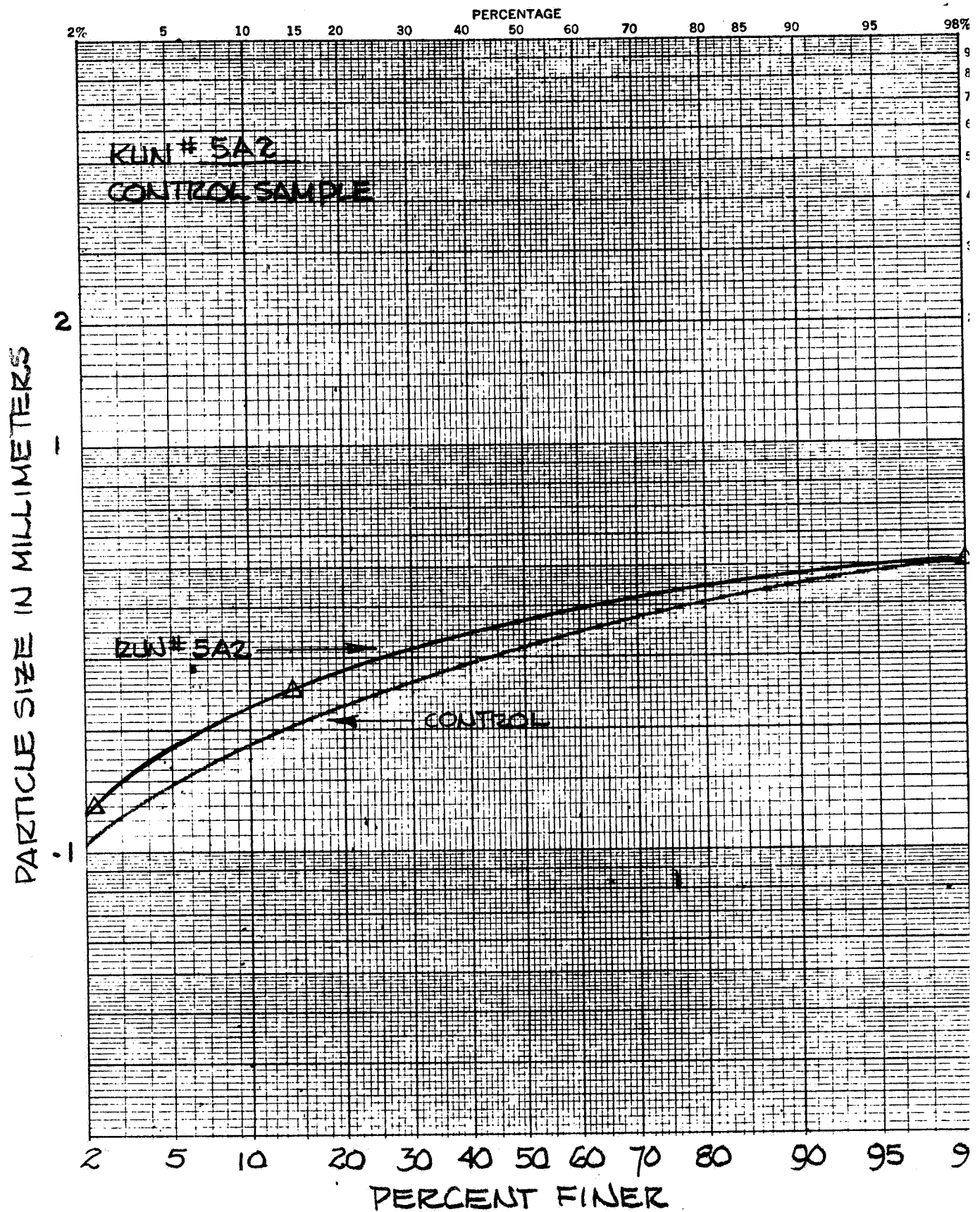


FIGURE D28 PARTICLE SIZE SUMMATION CURVE  
KELSO DUNE SAND



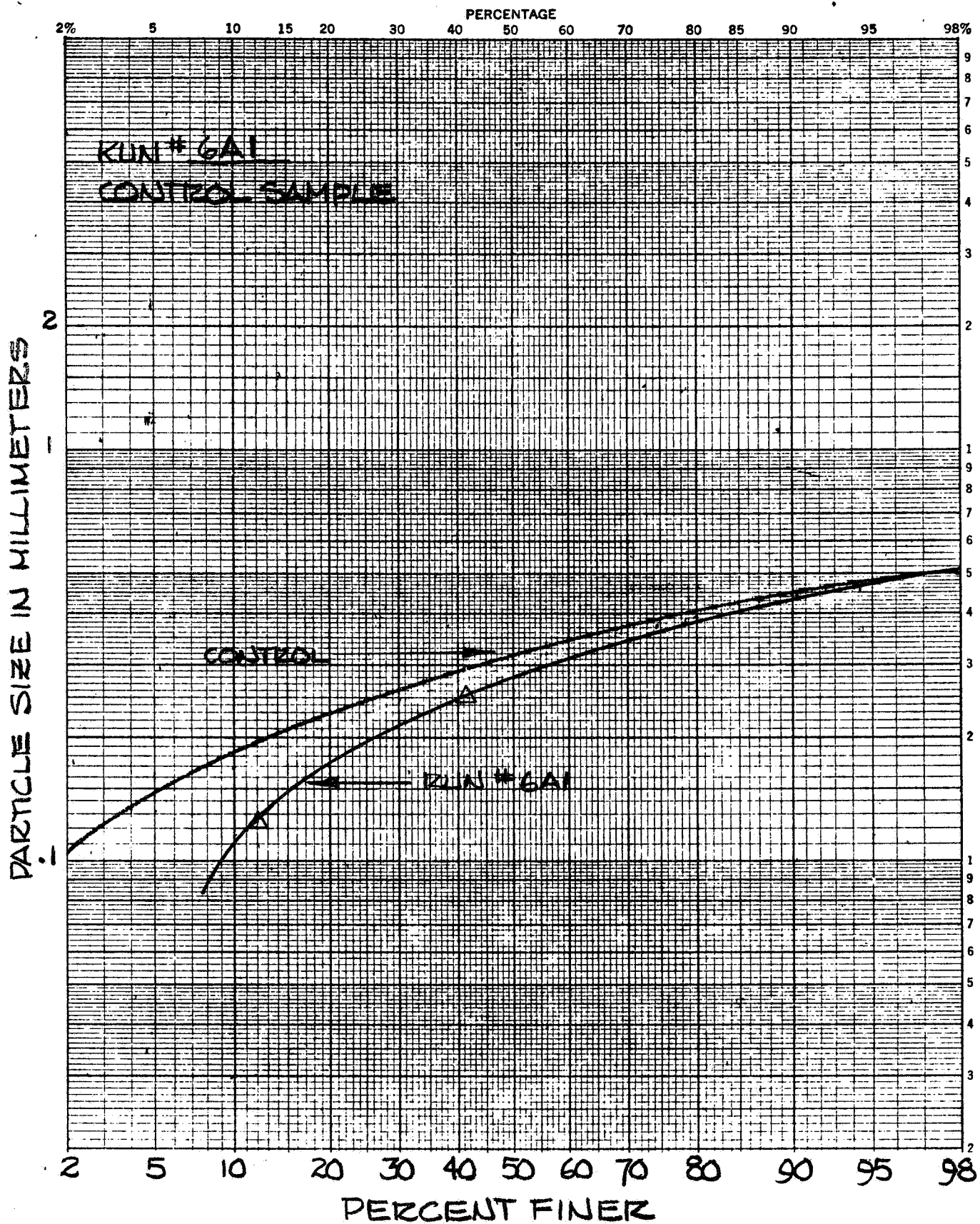


FIGURE D29 PARTICLE SIZE SUMMATION CURVE  
KELSO DUNE SAND



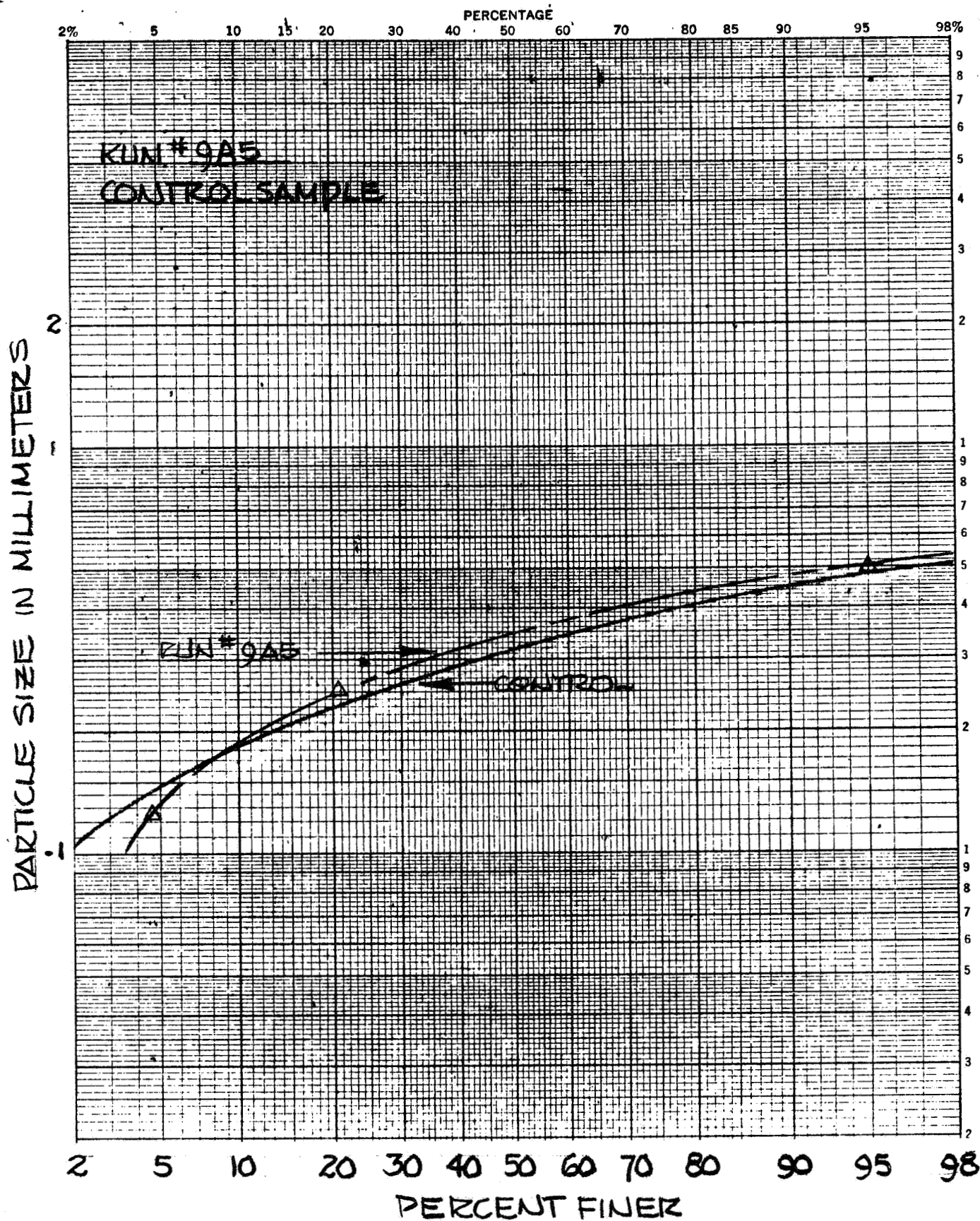


FIGURE D31 PARTICLE SIZE SUMMATION CURVE  
KELSO DUNE SAND

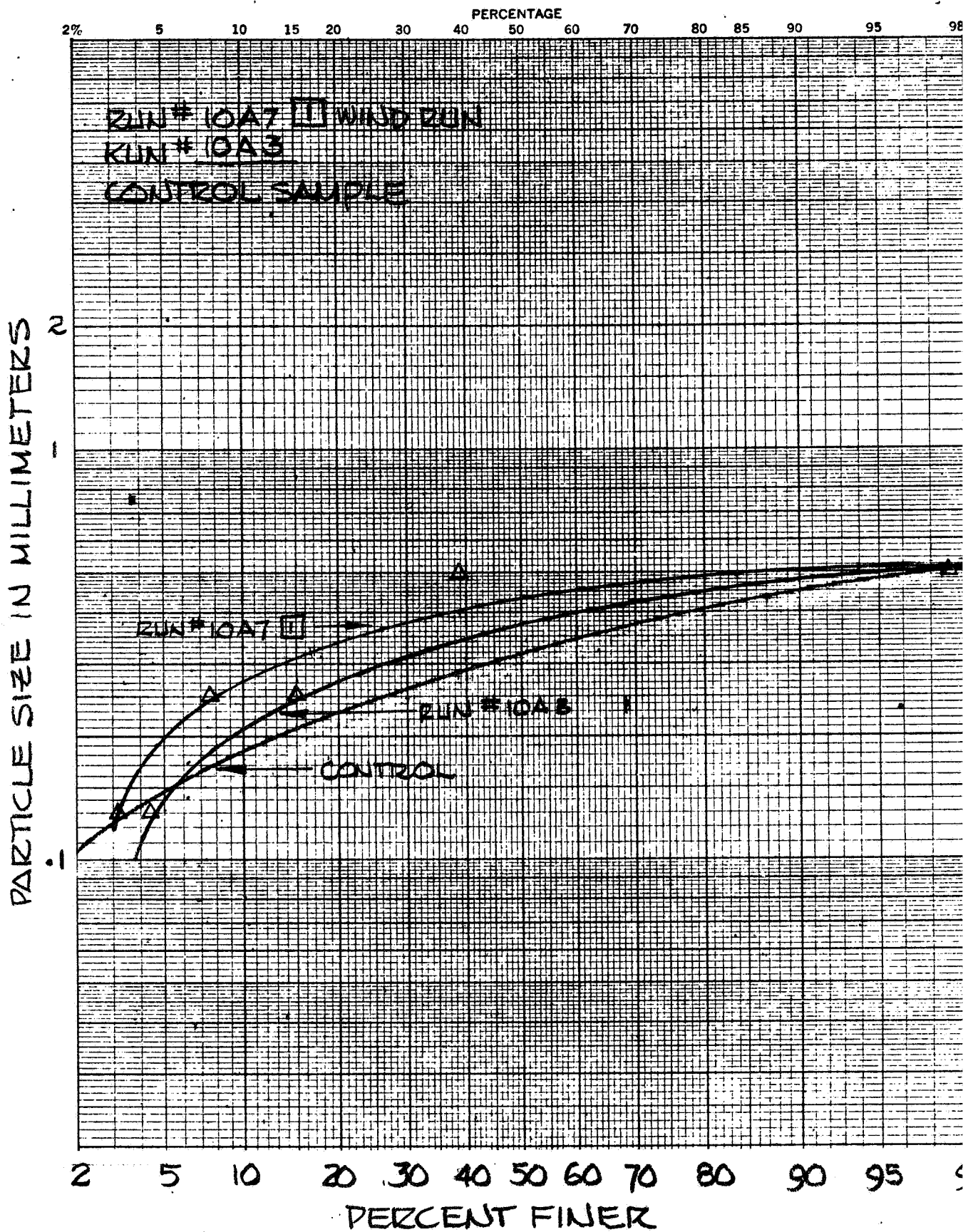


FIGURE D32 PARTICLE SIZE SUMMATION CURVE  
KELSO DUNE SAND



MODEL

DATE

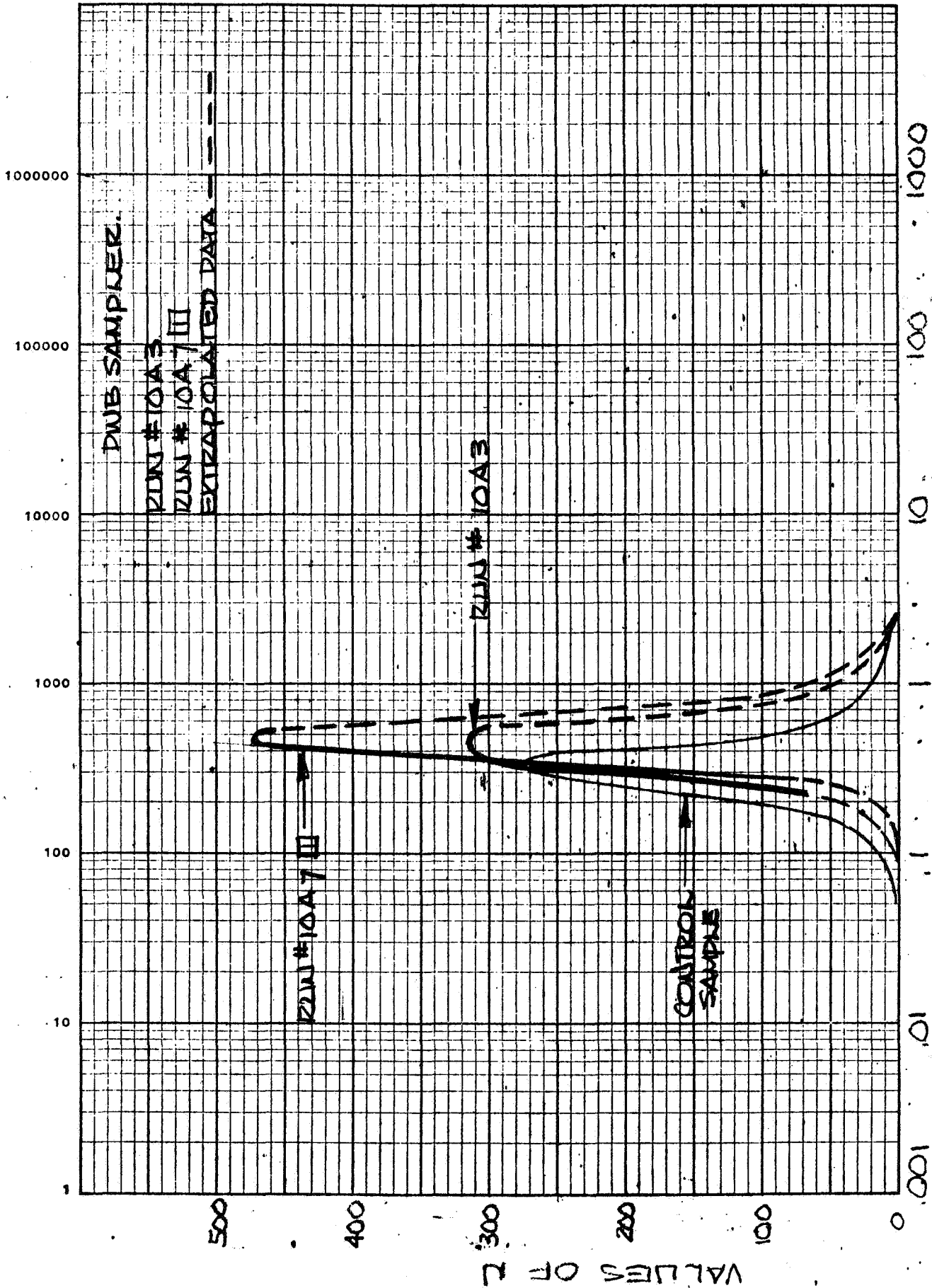


FIGURE D-63 PARTICLE SIZE DISTRIBUTION KELLO DUNE SAND

PARTICLE SIZE IN MILLIMETERS

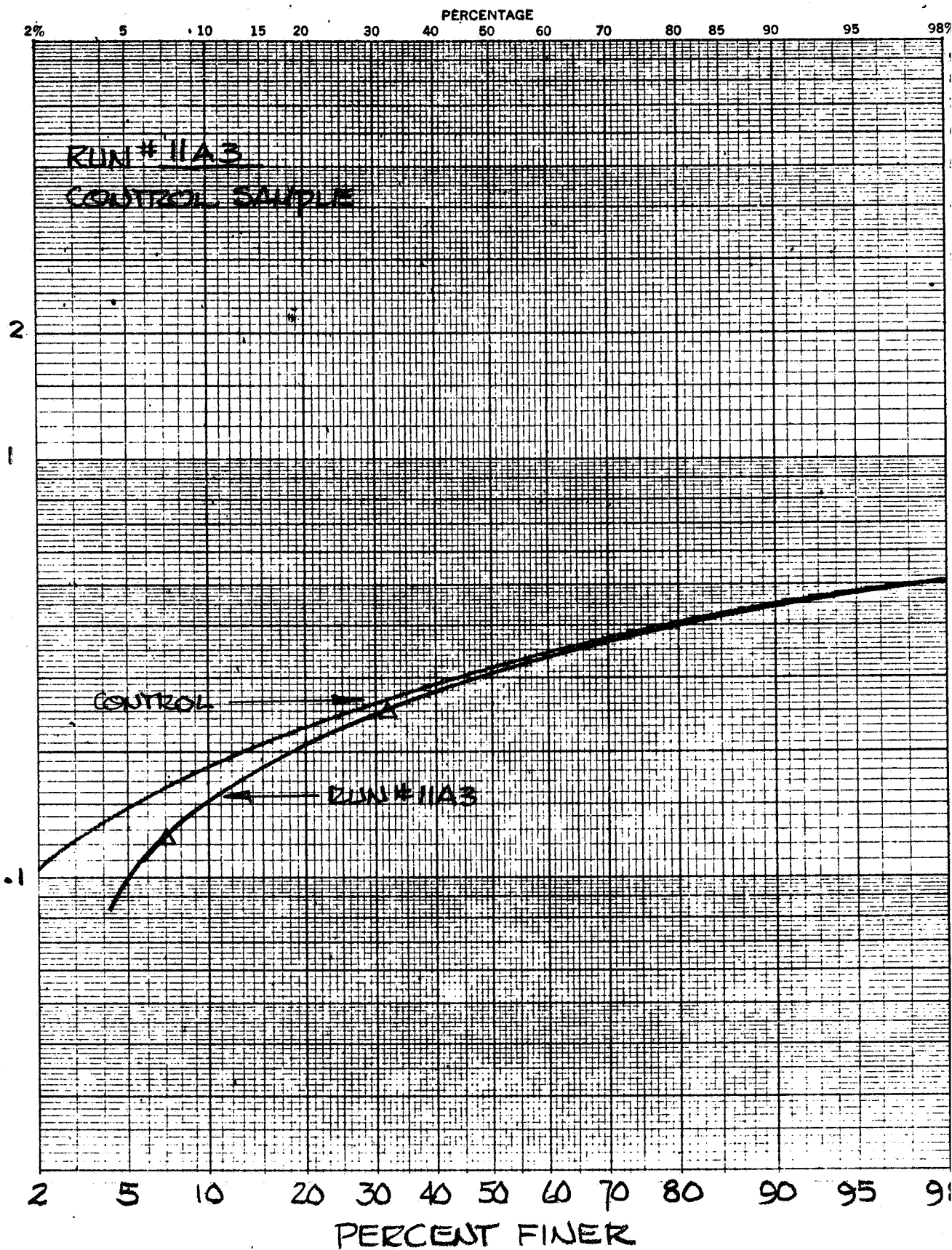


FIGURE D34 PARTICLE SIZE SUMMATION CURVE  
KELSO DUNE SAND

MODEL

DATE

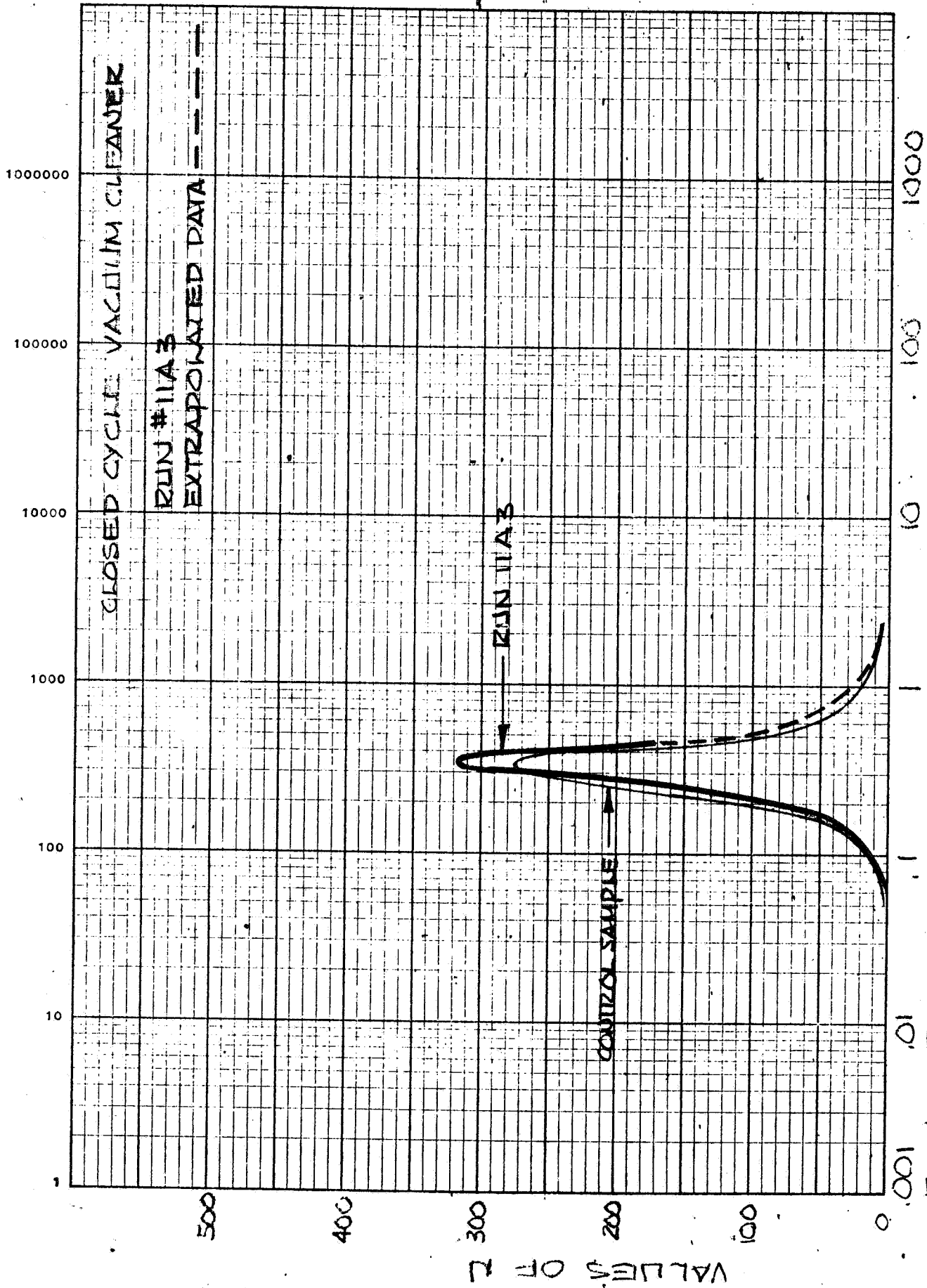


FIGURE D35 PARTICLE SIZE IN MILLIMETERS  
PARTICLE SIZE DISTRIBUTION KELSO DUNE SAND

This page intentionally blank.



#### D.3.2 TEST SITE B, DURICRUST

##### Particle Size Distribution Curves

### D.3.2 TEST SITE B, PISGAH DRYLAKE DURICRUST

This section contains Figures D-36 through D-46 for samples taken at site B.

It is more difficult to assess the results for this soil model because of the difficulty in arriving at a control standard. The results obtained by dry sieving should probably be used as a basis for comparison since the abrading action of the samplers is mechanical which more nearly approximates the sieving techniques used. In general it appears that most of the samplers do not substantially alter the distribution. Those samplers with noticeable characteristics were samplers 2, 7, and 10. In sample run 2B2, Figures D-36 and D-37, it is again noted that this sampler tends to collect substantially fine material with a broad distribution. It is interesting to note that the hump seen in the distribution curve of the control sample obtained by sedimentation procedures is reflected in the coarse grain limb of the distribution curve for the sample. More detailed analysis and testing would be required to evaluate this result.

In sample run 7B1 shown in Figures D-41 and D-42 it is seen that a very narrow distribution exists in the sample with a peak at 80 microns. This result is expected since the metal cased helical conveyor used on this sampler either rejects large particles or breaks them down into smaller sizes. With a lightly cemented material such as duricrust the agglomerated grains are easily broken down into smaller grains. The very narrow distribution of particle sizes for this sampler can be attributed to the action of the helical conveyor. The mean size is determined by the dimensions of the helical path through which the soil is transported.

The results of sample run 10B3 are given in Figure D-45 and D-46. Because of the very low flow velocities in the pneumatic transport mode, it is expected that any pneumatically collected sample would be very fine consisting of particles in the size range obeying Stoke's law; i.e., less than 70 microns. This is graphically substantiated by this analysis since the percentage by weight climbs to a maximum at about 25 microns. The sample obtained by the abrading wire brush in the gravity dump has a peak at the same place as that obtained by dry sieving except that the distribution is broader. This is probably true since the wire brush during acquisition does not work the material as severely or as long as is done in the sieving process. The narrow distribution on the fine limb of the distribution curve is probably due to the removal of some fines by the pneumatic collection of a sample; however, a stronger sorting action occurs when the sample is dumped by the inability of the cyclone collector to collect these fines. Large quantities of fine material were observed in the effluent from cyclone collector during the gravity dump of the sample.

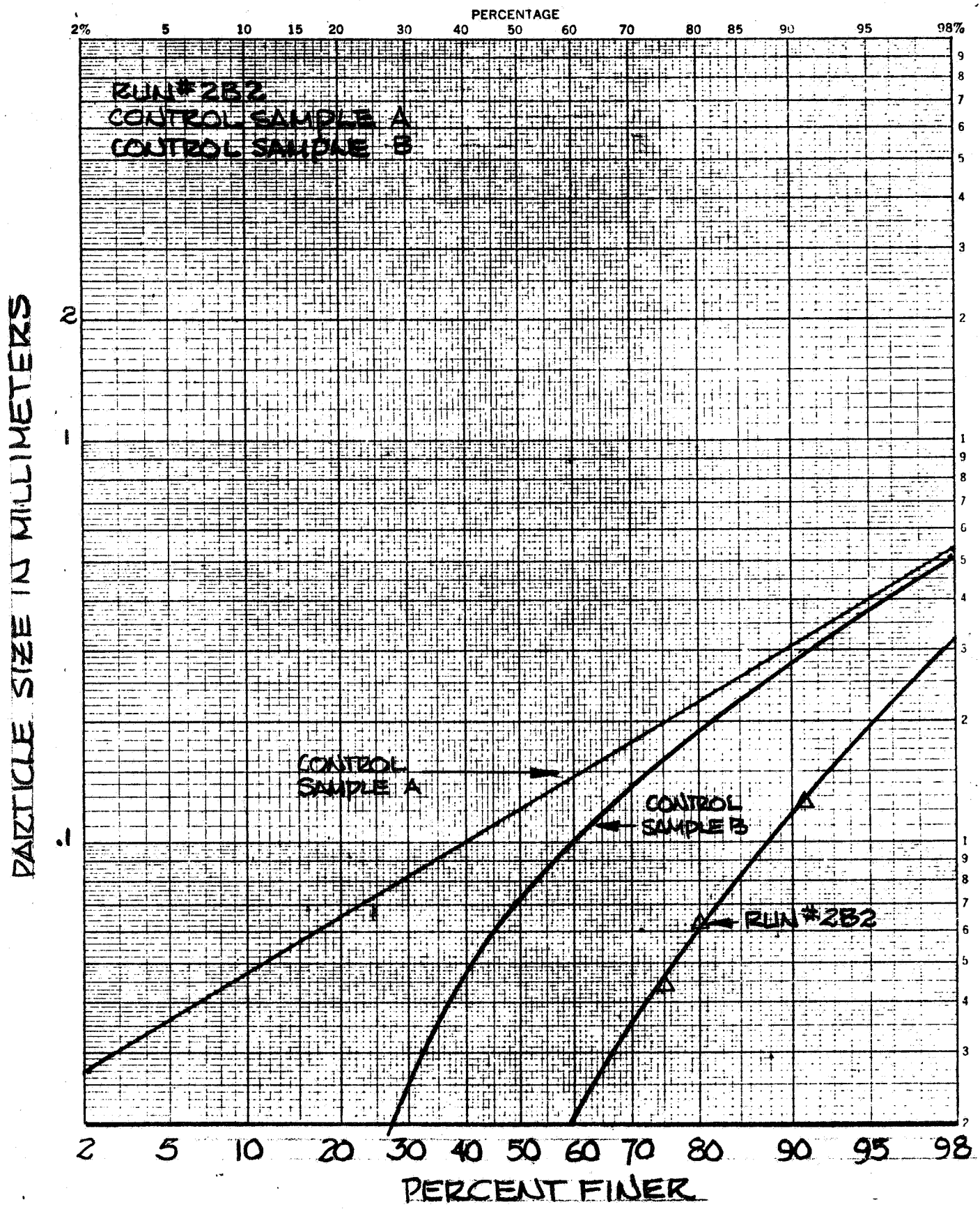


FIGURE D36 PARTICLE SIZE SUMMATION CURVE  
DURICRUST

MODEL

DATE

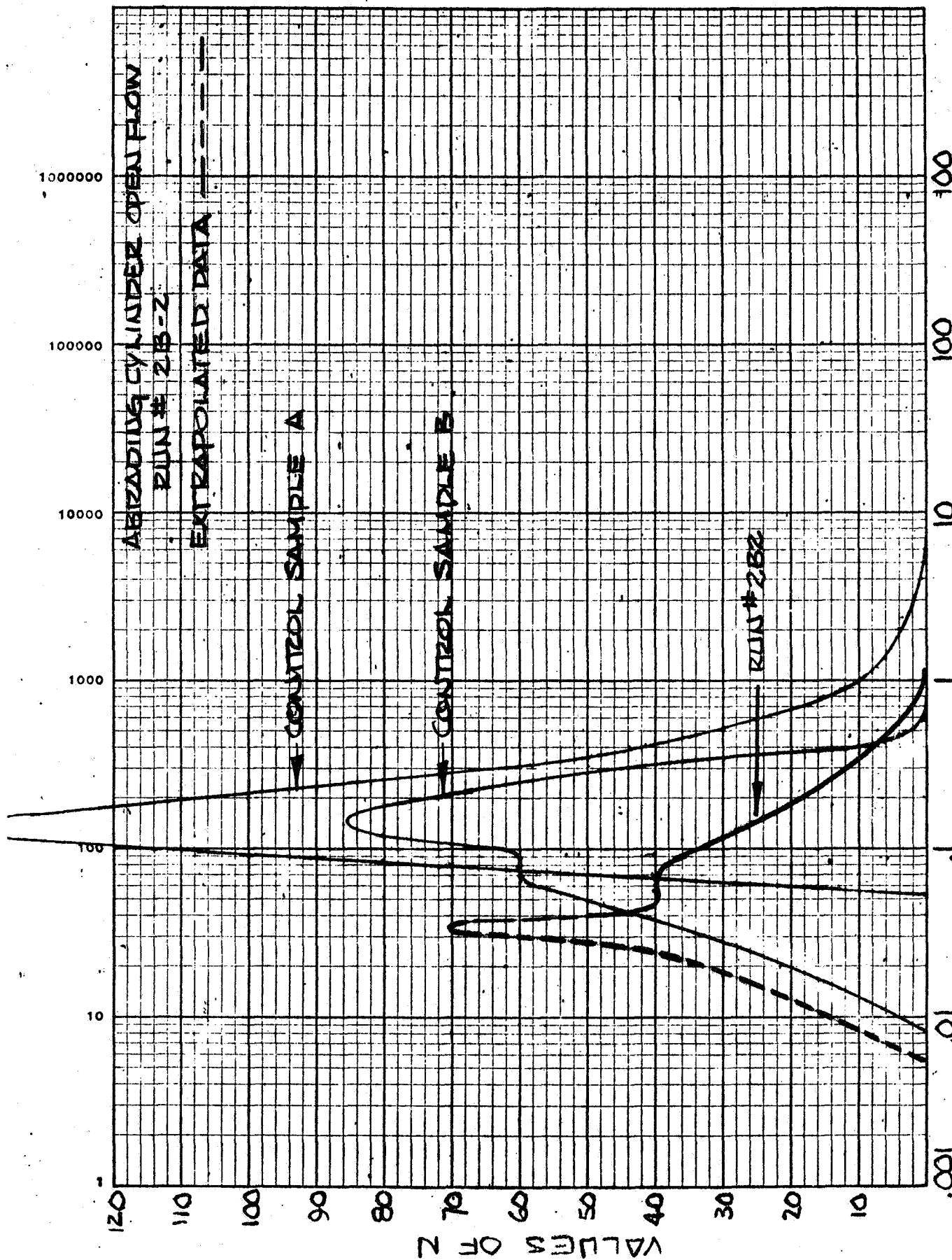


FIGURE D37  
PARTICLE SIZE DISTRIBUTION DURICRUST

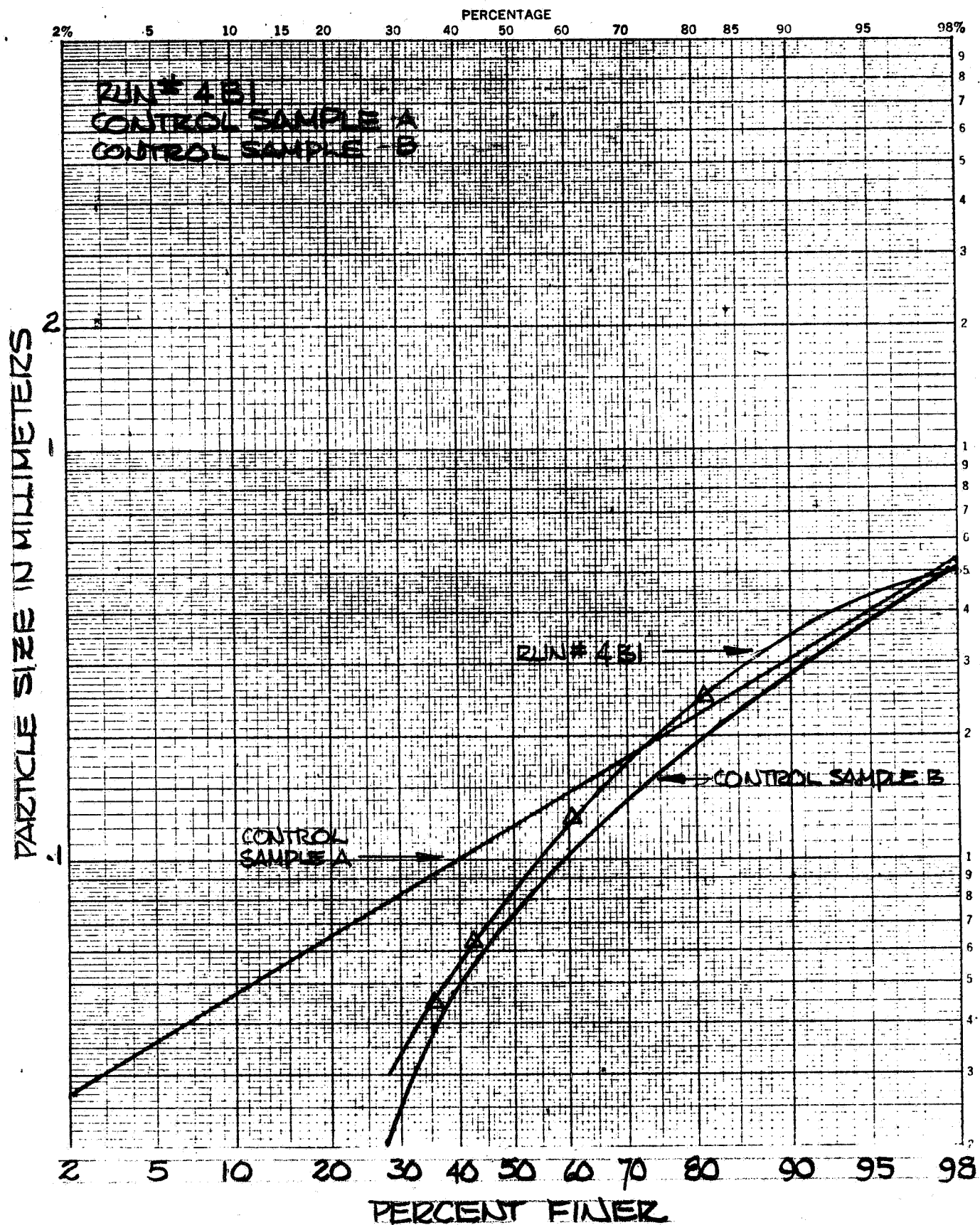


FIGURE D38 PARTICLE SIZE SUMMATION CURVE  
DURICRUST

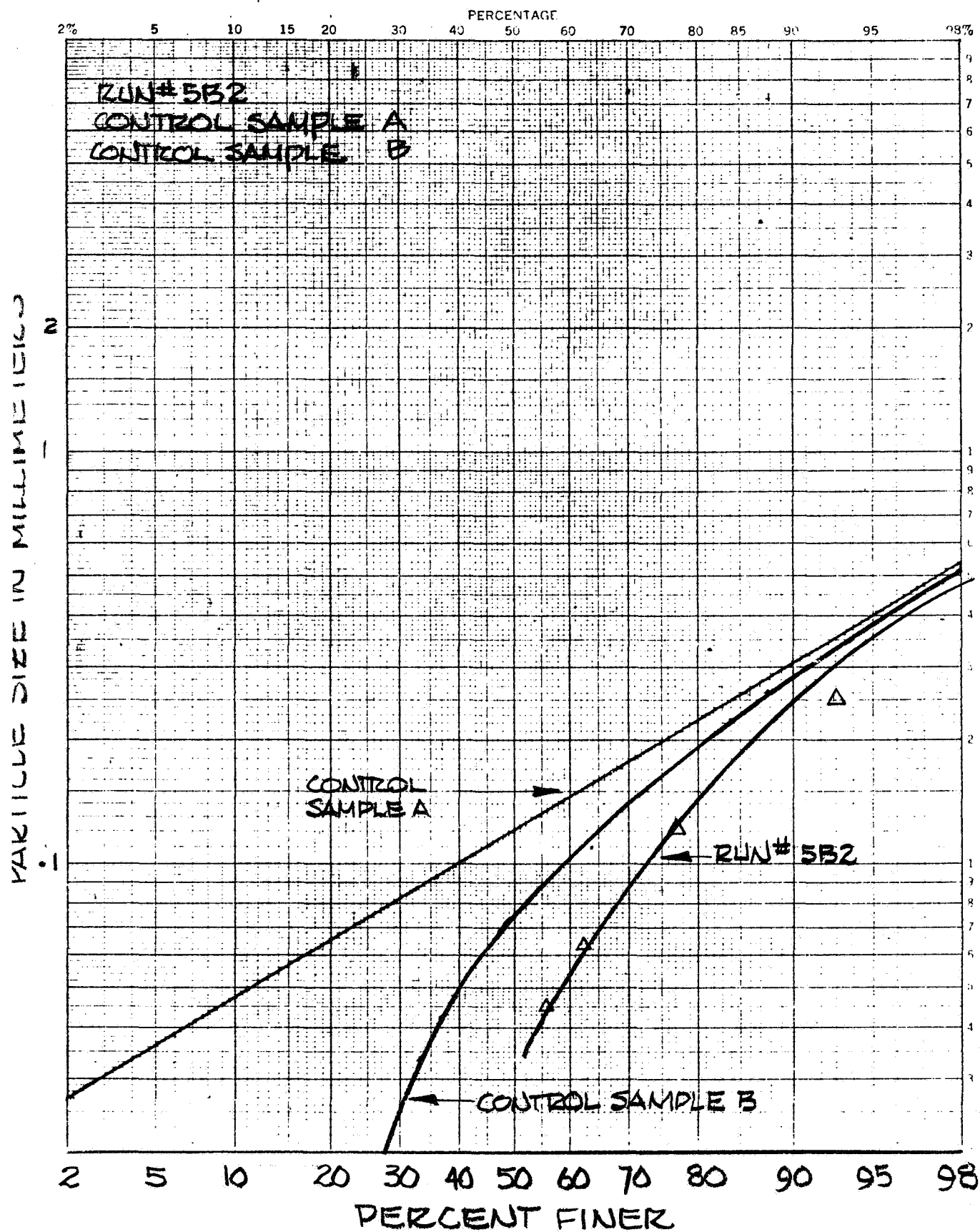


FIGURE D39 PARTICLE SIZE SUMMATION CURVE  
DURICRUST

PARTICLE SIZE IN MILLIMETERS

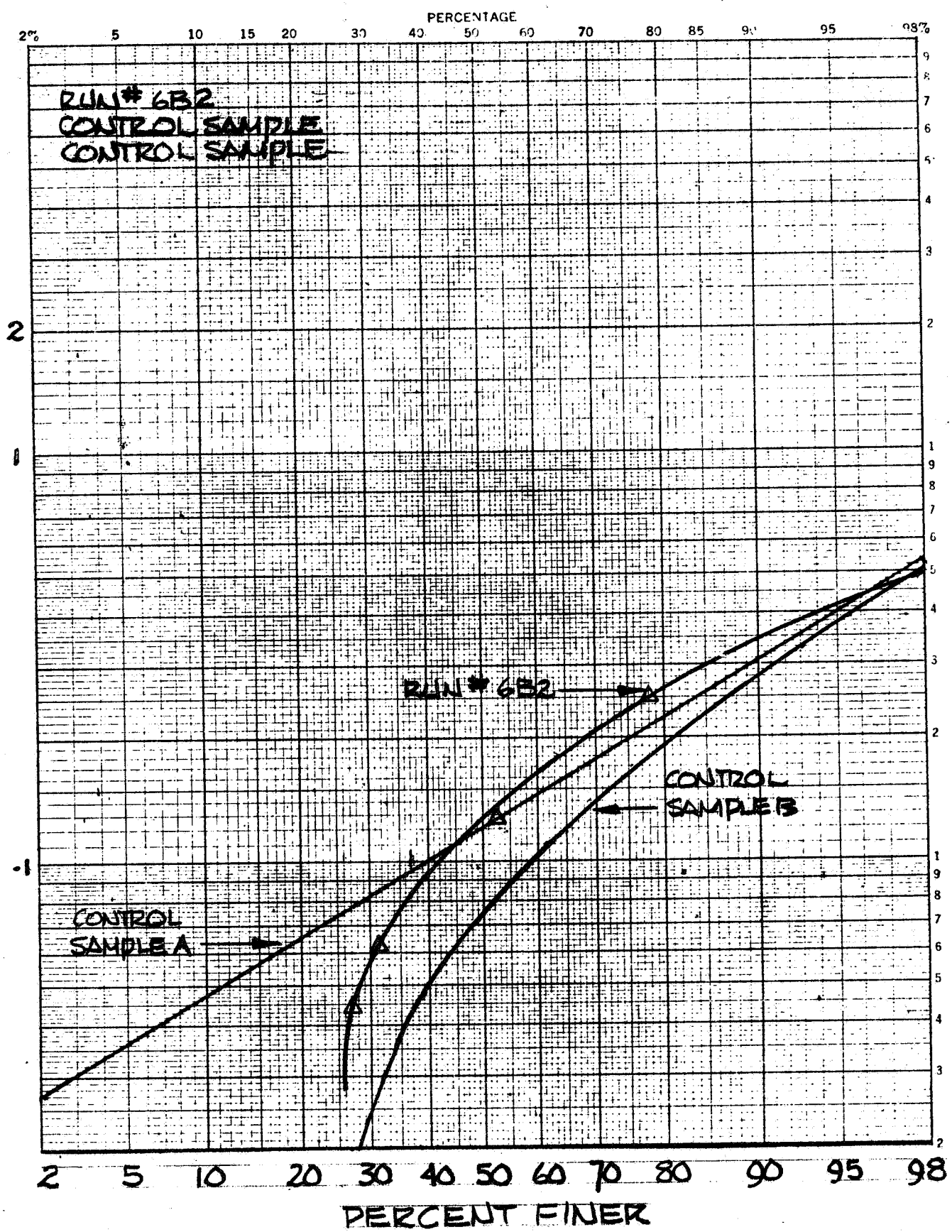


FIGURE D40 PARTICLE SIZE SUMMATION CURVE  
DURICIZHST

This page intentionally blank.



PARTICLE SIZE IN MILLIMETERS

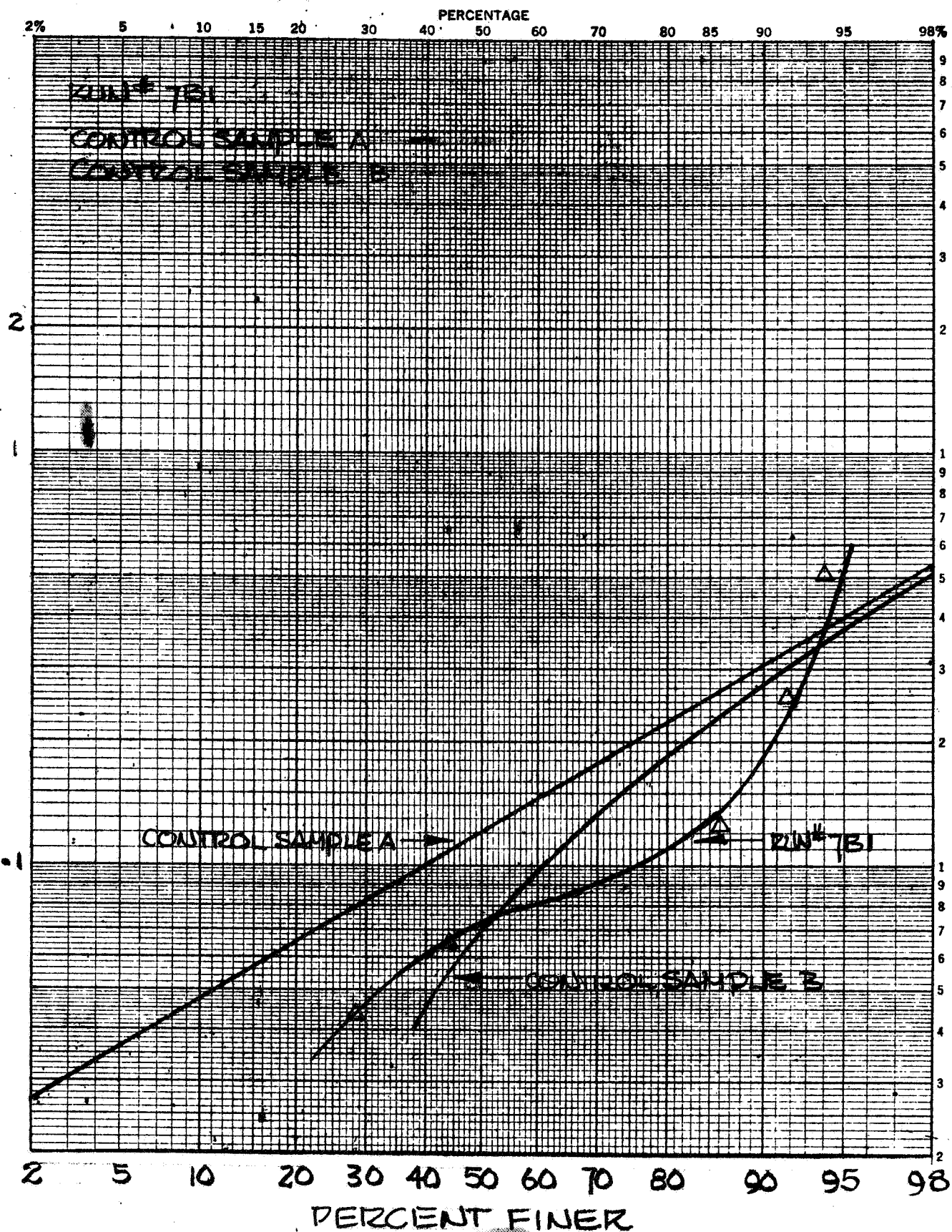


FIGURE DAI PARTICLE SIZE SUMMATION CURVE  
PRECEDING  
PAGE BLANK  
DURICRUST  
D-74

MODEL

DATE

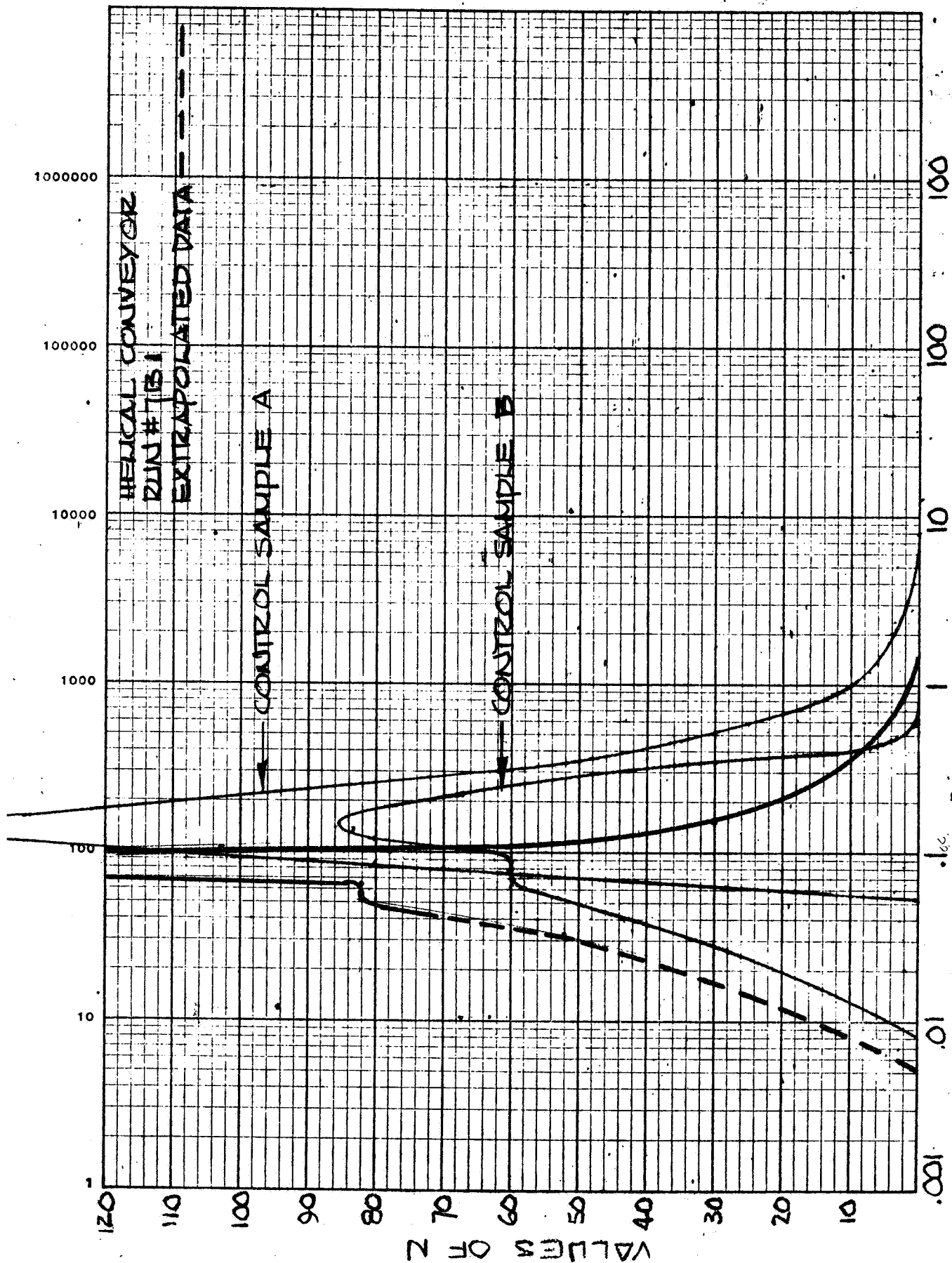


FIGURE D42 PARTICLE SIZE DISTRIBUTION DURICRUST

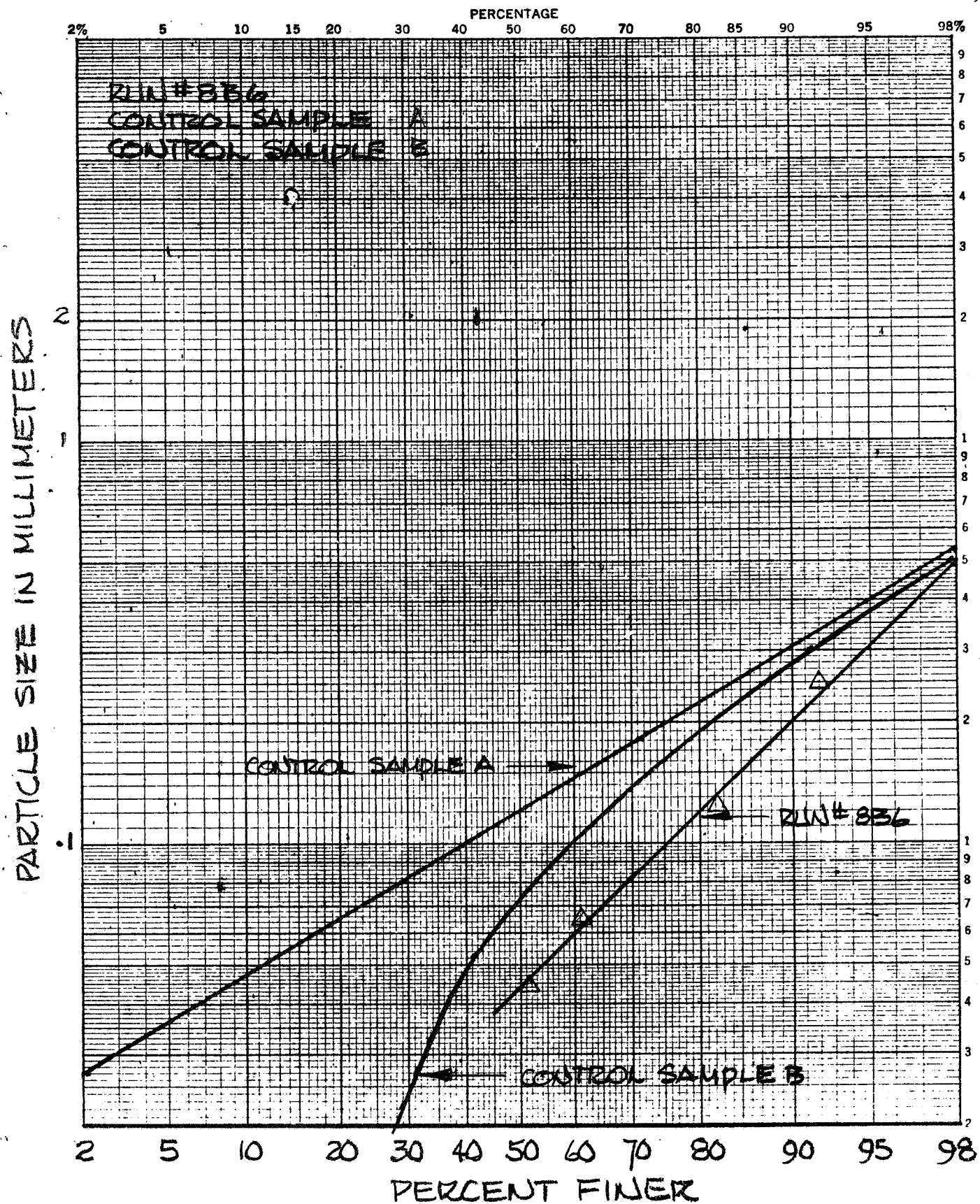


FIGURE D43 PARTICLE SIZE SUMMATION CURVE  
DURICRUST

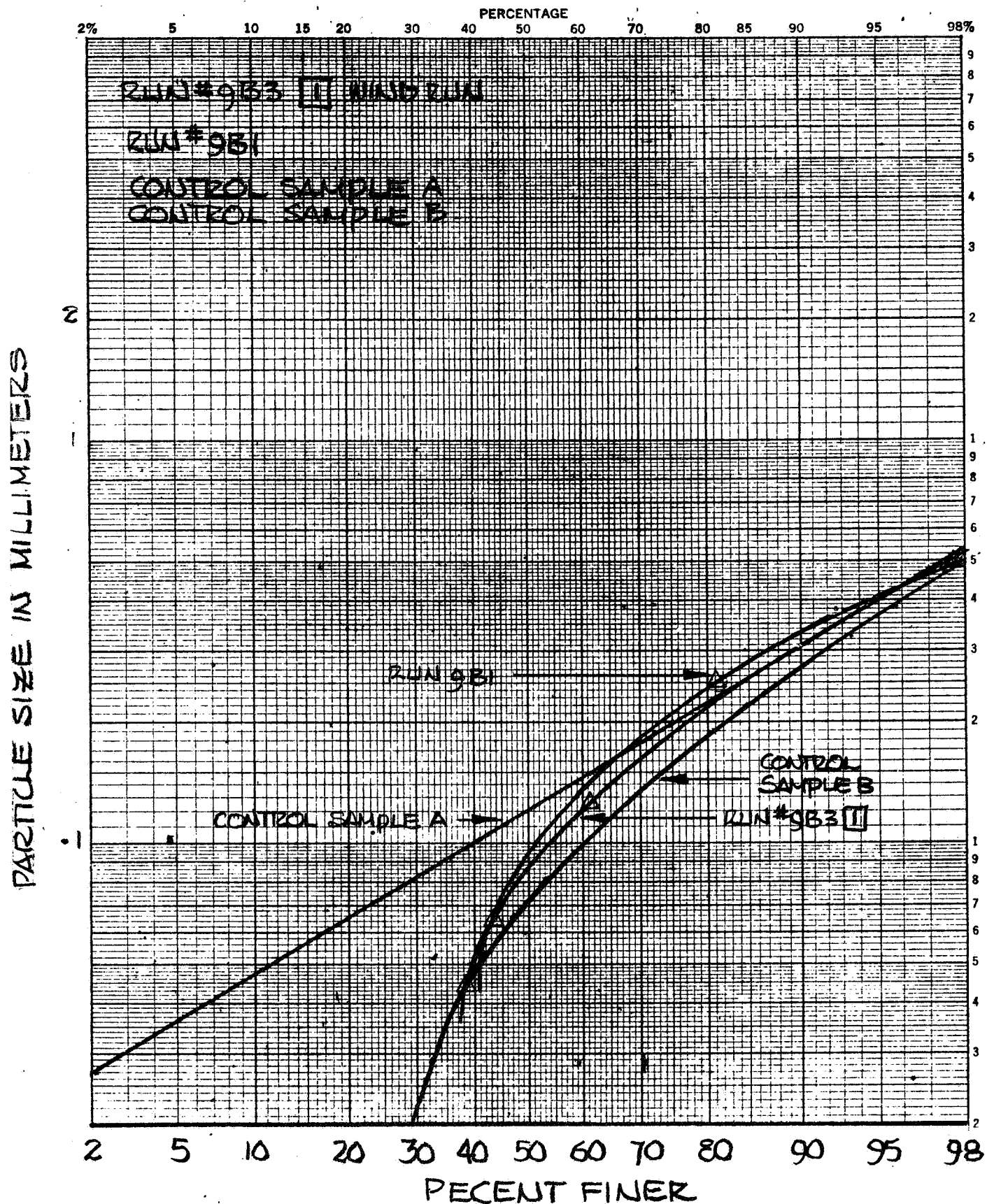


FIGURE D44 PARTICLE SIZE SUMMATION CURVE  
DURICRUST



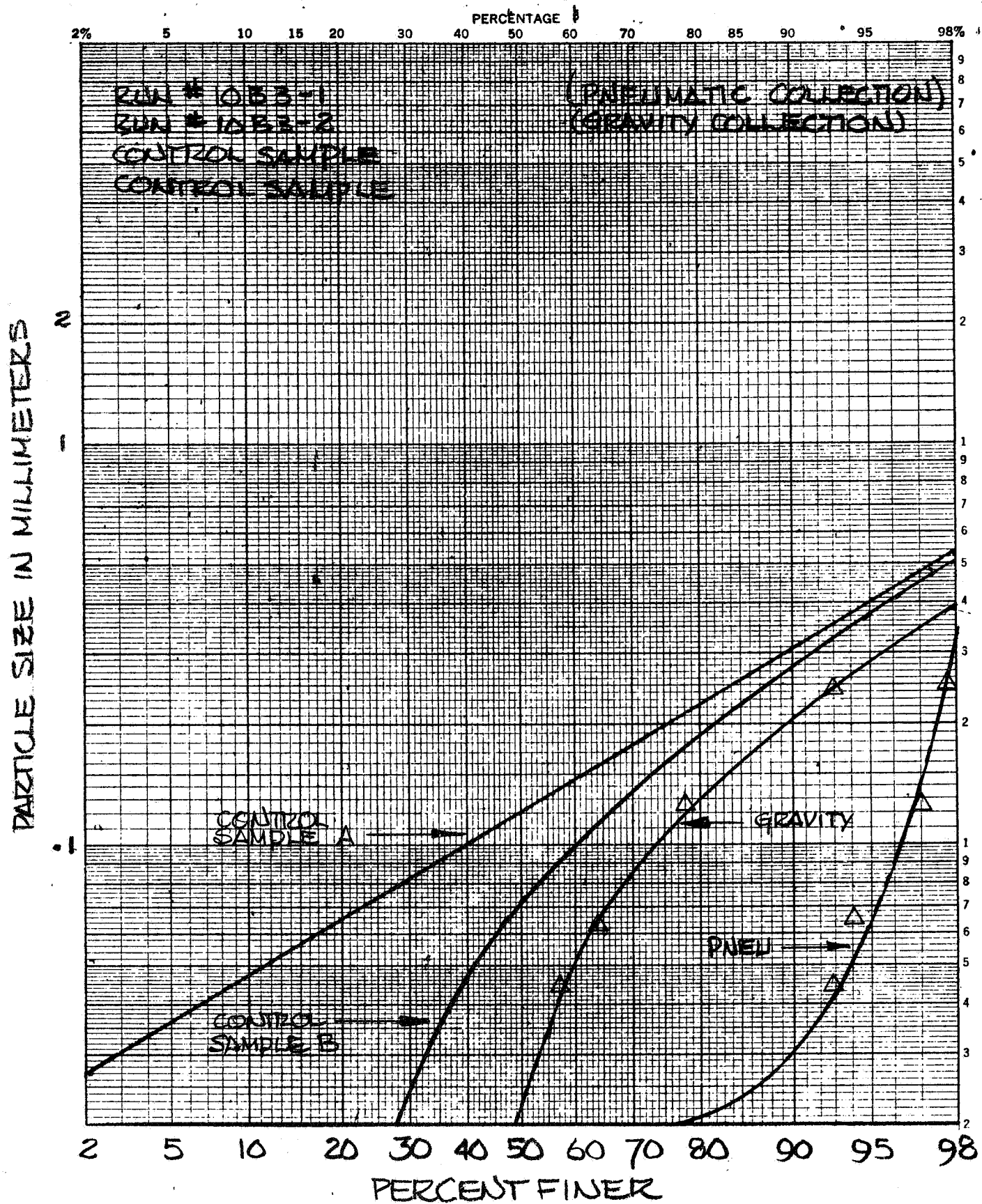


FIGURE D45 PARTICLE SIZE SUMMATION CURVE  
DURICRUST

MODEL

DATE

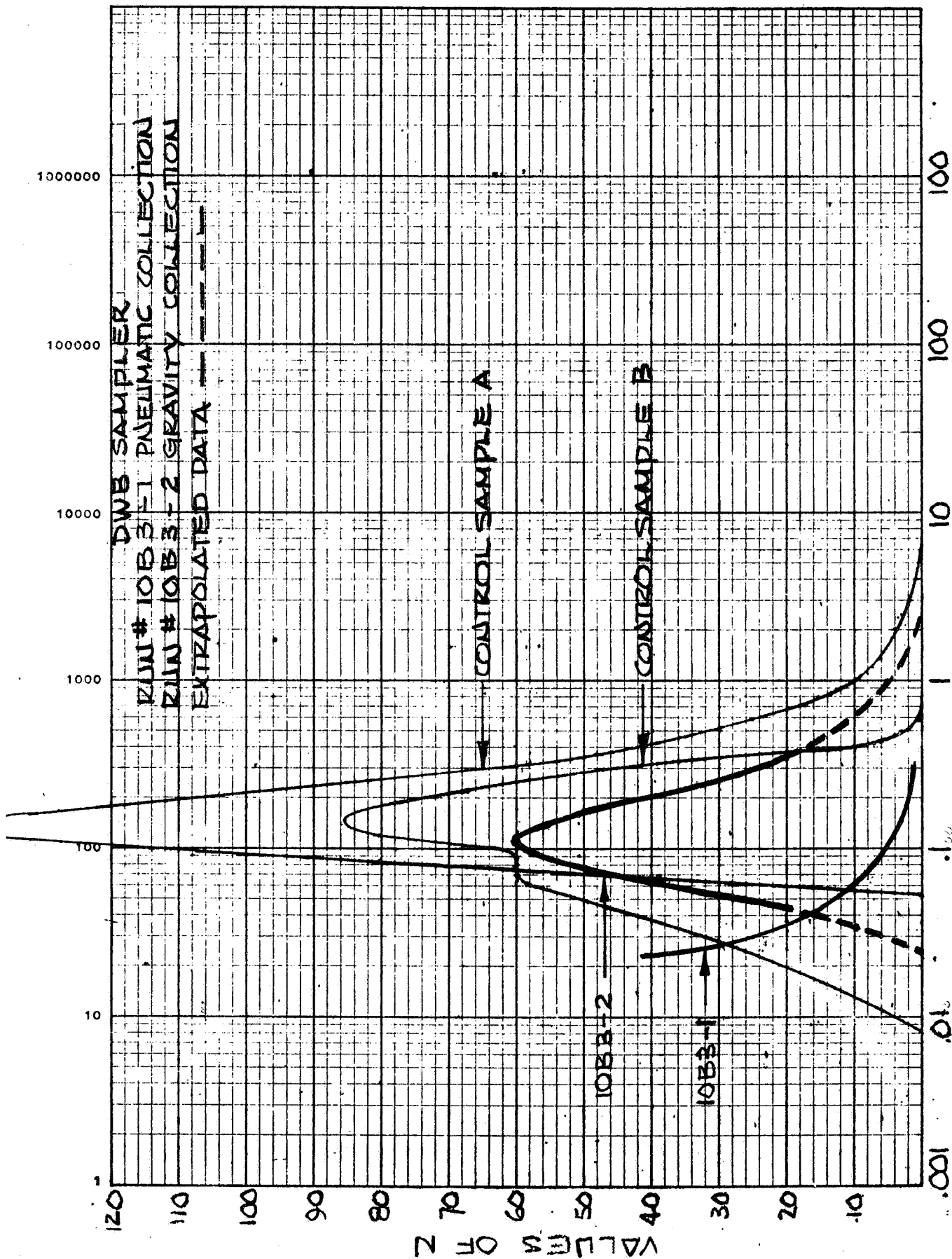


FIGURE D46 PARTICLE SIZE DISTRIBUTION DURICRUST

This page intentionally blank.

### D.3.3 TEST SITE E, COMPACTED CINDERS

#### Particle Size Distribution Curves



### D.3.3 TEST SITE E, COMPACTED CINDERS

This section contains Figures D-47 through D-58 for samples taken at site E.

In general, all the samplers rejected the gravel population and acquired the sample out of the fine material population. In this context, it should be pointed out that sampler 4 does acquire gravel size material but the quantity is not large enough to accurately assess the distribution in this analysis.

The samples collected at this site which appear to change the distribution of the fine population are samplers 7 and 9. From Figure D-53 and D-54, for run 7E1, it can be seen that sampler 7 again produces a very narrow distribution with a peak at about 70 microns in diameter. This peak coincides with the peak for the fine population of the control sample.

The results of sample run 9E1 are given in Figures D-55 and D-56. This is the only soil model in which a discriminating effect other than the rejection of the large gravel is evident. The steep slope of the fine limb of the distribution curve indicates a loss of fine material. A possible explanation can be made in terms of the spin dump cycle. It was at this site that poor engagement of the slip clutch driving the high speed spin dump mode was observed resulting in a slow spin with vibration. The finer material will slow down more rapidly due to air drag and begin to settle out. Since the velocity of the material is lower as it leaves the sampling head when the spin dump malfunctions in this manner, it can be expected that more material will be lost under these conditions by failing to cross the gap between the sampling head exit slit and the collection chamber. It can also be expected that the fine material is more apt to be lost than the coarser material. This effect could explain the distortion of the distribution curve shown in Figure D-56.

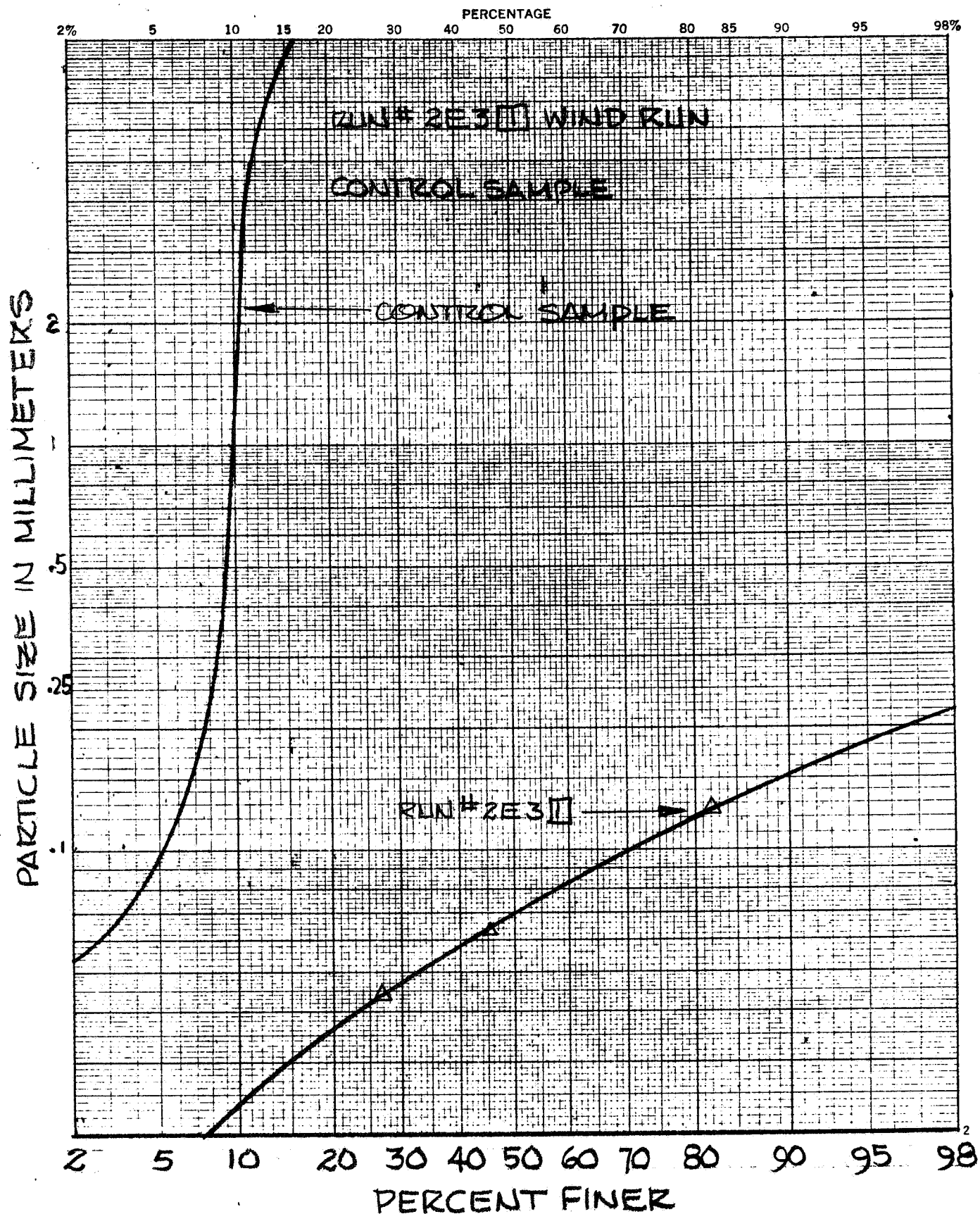


FIGURE D47 PARTICLE SIZE SUMMATION CURVE  
COMPACTED CINDERS

MODEL

DATE

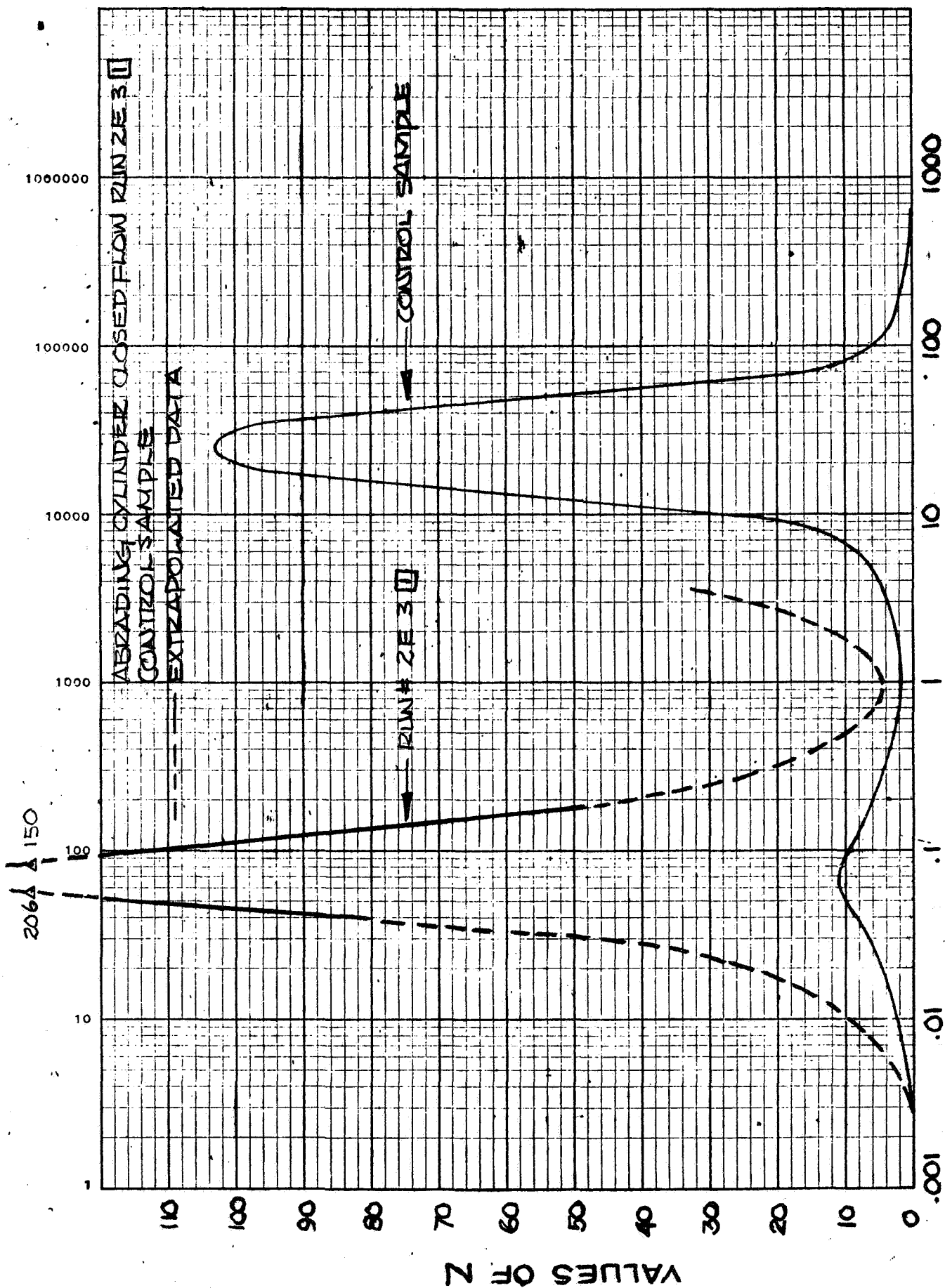


FIGURE D48 PARTICLE SIZE DISTRIBUTION COMPACTED CINDERS

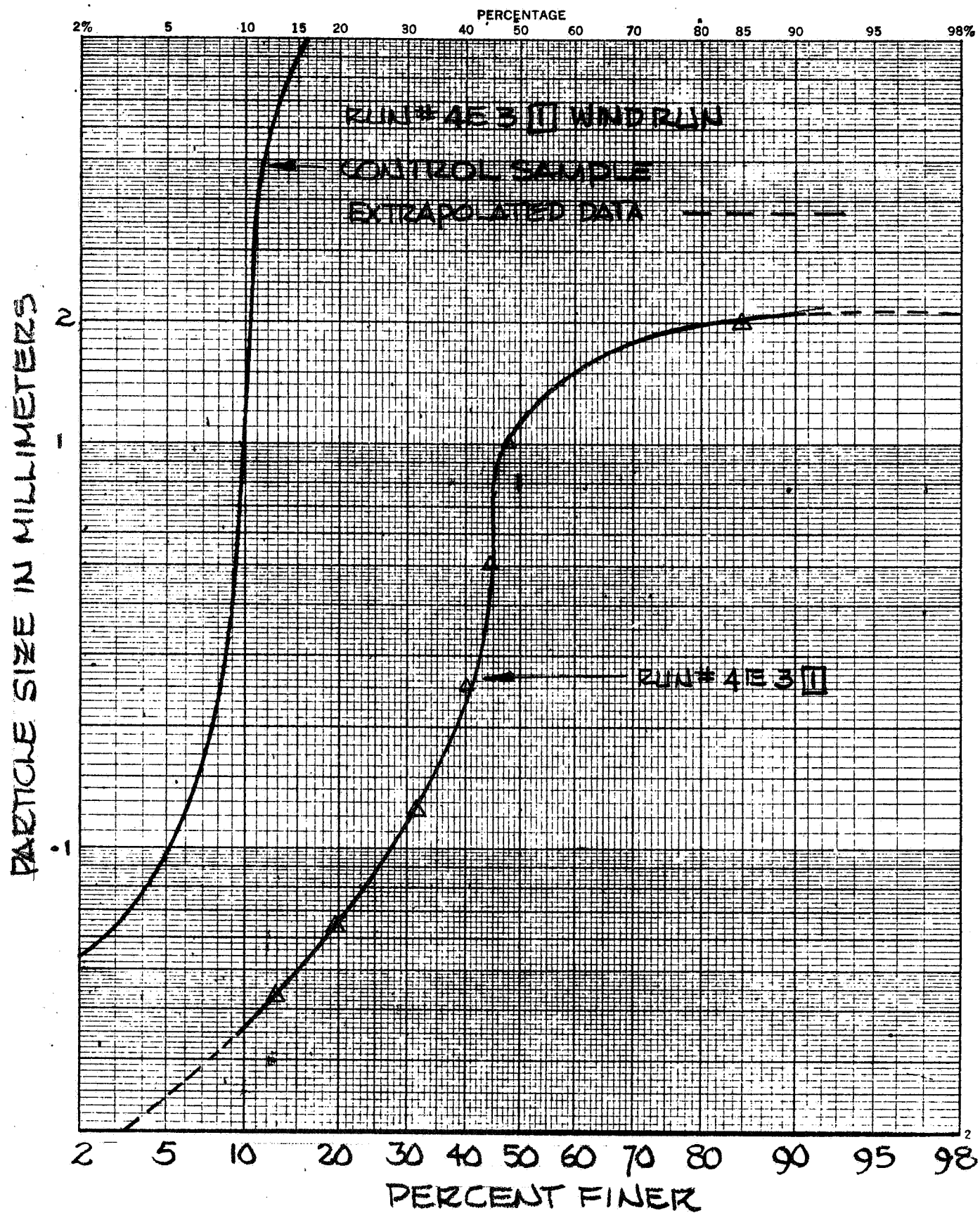


FIGURE D49 PARTICLE SIZE SUMMATION CURVE  
COMPACTED CINDERS

MODEL

DATE

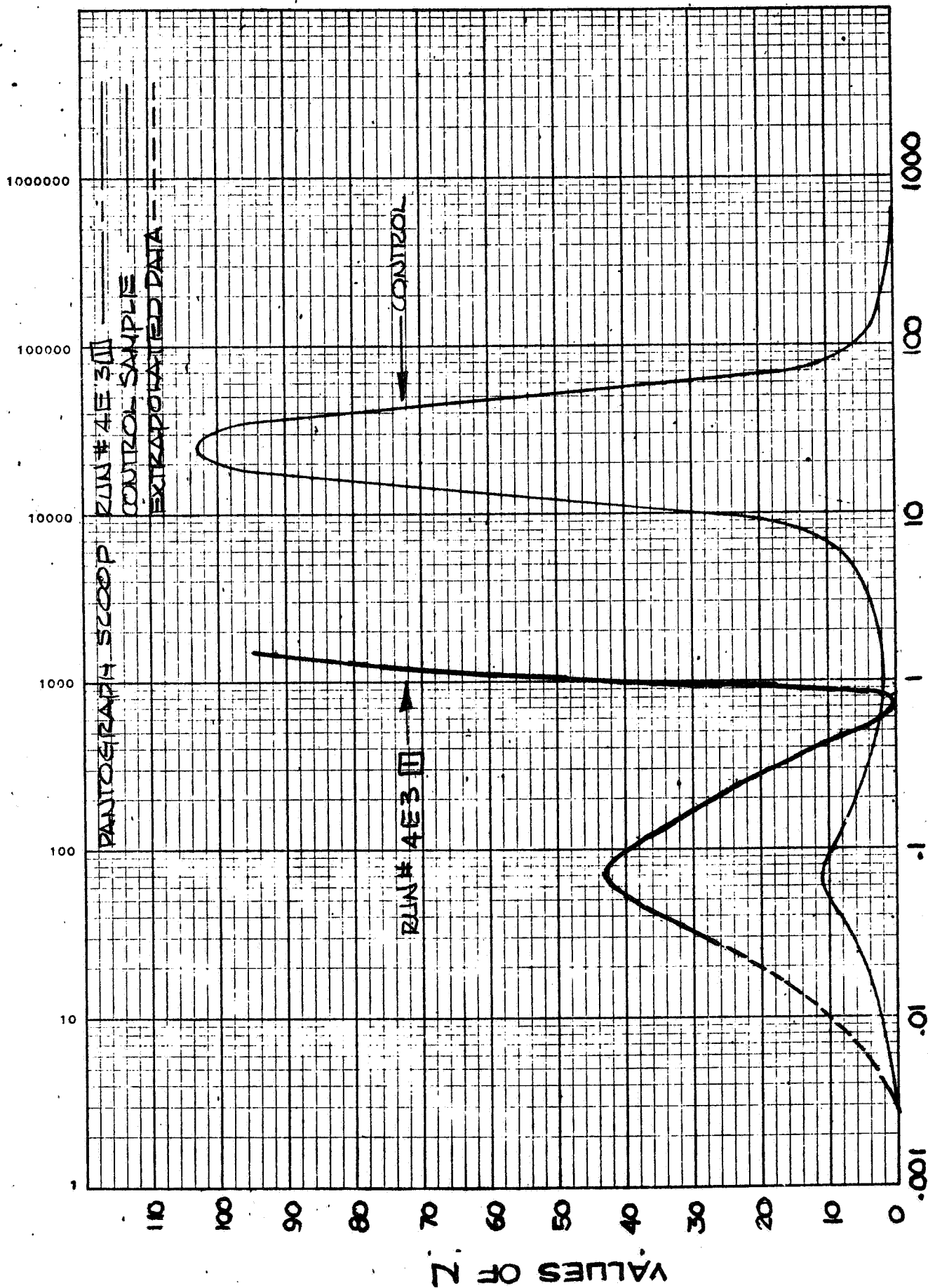


FIGURE D50 PARTICLE SIZE DISTRIBUTION COMPACTED CINDERS





MODEL

DATE

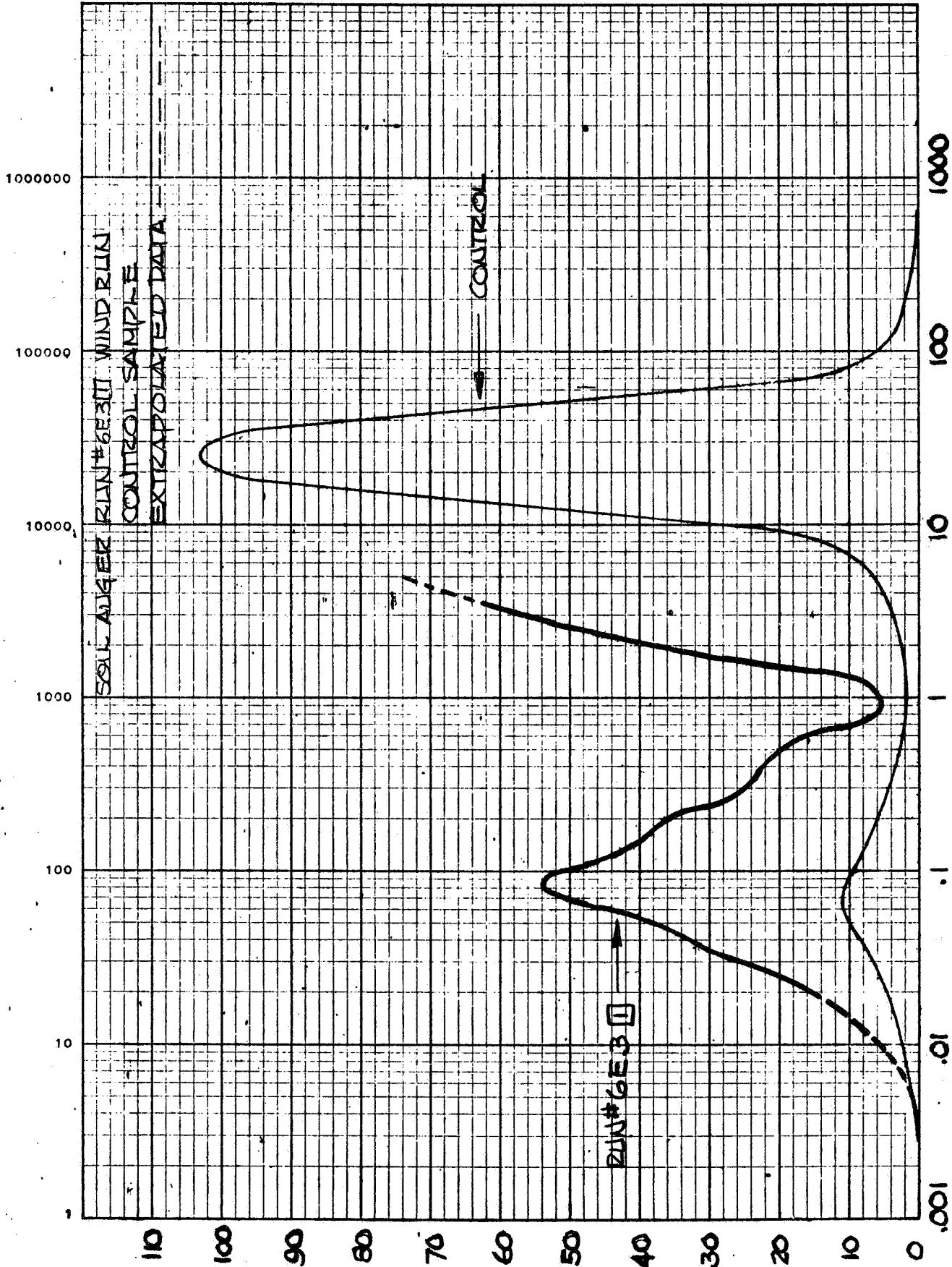


FIGURE D52 PARTICLE SIZE DISTRIBUTION COMPACTED CINDERS

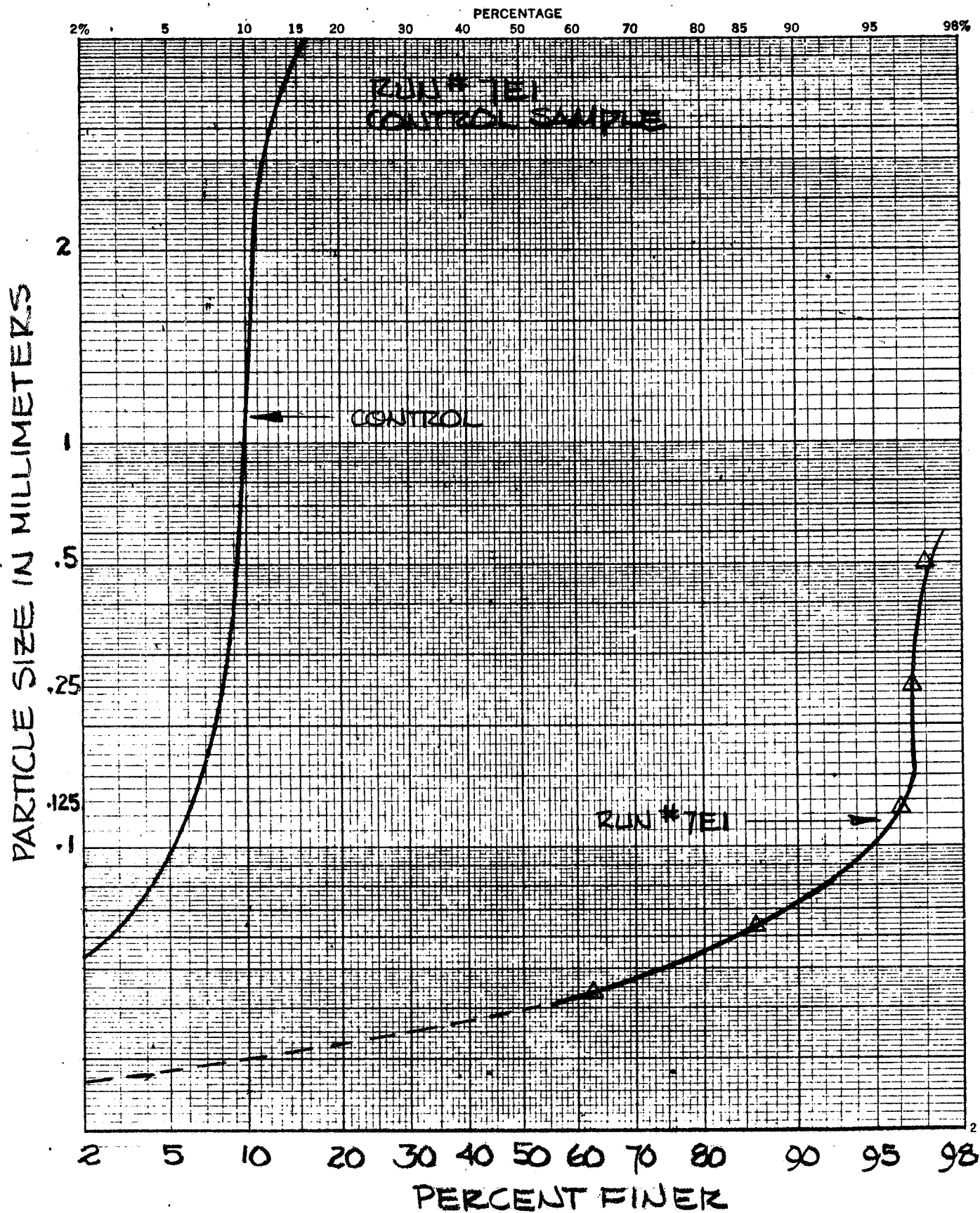


FIGURE D53 PARTICLE SIZE SUMMATION CURVE  
COMPACTED CINDERS



MODEL

DATE

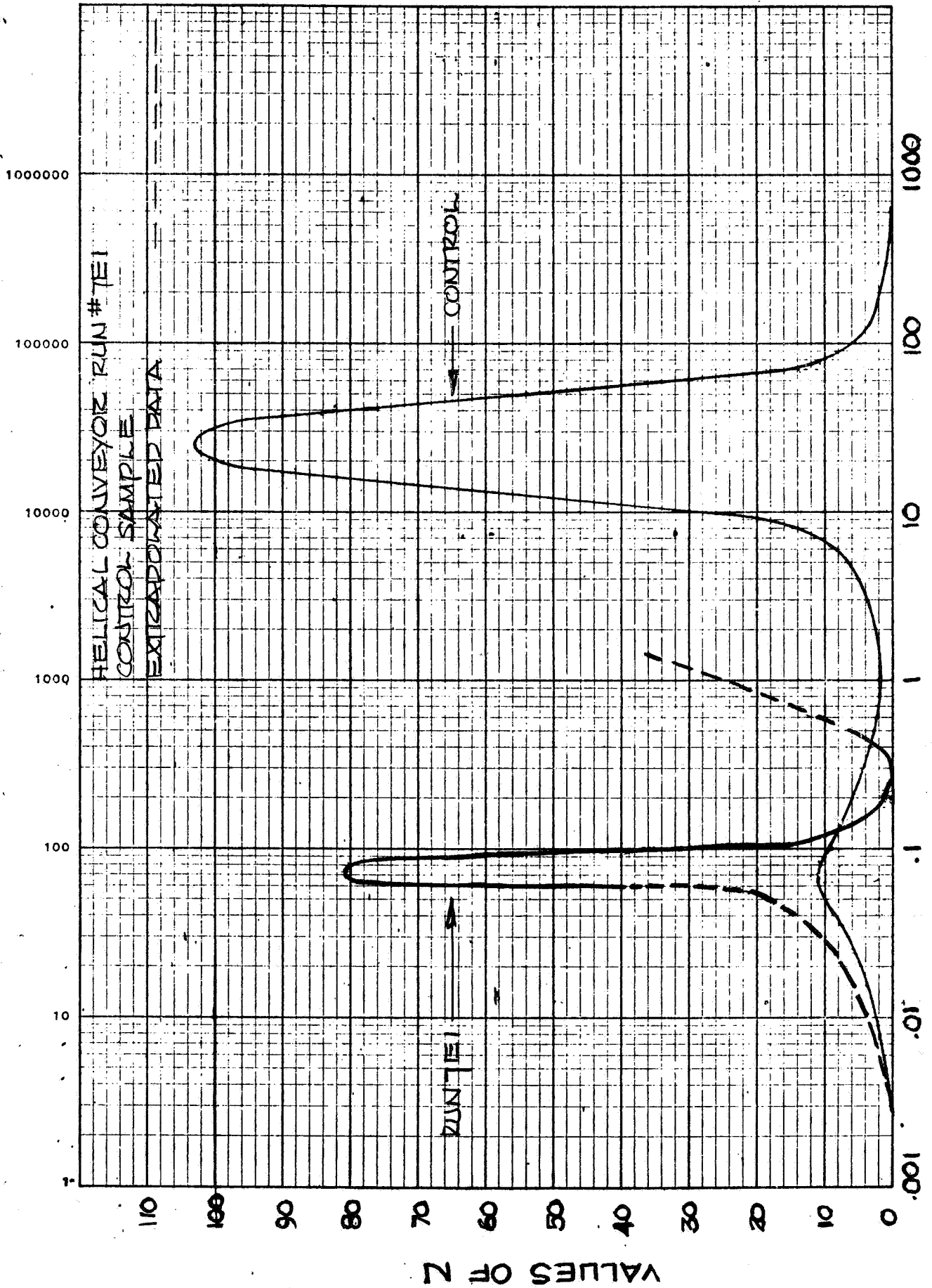


FIGURE D54 PARTICLE SIZE DISTRIBUTION COMPACTED CINDERS

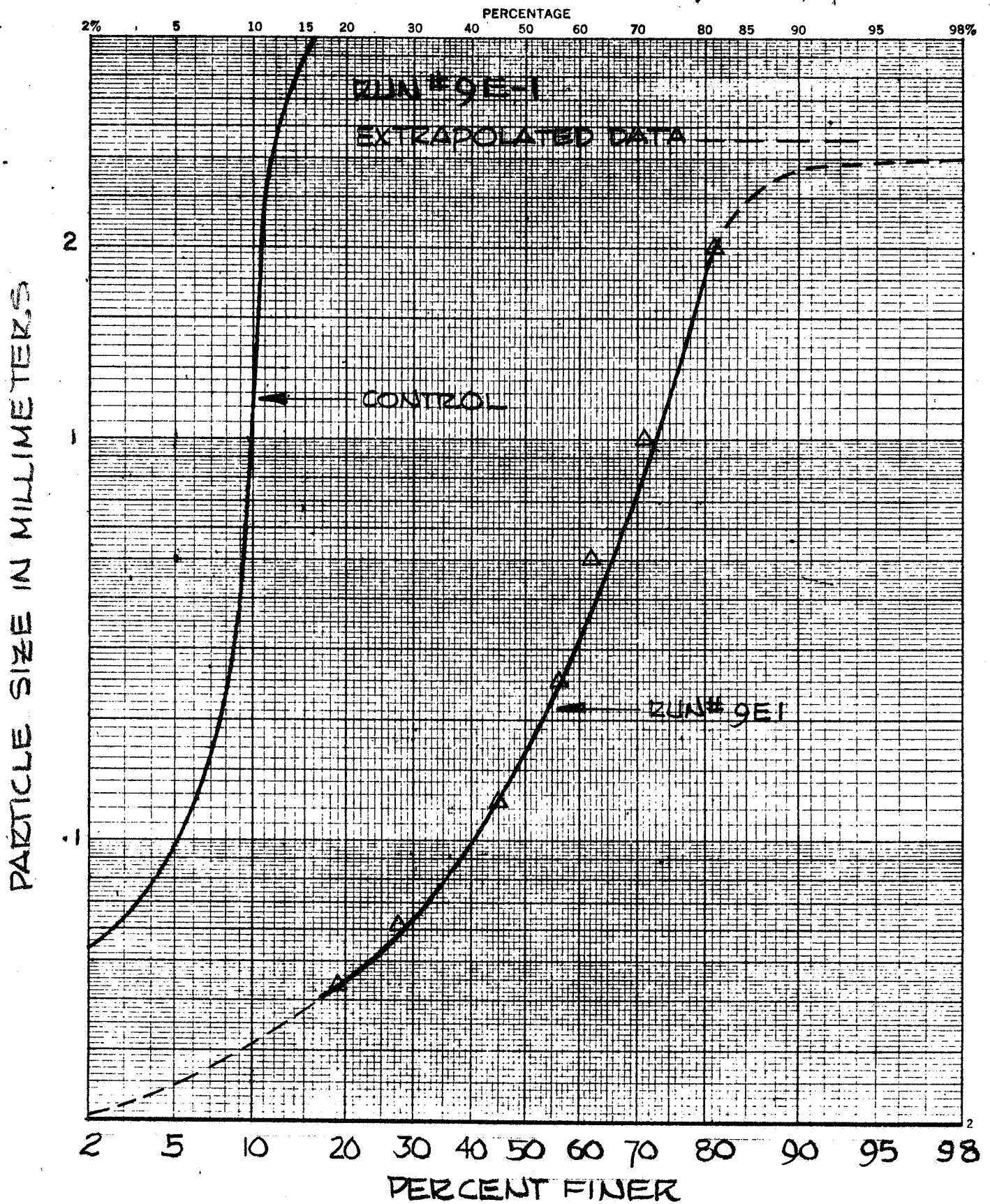


FIGURE D55 PARTICLE SIZE SUMMATION CURVE  
COMPACTED CINDERS

MODEL

DATE

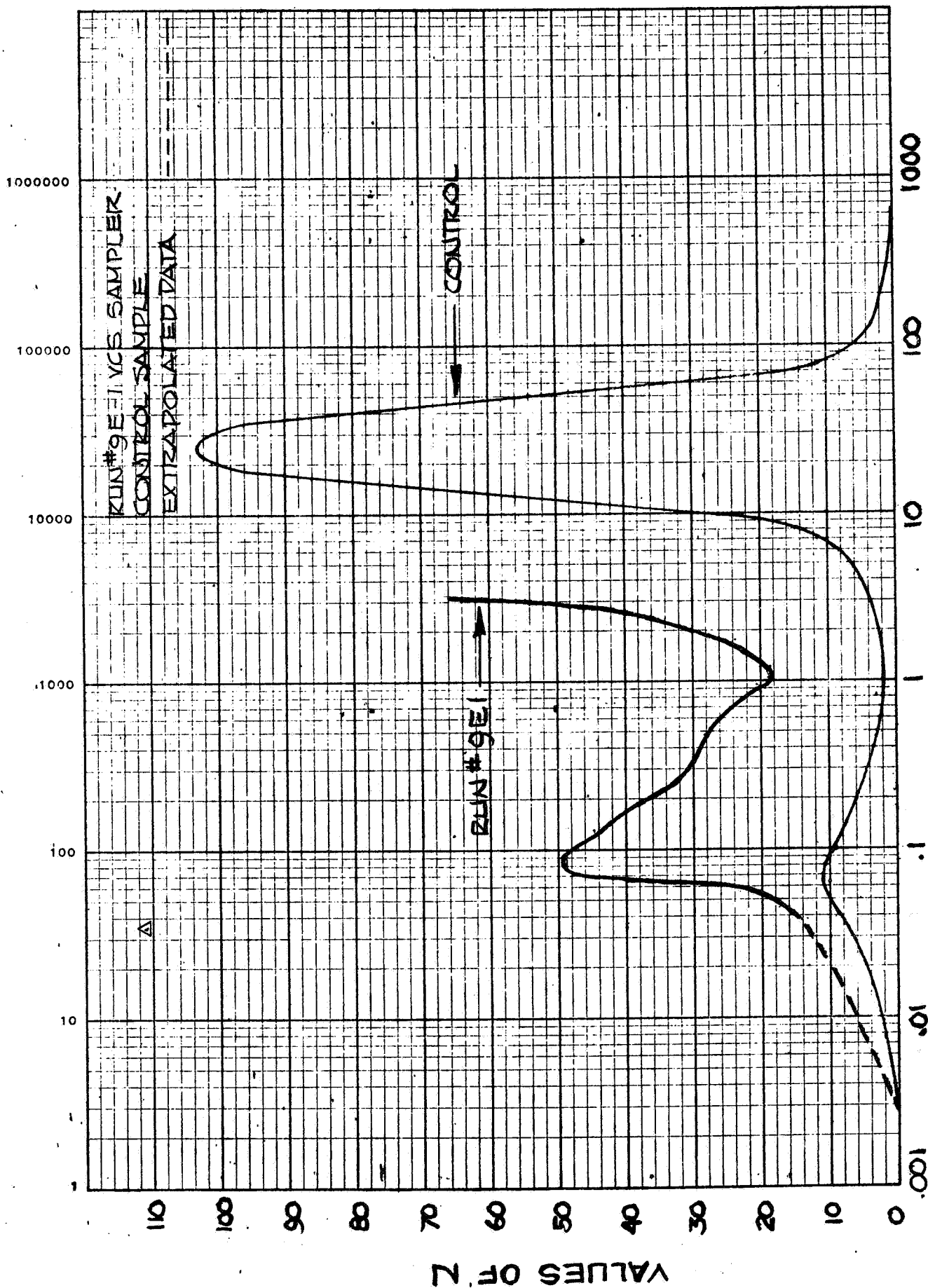


FIGURE D-91 PARTICLE SIZE DISTRIBUTION COMPACTED CINDERS

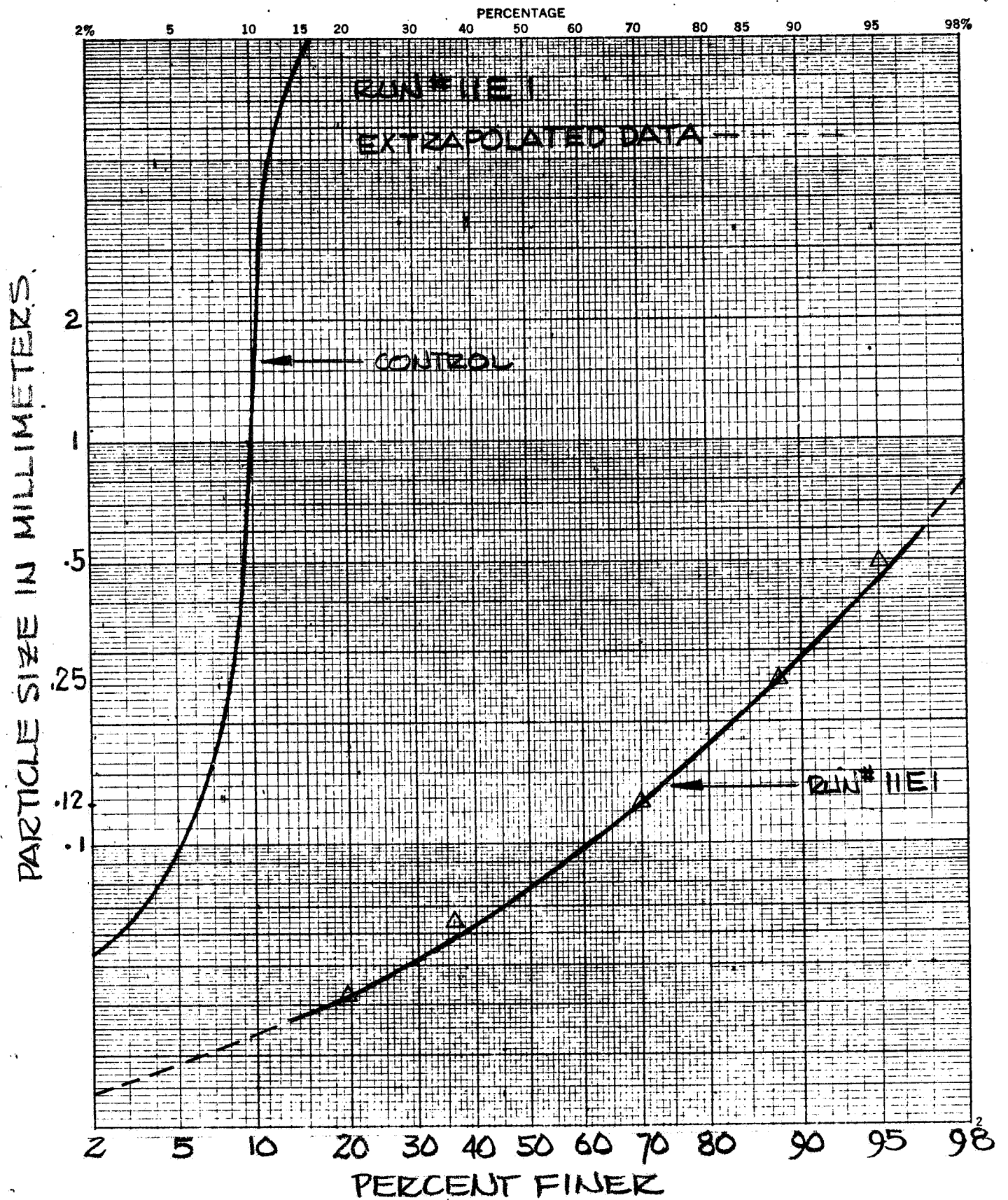


FIGURE 57 PARTICLE SIZE SUMMATION CURVE  
COMPACTED CINDERS

MODEL

DATE

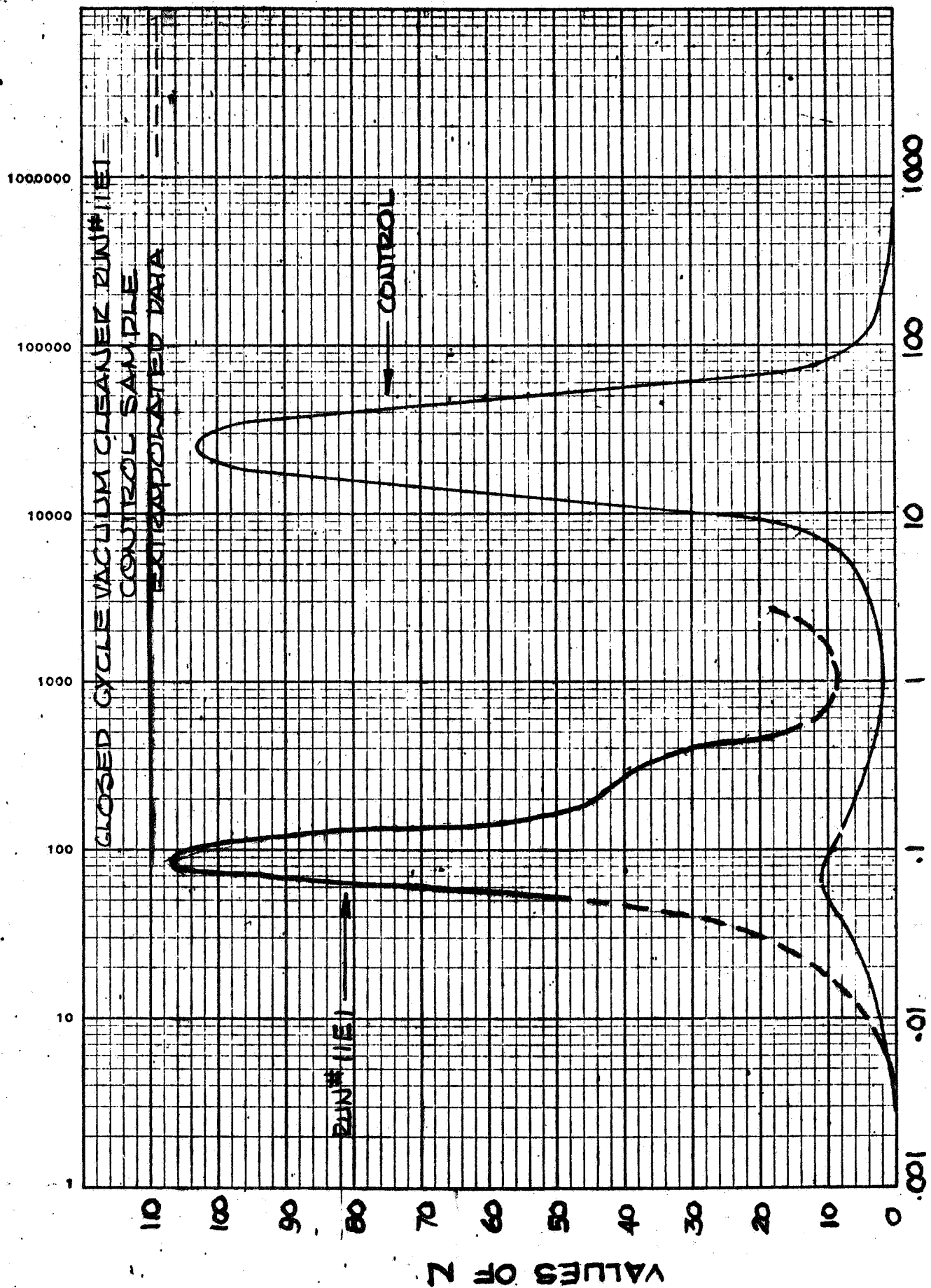


FIGURE D58 PARTICLE SIZE DISTRIBUTION COMPACTED CINDERS

This page intentionally blank.

D.3.4 TEST SITE F, DESERT PAVEMENT

Particle Size Distribution Curves

#### D.3.4 TEST SITE F, DESERT PAVEMENT

This section contains Figures D-59 through D-72 for samples taken at site F.

The control sample at this site consisted of a mixture of two equal populations of fine material with a peak at 100 microns and a coarser material with a peak at 4 or 5 millimeters. In every case the samplers collected predominately from the fine population without sorting or changing the shape of the distribution curve except for sampler 7. The results of sampling run 7F2 are shown in Figures D-67 and D-68 in which it can be seen that this sample has a very narrow distribution with a peak near 60 to 70 microns in diameter.



PARTICLE SIZE IN MILLIMETERS

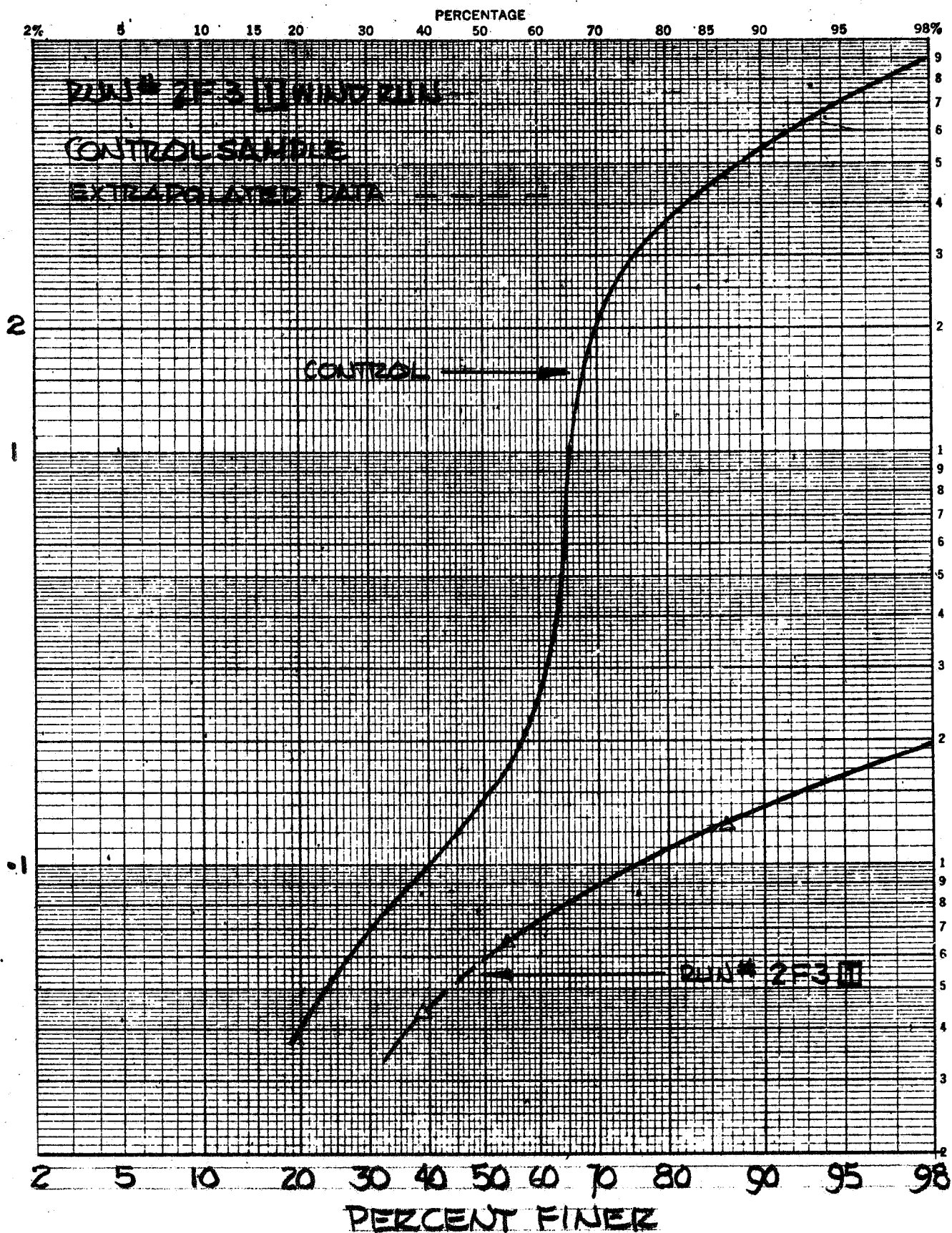


FIGURE D59 PARTICLE SIZE SUMMATION CURVE  
DESERT PAVEMENT

MODEL

DATE

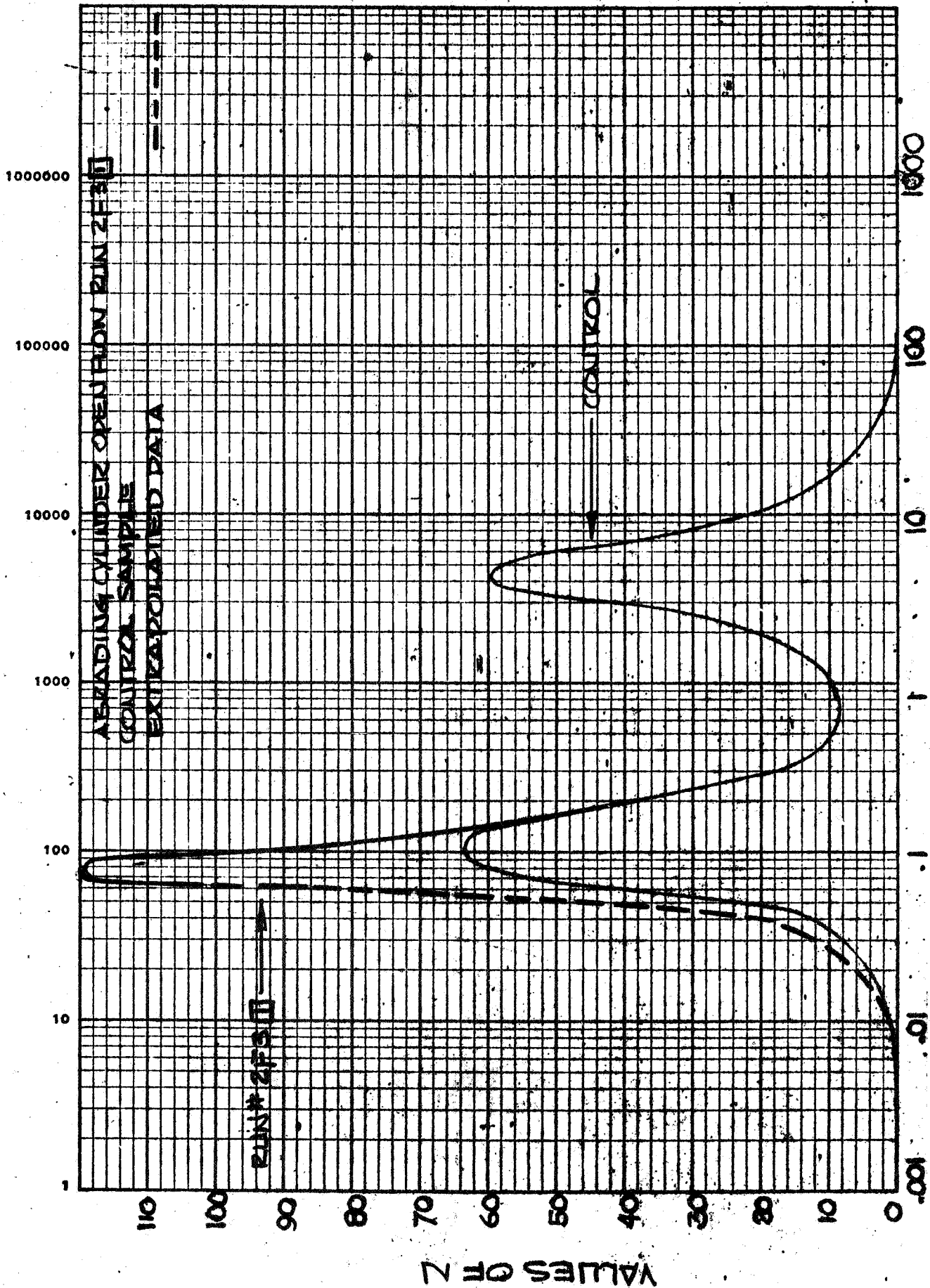
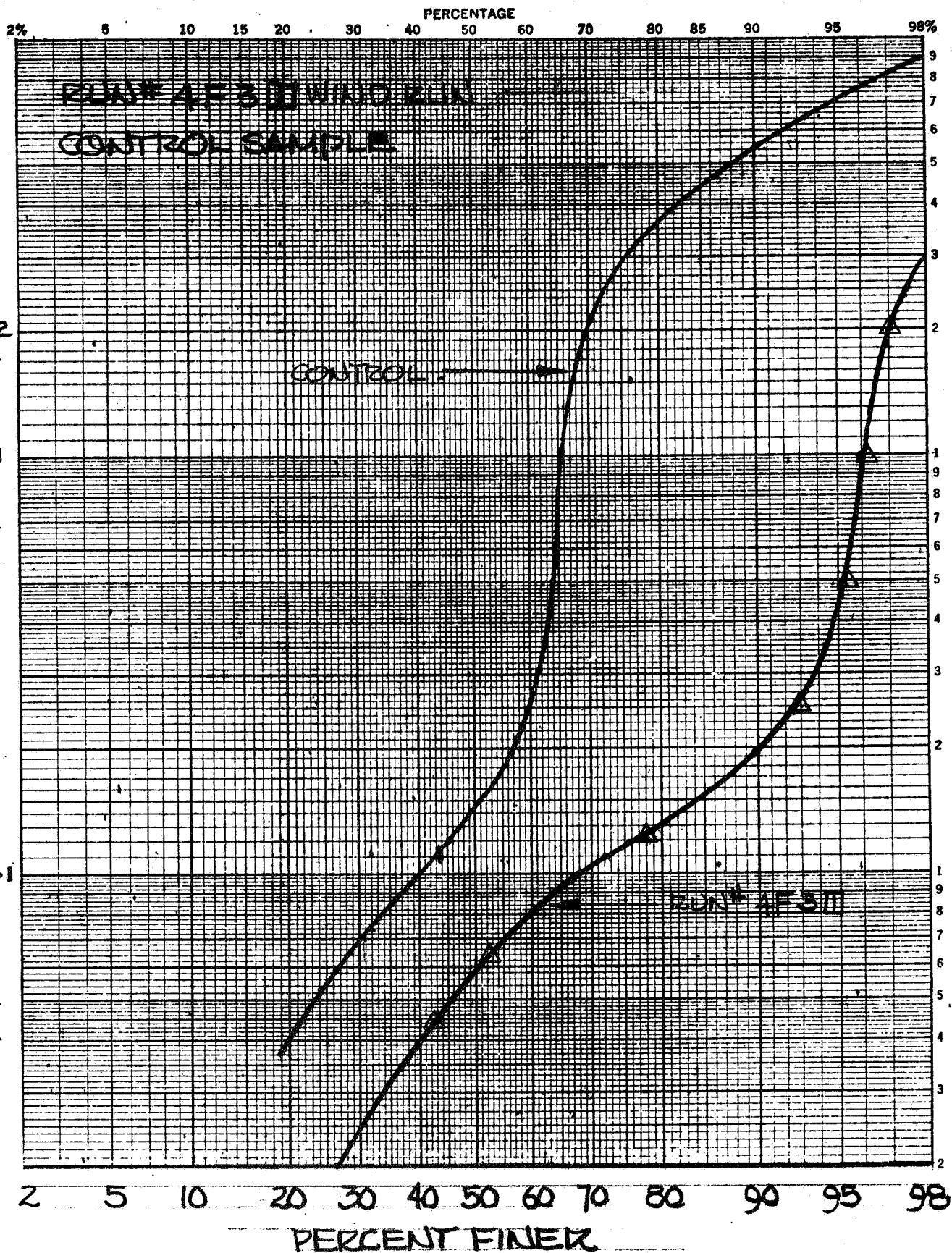


FIGURE D60  
PARTICLE SIZE DISTRIBUTION DESERT PAVEMENT

PARTICLE SIZE IN MILLIMETERS



PARTICLE SIZE SUMMATION CURVE

FIGURE D61 DESERT PAVEMENT

MODEL

DATE

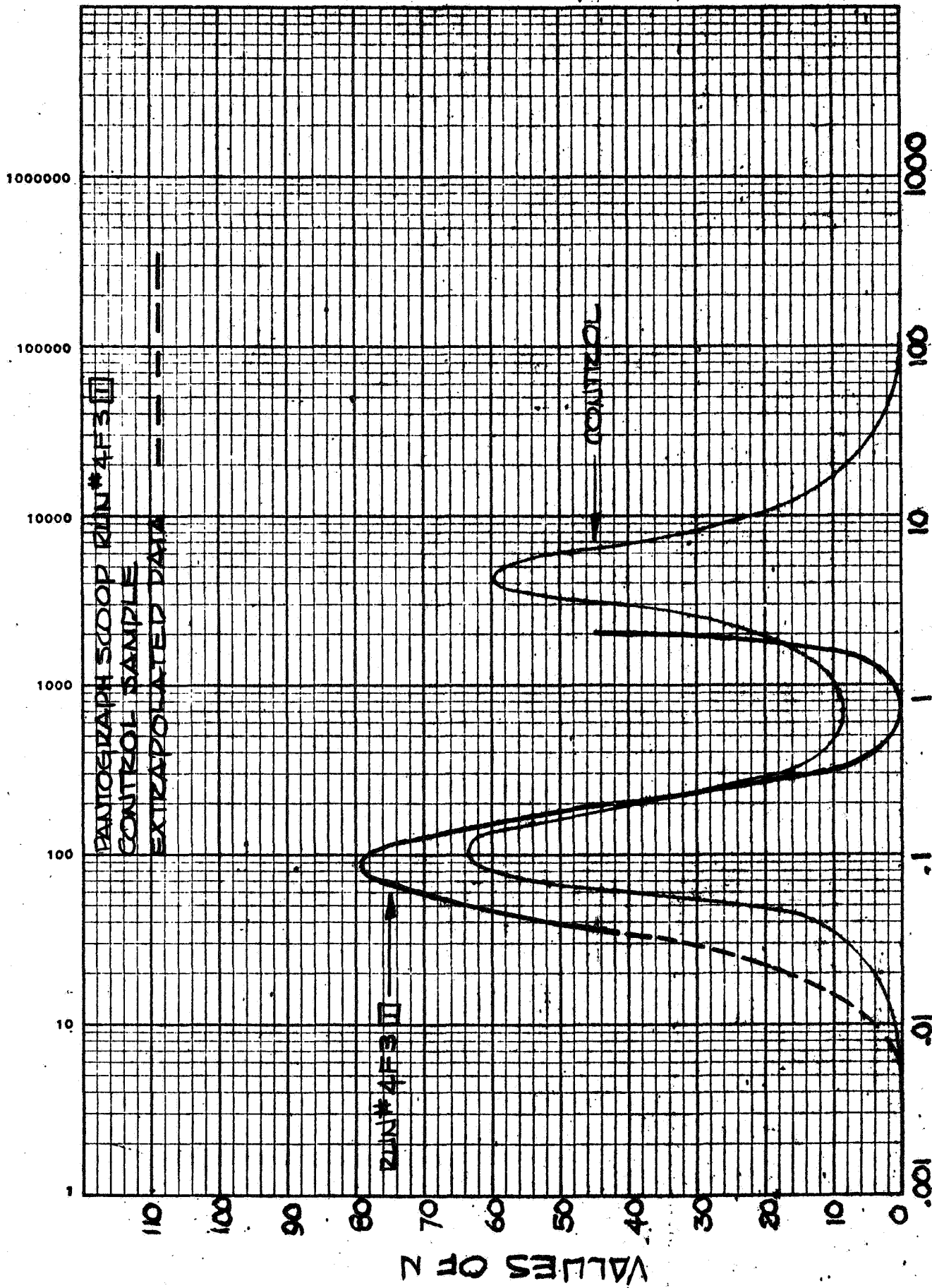


FIGURE D62  
PARTICLE SIZE DISTRIBUTION DESERT PAVEMENT



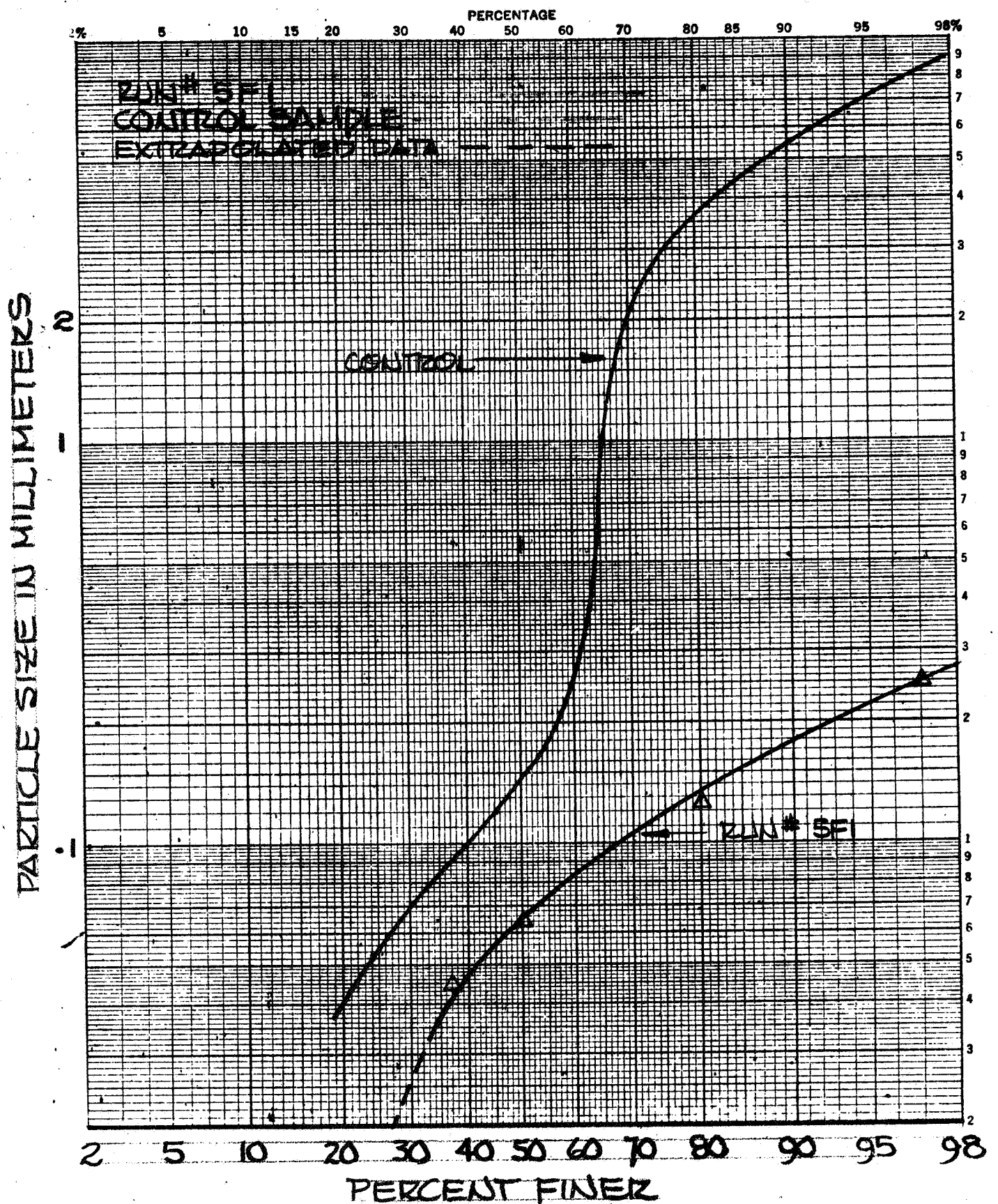


FIGURE D63 PARTICLE SIZE SUMMATION CURVE  
 DESERT PAVEMENT

MODEL

DATE

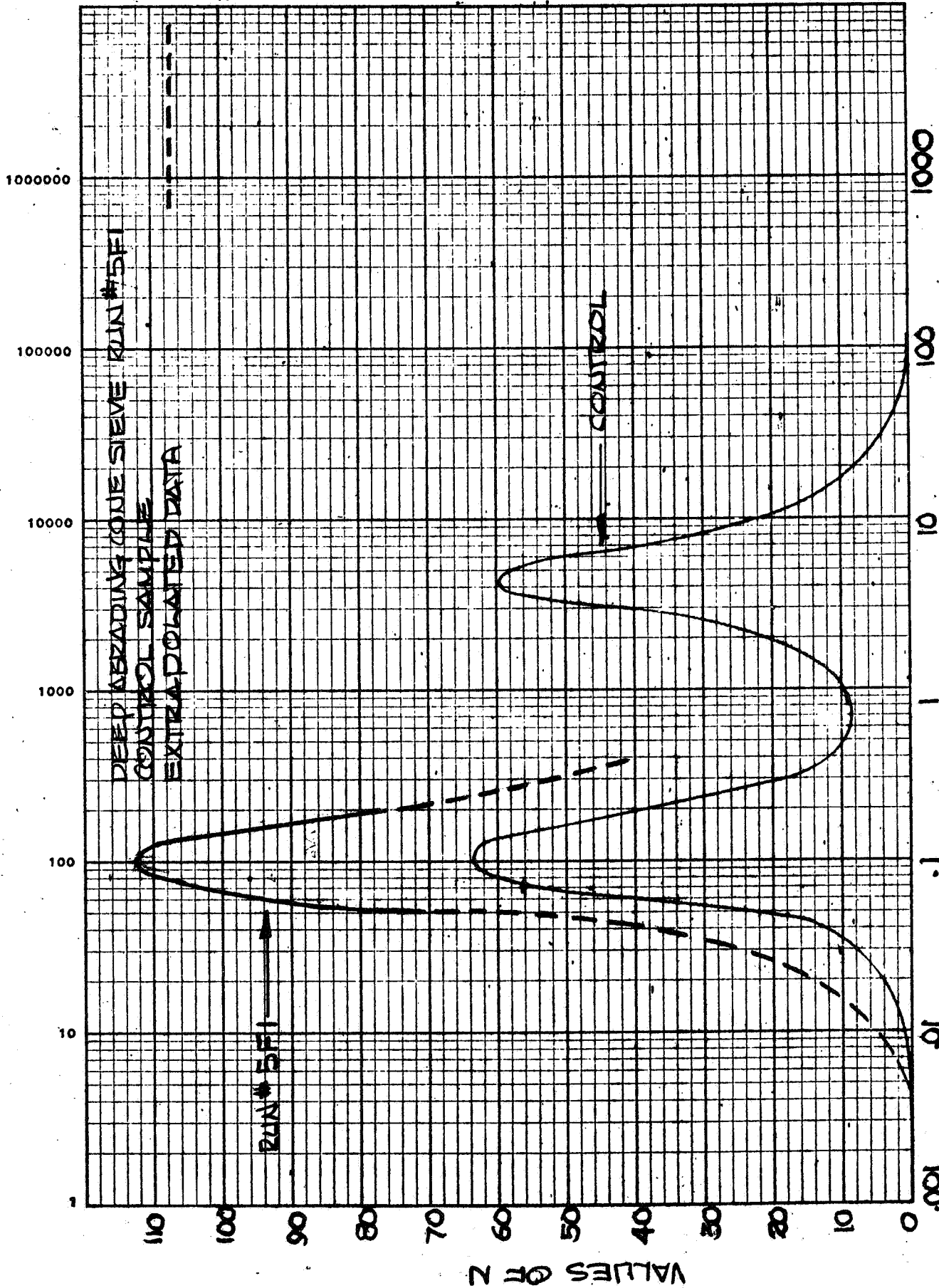


FIGURE D64 PARTICLE SIZE DISTRIBUTION DESERT PAVEMENT

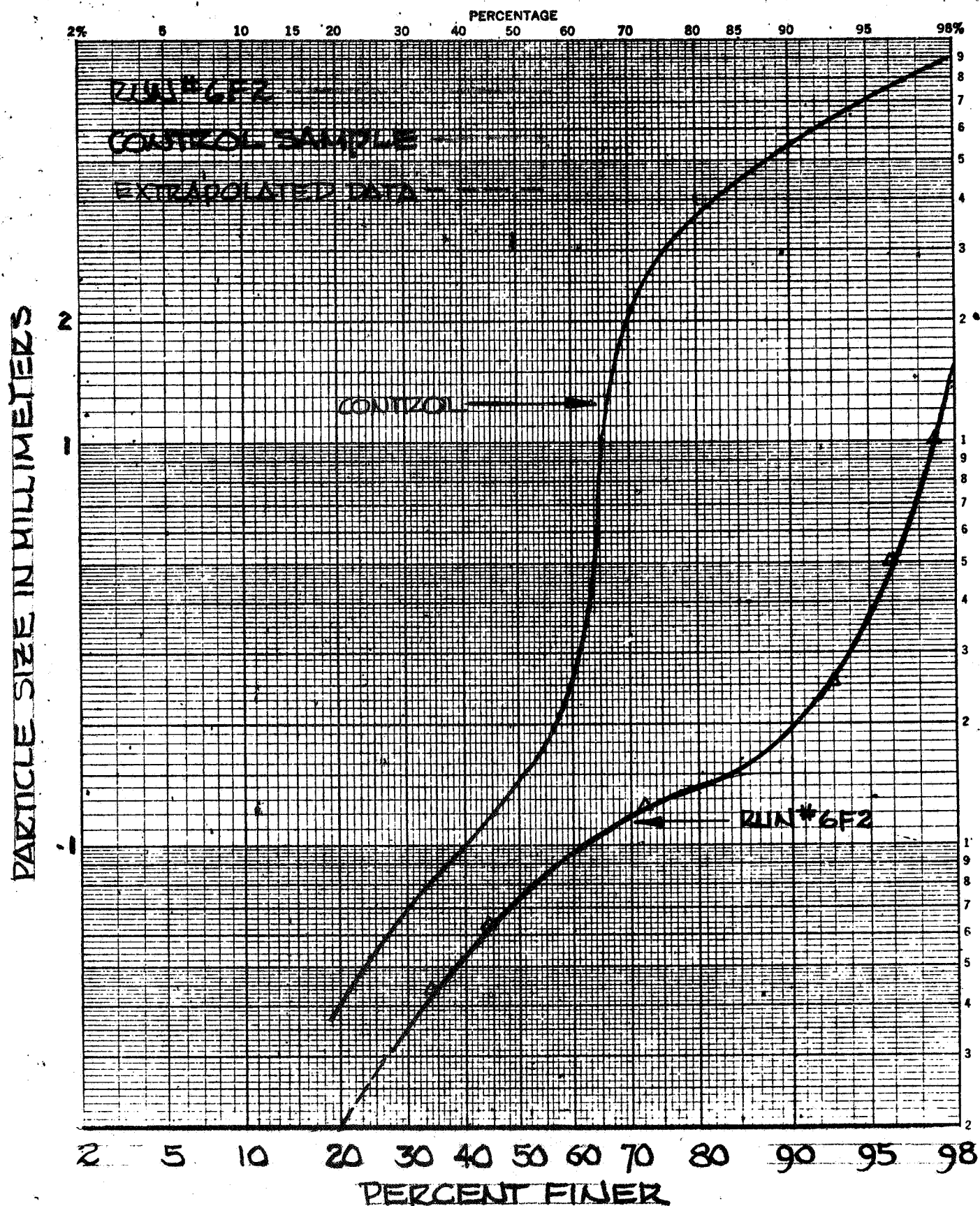


FIGURE D65 PARTICLE SIZE SUMMATION CURVE  
DESERT PAVEMENT

MODEL

DATE

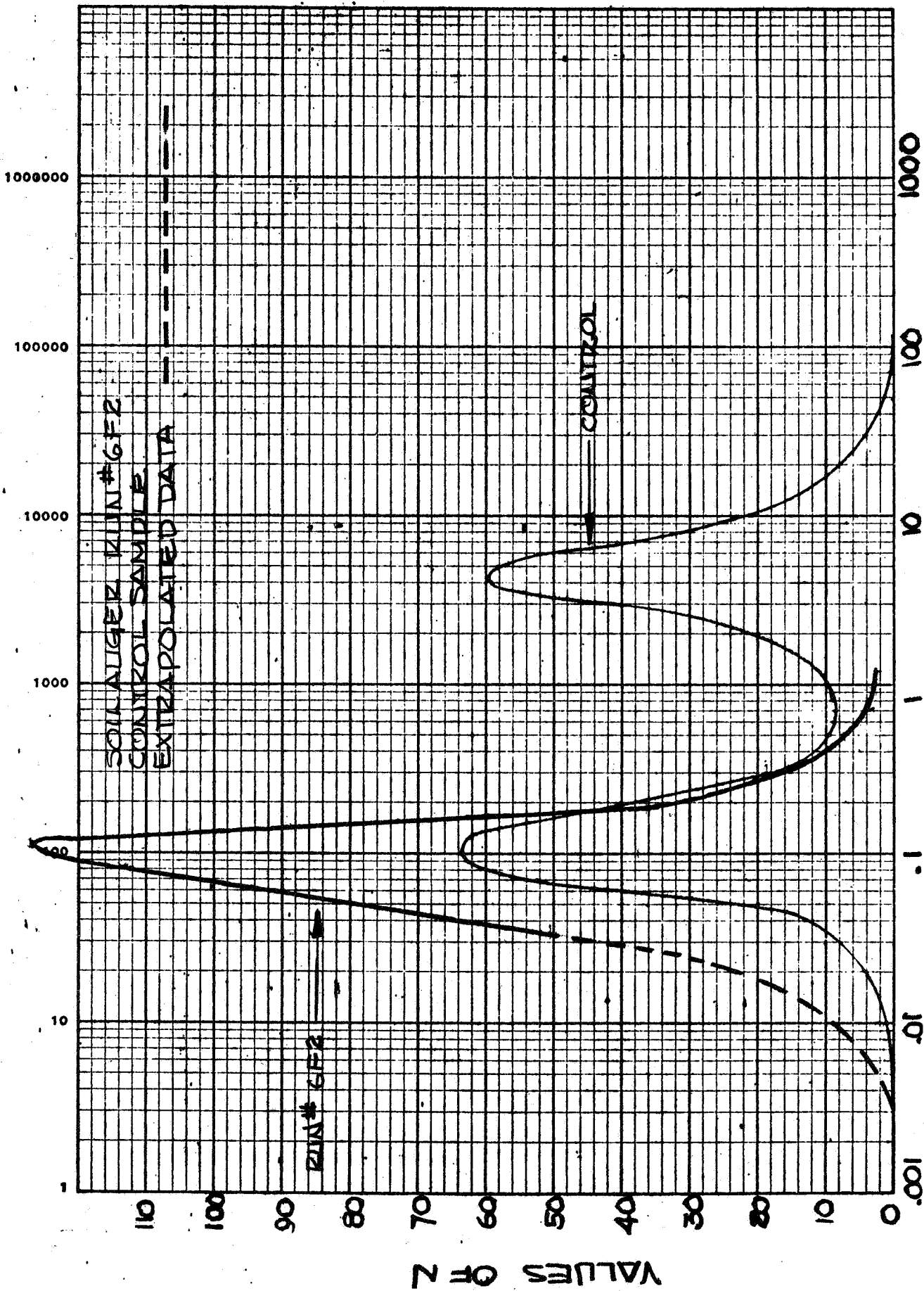


FIGURE D66 PARTICLE SIZE DISTRIBUTION DESERT PAVEMENT



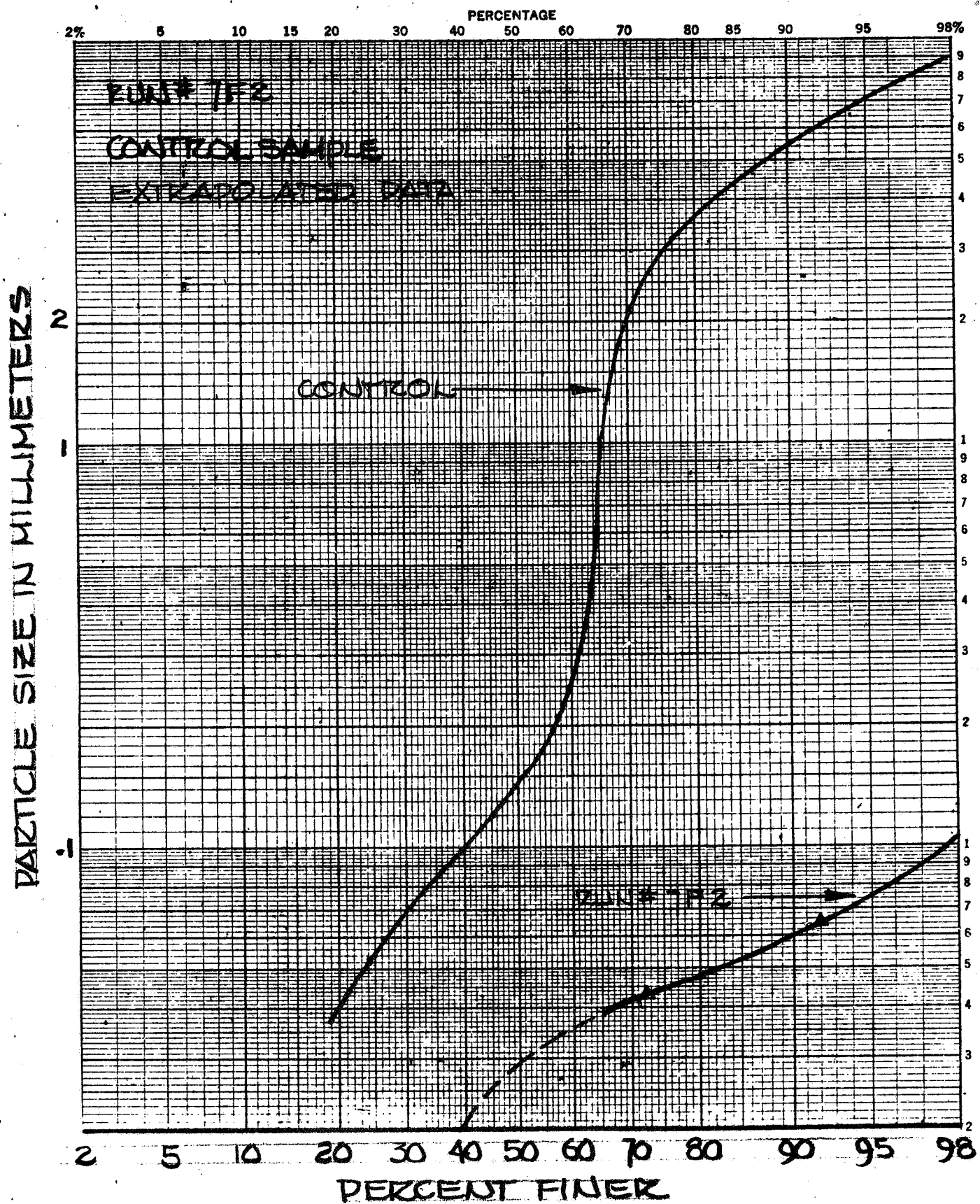


FIGURE D67 PARTICLE SIZE SUMMATION CURVE  
DESERT PAVEMENT

MODEL

DATE

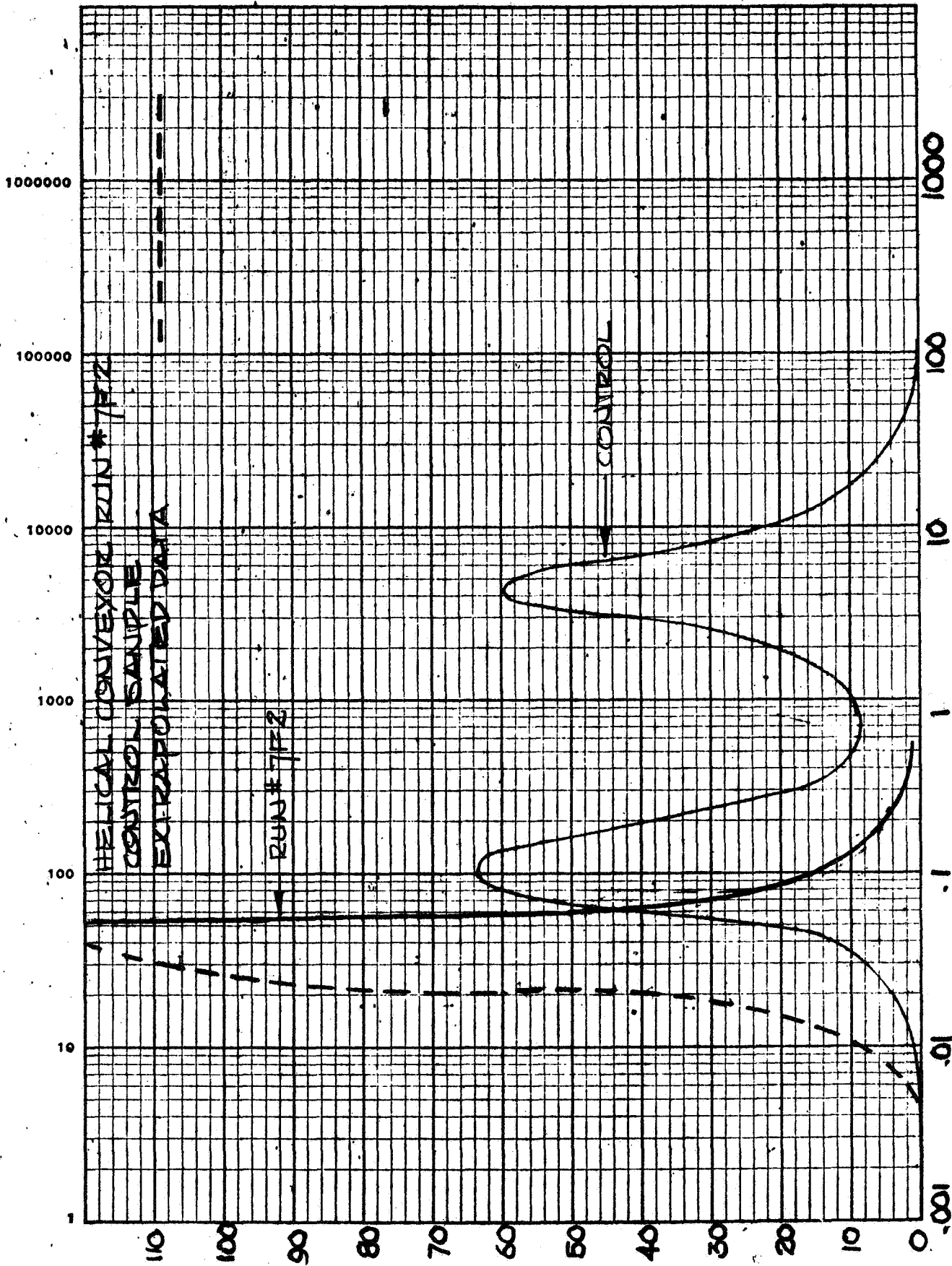


FIGURE D68 PARTICLE SIZE DISTRIBUTION DESERT PAVEMENT

VALUES OF N



MODEL

DATE

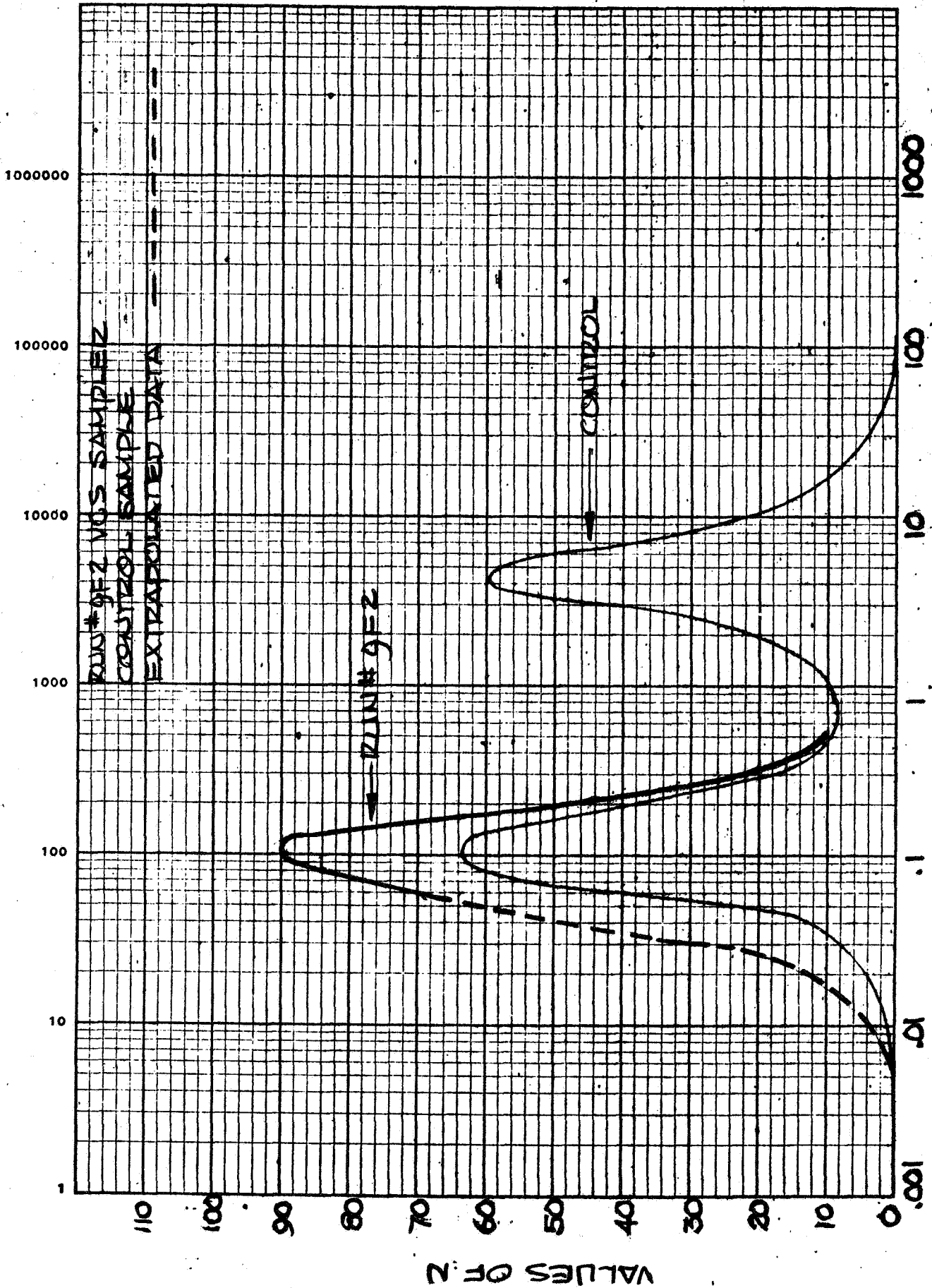


FIGURE D70 PARTICLE SIZE IN MILLIMETERS  
FIGURE PARTICLE SIZE DISTRIBUTION DESERT PAVEMENT

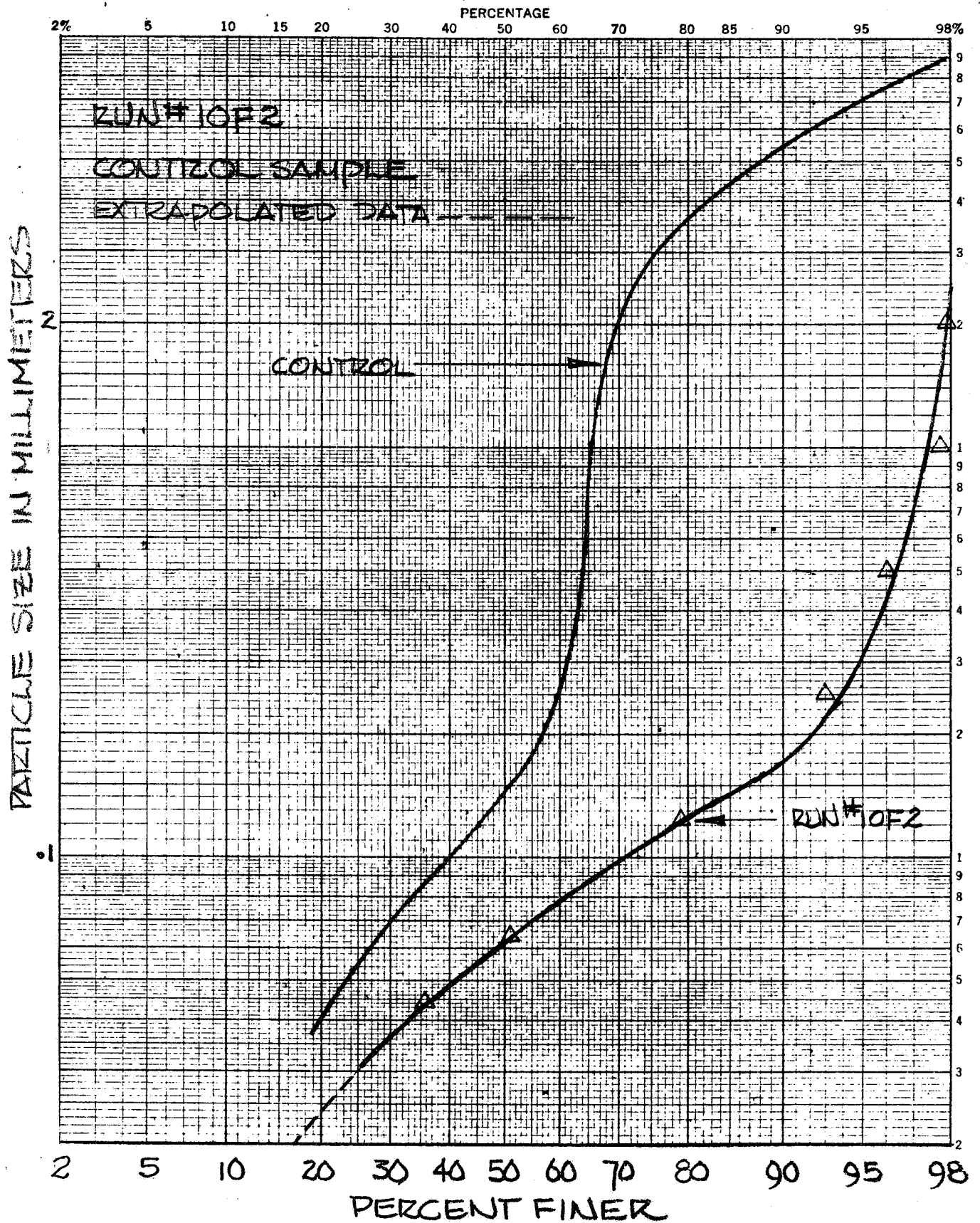


FIGURE D71 PARTICLE SIZE SUMMATION CURVE  
DESERT PAVEMENT



MODEL

DATE

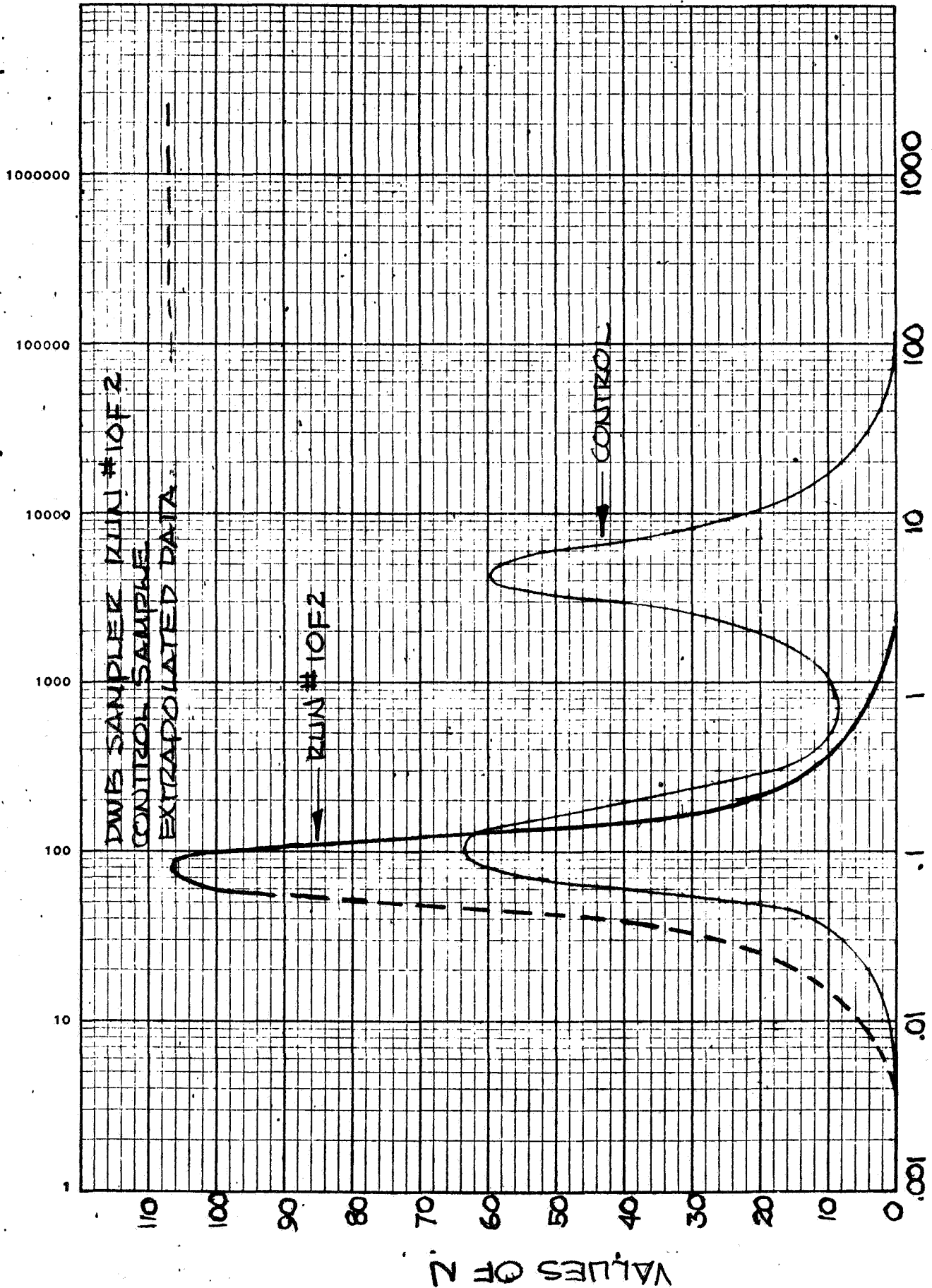


FIGURE D72 PARTICLE SIZE DISTRIBUTION DESERT PAVEMENT

#### REFERENCES

1. Bremner, J. M. (1965). In Methods of Soil Analysis, C. A. Black, Editor-in-Chief, American Society of Agronomy, Inc., Madison, Wisconsin, p 1238 ff.
2. Edwards, A. P. and J. M. Bremner, 1967. "Dispersion of Soil Particles by Sonic Vibration," J. Soil Science 18 (1):47-63.
3. Kunze, G. W. (1965). In Methods of Soil Analysis, C. A. Black, Editor-in-Chief, American Society of Agronomy, Madison, Wisconsin, p 568 ff.
4. Whittig, L. D. (1965). In Methods of Soil Analysis, C. A. Black, Editor-in-Chief, American Society of Agronomy, Madison, Wisconsin, p 671 ff.
5. Bagnold, R. A. (1941). The Physics of Blown Sand and Desert Dunes.
6. Bekker, M. G. (1961). Proceedings of the 1st International Conference on the Mechanics of Soil-Vehicle Systems.

APPENDIX E

PASSIVE SAMPLING BIBLIOGRAPHY



APPENDIX E  
PASSIVE SAMPLING BIBLIOGRAPHY

CONTENTS

- E.1 WIND/SOIL EROSION
- E.2 AIR POLLUTION/DUST COLLECTION/SURFACE CONTAMINATION
- E.3 METEOROLOGY/MICROMETEOROLOGY
- E.4 RADIOACTIVE CONTAMINATION
- E.5 AERO/FLUID DYNAMICS
- E.6 GEOLOGY
- E.7 PAPERS ON THE CHARACTERISTICS OF MARS

## E.1 WIND/SOIL EROSION

1. Akai, S., Meteorological Study of the Dunes of Tottori, Pt. 2, Japan. Meteorological Agency, Tokyo, Memoirs of Industrial Meteorology, 20(2): 29-37, Jan. 1957, 3 refs.
2. Bagnold, R. A., Physics of Blown Sand and Desert Dunes, Methuen & Co. Ltd., 1960.
3. Bagnold, R. A., (Royal Society, London), Surface Movement of Blown Sand in Relation to Meteorology. (In: International Symposium on Deserts Research, Jerusalem, May 7-14, 1952, Proceedings, p 89-96, pub. 1953.)
4. Bagnold, R. A., The Flow of Cohesionless Grains and Fluids, Phil. Trans. A249, 235, 1956.
5. Chepil, W. S., The Use of Evenly Spaced Hemispheres to Evaluate Aerodynamic Forces on a Soil Surface, Trans. Am. Geophys. Union, 39, 397-404, 1958.
6. Chepil, W. S., Sedimentary Characteristics of Dust Storms, Pt. 1, Sorting of Wind-Eroded Soil Material. American Journal of Science, New Haven, Conn., 255 (1):12-22, Jan. 1957, 3 figs., 4 tables, 12 refs.
7. Chepil, W. S. and Woodruff, N. P., Pt. 2, Visibility and Dust Concentration, Ibid., 255 (2):104-114, Feb. 1947, 3 figs., table, 5 refs., 10 eqs.
8. Chepil, W. S., Pt. 3, Composition of Suspended Dirt, Ibid., 255(3): 206-213, March 1957.
9. Chepil, W. S. (U.S. Dept. of Agri. & Kansas Agri. Experiment Sta., Manhattan), Transport of Soil and Snow by Wind. Meteorological Monographs, Boston, 6(28):123-132, July 1965.
10. Clements, T., R. O. Stone, J. F. Mann, Jr., and J. L. Eymann, A Study of Windborne Sand and Dust in Desert Areas, Army Natick Labs. Tech. Rept. ES8, 1963.

11. Chepil, W. S., Dynamics of Wind Erosion, Pts. I to IV, Soil Science, 60, 305, 1945; *ibid* 60, 397; *ibid* 60, 475 and *ibid* 61, 167, 1946.
12. Fristrup, Borge, Wind Erosion within the Arctic Deserts. Geografisk Tidsskrift, Copenhagen, 52:51-65, 1952/53.
13. Gael', A. G. and Smirnova, L. F. (both, Moscow Gosudar, Univ.), K voprosu sifikatsii legkikh pochv po stepeni ikh vetrovoi erodirovannosti, (Classification of Soils According to their Wind Erodibility) Pochvovedenie, Moscow, No. 4:1-15, April.
14. Grosse, Bernhard, Die Erodierbarkeit von Boden durch Wind, (Wind Erosion of the Soil), Geologisches Jahrbuch, Hanover, 71:527-530, 1956.
15. Hilst, Glenn R. and Nickola, Paul W., (Gen. Electric Co., Richland, Wash.), On the Wind Erosion of Small Particles, American Meteorological Society, Bulletin, 40(2):73-77, Feb. 1959.
16. Kiselev, A. N., Sviaz' mezhdv vodnoi eroziei i defliatsiei pochovy. (Relation between water and wind erosion.) Pochvovedenie, Moscow, No. 9:840-850, Sept. 1952.
17. Parkinson, G. R., Dust Storms over the Great Plains, Bull. Am. Meteorol. Soc., 17, 127-135, 1936.
18. Roberts, Edd and Bunch, Clarence E., Wind Erosion in Oklahoma, Oklahoma Univ., Circular 3-667m (1958).
19. Smith, G. O., Illinois Loess-Variations in its Properties and Distribution, Univ. Illinois Agr. Expt. Sta. Bull. 490, 1942.
20. Tanaka, S., Sano, H. and Kakinuma, S., Relation of Soil Moisture to the Wind Velocity Required to Initiate Soil Movement, (Study on the control of wind-erosion, Pt. 1), Jour. of Agri. Meteorology, Tokyo, 10(1/2):57-60, Dec. 1954.
21. Tanaka, Sadao; Tanizawa, Tsuneo and Kodera, Shinji (Kanto-Tosan Agric. Exper. Sta.), On the Wind Erosion of Cultivated Field, Pt. 1, Jour. of Agri. Meteorology, Tokyo, 9(3/4):125-126, Aug. 1954.
22. Tamura, T., Characteristics of Eolian-Influenced Soils in Connecticut, 2, Soil Sci. Soc. Am. Proc., 21, 536-539, 1957.
23. Waggoner, P. E., and L. Bingham, Depths of Loess and Distance from Source, Soil Sci., 92, 396-401, 1961.
24. Warn, G. F., Some Dust Storm Conditions of the Southern High Plains, Bull. Am. Meteorol. Soc., 33, 240-243, 1952.

25. Zingg, A. W. (U. S. Bur. of Plant Ind., Soil and Agr. Engr., Manhattan, Kansas), The Wind Erosion Problem in the Great Plains, American Geophys. Union, Trans., 35(2):252-258, April 1954.

## E.2 AIR POLLUTION/DUST COLLECTION/SURFACE CONTAMINATION

1. Bagnold, R. A., The Re-entrainment of Settled Dusts, Int. J. Air Poll. 2, 357, 1960.
2. Billings, C. E., L. Silverman, R. Dennis and L. H. Levenbaum, Shock Wave Cleaning of Air Filters, J. Air Poll. Control Assn., 10, 318, 1960.
3. Bock, P., Some Physical Aspects of Flow Near Surfaces, Trans. New York Acad. Sci., 25, Ser. II, 902, 1963.
4. Browning, W. E., Jr., and M. H. Fontana, unpublished report (1963).
5. Bradley, R. S., The Cohesive Force Between Solid Surfaces and the Surface Energy of Solids, Phil. Mag. 13, 853, 1932.
6. Chamberlain, A. C., Aspects of Travel and Deposition of Aerosol and Vapour Clouds, AERE Report HP/R, 1261.
7. Chamberlain, A. C., Transport of Particles Across Boundary Layers, AERE-M 1122, 1962.
8. Corn, M., The Adhesion of Solid Particles to Solid Surfaces, I and II, J. Air Poll. Control Assn., 11, 523, 566, 1961.
9. Corn, M., and F. Stein, Re-entrainment of Particles from a Plane Surface, Amer. Ind. Hyg. Assoc., J. 26, 325, 1965.
10. Davies, C. N., M. Aylward and D. Leacey, Impingement of Dust from Air Jets, AMA Arch. Ind. Hyg. and Occ. Med. 4, 354, 1951.
11. Davies, C. N., Nature, 195 (4843), 768, 1952; ib. 201 (4922), 905, 1964; Recent Advances in Aerosol Research, Pergamon Press, Oxford, 1964.
12. Deryaguin, B. F. and Bakanov, S. P., Dokl. Acad. Nauk SSSR. 147, 139, Nature 196, 669, 1962.
13. Deryaguin, B. V. and Dukhin, S., Dokl. Acad. Nauk SSSR. 111, 613, 1956.
14. Deryaguin, B. V., and A. D. Zimon, Adhesion of Powder Particles to Plane Surfaces, Kolloidn. Zh. 23, 454, 1961. Translation by the Consultants Bureau, Chicago, Ill.

15. Fage, A. and H.C.H. Townend, An Examination of Turbulent Flow with an Examination of Turbulent Flow with an Ultramicroscope, Proc. Roy. Soc. (London) 135 Ser. A, 656, 1932.
16. Fish, B. R., Surface Contamination, Pergamon Press Ltd., 1967.
17. Foster, W. W., Brit. J. Appl. Physics. 10 (5), 206, 1959.
18. Friedlander, S. R., and H. F. Johnstone, Deposition of Suspended Particles from Turbulent Gas Streams, Ind. and Eng. Chem. 49, 1151, 1957.
19. Fuchs, N. A., The Mechanics of Aerosols, Enl. edn. Pergamon Press, Oxford, 1964.
20. Gerrard, J. H., An Experimental Investigation of the Initial Stages of the Dispersion of Dust by Shock Waves, Brit. J. Appl. Phys. 14, 186, 1963.
21. Gish, O. H., Universal Aspects of Atmospheric Electricity, in Compendium of Meteorology, (T. F. Malone, Ed.), American Meteorological Soc., Boston, Mass., 1951, p 101.
22. Green, H. L., and W. R. Lane, Particulate Clouds: Dusts, Smokes and Mists, Van Nostrand, New York, pp 70-78, 1957.
23. Heating, Ventilating and Air Conditioning Guide, V. 34, Amer. Soc. Htg. and Air Cond. Engrs., New York, 1956, pp 705-706.
24. Hinkle, B. L., C. Orr and J. M. Dallavalle, A New Method for the Measurement of Aerosol Electrification, J. Coll. Sci. 9, 70, 1954.
25. Jacobs, M. B., A. Monoharan and L. J. Goldwater, Comparison of Dust Counts of Indoor and Outdoor Air, Int. J. Air and Water Poll. 6, 205, 1962.
26. Jordan, D. W., The Adhesion of Dust Particles, Brit. J. Appl. Phys. 3, S194, 1954.
27. Kunkel, W. B., Charge Distribution in Coarse Aerosols as a Function of Time, J. Appl. Phys. 21, 833, 1950.
28. Larsen, R. I., The Adhesion and Removal of Particles Attached to Air Filter Surfaces, Amer. Ind. Hyg. Assoc. J. 19, 265, 1958.
29. Magill, P. L., F. R. Hoiden, C. Ackley, Air Pollution Handbook, McGraw-Hill Book Co., Inc., 1956.

30. Owe Berg, T. G., and N. Brunetz, Behavior of Charged Particles on Glass Slides, Arch. Env. Health 5, 22, 1962.
31. Penney, G. W., and E. H. Klinger, Contact Potentials and the Adhesion of Dust, AIEE Conf. Paper, New York, N.Y., Jan. 29-Feb. 3, 1961.
32. Perry, J. H., Chemical Engineers Handbook, Gas-Solids Separations Section 20, pp 62-96, McGraw-Hill Book Co., 1963.
33. Pich, J., Staub. 22 (1), 15, 1962.
34. Rohatschek, H., Acta Phys. Austriaca, 10 (3), 227, 267, 1956.
35. Spinrad, H., Schorn, R., Moore, R.
36. Stern, A. C., Air Pollution, Vol. I and II, Academic Press, 1962.
37. Symposium, Atmospheric Diffusion and Air Pollution, Academic Press, 1959.
38. Thomas, J. W., The Diffusion Battery Method for Aerosol Particle Size Determination, ORNL-1648, Dec. 14, 1953.
39. Vogelpohl, G., and D. Mannesmann, Flow Investigation with the Aid of the Ultramicroscope (1937); Translation, National Advisory Committee for Aeronautics, Technical Memorandum No. 1109 (1946).
40. Waldmann, L., Zeits. Naturforsch. 14a (7), 589, 1959.
41. White, H. J., Industrial Electrostatic Precipitation, Addison-Wesley, Reading, Mass., 1963, p 331.
42. Zenz, F. A., Conveyability of Materials of Mixed Particle Size, I, and E.C. Fundamentals, 3, 65, 1964.

### E.3 METEOROLOGY/MICROMETEOROLOGY

1. Barad, M. L., Project Prairie Grass: A Field Program in Diffusion, Vols. 1 and 2, Geophys. Research Papers 59, U.S. Air Force, Geophys. Research Directorate, 1958.
2. Batchelor, G. K., Application of the Similarity Theory of Turbulence to Atmospheric Diffusion, Quart. J. Roy. Met. Soc. 76, 133-146, 1950.
3. Blamont, J. E., and C. deJager, Upper Atmosphere Turbulence Near the 100 km Level, Annales de Geophysique 17, 134-144, 1961.
4. Bolgiano, R., Jr., Turbulence Spectra in a Stably Stratified Atmosphere, J. Geophys. Res. 64, 2226-2229, 1959.
5. Cadle, R. D., Particles in the Atmosphere and Space, Reinhold Pub. Co., 1966.
6. Chapman, S., and T. G. Cowling, The Mathematical Theory of Non-Uniform Gases, Cambridge Univ. Press, 431 pp. 1951.
7. Charnock, H., Note on the Eddy Diffusion in the Atmosphere Between One and Two Km., Quart. J. Roy. Met. Soc. 77, 654-658, 1951.
8. Charnock, H., J. R. D. Francis, and P. A. Sheppard, An Investigation of Wind Structure in the Trades, Anegada 1953.
9. Atmospheric Contaminants, paper presented at National Conference of Applied Meteorology, American Meteorological Society, Oct. 1957.
10. Cramer, H. E., F. A. Record and J. E. Tillman, Measurements of the Inertial Scales of Turbulence and Dissipation Rates in the Atmospheric Surface Layer, Paper presented at 44th Annual Meeting American Geophysical Union, Washington, D. C., April 17-20, 1963.
11. Ellison, T. H., Meteorology, Sci. Prog. 47, 495-506, 1959.
12. Frenkiel, F. N., and I. Katz, Studies of Small-Scale Turbulent Diffusion in the Atmosphere, J. Meteor. 13, 388-394, 1956.
13. Gifford, F., Jr., Relative Atmospheric Diffusion of Smoke Puffs, J. Meteor. 14, 410-414, 1957.



14. Gifford, F., Jr., Further Data on Relative Atmospheric Diffusion, J. Meteor. 14, 475-476, 1957.
15. Gifford, F., Jr., Statistical Properties of a Fluctuating Plume Dispersion Model, Atmospheric Diffusion and Air Pollution, edited by F. N. Frenkiel and A. S. Monin, Turbulence in Shear Flow with Stability, J. Geophys. Res. 64, pp 2224-2225, 1959.
16. Gifford, F., Jr., The Interpretation of Meteorological Spectra and Correlations, J. Meteor. 16, 344, 1959.
17. Gifford, F., Jr., Use of Routine Meteorological Observations for Estimating Atmospheric Dispersion, Nuclear Safety 2 (4), 1961.
18. Gifford, F., Jr., Diffusion in the Diabatic Surface Layer, J. Geophys. Res. 67, 3207-3212, 1962.
19. Greenhow, J. S., Eddy Diffusivity and its Effect on Meteor Trails, J. Geophys. Res. 64, 2208-09, 1959.
20. Haltiner, G. J., and F. L. Martin, 1957, Dynamical and Physical Meteorology, McGraw-Hill, New York.
21. Haugen, D. A., Project Prairie Grass: A Field Program in Diffusion, Vol. 3, Geophys. Research Papers 59, U.S. Air Force, Geophys. Research Directorate, 1958.
22. Hinze, J. O., Turbulence, McGraw Hill, New York and London, 586 pp., 1959.
23. Kellog, W. W., Diffusion of Smoke in the Stratosphere, J. Meteor. 13, 241-250, 1956.
24. Kuo, H. L., Dynamics of Convective Vortices and Eye Formation, in The Atmosphere and the Sea in Motion, ed. by B. Bolin, Rockefeller Inst. Press, New York, 1959.
25. Lettau, H., Wind Profile, Surface Stress and Geostrophic Drag Coefficients in the Atmospheric Surface Layer, Advances in Geophysics Vol. 6, Academic Press, New York, London, pp. 241-247, 1959.
26. Munn, R. E., Descriptive Micrometeorology, Academic Press, 1966.
27. Pasquill, F., Atmospheric Diffusion, D. Van Nostrand, London, 1962.
28. Priestly, C. H. B., Turbulent Transfer in the Lower Atmosphere, Chicago Univ. Press, 130 pp. (p 60), 1959.

29. Seneca, J., Mesures de Diffusivite Turbulente sur des Flacons de Fumie, J. Sci. Meteor. 71, 221-225, 1955.
30. Sheppard, P. A., Advances in Geophysics 6, 117, Academic Press, 1959.
31. Sutton, O. G., Micrometeorology, McGraw-Hill, 1953.
32. Tank, W., The Use of Large-Scale Parameters in Small-Scale Diffusion Studies, Bull. Amer. Meteor. Soc. 38, 6-12, 1957.
33. Wilkins, E. M., Observations on the Separation of Pairs of Neutral Balloons and Applications to Atmospheric Diffusion Theory, J. Meteor. 15, 327, 1958.
34. Wilkins, E. M., Decay Rate for Turbulent Energy Throughout the Atmosphere, J. Atmos. Sci. 29 (5), 1963.

#### E.4 RADIOACTIVE CONTAMINATION

1. Bailey, J. C. and Rohr, R. C., Airborne Contamination Resulting from Transferable Contamination on Surfaces, Oak Ridge Gaseous Diffusion Plant. Report K1088, 24 November 1953.
2. Chamberlain, A. C. and Stanbury, G. R., The Hazard from Inhaled Fission Products in Rescue Operations after an Atomic Bomb Explosion, AERE Report No. HP/R.737.
3. Dunning, N. J., "Comprehensive List of Nuclides with a Statement of Atomic Mass," Half-Life and Specific Activity, AHSB Report 44.
4. Dunster, H. J., The Derivation of Maximum Permissible Levels on Contamination of Surfaces of Radioactive Materials, AERE Report No. HP/R.1495.
5. Dunster, H. J., Atomics 6, No. 3, August 1955.
6. Dunster, H. J., "Surface Contamination Measurements as an Index of Control of Radioactive Materials," Health Physics, Pergamon Press, 8, 353-356, 1962.
7. Garland, J., Experiments on the Possible Spread of Airborne Contamination of Clothing, Internal Report.
8. McKinnon, D. S., Estimation of Plutonium Contamination Levels in Air in the New Change-room, Internal Report.
9. Sherwood, R. J. and Stevens, D. C., A Phosphor-Film Technique to Determine the Activity of Individual Particles on Air Sample Filters, AERE R.4310.
10. Sherwood, R. J., On the Interpretation of Air Sampling for Radioactive Materials, AERE R.4491. Recommendations of the International Commission on Radiological Protection. Report of Committee II, 1959.
11. Stevens, D. C., "Location and Examination of Alpha Active Airborne Dust Particles collected on Glass Fibre Filter Paper," Ann. Occup. Hyg. 6, 31-38.

12. Stewart, K., Particulate Material formed during the Combustion of Plutonium and Polonium, International Conference on the Radioactive Pollution of Gaseous Media, Saclay, France, 1963.
13. Tagg, B., Airborne Contamination Levels in Change-room Number 4, Internal Report.
14. United Kingdom Atomic Energy Authority Health and Safety Code, Maximum Permissible Doses from Inhaled and Ingested Radioactive Materials, Authority Code No. E. 1. 2., Issue No. 1, June 1961.
15. Wilkins, E. M., "Effective Coefficients of Diffusivity for Atomic Bomb Clouds at 1000 to 2000 Miles," Trans. Amer. Geophys. Union, 1958.

#### E.5 AERO/FLUID DYNAMICS

1. Goldstein, S., ed., Modern Developments in Fluid Dynamics, Vols. 1 and 2, Oxford University Press, 1938.
2. Prandtl, L., and Tietjens, O. G., Applied Hydro- and Aeromechanics, McGraw-Hill Book Company, New York, 1934.
3. Prandtl, L., Fluid Dynamics, Hafner Publishing Company, New York, 1952.
4. Schlichting, M., Boundary Layer Theory, McGraw-Hill Book Company, New York, 1960.

## E.6 GEOLOGY

1. Bessonova, T. D., (Astro. Obs., LGU), Proverka gipotezy limonitovogo pokrova na Marse indikatometricheskim putem. (Verification of the hypothesis of the limonitic cover of Mars using the indicatometric method.) (In: Akademiia Nauk Ukrainskoi RSR, Voprosy astrofiziki (issledovanie atmosfer Venery i Marsa). Kiev, 1965.
2. Lyon, R. J. P., "Infrared Emission Spectra of Natural, Polished and Powdered Rocks," Notes from 3rd Annual Meeting of Extraterrestrial Resources Working Group, Cocoa Beach, Florida, 19 November 1964.
3. Zebal, G. P., A Preliminary Synthesis of the Geology of Mars, Philco-Ford Corporation Memo.

#### E.7 PAPERS ON THE CHARACTERISTICS OF MARS

1. Adamcik, J. A., "The Water Vapor Content of the Martian Atmosphere as a Problem of Chemical Equilibrium," Planetary and Space Science, Vol. II, 1963.
2. Anderson, Albert D., Spherical Particle Terminal Velocities in the Martian Daytime Atmosphere from 0 to 50 Kilometers, Rept. No. LMSC-6-76-66-21, Lockheed Missiles and Space Co., Palo Alto California Research Labs, September 1966.
3. Anderson, Albert D., revised ed. 14 December 1966, 8 p., unclassified report. Revision of manuscript submitted 7 October 1966. Journal of Geophysical Research, Vol. 72, No. 7, p 1951-8, April 1, 1967.
4. Antoniadi, E. M., La planete Mars, 1659-1929, Hermann et Cie., Paris, 1930, 239 pp.
5. Avigliano, D. P., "Mars, 1954," The Strolling Astronomer, Vol. 8, Nos. 9-10, Sept.-Oct. 1954, p 109.
6. Barabashov, N. P. and Garazha, V. I., "Some Remarks on the Dust and Haze Formations on Mars," Aston. Zhur., 37, 501-507, 1960.
7. Campbell, W. W., "Notices of the Lick Observatory," Publications, Astronomical Soc. of the Pacific, Vol. 2, No. 10, 1890, pp 248-249.
8. Campbell, W. W., "Notices of the Lick Observatory," Publications, Astronomical Soc. of the Pacific, Vol. 6, No. 35, 1894, pp 104-112.
9. De Vaucouleurs, G., Physics of the Planet Mars, Faber and Faber Ltd., London, 1954.
10. De Vaucouleurs, G., The Atmospheric Environments of Mars and Venus, in Southwest Res. Inst. Bioastronautics and the Exploration of Space, December 1965.

11. Dollfus, A., "Visual and Photographic Studies of the Planets at the Pic du Midi," Planets and Satellites, pp 534-571, edited by G. P. Kuiper and B. M. Middlehurst, Univ. of Chicago Press, 1961.
12. Dollfus, A., Proceedings of Lunar and Planetary Exploration Colloquium, 2 (3), pp 17-37, 1961.
13. Dollfus, A., Study of the Planet Mars from 1954 to 1958 (Etude de la Planete Mars de 1954 a 1958), Annales d'Astrophysique, Vol. 28, July-August 1965.
14. Dollfus, A., "Polarization Studies of Planets," pp 343-399, The Solar System, Vol. 3, Planets and Satellites, G. P. Kuiper and B. M. Middlehurst (eds.), Univ. of Chicago Press, Chicago, 1961 (see p 386).
15. Douglass, A. E., Annals of Lowell Observatory, Vol. 1.
16. Douglass, A. E., "A Cloud-like Spot on the Terminator of Mars," Astrophysical Journal, Vol. 1, No.2, February 1895, pp 127-130.
17. Evans, D. E., Pitts, D. E. and Kraus, G. L., Venus and Mars Nominal Natural Environment for Advanced Manned Planetary Mission Programs, NASA SP-3016, 1965.
18. Flammarion, C., La planete Mars, Gauthier-Villars et Cie., Paris, 1909.
19. Gifford, F., "The Problem of the Martian Yellow Clouds," Monthly Weather Review, Vol. 91, Nosx 10-12, October-December 1963, pp 610-612.
20. Gifford, F., "A Study of Martian Yellow Clouds that Display Movement," Monthly Weather Review, Vol. 92, No. 10, 1964.
21. Gifford, F., The Martian Canals According to a Purely Aeolian Hypothesis, Icarus, Vol. 3, July 1964.
22. Gifford, F., "The Surface-Temperature Climate of Mars," Astrophysical Journal, Vol. 123, No. 1, January 1956, pp 154-161.
23. Goody, R. M., "The Atmosphere of Mars," The Origin and Evolution of Atmospheres and Oceans, P. J. Brancasio and A. G. W. Cameron, eds., John Wiley and Sons, New York, 1963.
24. Goldstein, R. M. and Gillmore, W. F., "Radar Observations of Mars," Science, Vol. 141, 1963.
25. Heintz, W. D., "On the Martian Yellow Cloud in 1956," The Observatory, Vol. 78, 1958, pp 203-204.



26. Hess, D. S. and Pounder, E., Draft, Voyager Environmental Predictions Document, JPL, 26 October 1966.
27. Hess, S. L., "Some Aspects of the Meteorology of Mars," J. Meteorol., 7, 1-13, 1950.
28. Hertzler, Richard G., Wang, Emile S. J. and Wilbers, Ollie J. (McDonnell Aircraft Corp., St. Louis, Mo.), Development of a Martian Environmental Simulation Facility, The American Institute of Aeronautics and Astronautics, Institute of Environmental Sciences, and American Society for Testing and Materials, Space Simulation Conference, Houston, Texas, September 7-9, 1966. Technical Papers (A66-40204 22-11).
29. Johnson, R. W., Terrain and Soil of Mars, paper presented at the Ninth Annual American Astronautical Society Meeting, Los Angeles, California, January 15-17, 1963.
30. Kaplan, L. D., Munch, G. and Spinrad, H., "An Analysis of the Spectrum of Mars," *Astrophys. J.* 139, 1-15, 1964.
31. Koval, I. K. and Morozhenko, A. V., "Several Properties of the Yellow Haze Observed on Mars during 1956," *Astron. Zhur.* 39, 65-72, 1962.
32. Kuiper, G. P., in Proceedings of Lunar and Planetary Exploration Colloquium, 2 (3), p 32, 1961.
33. Kuiper, G. P., "Planetary Atmospheres and their Origin," The Atmospheres of the Earth and Planets, Univ. of Chicago Press, 1952.
34. Lamar, D. L., Optical Ellipticity and Internal Structure of Mars, *Icarus*, Vol. 1, No. 3, 1962.
35. Leighton, R. B. and Murray, B. C., Behavior of Carbon Dioxide and Other Volatiles on Mars, *Science*, Vol. 153, 8 July 1966.
36. Loomis, A. A., "Some Geologic Problems of Mars," Tech. Rept. 32-400, Jet Propulsion Laboratory, California Institute of Technology, March 1963.
37. Loomis, A. A., Geological Society of America Bulletin, Vol. 76, Oct. 1965.
38. Lowell, P., Drawings of Mars, 1905, Lowell Observatory, 1906.
39. Lowell, P., Mars and Its Canals, Macmillan Co., New York, 1911, 393 pp.

40. Mintz, Y., 1961: A Note on the Temperature of the Equatorial Troposphere of Mars, in RM-2769-JPL, 81-96.
41. Mintz, Y., "The General Circulation of Planetary Atmospheres," pp 107-146, The Atmospheres of Mars and Venus, Report of the Space Science Board, National Academy of Sciences - National Research Council, Pub. 944, Washington, 1961.
42. Miyamoto, S., Observational Study of the General Circulation of Martian Atmosphere - Cloud Observations During the 1963 Opposition, edited by M. Florkin and A. Dollfus, Amsterdam, North-Holland Publishing Co., New York, Interscience Publishers, 1964.
43. Miyamoto, S. and Nakai, Y., "Meterological Observations of Mars During 1960-61 Opposition," Contribution No. 105, Inst. of Astrophysics and Kwasan Observatory, University of Kyoto, 1961, 49 pp.
44. Miyamoto, S., 1964: "Observational Study of the General Circulation of Martian Atmosphere," in Life-Sciences and Space Research, II, eds. M. Florkin and A. Dollfus, Interscience, Amsterdam, 238-245.
45. Neubauer, F. M. (Inst. fur Geophys. & Met. der Tech. Hochschule, Braunschweig, Ger.) Thermal Convection in the Martian Atmosphere. Journal of Geophysical Research, Washington, D. C., 71 (10):2419-2426, May 15, 1966.
46. Observatoires Jarry-Desloges, Observations des Surface Planetaires, Vols. 1 to 10 (for the Apparitions of 1907 to 1941), Gauthier-Villars et Cie, Paris, various dates, 1908 to 1946.
47. Opik, Ernst J., "The Martian Surface," Science (Maryland, University, College Park, Md., Armagh Observatory, Armagh, Northern Ireland), Vol. 153, July 15, 1966.
48. Palm, A. and Basu, B. (both, Univ. of Calif., Berkeley), Blue Haze of Mars, 16.11-687, New York, 4(2):111-118, May 1965.
49. Peterson, R. E., Winds on Mars, Voyager Memo, L374-012, 28 Dec. 1965.
50. Peterson, R. E., Maximum Martian Surface Winds, Voyager Memo, 20 April 1966.
51. Pettit, E. and Richardson, R. S., "Observations of Mars Made at Mount Wilson in 1954," Report of the International Mars Committee, Lowell Observatory, 1955, 113 pp. (also in Publications, Astronomical Society of the Pacific, Vol. 67, No. 395, April 1955, pp 62-73).

52. Pickering, W. H., Mars Reports, Nos. 1 to 44, Popular Astronomy, Vols. 22-38, 1914-1930.
53. Ryan, J. A., Notes on the Martian Yellow Clouds, Geophysical Research Journal, Vol. 69, No. 18, September 1964.
54. Sagan, C., Phaneuf, J. P. and Inat, M., "Total Reflection Spectrophotometry and Thermogravimetric Analysis of Simulated Martian Surface Materials," Icarus, Vol. 4, 1965.
55. Sagan, C. and Pollack, J. B., Sky and Telescope, November 1966.
56. Sharonov, V. V., Dust Covers on the Surface of Planets and Satellites, edited by M. Florkin and A. Dollfus, Amsterdam, North-Holland Pub. Co., New York, Interscience Publishers, 1964.
57. Sharonov, V. V., "A Lithologic Interpretation of Photometric and Colorimetric Studies of Mars," Soviet Astron., AJ, English Transl., 5, 199-201, 1961.
58. Sinton, W. M., and Strong, J., 1960: Radiometric Observations of Mars, Astrophys. J., 131, 459-469.
59. Slipher, E. C., Mars, the Photographic Story, Sky Pub. Co., Cambridge, Mass., 1962, 168 pp.
60. Spencer, D. F., 1966: Our Present Knowledge of the Martian Atmosphere, at AIAA/AAS Stepping Stones to Mars Meeting, Baltimore, Md., March 28-30, 1966.
61. Stone, Irving, 1965: Atmosphere Data to Alter Voyager Design, Av. Wk. Space Tech., 83, p 69.
62. Tang, W., 1965: Some Aspects of the Atmospheric Circulation on Mars, NASA Cr-262.
63. Tang, W., On the Steady Symmetrical Regime of the General Circulation Martian Atmosphere. GCA Corp., Bedford, Mass., GCA Tech. Rpt. 66-8-N, March 1966 (Contract NASw-1227)
64. Tombaugh, Clyde W. (N.M. State Univ. Obs., Univ. Park), (Comments on) R. A. Wells, "Evidence that the Dark Areas on Mars are Elevated Mountain Ranges" and (Reply by) Wells, Nature, London, 209 (5030): 1338-1339, March 26, 1966.
65. Van Tassel, R. A. and Salisbury, J. W., "The Composition of the Martian Surface," Icarus, Vol. 3, 1964.

66. Wells, R. A. (London, University, University College, London, England)  
"An Analysis of Martian Clouds and their Topographical Relationship,"  
Cospar, International Space Science Symposium, 7th, Vienna, Austria,  
May 10-19, 1966, Paper.

**APPENDIX F**  
**SOIL TRANSPORT ANALYSIS**

## APPENDIX F

### SOIL TRANSPORT ANALYSIS

#### F.1 INITIATION OF SOIL MOVEMENT

F.1.1 Boundary Layer Velocity Distribution

F.1.2 Threshold Velocity

#### F.2 MODES OF TRANSPORT

F.2.1 Characteristics of Saltation

F.2.2 Characteristics of Particles in Suspension

## SYMBOLS

$R_n$	Reynold's Number, $\frac{\rho v l}{\mu}$
$\mu$	Absolute viscosity, lb-sec/ft ²
$\rho$	Fluid density, slugs/ft ³
$\sigma$	Particle density, slugs/ft ³
$\tau$	Shear force or surface drag, lbs/ft ²
$d$	Effective diameter of surface particle, ft
$h$	Height of particle rise, ft
$l$	Length of particle traverse, ft
$l$	Characteristic dimension, ft
$z$	Vertical height above surface, ft
$\alpha$	Slope of velocity distribution curve
$m$	Tangent of the slope
$v$	Velocity, ft/sec
$v_*$	Equivalent drag velocity, without soil movement, ft/sec
$v'_*$	Equivalent drag velocity with soil movement, ft/sec
$v_t$	Impact threshold velocity of grain movement, ft/sec
$K_0$	Characteristic height, $v = 0$ , no soil movement, ft
$K'$	Characteristic height, $v = \text{constant}$ , with soil movement, ft
$g$	Gravitational constant, ft/sec ²
$q$	Weight of material transported, gm/ft sec
$q_s$	Weight of material transported by saltation, gm/ft sec
$A$	Effective drag velocity coefficient
$C$	Soil transport coefficient
$\beta$	Angle of impact for saltating particle

LIST OF TABLES

TABLE		PAGE
F-1	Value of Coefficient C . . . . .	F-18



## LIST OF FIGURES

FIGURE		PAGE
F-1	Typical Boundary Layers . . . . .	F-5
F-2	Wind Velocity Distribution. . . . .	F-6
F-3	Forces Acting on a Particle at Incipient Movement . . .	F-8
F-4	Effective Drag Velocity . . . . .	F-10
F-5	Effective Drag Velocity Coefficient "A" . . . . .	F-11
F-6	Fluid Threshold Velocity $v_*$ . . . . .	F-13
F-7	Characteristic Path of Saltating Particle . . . . .	F-15
F-8	Ratio of Height of Rise to Length of Traverse for Saltating Particle. . . . .	F-15
F-9	Soil Transported as a Function of Velocity for Hatton Fine Sandy Loam . . . . .	F-19
F-10	Soil Transported as a Function of Velocity for Sceptre Heavy Clay. . . . .	F-20
F-11	Variation in Soil Transported as a Function of Height Above Surface . . . . .	F-21
F-12	Distribution of Dust Carried in Suspension at Various Heights . . . . .	F-23

## APPENDIX F

### SOIL TRANSPORT ANALYSIS

This appendix presents the analysis methods used to extrapolate the data for earth to conditions for Mars as given in Section 6. The methods are in general the methods used by Bagnold², Chepil¹¹ and Ryan⁵³.

#### F.1 INITIATION OF SOIL MOVEMENT

This section presents the dynamics of the boundary layer of the wind at the surface with the loose particulate material lying on the surface.

##### F.1.1 BOUNDARY LAYER VELOCITY DISTRIBUTION

The mechanism by which a grain lying on the surface is dislodged and lifted into the fluid flowing over the surface begins with the boundary layer interaction with the surface. Depending on the Reynold's number of the flow, this boundary layer can be either laminar or turbulent. The laminar flow boundary layer is a linear function of the height above the surface whereas the turbulent boundary layer is not. These velocity profiles are shown qualitatively in Figure F-1.

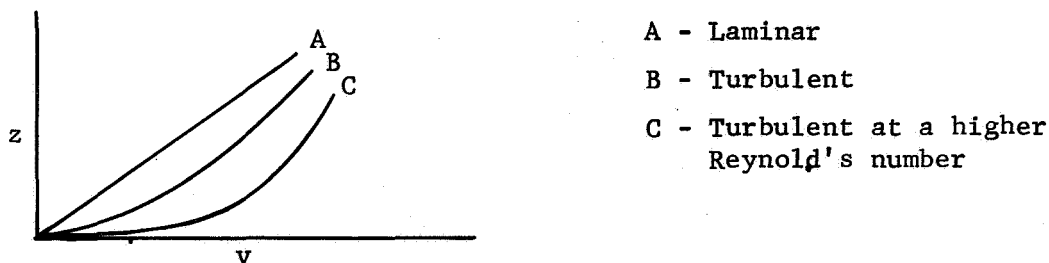


FIGURE F-1. TYPICAL BOUNDARY LAYERS

The transition from laminar to turbulent flow has been shown to occur for  $R_N > 2000$ , which is usually the case for winds on earth over a rough surface. The velocity distribution in a turbulent boundary layer is given by Bagnold as

$$v = 5.75 v_* \log \left( \frac{z}{K_0} \right) \quad (1)$$

which is attributed originally to Prandtl. The value  $v_*$  is defined as the effective drag velocity such that the surface drag can be expressed as  $\tau = \rho v_*^2$  (2). This is a convenient definition by which the characteristics of a flow can be compared with another. The equation given in (2) can be shown graphically in a semilog plot shown as curve A in Figure F-2.

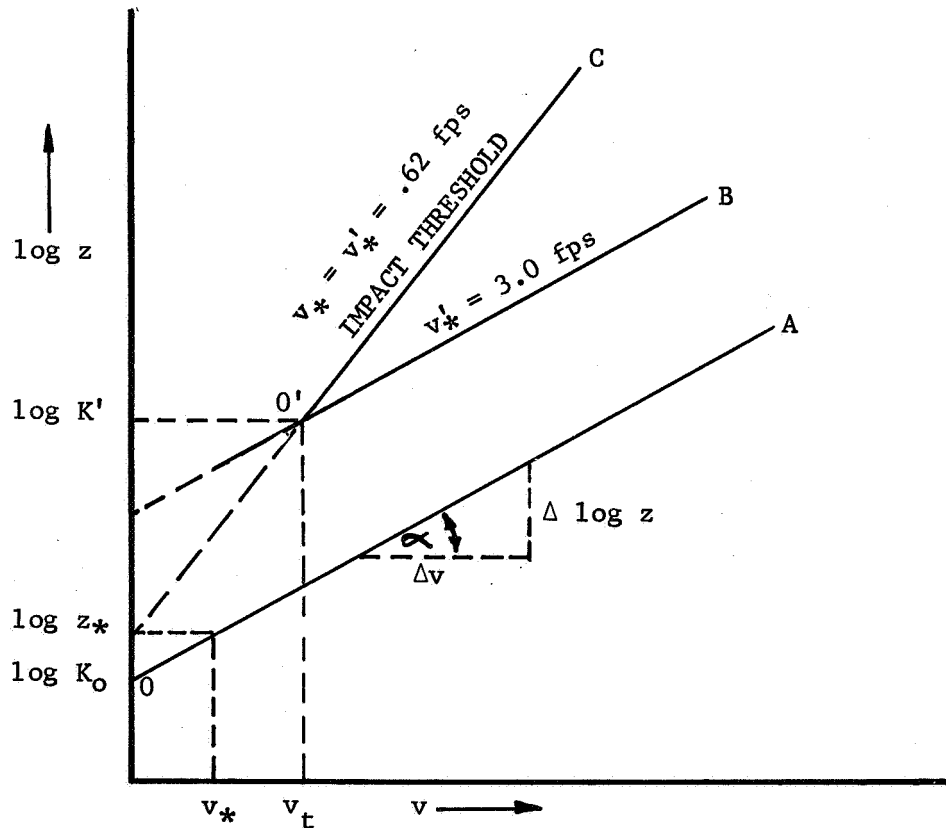


FIGURE F-2. WIND VELOCITY DISTRIBUTION

It is seen that this distribution appears as a straight line in this plot which can be defined by an equation of the form

$$\log z = mv + \log K_0 \quad (3)$$

from which

$$v = \frac{1}{m} (\log z - \log K_o) = \frac{1}{m} \log \left( \frac{z}{K_o} \right) \quad (4)$$

The effective drag velocity can be related to the slope,  $\alpha$ , by expressing it in terms of (4)

$$v_* = \frac{1}{m} \log \left( \frac{z_*}{K_o} \right) \quad (5)$$

from which

$$\frac{1}{m} = \frac{v_*}{\log \left( \frac{z_*}{K_o} \right)} = 5.75 v_* \quad (6)$$

It has been found that  $v_*$  is related to  $m$  by a constant having a value of 5.75. Thus, the effective drag velocity can be conveniently determined from empirical data by measuring the wind velocity above the surface. It has also been observed that the value of  $K_o$  is related to the surface roughness through another constant of proportionality which is

$$K_o = \frac{d}{30} \quad (7)$$

where  $d$  is the predominant grain diameter on the surface.

Thus, equation (1) can be rewritten as

$$v = 5.75 v_* \log \left( \frac{30 z}{d} \right). \quad (8)$$

It is pointed out here that Equation (8) is valid as long as no soil movement occurs. Bagnold has determined that once soil movement occurs, there is an effective increase in the surface drag resulting in a velocity reduction at a given height  $z$ . Curves B and C of Figure F-2 show the effect of this on the velocity distribution. He observed that all velocity distribution curves now passed through a common point,  $o'$ , which he suggested could be related to the ripple height for a particular sand. The location of the point  $o'$  is related to the mean grain size of the sand which is discussed in Section F.1.2. This can again be expressed by an equation of the form

$$\log z - \log K' = m(v - v_t) \quad (9)$$

from which

$$v = 5.75 v_* \log \left( \frac{z}{K_r} \right) + v_t. \quad (10)$$

The effect is to displace the velocity distribution upward as an apparent increase in surface roughness caused by the additional drag imposed by the airborne material near the surface.

#### F.1.2 THRESHOLD VELOCITY

If the wind velocity passing over a surface of loose particles is gradually increased, a velocity is finally reached at which the forces acting on the grain are sufficiently large to overcome the forces of gravity holding the grain in position.

These forces are shown in Figure F-3.

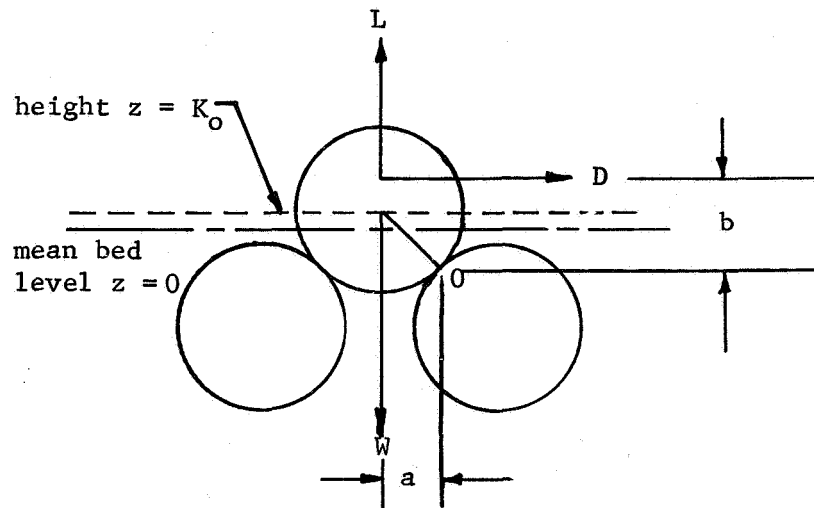


FIGURE F-3. FORCES ACTING ON A PARTICLE AT INCIPIENT MOVEMENT

At the time when incipient movement exists, the forces acting on the particle tending to cause it to rotate about 0 are in equilibrium; i.e., the summation of moments about point 0 are zero. Bagnold did not originally include the lift force; however, wind tunnel measurements made on hemispheres resting on a flat surface by Chepil⁵ indicates that the lift to drag ratio varied from 0.7 to 1.3. The manner in which grains leave the surface is very complex and difficult to treat theoretically. Chepil observed that most of the grains appeared to leave the surface by jumping in a nearly vertical direction, the majority leaving at angles between 75 and 90 degrees from the horizontal. He accounted for this behavior with several effects. As the grain starts to move, it rotates about point 0 and at the same time moves up into the more energetic boundary layer. Thus, the particle is spinning and has some vertical velocity due to the action of leaving the surface. This vertical acceleration is further enhanced by the fact that a rotating sphere in a uniform flow generates lift in the direction of the side of the body where the flow velocity and the tangential velocity of the surface of the body add. This effect is further increased by the fact that the flow velocity on top of the grain is higher than the velocity on the lower side because of the velocity gradient in the boundary layer. In addition, some vertical velocity is probably imparted by the vertical component of turbulence in the fluid.

The effective drag velocity,  $v_*$ , at which a particle begins to move can be shown to be

$$v_* = A \left( \frac{\sigma - \rho}{\rho} g d \right)^{\frac{1}{2}} \quad (11)$$

For a grain moving in air, the density of the fluid is small compared to the density of the particle and Equation (11) can be rewritten as

$$v_* = A \left( \frac{\sigma}{\rho} g d \right)^{\frac{1}{2}} \quad (12)$$

The coefficient A has been determined empirically and is essentially a constant equal to 0.1 for  $R_N > 3.5$ . For very low  $R_N$ , which is a result of low flow velocities or very smooth surfaces, this coefficient increases with decreased particle size as shown in Figure F-4 for particles moving in earth's atmosphere. The effective drag velocity required to initiate grain movement in this manner is referred to as the fluid threshold velocity. Once movement has started, the impacting grains moving in saltation tend to augment the process of particle movement. Thus, it has been observed in wind tunnel measurements that the velocity at which soil movement ceases, once it has been initiated, is lower than that required to start soil movement. This has been defined as the impact threshold velocity. The effective drag velocity coefficient A is primarily, although not totally, a function of Reynold's number and is presented in this way in Figure F-5. The dashed curve gives the variation for the impact threshold. Using these

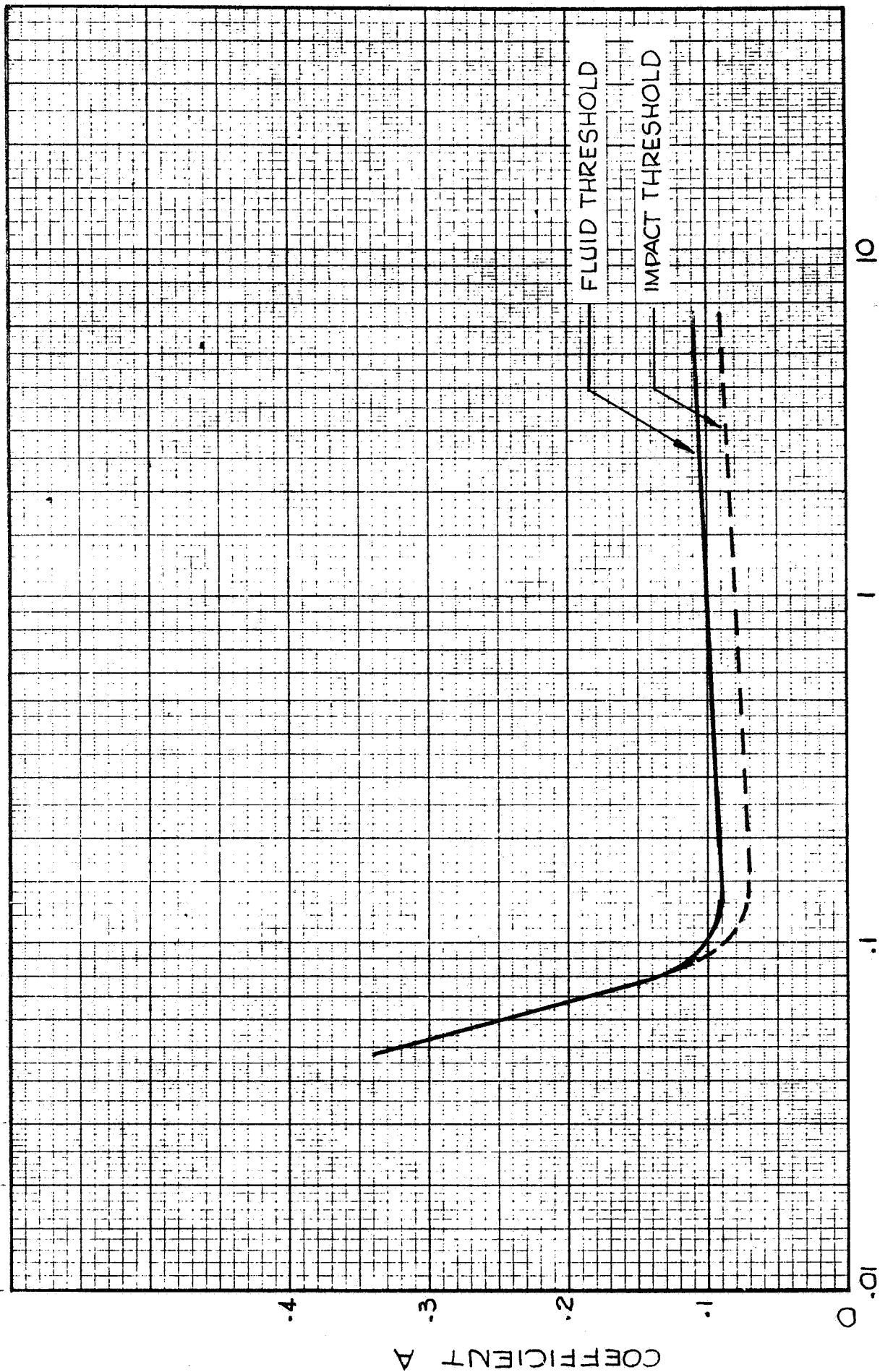


FIGURE F4 EFFECTIVE DRAG VELOCITY

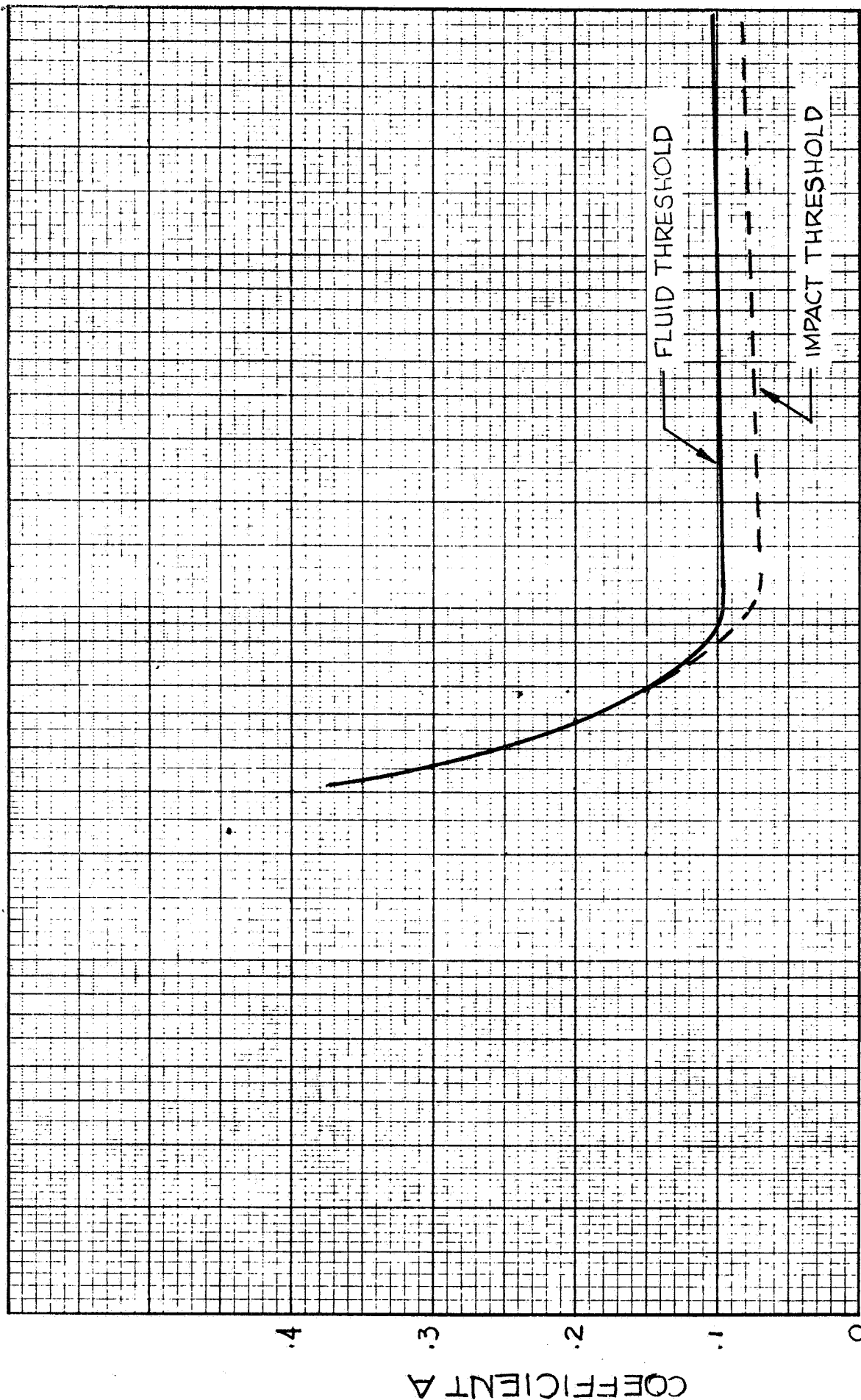


FIGURE F-5 EFFECTIVE DRAG VELOCITY COEFFICIENT 'A'



values for the coefficient A, with Equation (12), makes it possible to plot the effective drag velocity as a function of particle size. Such a plot is shown in Figure F-6. From this plot it can be seen that there is a particular particle size for which the required effective drag velocity is a minimum. This is the material most easily moved and for most earth dune sands coincides approximately with the lower limit of the grain size in the sand distribution. Bagnold and Chepil plotted the square root of the grain diameter so that the right hand portion would be a straight line. This same result can be achieved on a log-log plot and, for the data in this case, it also makes the left hand portion of the curve a straight line. This curve was derived essentially from Chepil's data¹¹; however, it agrees well with Bagnold's data even though Bagnold obtained his for dune sand while Chepil obtained his for cultivated soils. The upper limit of grain size is probably determined by the average value of the prevailing winds at the point where the effective drag velocity coincides with the impact threshold velocity. Dune sands have an upper limit of approximately one millimeter diameter grains. This corresponds to a  $v_*$  of 1.5 fps. Using Equation (1), this yields a wind velocity of 43 fps or 30 mph at an elevation of 10 feet. This agrees fairly well with the observed average winds in these types of areas.

In order to find the fluid threshold velocity in other than an earth atmosphere, it is necessary to satisfy the requirement of equivalent Reynold's number when using Equation (12). This is most easily done by solving Equation (12) and the Reynold's number parameter simultaneously in terms of  $v_*$  and d. The value for  $v_*$  is then given by

$$v_* = \left( \frac{\sigma g \mu}{2} \right)^{1/3} (A^2 R_n)^{1/3} \quad (13)$$

and the associated value of d is given by

$$d = \frac{\mu^{2/3}}{(\sigma \rho g)^{1/3}} \left( \frac{R_n}{A} \right)^{2/3} \quad (14)$$

The fluid threshold velocities for Mars, given in Section 6, were derived using these equations.

## F.2 MODES OF SOIL TRANSPORT

Soil that is eroded and carried by the wind is moved in three modes of transport; i.e., suspension, saltation and surface creep. Of these three modes of transport, the movement of material by saltation, consisting of a series of leaps and flat trajectories near the surface, is the most powerful in terms of quantity of soil moved, effect on the wind, and erosive capability. The grains which move in saltation are those which have the

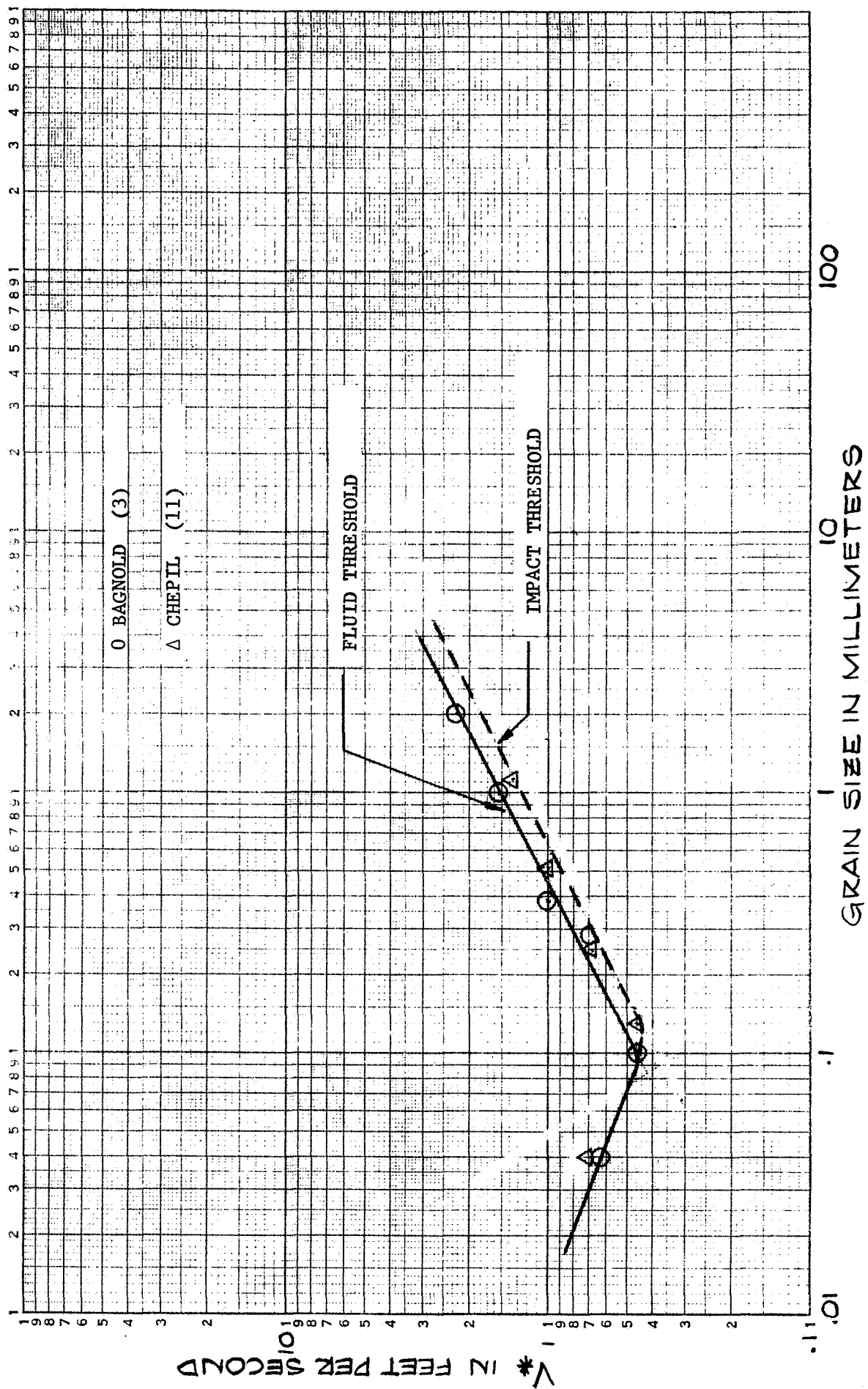


FIGURE F-6 FLUID THRESHOLD VELOCITY  $V^*$

required combination of mass and drag area. These are the particles which are most easily moved by the wind and are also the first to be effected. The impact of saltating particles on the surface is the mechanism whereby finer particles are lifted into the wind and carried along in suspension. On earth, these are particles of 80 to 100 microns in diameter. Material carried in suspension is essentially particles of or near a size so that they do not materially affect the flow characteristics. The majority of these particles are of a size such that they obey Stoke's law, those in which inertia effects are small with respect to drag forces. This material is carried high into the atmosphere and is moved far from the site at which it is picked up. On the other hand, particles which move in surface creep are those in which inertia effects are large with respect to drag or lift forces. These particles are too large to be lifted into the fluid flow and obtain their mobility by virtue of the energy transferred on impact at the surface by the saltating particles. Bagnold has estimated that approximately one fifth to one fourth of the total mass of particle flow past a given point per unit width per unit time is transported in this manner. He has also shown that for typical dune sand, the quantity of material transported in true suspension is very low; however, Chepil has shown, that for cultivated soils or soils with wide particle size distributions, the amount of material carried in suspension can be appreciable. In general, particles moving in surface creep remain in the immediate area while those traveling in saltation move into adjacent areas - the distance traveled being determined by the strength and duration of the wind and the ability of these adjacent surfaces to trap the saltating particles.

#### F.2.1 CHARACTERISTICS OF SALTATION

As mentioned earlier, particles moving in saltation are lifted into the fluid flow by a combination of impact forces and aerodynamic forces. The majority of the particles tend to rise nearly vertically from the surface and, as the vertical component of their velocity approaches zero, to be accelerated by the wind horizontally producing a typical trajectory as shown in Figure F-7.

The height,  $h$ , to which the particle rises is a function of the initial velocity vector, the size of the particle, and the velocity of the wind which determines the length over the surface traversed by the particle and the final impact velocity. The height of the trajectory is also affected by the character of the surface; i.e., particles rebounding from a hard surface rise higher than from a yielding surface. It has been observed that the material traveling in saltation rarely rises higher than two or three feet on earth and can be considerably less. Other characteristics of these saltating particle trajectories observed is that the impact angle,  $\beta$ , is most commonly 6 to 12 degrees and that, where the particle size is appropriate, the length of ripples formed on the surface corresponds very closely with the traversed path length,  $\ell$ . Chepil¹¹

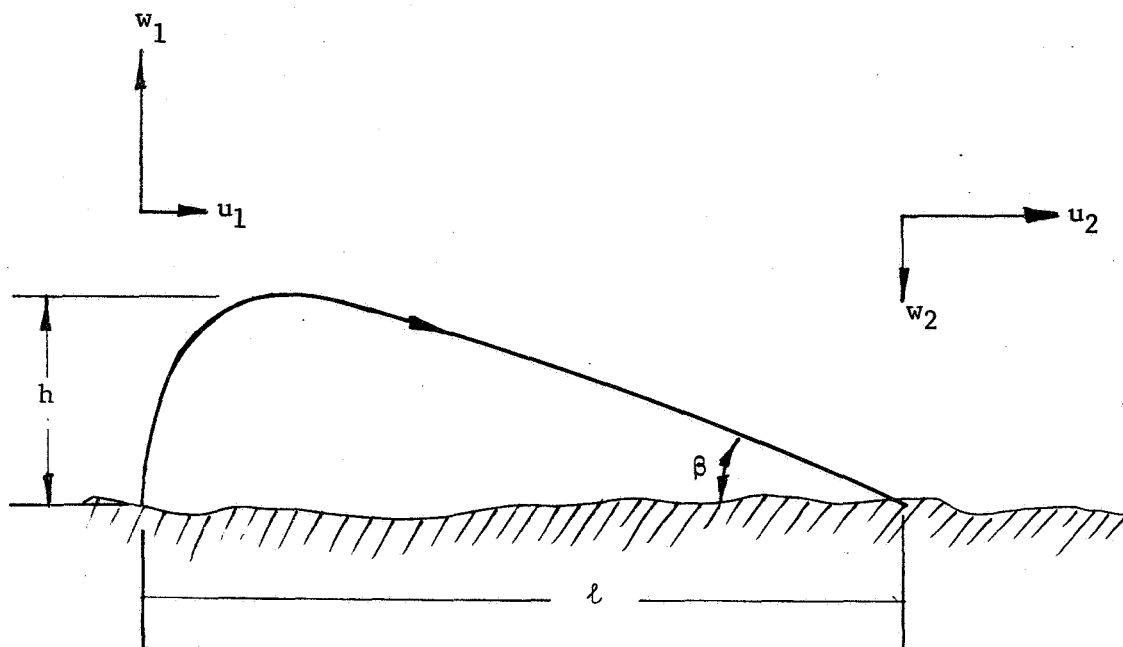


FIGURE F-7. CHARACTERISTIC PATH OF SALTATING PARTICLE

observed that the ratio of height of rise to length of traverse for most cases with earth soils varied from a ratio of 1:7, for particles rising to height of 2 inches, to a ratio of 1:10 for particles rising higher than 6 inches. The variation in this ratio as a function of height of rise is shown in Figure F-8 as determined by Chepil.

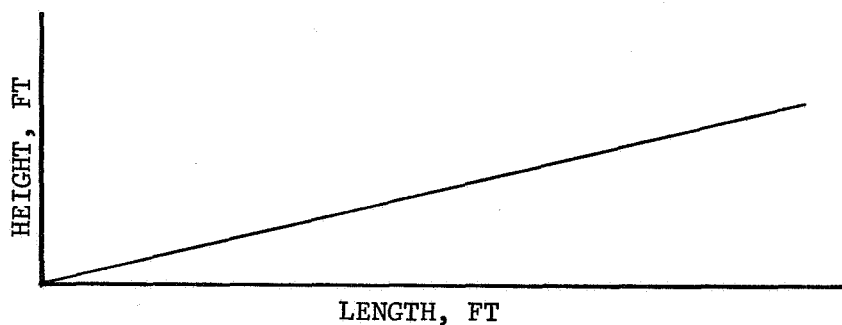


FIGURE F-8. RATIO OF HEIGHT OF RISE TO LENGTH OF TRAVERSE FOR SALTATING PARTICLE

In order to estimate the effect of a Martian environment, the differences in gravity and aerodynamic drag forces should be considered. To do this precisely, the trajectory should be computed using numerical methods; however, the limited scope of this effort did not allow for this. A first order estimate of the height of rise, which is determined largely by gravity, can be made by comparing the height of vacuum trajectories. Since the drag forces due to the wind dominate in determining the length of traverse, the relative drag forces can be used to estimate the ratio of height of rise to length of traverse. The height of rise for a particle traveling a vacuum ballistic trajectory is given by

$$h = \frac{v_o^2 \sin^2 \theta_o}{2g} \quad (15)$$

For the typical saltating particle trajectory, the initial angle is vertical ( $\theta_o = 90^\circ$ ) and the initial velocity is proportional to  $v_*$ , thus

$$h \sim \frac{v_*^2}{g} \quad (16)$$

From this the ratio of height on Mars to earth can be estimated

$$\frac{h_m}{h_e} = \frac{\frac{v_{*m}^2}{g_m}}{\frac{v_{*e}^2}{g_e}} \quad \text{and} \quad (17)$$

$$h_m = h_e \left( \frac{v_{*m}}{v_{*e}} \right)^2 \frac{g_e}{g_m} \quad (18)$$

From this relation, it can be seen that saltating particles can be expected to rise higher on Mars since  $v_*$  for Mars is high and gravity is reduced. In a similar way, the drag effects can be estimated. The drag on a particle is given by

$$D = \frac{1}{2} \rho v^2 C_D A \quad (19)$$

Assuming that the drag coefficient is the same and that the length of traverse is proportional to the drag forces, then

$$l \sim \rho v_*^2 d^2 \quad (20)$$

from which

$$\frac{\ell_m}{\ell_e} = \frac{\rho_m v_{*m}^2 d_m^2}{\rho_e v_{*e}^2 d_e^2} \quad (21)$$

In this relation, the diameter and velocity used are those associated with the particle most easily moved or the minimum obtained from the fluid threshold curve. Thus, the length of traverse on Mars is given by

$$\ell_m = \ell_e \frac{\rho_m}{\rho_e} \left[ \frac{v_{*m}}{v_{*e}} \right]^2 \left[ \frac{d_m}{d_3} \right]^2 \quad (22)$$

A final property of saltating particulate material required to describe the transport of soil is the quantity of material transported. Bagnold² determined from momentum considerations that the quantity of material being transported in saltation is proportional to the horizontal component of the impact velocity ( $u_2$  of Figure F-7) and inversely proportional to the length of path traversed. Also, the final velocity  $u_2$  is proportional to  $w_1$ , the initial vertical component of the velocity which is directly related to  $v_*$ . Thus, he gives the expression

$$q_s = \frac{8}{10} \rho v_*^3 \quad (23)$$

knowing that approximately one-fourth of the material is transported by surface creep, he obtains the expression

$$q = \frac{4}{3} \cdot \frac{8}{10} \rho v_*^3 \quad (24)$$

for the total quantity of dune sand being transported. He further determined that the quantity transported is also a function of the particle size and the distribution of sizes existing in a soil. Thus, the expression given in (24) becomes

$$Q = C \left( \frac{d}{D} \right)^{\frac{1}{2}} \rho v_*^3 \quad (25)$$

The values for C are listed in Table F-1.

TABLE F-1

## VALUE OF COEFFICIENT C

C	Soil Characteristics
1.5	Sand with a narrow deviation of particle size
1.8	Naturally graded dune sand
2.8	Sand with a wide deviation of particle size

Typical variations of quantity of material transported as a function of wind velocity was determined in wind tunnel tests by Chepil¹¹ and are shown in Figures F-9 and F-10 for two types of soil. It is seen that for these soils, considerable material is carried in suspension, although less so for the coarser silt and heavy clay. In addition, Chepil¹¹ also determined the variation of the quantity of material being transported per unit area normal to the flow as a function of height above the surface. This is shown in Figure F-11 for the same two soils. Chepil stresses that these are only average values and apply for winds with velocity range of 13 to 30 fps measured at a height of one foot above the surface.

## F.2.2 CHARACTERISTICS OF PARTICLES IN SUSPENSION

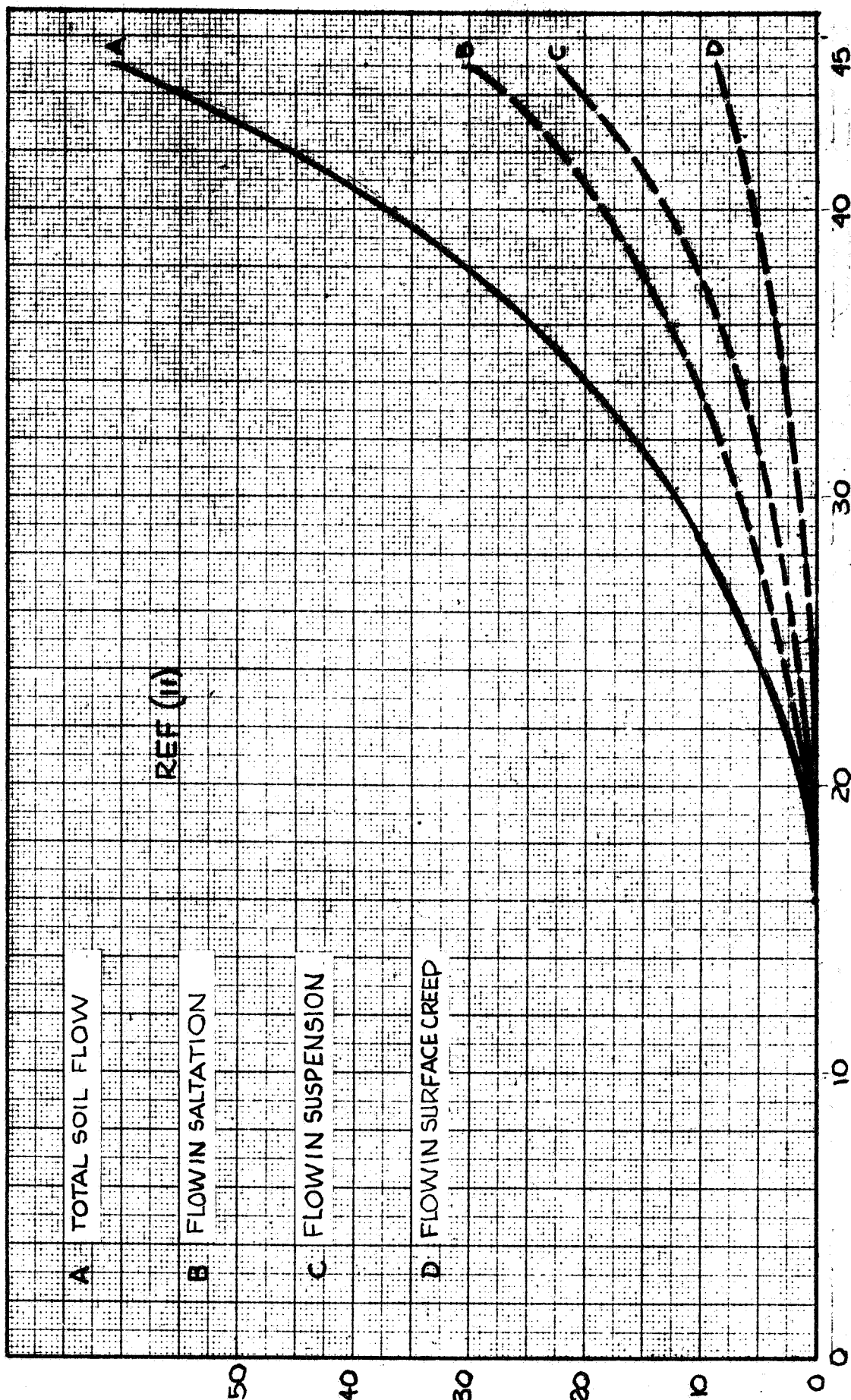
These are particles of a size such that they essentially do not interfere with the fluid flow nor absorb energy continuously from it. In general, these particles obey Stoke's law so that they quickly acquire the velocity of the fluid flow, are easily carried upward with any vertical components of flow due to turbulence, and finally fall out at some low terminal velocity when the wind has ceased. This terminal velocity is given by

$$v = \frac{g \sigma d^2}{18\mu} \quad (24)$$

where the fluid density is small compared to the particle density,  $\sigma$ . This equation is fairly accurate up to a Reynold's number of two which is slightly higher than the minimum effective drag velocity of the fluid threshold curve. It is seen that this terminal velocity is a function only of the particle properties, the gravitational constant, and the viscosity of the fluid through which the particle is falling. The terminal velocity in a Mars environment for a given particle size is given by

$$v_m = v_e \left[ \frac{g_m}{g_e} \right] \left[ \frac{\mu_e}{\mu_m} \right] \quad (25)$$

RATE OF SOIL MOVEMENT IN GRAMS/FOOT WIDTH/SECOND



WIND VELOCITY AT 1 FOOT HEIGHT, FEET PER SECOND

FIGURE F-9 SOIL TRANSPORTED AS A FUNCTION OF VELOCITY FOR HATTON FINE SANDY LOAM



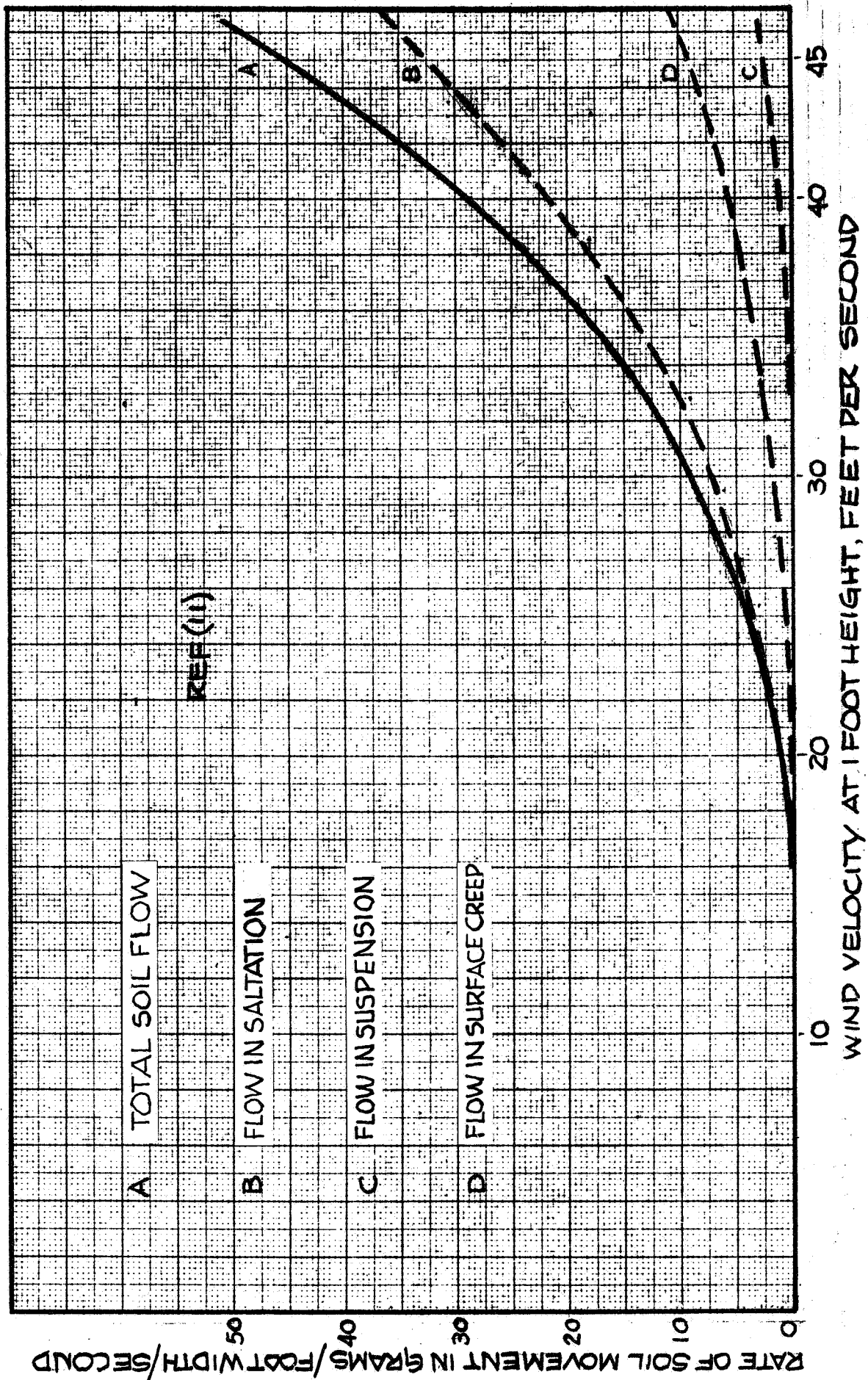


FIGURE F-10 SOIL TRANSPORTED AS A FUNCTION OF VELOCITY  
FOR SCEPTRE HEAVY CLAY

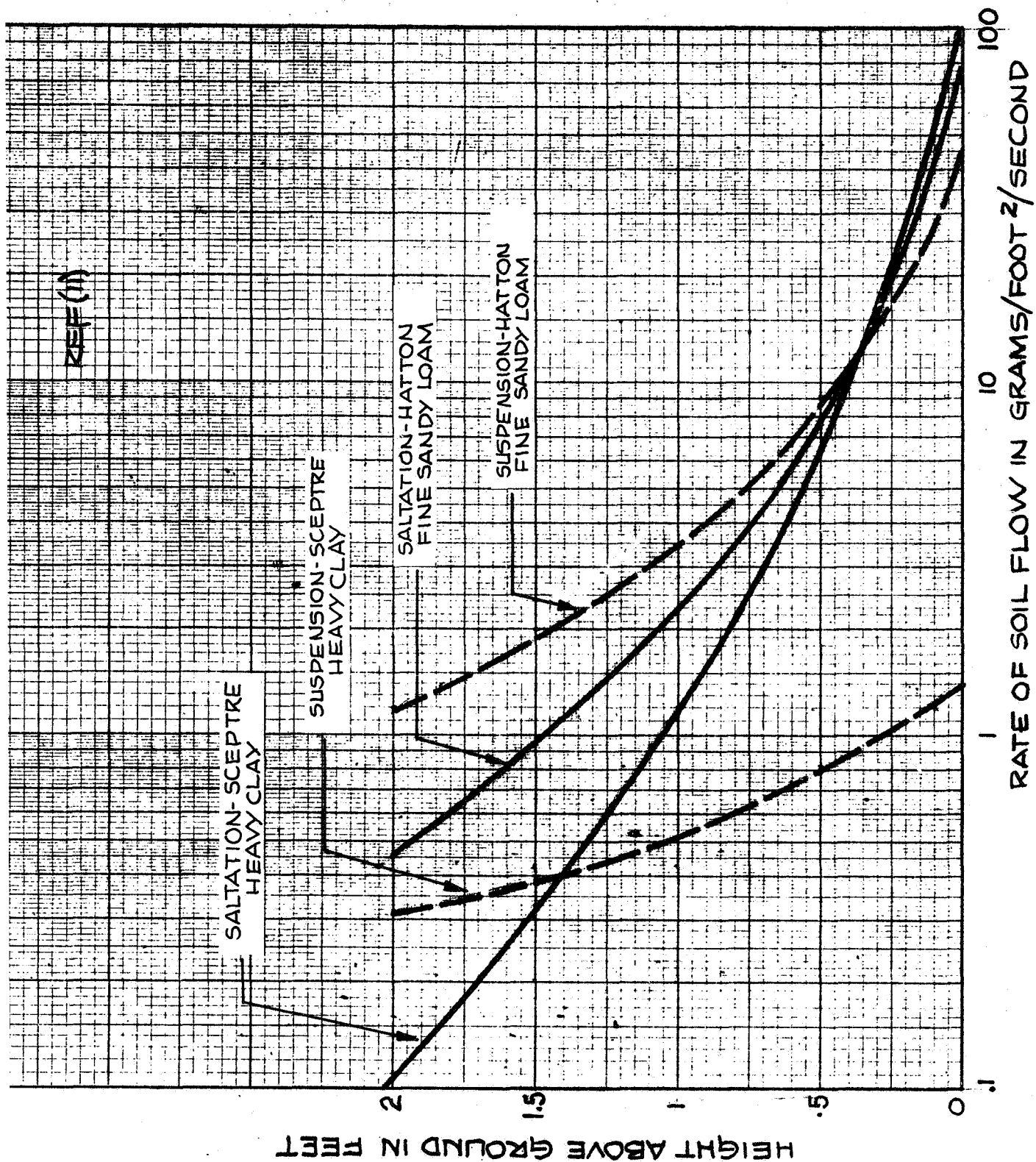


FIGURE F-11 VARIATION IN SOIL TRANSPORTED AS A FUNCTION OF HEIGHT ABOVE SURFACE

The material carried in suspension can therefore be assumed to be fairly uniformly distributed throughout a turbulent wind gradient. Chepil⁸ confirmed this to a certain extent in determining the particle size distribution at various heights above the surface. This data is shown in Figure F-12 for heights of 2, 5, 11, and 20 feet. A slight tendency for the peak of the distribution curve to shift towards the finer material with increased altitude is shown for the silt loam soil but is not as apparent for the sandy soil. Sorting by size probably does occur when the soil in suspension is carried to extreme heights since the larger particles have higher terminal velocities and are not as easily supported in the more tenuous upper atmosphere. This was not investigated in this study.

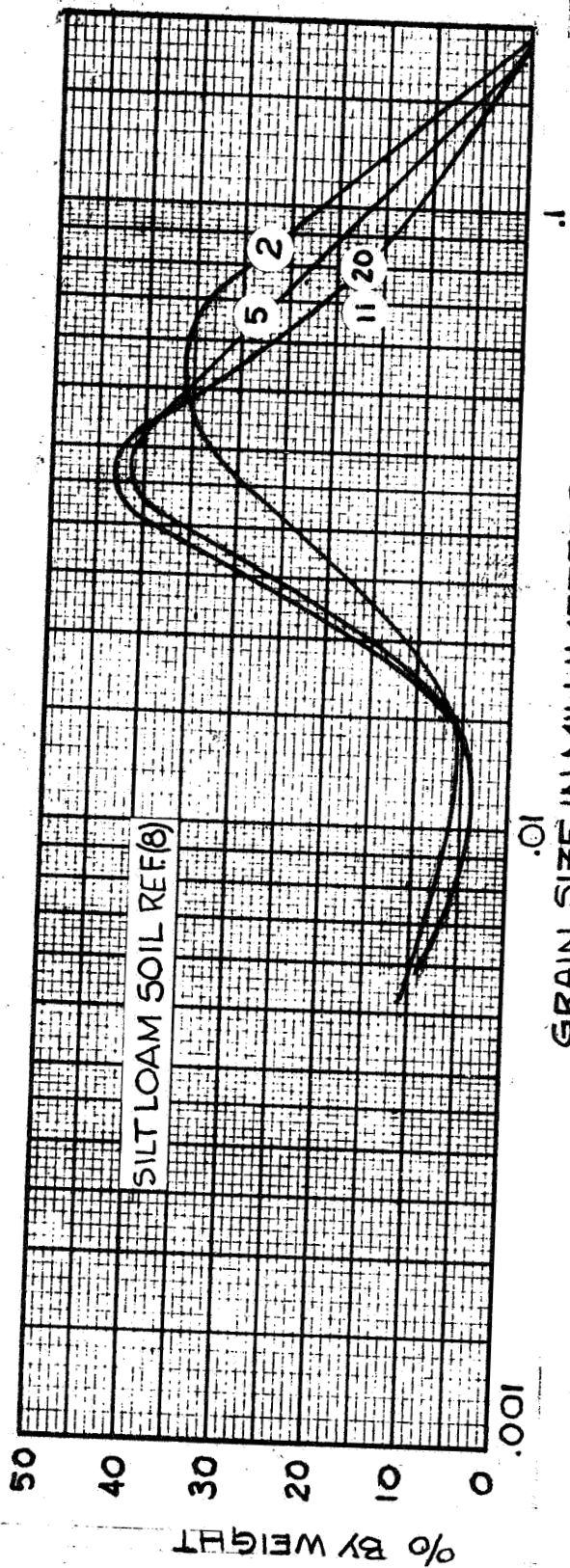
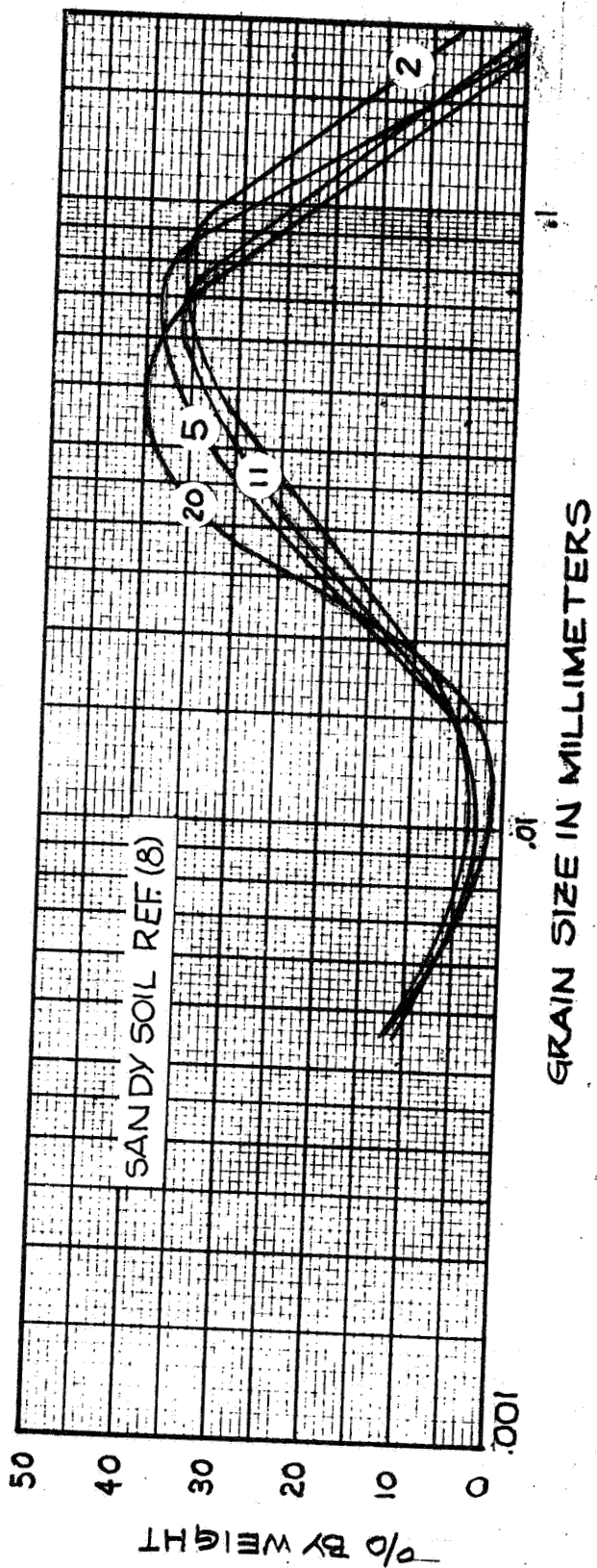


FIGURE F-12 DISTRIBUTION OF DUST CARRIED IN SUSPENSION AT VARIOUS HEIGHTS